Oxygen carriers for a novel bio-artificial liver support system

By Francis Sean Moolman

Submitted in partial fulfilment of the requirements for the degree Ph.D. (Chemical Engineering) in the Faculty of Engineering, Built Environment and Information Technology

University of Pretoria

Pretoria

May 2003

Oxygen carriers for a novel bio-artificial liver support system

Author: Francis Sean Moolman
Promoters: W.W. Focke, M.D. Heydenrych
Department: Dept. of Chemical Engineering, UP
Degree: Ph.D. (Chemical Engineering)

ABSTRACT

The purpose of the investigation was the design and development of an oxygen carrier system for oxygenation of liver cells (hepatocytes) in a bio-artificial liver support system.

Acute liver failure is a devastating condition with higher than 80% mortality. Currently the only successful treatment is orthotopic liver transplantation. The high mortality rate could be reduced if a system could be developed that could bridge the patient either until recovery (due to the liver's well-known regeneration ability) or until transplantation.

Such a system requires a bioreactor with a high density of cultured cells. Sufficient oxygen delivery to the cells is critical to ensure efficient cell function. The CSIR and University of Pretoria (UP) have designed and developed a novel bio-artificial liver support system (BALSS) that utilizes perfluorooctyl bromide (PFOB) as artificial oxygen carrier. As the PFOB is not miscible with water, it needs to be emulsified. To enable the use of the PFOB emulsion in the UP-CSIR BALSS, a study was carried out to investigate relevant aspects relating to the PFOB emulsion, i.e. the formulation, manufacturing procedure, stability, rheology and mass transfer characteristics.

The study results are reported in this dissertation, including a proposed mass transfer model for describing oxygen mass transfer to and from the PFOB emulsions. Emulsion stability can be improved through control of the droplet size and size distribution, limiting Ostwald ripening, and control of zeta potential of the dispersed phase droplets.

PFOB emulsions with dispersed phase (PFOB) volume fractions between 0.4 and 0.5 and Sauter mean droplet diameter between 100 and 200 nm were found to be optimal for oxygen mass transfer in cell culture systems. The PFOB emulsion in the UP-CSIR BALSS can be concentrated and recirculated using ultrafiltration. Quantitative recovery of PFOB from its emulsions can be carried out using distillation with orthophosphoric acid.

Experimental overall mass transfer coefficients for membrane oxygenators obtained without PFOB compared well with literature reported values of 2.5×10^{-5} m/s by Goerke et al. (2002) and $1 - 3\times10^{-5}$ m/s by Schneider et al. (1995) for similar systems. The addition of 0.2 v/v PFOB leads to an increase in the membrane oxygenator mass transfer coefficient by a factor of about 30, and an increase in oxygen carrying capacity by a factor of about 4.5.

It was also shown that suitable PFOB emulsions can have a significant impact on the growth and function of hepatocytes in a BALSS.

Key words: bio-artificial liver, liver support, oxygen carrier, perfluorocarbon

SAMEVATTING

Die doel van die ondersoek was die ontwerp en ontwikkeling van ‘n suurstofdraerstelsel vir suursfofvoorsiening aan lewerselle (hepatosiete) in ‘n kunslewerondersteuningstelsel.

Akute lewerversaking is ‘n dodelike toestand met ‘n oorlewing van minder as 20%. Huidiglik is leweroorplanting die enigste beskikbare suksesvolle behandeling. Die oorlewing van pasiënte met akute lewerversaking sou verbeter kon word indien ‘n stelsel ontwikkel kon word om die pasiënt te brug tot leweroorplanting of herstel (as gevolg van die lewer se inherente herstelvermoë).

So ‘n stelsel benodig ‘n bioreaktor met ‘n hoë seldigtheid. Genoegsame suurstoftoevoer na die selle is van kritieke belang om effektiewe selfunksie te verseker. Die WNNR en UP het ‘n unieke stelsel ontwerp en ontwikkel wat ‘n kunsmatige suurstofdraer, perfluorooktiel-bromied (PFOB), gebruik om suurstoflewering aan die selle in die bioreaktor te verbeter. Aangesien die PFOB nie mengbaar met water is nie, moet dit ge-emulsifiseer word.

Om die gebruik van die PFOB emulsie in die UP-WNNR stelsel moontlik te maak, is ‘n studie uitgevoer van relevante aspekte van die PFOB emulsie, soos formulasie, vervaardigingsprosedure, stabiliteit, rheologie en massa-oordragseienskappe.

Die resultate van die studie word in hierdie proefskrif weergegee, en sluit ‘n voorgestelde massa-oordragmodel vir beskrywing van suurstof massa-oordrag na en van die PFOB emulsies in. Emulsie-stabiliteit kan verbeter word deur beheer van die druppelgroottes en druppelgrootteverspreidings, vermindering in molekulêre diffusie, en beheer van die zeta-potensiaal van die emulsie druppels.

PFOB emulsies met PFOB volume fraksies tussen 0.4 en 0.5 en Sauter gemiddelde druppel-diameter tussen 100 en 200 nm is optimaal vir suurstof massa-oordrag in selkultuur-stelsels. Die PFOB emulsie in die UP-WNNR stelsel kan gekonsentreer en hersirkuleer word deur middel van ultrafiltrasie. Kwantitatiewe herwinning van PFOB uit sy emulsies kan gedoen word deur distillasie met ortofosforsuur.

Eksperimentele algehele massa-oordragskoeffisiënte vir membraan-suurstoflaaiers sonder PFOB was in die omgewing van 3×10^{-5} m/s, wat goed vergelyk met literatuurwaardes van 2.5×10^{-5} m/s (Goerke, Leung and Wickramasinghe, 2002) en $1 – 3\text{x}10^{-5}$ m/s (Schneider et al., 1995) vir soortgelyke stelsels. Die byvoeging van 0.2 v/v PFOB lei tot ‘n verhoging in die algehele massa-oordragkoeffisiënt met ‘n faktor van ongeveer 30, en ‘n verhoging in die totale suurstofdravermoë met ‘n faktor van ongeveer 4.5.

Die studie wys dat PFOB emulsies met die regte formulasie en eienskappe ‘n betekenisvolle impak het op die groei en funksie van hepatosiete in die UP-WNNR kunslewerondersteuningstelsel.

Sleutelwoorde: kunslewer, lewerondersteuning, suurstofdraer, perfluorokoolstof

"Only two things are infinite, the universe and human stupidity, and I'm not so sure about the former"

Albert Einstein (1879 – 1955)

ACKNOWLEDGEMENTS

I would like to thank the following people and organization(s) for the part they played in the work that culminated in this dissertation:

- Dr. Patricia Truter at the CSIR for allowing me the space and time to write in for the degree and to complete the dissertation;
- Dr. Heidi Rolfes for the many fruitful discussions and her assistance in the model development;
- The CSIR and SERA for the financial and other support of the project;
- Prof. Walter Focke for his time and advice on the model development and the dissertation;
- Prof. Mike Heydenrych for his advice and assistance with the dissertation;
- Dr. Wim Mandersloot for his assistance in the editing of papers;
- Dr. Schalk van der Merwe for his assistance with the physiological aspects and the reviewing of draft papers;
- Jack Ledwaba for all his hard work on the experiments;
- Gordon Brindley for his excellent work on the perfluorocarbon recovery method;
- Juul Cuijpers, Bauke Vermaas and Tuliameni Haufiku for their assistance on the experimental work, literature surveying and raw material ordering.

CONTENTS

LIST OF TABLES

LIST OF FIGURES

LIST OF FIGURES

DEFINITIONS AND ABBREVIATIONS

Most of the medical term definitions were obtained from the Online Medical Dictionary maintained by the CancerWeb Project (University of Newcastle upon Tyne, 2003).

ALF	Acute liver failure
Allogeneic	From another person
AMC	Amsterdam Medical Center
Anaphylactoid	Refers to anaphylaxis - immediate, transient allergic reactions
BALSS	Bio-artificial liver support system
Cerebral edema	Build-up of abnormally large amounts of fluids in the brain
cmc	Critical micelle concentration (concentration at which a surfactant begins forming micelles)
CSIR	Council for Scientific and Industrial Research
DSD	Droplet size distribution
EDTA	Ethylenediaminetetraacetic acid
Encephalopathy	Degenerative disease of the brain
Extracorporeal	Occurring outside the body
EYP	Egg yolk phospholipids or egg yolk lecithin
FF-TEM	Freeze-fracture transmission electron microscopy
FHF	Fulminant hepatic failure
Fibroblast	Resident cell of connective tissue
GC-MS	Gas chromatography combined with mass spectrometry
Globin	The polypeptide moiety of hemoglobin, linking the heme groups
Hematocrit	Relative volume of blood occupied by red blood cells or erythrocytes
Heme	Compounds of iron complexed in a porphyrin ring - the oxygen carrying moieties in hemoglobin
Hemoglobin	A conjugated protein containing four heme groups and globin
Hepatocytes	Epithelial cells of the liver that perform most of the liver functions
HLB	Hydrophilic-lipophilic balance
HPH	High-pressure homogenized
Hypoxic	Oxygen supply is below physiological levels
Kupffer cells	Phagocytic cells lining the walls of the sinusoids of the liver
LD_{50}	Lethal Dose 50 - the amount of a substance that, when administered by a defined route (e.g. oral, dermal), is expected to cause death in 50% of the defined animal population.
Leukocytes	Cells that help the body fight infections and diseases (white blood cells)
Micelle	A colloid particle formed by surfactants in aqueous solution, with hydrophobic parts pointing inward, and hydrophilic (polar) parts outward. A reverse micelle is a micelle formed in oil solution, with hydrophilic part pointing inward.

DEFINITIONS AND ABBREVIATIONS

MLV	Multilamellar vesicle – vesicle with multiple surfactant layers
MWCO	Molecular weight cut-off of an ultrafiltration membrane
NRF	National Research Foundation
Osmolarity	The concentration of osmotically active particles in solution
Ostwald ripening	Molecular diffusion of dispersed phase in an emulsion from smaller to larger droplets, due to a small difference in chemical potential between smaller and larger droplets caused by a difference in surface curvature. Only significant in sub-micron emulsions.
Parenchymal	Functional elements of an organ (as opposed to its framework)
Parenteral	Administration by injection
PC	Phosphatidyl choline
PE	Phosphatidyl ethanolamine
Perfusion	Passage of a fluid through an organ or tissue
PFC	Perfluorochemical
PFDB	Perfluorodecyl bromide
PFOB	Perfluorooctyl bromide
Phagocytic	Pertaining to uptake and digestion or killing of particulate material
Polydisperse	Wide droplet size distribution (as opposed to monodisperse, where all droplets are of the same or very similar size)
Porphyrin	Protein pigments that chelates metals – constituents of, amongst others, hemoglobin
PTFE	Polytetrafluoroethylene
RCF	Relative centrifugal force
RES	Reticuloendothelial system – phagocytic system of the body, responsible for breakdown and clearance of foreign particles
RPM	Revolutions per minute
SEM	Scanning electron microscopy
SMD	Sauter mean diameter (surface/volume average diameter)
SUV	Single unilamellar vesicle – a vesicle with a single bilayer
TEM	Transmission electron microscopy
Tumorigenic	Tumor causing
UF	Ultrafiltration
UP	University of Pretoria
Vesicle	A spherical particle formed in solution from a surfactant bilayer, with polar groups on the outside
WHO	World Health Organization
Xenogenic	Originating outside an organism, or from a foreign substance introduced in the organism
Zoonosis	The transmission of a disease from an animal or non-human species to a human

NOTATION

SYMBOL	DEFINITION	UNITS
a	Specific surface area	m^2/m^3
A	Area	m^2
a_a	Specific surface area of a per unit total volume	m^2/m^3
a_{ab}	Interfacial specific surface area between a and b per unit total volume	m^2/m^3
A_{ab}	Surface area between phases a and b	m^2
$A_{cross\text{-}section}$	Total cross-sectional area of membrane oxygenator	m^2
A_{flow}	Effective cross-sectional area in membrane oxygenator available for emulsion flow	m^2
a_i	Constants used in solving differential equations (Appendix A)	
$A_{p,proj}$	Projected surface area of PFOB in bioreactor	m^2
A_{ps}	Interfacial surface area between PFOB and hepatocytes in BALSS bioreactor	m^2
$A_{sb,proj}$	Projected surface area of hepatocyte spheroids in bioreactor	m^2
A_{surf}	Total surface area in bioreactor	m^2
$A_{surface}$	Shell-side total surface area of hollow fibres in membrane oxygenator	m^2
B	Constant used in average viscosity calculations	$[kg/m^{(2-1/n)}.s]$
Bi_m	Mass transfer Biot number	
c	Molecular solubility of PFOB in water $= S_p M_p / \rho_p$	
C_a	Concentration of oxygen in phase a	mol/m^3
$C_{a,g}$	Concentration of oxygen in phase a, at phase boundary with gas phase	mol/m^3
C_{blood}	Oxygen concentration in blood	mol/m^3
C_{BRi}	Concentration of component i in bioreactor	mol/m^3
C_{cell}	Equivalent oxygen concentration in plasma at hepatocyte surface	mol/m^3
C_{Hb}	Hemoglobin content of blood	kg Hb / m^3 blood
C_i	Concentration of rate-limiting nutrient i	mol/m^3
c_i	Constants used in solving differential equations (Appendix A)	
$C_{m,equil}$	Equilibrium oxygen concentration in medium at phase boundary with PFC	mol/m^3
C_{Pi}	Concentration of component i in patient's blood	mol/m^3
D	Diffusion coefficient	m^2/s
d_f	Internal diameter of hollow fibre	m

NOTATION

d_h	Hydraulic diameter	m
d_{hp}	Hepatocyte diameter	m
d_{hs}	Hepatocyte spheroid diameter	m
d_i	Internal diameter of membrane oxygenator unit	m
d_{imp}	Impeller diameter in agitated tank	m
d_n	Number average droplet diameter	m
D_{oa}	Binary diffusion coefficient of oxygen in phase a	m^2/s
d_{or}	Diameter of gas orifices in gas-sparged oxygenator	m
D_p	Molecular diffusion coefficient of PFOB in water	m^2/s
d_{ai}	Average diameter of i'th droplet/bubble size interval of phase a	m
d_{sa}	Sauter mean diameter of droplets/bubbles of phase a	m
e	Constant used in Equation 4-59	
E	Oxygen transfer enhancement factor, as defined in Equation 4-88	
E_a	Hole nucleation activation energy	J
f	Constant used in Equation 4-59	
F_c	Centrifugal force	N
g	Gravitational acceleration = 9.8	m/s^2
G_{form}	Gibbs free energy of formation (emulsion)	J/mol
h	Thickness of boundary layer around gas bubble or membrane	
h_b	Membrane wall thickness	m
h_f	Thickness of thin film between gas and PFC droplets in boundary layer	m
$H_{g\text{-}l}$	Henry's constant for gas g in liquid l	$bar.m^3/mol$
H_x	Henry's constant as defined in Equation 4-8	bar
i	i'th size interval	
j	Diffusional flux	$mol/m^2.s$
j_{ab}	Flux of oxygen from phase a to phase b	$mol/m^2.s$
k	Mass transfer coefficient	m/s
K	Distribution coefficient of oxygen between PFOB and medium	
k_0	Factor making provision for associated liquid volume around emulsion droplets	
k_{ab}	Convection mass transfer coefficient from a to b	m/s
k_{ph}	Convection mass transfer coefficient from PFOB to hepatocytes	m/s
K_c	Consistency index (power law coefficient)	$kg/m.s^{2-n}$
K_{Ci}	Saturation constant for nutrient i	mol/m^3

k_h	Membrane hydraulic permeability	m^2
l	Thickness of thin film	m
L_b	Length of hollow fibre in membrane oxygenator	m
L_{CR}	Length of concentration entrance region	m
L_{HR}	Length of hydrodynamic entrance region	m
m	Mass	kg
M_a	Molar mass of molecule / phase a	kg/kmol
m_i	Variable used in solving differential equations (Appendix A)	
N	Total number of droplet/bubble size intervals	
n	Power law exponent	
n_a	Number of moles of phase a	mol
N_b	Number of hollow fibres per unit oxygenator process volume	m^{-3}
N_h	Number of hepatocytes required in a BALSS for human liver support	
N_{hs}	Number of hepatocytes per hepatocyte spheroid	
N_{sb}	Number of hepatocyte spheroids in bioreactor	
$\dot{n}_h$	Steady-state oxygen consumption of hepatocytes	nmol/s/10^6 cells
$\dot{n}_{h,\max}$	Maximal oxygen consumption of hepatocytes	nmol/s/10^6 cells
n_i	Number of droplets/bubbles in droplet/bubble size interval i	
N_{imp}	Impeller speed	rev/s
$\dot{n}_{O_2,in}$	Rate of oxygen entering bioreactor	mol/s
N_p	Impeller power number	
$\dot{n}_p$	Molar flow rate of oxygen into or out of PFOB phase	mol/s
$OR_{h,max}$	Oxygen requirements of hepatocytes in bioreactor	mol/s
ΔP_b	Trans-membrane pressure drop	Pa
P	Pressure	Pa
P_a	Partial pressure of gas a in gas phase	bar
P_{ag}	Agitator power input in gas sparger	W
P_{aO_2}	Arterial partial oxygen pressure	bar
P_{atm}	Atmospheric pressure = 1.01325	bar
P_{CO_2}	Partial carbon dioxide pressure	bar
PD	Polydispersity of emulsion droplet size distribution	
pH	Negative log of the hydrogen ion concentration in an aqueous environment	

NOTATION

P_{O_2}	Partial oxygen pressure	bar
P_{vO_2}	Venous partial oxygen pressure	bar
Q	Volumetric flow rate	m^3/s
Q_e	Volumetric flow rate of emulsion through membrane oxyg.	m^3/s
Q_g	Volumetric flow rate of gas in gas sparger	m^3/s
Q_{in}	PFOB-plasma circulation rate through bioreactor	m^3/s
r	Radial distance measured from axis of hollow fibre	m
R	Gas constant = 8.314	J/mol.K
r^2	Coefficient of determination – indicates goodness of fit in simple regression (values closer to 1 indicate better fit)	
R_b	Intrinsic (clean) membrane resistance for water flow	m^{-1}
r_{BRi}	Rate of production / consumption of component i in bioreactor	mol/s
r_c	Distance of particle or droplet from axis of rotation in centrifuge	m
R_c	Membrane solute cake layer resistance	m^{-1}
R_d	Radius of droplet	m
Re	Reynolds number	
Re_g	Reynolds number for gas bubble in gas sparger	
Re_{imp}	Impeller Reynolds number	
Re_{MR}	Metzner-Reed Reynolds number for power law fluids	
R_f	Internal radius of hollow fibre = $½d_f$	m
R_h	Hydraulic radius	m
R_i	Membrane fouling resistance (due to pore plugging and adsorption)	m^{-1}
r_{Pi}	Rate of production / consumption of component i in patient	mol/s
R_T	Total membrane resistance	m^{-1}
s	Distance along length of membrane oxygenator	m
$Sat\%$	Oxygen bound to hemoglobin as a percentage of hemoglobin oxygen carrying capacity	
Sc	Schmidt number	
S_{config}	Configurational entropy for emulsion	J/mol.K
Sh	Sherwood number	
S_{Hb}	Oxygen solubility in hemoglobin	m^3 O_2 / kg Hb
S_i	Rate of consumption of nutrient i	$mol/m^3.s$
S_p	PFOB solubility in water	$kmol/m^3$
S_{pl}	Oxygen solubility in blood plasma	m^3 O_2 / bar / m^3 blood

NOTATION

t	Time	s
T	Temperature	K
t_m	Average time spent in membrane oxygenator by unit cell of emulsion	s
u	Velocity	m/s
u_c	Settling velocity of particle or droplet in centrifuge	m/s
u_e	Bulk (average) emulsion velocity	m/s
u_{or}	Gas bubble velocity through orifice (gas-sparged oxygenator)	m/s
u_t	Terminal velocity of a single settling particle or droplet	m/s
$u(t\text{-}t_{lag})$	Step function making provision for cell growth lag time	
u_{th}	Hindered terminal settling velocity in a suspension or emulsion	m/s
V	Volume	m^3
V_{BR}	Bioreactor volume	m^3
V_{gs}	Total volume in gas-sparged oxygenator = $V_p+V_m+V_g$	m^3
$V_{m,p}$	Molar volume of PFOB	m^3/mol
V_{open}	Free volume in bioreactor	m^3
V_P	Volume of blood in patient	m^3
V_t	Total system volume in membrane oxygenator = $V_p+V_{gb}+V_m+V_b$	m^3
$w_{a\text{-}b}$	Mass fraction of solute a in solvent b	
$W_{a\text{-}b}$	Mass of solute a in solvent b	kg
X	Cell density	cells/m^3
x_g	Mole fraction of gas	
X_{max}	Maximum cell density	cells/m^3
$Y_{X/Ci}$	Yield factor relating amount of nutrient consumption to amount of cells	mol/cell
z	Distance	m

Greek symbols

Δ	Change	
ε_c	Cross-sectional void fraction (shell side) of hollow fibre membrane oxygenator	
ε_{PU}	Polyurethane foam porosity	
ϕ_g	Volume fraction gas in medium = $V_g/(V_p+V_g+V_m)$	
ϕ_p	Vol. fraction PFOB in emulsion = $V_p/(V_p+V_m)$	
ϕ'_{pg}	Fraction of specific surface area of gas bubbles that is in 'direct' contact with PFOB	
$\dot{\gamma}$	Shear rate	s^{-1}

NOTATION

η	Dynamic viscosity	Pa.s
η_r	Reduced viscosity = η_e/η_m	
λ	Cell death constant	s^{-2}
μ	Specific growth rate of cells	s^{-1}
μ_{max}	Maximum specific growth rate	s^{-1}
ν	Cell age	s
ρ	Density	kg/m^3
σ	Standard deviation of emulsion droplet diameters	
σ_s	Surface tension	N/m
σ_t	Interfacial tension	N/m
τ_e	Emulsion residence time in membrane oxygenator	s
τ_w	Shear stress at the wall in membrane oxygenator	Pa
ω	Ostwald ripening rate (rate of increase of average droplet volume)	m^3/s
ω_c	Angular velocity	rad/s

General subscripts

ave	Average
b	Membrane
c	Centrifugal
e	Emulsion
g	Gas
Hb	Hemoglobin
hp	Hepatocyte
hs	Hepatocyte spheroid
m	Medium (continuous phase of emulsion)
p	PFOB
pl	Plasma
PU	Polyurethane
r	Reduced value of parameter
sb	Hepatocyte spheroids in bioreactor
w	Property evaluated at the wall

1. INTRODUCTION*

"The longest part of the journey is said to be the passing of the gate." – Marcus Terrentius Varro (116 BC – 27 BC).

1.1. Problem background

Acute liver failure is a devastating condition with high mortality rates (higher than 80% - Dixit and Gitnick, 1996:101). Orthotopic liver transplantation is currently the only available treatment. The high mortality rate is due to a number of reasons, including shortage of suitable donors, short time window between onset of acute liver failure and death (a few weeks) and the availability of medical centers able and equipped to perform the procedure.

The high mortality rate of patients suffering from acute liver failure could be reduced if a therapy was available that could support the patient's liver functions, either until patient recovery (due to the liver's well-known regeneration ability) or until liver transplantation.

Such a therapy or treatment system would have to meet a number of requirements in order to bridge the patient until transplantation or recovery:

- It must perform 20 – 40% of normal adult human liver function (Tsiaoussis et al., 2001:5; Olson, Bradley and Mate, 1999; Sussman and Kelly, 1997:S67). There is still uncertainty as to exactly which of the large number of liver functions (some of which are still not understood) are essential for patient survival (Allen, Hassanein and Bhatia, 2001:447; Brems et al., 2001; Park, Iwata and Ikada, 2001:296). Some authors think that as little as 3-5% of total liver mass could make a difference (Kamohara, Rozga and Demetriou, 1998:278).
- There must be a sufficient rate of exchange / circulation of blood between patient and system to have an impact on levels of relevant molecules in patient's blood (Iwata, Park and Ikada, 1998:235).
- Immune reactions & risk of zoonosis (incl. cell debris) must be minimized / properly managed
- The system must be as easy to use as possible (e.g. must fit on a bedside trolley; require minimal human intervention)
- The system must be cost-effective and costs should compare favourably with normal intensive care treatment for patients suffering from acute liver failure.

Extracorporeal support for liver failure patients has been researched for over 40 years (Allen, Hassanein and Bhatia, 2001:447), but no commercial system is available that has had clinical success.

---

* Please note that all raw experimental data is contained in spreadsheets (Microsoft Excel 2000) included on a CD attached to the inside back cover of this dissertation.

Due to the complexity of the liver, a simple filtration system (analogous to the kidney dialysis machine) is not sufficient for liver support. The liver performs a large number of functions, including metabolic, regulatory and secretory functions. This complexity necessitates the inclusion of live liver cells (hepatocytes) in any system that has to support or perform liver functions.

Systems containing hepatocytes in a bioreactor for the purpose of liver support are generally referred to as Bio-artificial Liver Support Systems (BALSS). The inclusion of hepatocytes in the system adds additional requirements to the BALSS:

- A suitable environment / surface for cell adhesion and proliferation (hepatocytes are anchorage-dependent – Busse and Gerlach, 1999:328);
- Oxygen and nutrient supply for sustaining cell growth and function – hepatocytes have very high oxygen demands compared to most other mammalian cells (Hay, Veitch and Gaylor, 2001:119);
- Regulation of carbon dioxide levels for optimal cell functioning - carbon dioxide levels in blood plasma influence the pH of the blood plasma due to the dissociation of dissolved carbon dioxide (H_2CO_3) into bicarbonate (HCO_3^-) and hydrogen (H^+) ions. Proper control of the pH in the circulation system is of critical importance to maintain optimal cell function. Acidosis could occur if carbon dioxide generated by the cells is not removed. The pH of blood plasma is directly related to the carbon dioxide partial pressure and can be calculated from the Henderson-Hasselbalch equation (Ludwig, 2002):

$$pH = 6.1 + \log \frac{\left[HCO_3^-\right]}{22.5 P_{CO_2}} \tag{1-1}$$

- Immune protection for both patient and hepatocyte bioreactor;
- Effective mass transfer between hepatocytes and exchange fluid (either whole blood or blood plasma) from patient (Flendrig, Te Velde and Chamuleau, 1997:1177).

The above set of requirements contains two conflicting requirements: effective mass transfer vs. immune protection. While a barrier such as a membrane could provide immune protection, it simultaneously introduces but introduces an additional mass transfer resistance. The solution to this problem is currently approached in one of two ways:

1. **Whole blood – indirect contact:** A barrier or membrane is provided, with main purpose to protect the hepatocytes from leukocytes (white blood cells) while still allowing exchange of smaller molecules. Whole blood is perfused on one side of the membrane, while hepatocytes are grown on the other side. The membrane unfortunately also introduces an additional resistance to mass transfer. Hepatocytes further away from the membrane are starved of oxygen, while also functioning sub-optimally due to decreased mass transfer of metabolites, toxins, etc. (because of increased diffusional distance).

2. **Blood plasma – direct contact:** Blood plasma is separated from whole blood through filtration, and only the blood plasma is contacted with the hepatocytes. Most molecules related to liver

function are dissolved in the blood plasma, allowing liver support through treatment of blood plasma alone (Kamohara, Rozga and Demetriou, 1998:279). As the white blood cells or leukocytes are removed, the risk of immune response activation is reduced, allowing direct perfusion of the blood plasma over the hepatocytes. While this allows higher mass transfer rates between cells and blood plasma compared to membrane-type BALSS, another problem is created.

During plasma filtration, red blood cells (hemoglobin) are also separated from the plasma. These cells are very important for hepatocyte function in terms of their oxygen supply and carbon dioxide removal functions. Thus, there is a major problem in terms of oxygen supply in BALSS treating blood plasma alone (Allen, Hassanein and Bhatia, 2001:451). This problem can be partially solved through the inclusion of oxygen supply tubes (membranes) within a BALSS bioreactor. Although some success has been achieved with this approach (Flendrig et al., 1997 and Gerlach, 1996), the membranes still represent a barrier to oxygen mass transfer between the oxygen supply and the cells.

If it is accepted that 100 µm is approximately the maximum diffusion transport distance that oxygen should travel between the source and the hepatocytes (McClelland, MacDonald and Coger, 2003:12), these membranes could represent a significant diffusional barrier, depending on their wettability by plasma. The oxygenation hollow fibres in the AMC BAL for example (Flendrig et al., 1997:1381), have a wall thickness of 330 µm, and the hollow fibres are spaced approximately 2 mm or 2000 µm apart.

The CSIR and the University of Pretoria (UP) have designed and developed a novel bio-artificial liver support system. A detailed description is presented in Section 2.4. The system follows the general approach described in point 2 above, but solves the oxygen supply problem through the addition of a synthetic oxygen carrier to the BALSS.

Oxygen carriers are well known in the field of 'blood substitutes' where they are mainly intended to reduce dependency on allogeneic (donor) blood transfusion during e.g. general surgery. There are a number of systems in various stages of clinical development (Riess, 2001:2799). The oxygen carriers are either synthetic (perfluorocarbon-based) or semi-synthetic (hemoglobin-based) – see Section 3.1 for a detailed discussion.

The UP-CSIR BALSS uses perfluorooctyl bromide (a perfluorochemical) as oxygen carrier. Perfluorochemicals (PFC's) generally have exceptional stability and very high solubility of gases, rendering them appropriate for oxygen carrying applications. As PFC's are not miscible with water, they need to be emulsified in order to function as oxygen carrier in aqueous environments. In the UP-CSIR BALSS, the perfluorooctyl bromide (PFOB) emulsion is recirculated in the BALSS during treatment of patients.

The PFOB emulsion needs to be recirculated in the BALSS for three reasons:

a) The patient's blood volume cannot be increased continuously during treatment;
b) The high cost of the PFOB;
c) The patient would be exposed to very high doses of PFOB on a continual basis during treatment if it were not recirculated.

1.2. Problem statement

To use PFOB emulsions in a BALSS as oxygen carriers, several aspects of the material and emulsion need to be investigated and understood. These include:

- How should the emulsion be formulated for maximum stability?
- How can the emulsion be sterilized?
- What surfactants should be used for emulsification?
- What emulsion manufacturing procedure should be used?
- Does the use of the emulsion result in enhanced oxygen mass transfer compared to plasma only?
- If so, what is the mass transfer enhancement mechanism?
- What are the optimum emulsion droplet sizes and volume fractions that maximize mass transfer and oxygen carrying capacity?
- What separation method can be used to keep the emulsion in circulation in the BALSS without causing it to break?
- How can the PFOB be recovered from spent emulsions?
- Does the emulsion improve BALSS function?

These key issues are addressed in subsequent chapters. Chapter 2 looks at human liver function, the epidemiology of liver diseases and the history of liver support systems. It discusses the UP-CSIR BALSS system and design in detail, highlighting the important role of the PFOB oxygen carrier. In Chapter 3, aspects relating to the formulation, manufacture and resultant properties (such as stability, viscosity, etc.) of PFOB emulsions are discussed, as well as the development of emulsion separation methods. Chapter 4 presents a model for describing and predicting oxygen mass transfer to and from PFOB emulsions, as well as experimental verification of the model results using gas-sparged and membrane oxygenators. Chapter 5 discusses the impact of PFC emulsions on cell function and cell growth kinetics. Chapter 6 reviews results obtained in the study and discusses their implications.

1.3. Project background

In 1998, Dr. Schalk van der Merwe, a gastroenterologist at Unitas Hospital and visiting lecturer at the Department of Internal Medicine at University of Pretoria, approached the Centre for Polymer Technology at the CSIR to discuss collaboration on the encapsulation of hepatocytes in hydrogel beads made from calcium alginate, with the intention of using these beads in a BALSS. Although the encapsulation of viable hepatocytes

was achieved successfully in 1999, it became evident from the literature that, owing to mass transfer limitations, the international research focus was moving away from hydrogel beads as membranes for hepatocytes.

Thus, in the beginning of 2000 it was decided that a novel approach to BALSS design was required. The UP-CSIR BALSS design was developed by a team of four persons: Dr.'s Schalk van der Merwe and Rob Bond (both of UP Dept. of Internal Medicine), Kobus van Wyk (UP Dept. of Mechanical Engineering) and Sean Moolman (CSIR Centre for Polymer Technology).

Funding for Phase I of the project (development of the system up to animal trials) was obtained from UP and CSIR's executive management, with administration of funds handled by SERA (Pty) Ltd. Recently, funding for Phase II of the project (completion of animal trials and preliminary human clinical trials) was awarded by NRF (National Research Foundation) through the Innovation Fund (funded by the Department of Science and Technology).

Currently (May 2003), the core team comprises Dr. Schalk van der Merwe (gastroenterologist), Dr. Rob Bond (medical doctor), Kobus van Wyk (mechanical engineer), Sean Moolman (chemical engineer) and Martin Nieuwoudt (medical scientist).

2. LIVER SUPPORT SYSTEMS

"The liver, you see, is a large, ugly mystery to us. We're pretty sure today that the liver exists and we have a fairly good idea of what it does whenever it's doing what it's supposed to be doing. Beyond that, we're really in the dark." – from *Catch 22* by Joseph Heller, 1962 (published by Simon & Schuster, New York).

2.1. The human liver

Detailed descriptions of the liver and liver function are given by Lee (2000) and Guyton and Hall (1996).

2.1.1. Normal liver function

The liver is one of the body's most complex organs. Where most other organs have clear-cut functions (e.g. heart = blood pump, kidneys = filters), the functions of the liver are complex and diversified. An incomplete list of liver functions is as follows (British Liver Trust, 2001; Olson, Bradley and Mate, 1999):

- Processing digested food
- Fat, lipid and protein metabolism
- Glucose regulation (glyconeogenesis and glycogenolysis)
- Combating infections
- Clearing the blood of particles like bacteria
- Detoxification
- Manufacturing bile, which is important for digestion of fats
- Storing iron, vitamins and other essential chemicals
- Carbohydrate metabolism
- Synthesis of lipoproteins and cholesterol
- Manufacturing and regulation of numerous hormones, including sex hormones
- Manufacturing enzymes and proteins that are responsible for most chemical reactions in the body, such as those involved in blood clotting and repair of damaged tissue.

The liver is the largest organ in the body and weighs approximately 1.25 kg in a healthy adult (British Liver Trust, 2001). The blood draining from the intestines in the portal vein first flows through the liver before being returned to the heart and lungs. In this way, toxins and other food products are removed from the blood before it returns to the heart. The liver also has a second blood supply – oxygen-rich arterial blood is supplied through the hepatic artery. The main function of this blood is the supply of oxygen to the liver cells. The hepatocytes receive about 25% of the total cardiac output (Lee, 2000). The liver consumes approximately 20 – 33 % of total oxygen used by the body (McClelland, MacDonald and Coger, 2003:12).

Hepatocytes make up 80-90% of the total liver mass, and perform most of the liver's functions. Hepatocyte cell position in the liver is such that every cell operates in close contact with blood (Flendrig, Te Velde and

Chamuleau, 1997:1180). Other cells in the liver include Kupffer cells, responsible for particle (e.g. bacteria) filtration, and cells of Ito, responsible for storage of fat (Olson, Bradley and Mate, 1999).

2.1.2. Liver failure and epidemiology

Hepatic failure can be acute or chronic. Acute liver failure (ALF) can be caused by either primary liver disease (fulminant hepatic failure or FHF) or secondary failure due to major burns or septic shock (Sussman and Kelly, 1997:S66) and proceeds over days or weeks (Olson, Bradley and Mate, 1999), whereas chronic liver diseases develop over a number of years.

The main causes of acute liver failure are (Fontana, 1999:270):

1. Hepatotrophic viral infections (Hepatitis A, B or E)
2. Acetaminophen (paracetamol) toxicity
3. Other drugs / toxins
4. Indeterminate

Symptoms of FHF include hepatic encephalopathy and jaundice, and generally progresses to cerebral edema. FHF is generally associated with very rapid deterioration of the patient (Cao, Esquivel and Keeffe, 1998:87; Kamohara, Rozga and Demetriou, 1998:273).

There are currently about 12 million patients worldwide suffering from severe liver diseases. Approximately 700 000 of these would be treatable with some type of BALSS, where the following is indicated (Teraklin, 2002):

- Acute on chronic liver failure
- Fulminant hepatic failure
- Primary graft dysfunction (rejection or dysfunction of transplanted liver)
- Post-surgery

In the USA, it is estimated that about 2000 patients per year suffer from fulminant hepatic failure (FHF), and 250 000 patients per year suffer from chronic liver disease, with 25 000 deaths per year (Sussman and Kelly, 1997:S66). In South Africa, the number of acute liver failure patients is estimated at 300 patients per year, and chronic liver disease patients at 30 000 patients per year (Van der Merwe, 2002).

The number of patients awaiting liver transplantation in the United States has increased by a factor of eight over the past decade, while the number of transplantations only increased by 50% over the same period (Trotter et al., 2002:1074). This has resulted in an increase in the number of patients dying while on the waiting list – see Figure 2-1.

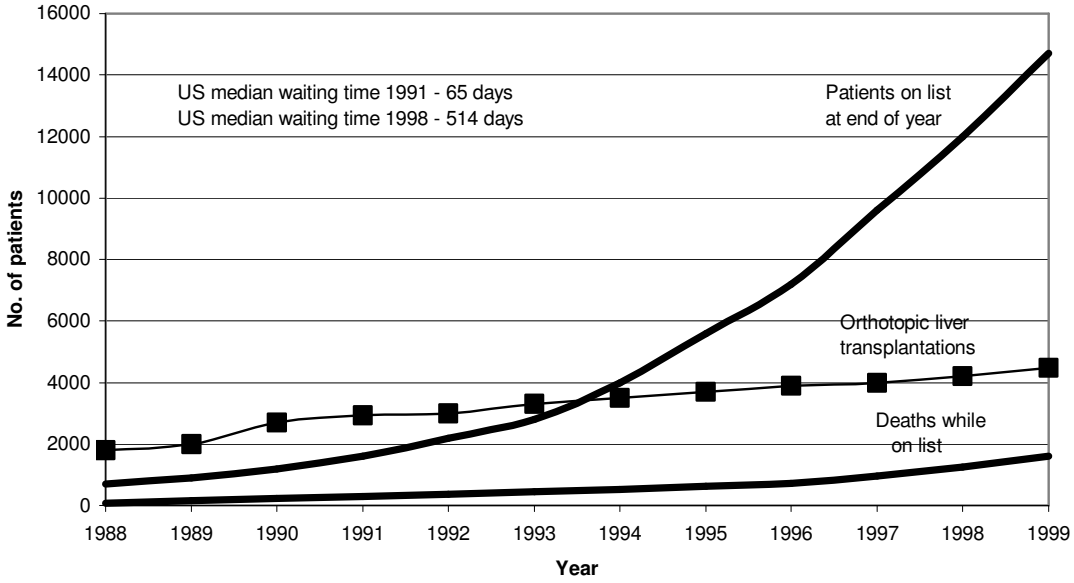

Figure 2-1. Waiting list for transplantation in the USA, 1991-1999 (Reproduced with permission from Trotter et al., 2002:1074).

2.2. History of liver support systems

Successful liver support systems would be applicable in both acute and chronic liver diseases. For acute liver failure, a liver support system could either bridge the patient until transplantation, or assist the patient's liver to recover. For chronic liver disease, a liver support system could alleviate time pressure on patients requiring transplantation through periodic treatments (Sussman and Kelly, 1997:S67). Historically, there are three basic approaches to liver support – artificial systems, biological approaches and bio-artificial systems.

2.2.1. Artificial systems

Artificial systems are systems where artificial components are used to substitute liver function. As it is impossible to mimic all of the liver's functions with a purely artificial system, these systems generally focus on one aspect of liver function only, namely its detoxifying function. The following approaches have been attempted (Legallais et al., 2001:82; Olson et al., 2000; Kamohara et al., 1998:274):

- Hemodialysis – blood is filtered with low-permeability membranes to remove toxins dissolved in plasma using some sort of membrane filtration system, analogous to kidney dialysis machines.
- Hemo- and plasmaperfusion – blood or plasma is perfused through an adsorption column (e.g. filled with activated carbon) to adsorb toxins.
- Immobilized enzyme systems – liver enzymes are immobilized in a substrate or encapsulated, and blood is perfused over the system.

As these approaches address only one specific liver function, namely detoxification, none of them was able to significantly improve survival of liver failure patients (Allen, Hassanein and Bhatia, 2001:447; Kamohara, Rozga and Demetriou, 1998:274; Dixit and Gitnick, 1996:101).

2.2.2. Biological approaches

These systems seek to utilize biological systems or entities for liver support. A number of example approaches are listed here (Legallais et al., 2001:82; Olson et al., 2000; Kamohara et al., 1998:274):

- Exchange transfusion or plasmapheresis – either the patient's blood or plasma is continuously removed while being replaced by fresh blood or plasma. The aim is to try to dilute toxins building up in the patient's circulation.
- Cross-circulation – the patient with failing liver is connected to a healthy, biocompatible individual and blood continuously exchanged (Olson, Bradley and Mate, 1999).
- Xeno-hemodialysis – the patient is connected to animals' (e.g. dogs) circulation systems or liver tissue through a dialysis membrane.
- Orthotopic liver transplantation – this is the transplantation of a cadaver's liver into a patient suffering from liver failure.
- Live-donor liver lobe transplantation – due to the liver's regenerative ability, a lobe from a healthy donor can be transplanted into patients with liver failure, with both livers then regenerating. Although this procedure is on the increase in the USA, some deaths of donors have occurred (Trotter et al., 2002:1079).

Of these approaches (in fact of all approaches), orthotopic liver transplantation is currently the only available successful treatment of liver failure (Sussman & Kelly, 1997:S66; Cao, Esquivel and Keeffe, 1998:85; Olson, Bradley and Mate, 1999), but the patient has to go on lifelong immunosuppression therapy to avoid rejection of the transplanted liver, and the risk of rejection of the organ remains (Gerlach, 1996:645). This makes the patient more susceptible to opportunistic diseases.

2.2.3. Bio-artificial systems

Bio-artificial systems include live liver cells (hepatocytes) for liver support, either implantable or in a bioreactor. The bio-artificial systems can be divided into three groups: encapsulation systems, membrane-based systems and direct perfusion systems. There are also two main approaches in terms of exchange between the patient and system: either whole blood or separated blood plasma is perfused through the bio-artificial system. The choice depends on the configuration of the bio-artificial system and considering immune protection of cells and patient, with plasma generally being used for direct perfusion, and whole blood being used in systems with some sort of membrane barrier.

Encapsulation systems

The basic approach of encapsulation systems is to encapsulate hepatocytes in a hydrogel matrix. This matrix is intended to function as a membrane through providing immune protection while at the same time allowing diffusion of smaller molecules to and from the encapsulated hepatocytes. The hydrogel beads can either be implanted or contained in some type of bioreactor.

The most common hydrogel material used in the encapsulation systems is alginate. While alginate is very biocompatible, it did not perform well as a membrane, and multilayer hydrogel coatings were developed, such as alginate-polylysine or polyacrylate hydrogels (Busse and Gerlach, 1999:326).

Initial UP-CSIR work focused on encapsulation of hepatocytes in hydrogel beads. This was achieved successfully, with hepatocytes remaining viable in alginate hydrogel beads for 14 days (see Figure 2-2). Ultimately, this approach was abandoned due to widespread indications from researchers in the field that the approach did not seem viable. Even though immune protection was successfully achieved with the beads (Joly et al., 1997:795), there are various problems associated with the beads, such as:

- The beads suffer from mass-transfer resistance problems (Goosen, 1999:97; Yuet, Harris and Goosen, 1995:110).
- The beads have reduced response time to chemical stimuli.
- Huge volumes are required for therapeutic effect due to the volume added by the beads (May and Sefton, 1999:126).
- Channeling and shear stress-related problems were observed (Legallais, David and Doré, 2001:90).

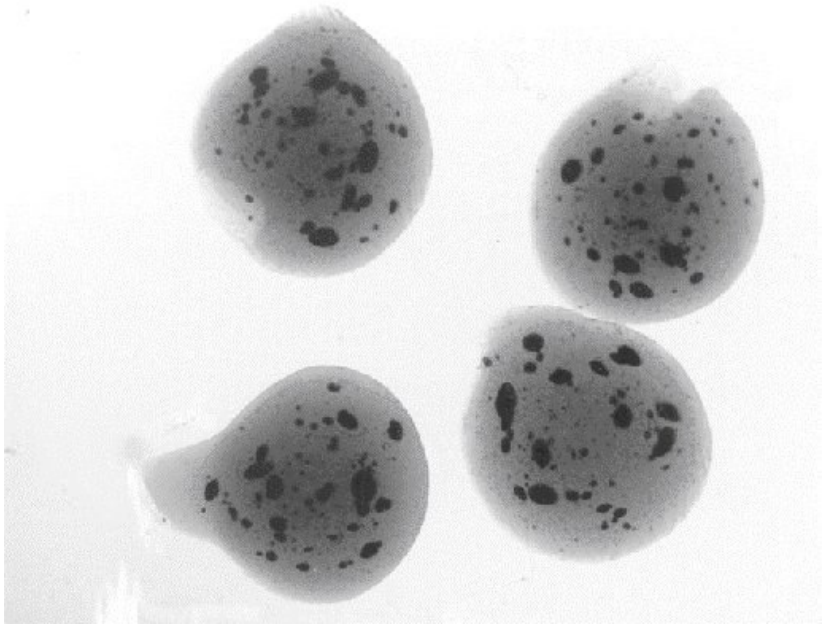

Figure 2-2. Hepatocytes in alginate hydrogel beads produced by UP-CSIR in 1999 remained viable for 14 days.

Membrane-based systems

The membrane-based systems are mainly based on perfusion of whole blood on one side of a semi-permeable membrane, and hepatocytes grown on the other surface of the membrane. The membranes generally have a molecular weight cut-off between 100 and 150 kDa, to allow free transport of carrier proteins such as albumin (60 kDa), while blocking immunoglobulins (≥150 kDa) and other larger molecules such as leukocytes (Allen, Hassanein and Bhatia, 2001:448; Te Velde et al., 1997:229).

One of the major limitations of these systems is achieving sufficient and effective mass transfer through the membrane of oxygen, toxins and other molecules that need to be processed by the hepatocytes (Flendrig, Te Velde and Chamuleau, 1997:1177; Gerlach, 1996:646). A recent theoretical and experimental analysis of the oxygen transfer in a hollow-fibre bio-artificial liver (the HepatAssist 2000) concluded that "a substantial proportion of the hepatocytes contained in the model device would be subjected to hypoxic conditions" (Hay, Veitch and Gaylor, 2001:129). Nevertheless, most of the current research on BALSS is being done on membrane-based systems (see Section 2.2.4).

Direct perfusion systems

Direct perfusion systems use bioreactors containing three-dimensional scaffolds on which hepatocytes are grown. Blood plasma is directly perfused through these scaffolds. The main limitation with these systems is oxygen supply to the cells. The bio-artificial liver group at AMC (Amsterdam Medical Centre) attempts to alleviate this problem through the inclusion of oxygen supply tubes in the bioreactor (Flendrig, Te Velde and Chamuleau, 1999).

The UP-CSIR BALSS (see Section 2.3) is a direct perfusion system with a three-dimensional polyurethane scaffold bioreactor that solves the problem of oxygen supply through the addition of an oxygen carrier to the perfused plasma.

2.2.4. Current development status of liver support systems

Table 2-1 gives an overview of the current development status of a number of liver support systems. Although there are a large number of systems under development, only the ones that are most advanced in terms of development are listed. The UP-CSIR system is also listed to indicate its comparative properties and development stage. Please note that inclusion on the table does not indicate clinical success in improvement of patient survival.

Table 2-1. Liver support systems currently under development (Legallais, David and Doré, 2001; Allen, Hassanein and Bhatia, 2001:452, Allen and Bhatia, 2002; Xue et al., 2001:826)

Company/group (system)	System	Perfusion type	Development phase
Artificial systems			
Teraklin (MARS®)	Hemodialysis	Blood	Commercially available
HemoTherapies (BioLogic-DT)	Hemodialysis & plasmaperfusion	Blood	FDA-approved multicenter
Bio-artificial - membrane-based systems			
Circe Biomedical (HepatAssist®)	Polystyrene hollow fibre membrane, cells grown on shell side, porcine hepatocytes, two charcoal columns	Plasma	Phase II/III multicenter
Vitagen (Hepatix®)	Cellulose acetate hollow fibre membrane, cells on shell side, C3A human cell line	Blood	Phase I/II clinical trials
Algenix (LIVERx 2000)	Hollow fibre membrane, porcine hepatocytes	Blood	Phase I
Excorp Medical (BLSS)	Polystyrene hollow fibre membrane, cells in fibre lumen, porcine hepatocytes	Blood	Phase I/II
Charite Virchow Clinic-Berlin (MELS)	Hollow fibre membrane, porcine hepatocytes, plasmapheresis	Plasma	Phase I/II
Chinese PLA General Hospital (TECA)	Hollow fibre membrane, porcine hepatocytes, cells on shell side	Plasma	Phase I
Bio-artificial - encapsulation systems			
UCLA	Alginate beads, fetal porcine hepatocytes	Blood	In vivo rats
Univ. of Detroit	Chitosan beads, rabbit hepatocytes	Culture medium	In vitro
Univ. of Rennes	Alginate beads, rat hepatocytes	Blood	In vivo rats
Bio-artificial – direct perfusion systems			
Univ. of Amsterdam	Spiral-wound polyester matrix with oxygen tubes, porcine hepatocytes	Plasma	Phase I/II clinical trials
Univ. of Tokyo	Wound polyester fabric, porcine hepatocytes	Whole blood	Pig model
Univ. of Pretoria & CSIR	**3D – polyurethane foam matrix, oxygen carrier, porcine hepatocytes**	**Plasma**	**Pig model**

One of the aspects currently not addressed in any of the BALSS under development, is bile excretion. It is suggested that the inclusion of a bile removal module, such as an albumin dialysis module, would improve BALSS performance (Allen, Hassanein and Bhatia, 2001:449).

The only system currently available commercially is the MARS® (Molecular Adsorbent Recirculation System) liver support therapy, which is a passive membrane-based dialysis system. Due to the absence of a biological component, this system cannot perform any of the metabolic or synthetic functions of the liver, as discussed in Section 2.2.1.

2.3. UP-CSIR bio-artificial liver support system

The UP-CSIR BALSS is an extracorporeal system used to contact a patient's blood with hepatocytes in a bioreactor designed to optimize hepatocyte growth and function and mass transfer between hepatocytes and blood plasma. The system is being patented in several countries worldwide: preliminary examination by the European Patent Office of PCT patent application no. WO0222775 was recently completed with a favourable ruling.

The basic process description is as follows (see Figure 2-3):

1. Venal blood is withdrawn from the patient and the blood plasma separated from the white blood cells, red blood cells and platelets in a plasma separator.
2. The blood plasma is pumped into the PFOB-plasma reservoir, where it is mixed with concentrated PFOB emulsion.
3. The blood plasma – PFOB blend is pumped through an oxygenator, where it is contacted with a gas mix consisting of 95% oxygen and 5% carbon dioxide. The carbon dioxide is required to maintain the blood plasma at physiological carbon dioxide concentration. Excess carbon dioxide picked up by the PFOB emulsion in the bioreactor is removed in the oxygenator.
4. The oxygenated blood plasma – PFOB blend is pumped through the bioreactor, where the hepatocytes are grown in open-cell polyurethane foam. The following actions take place within the bioreactor:
   - The hepatocytes absorb nutrients from the plasma and oxygen from the PFOB emulsion droplets, while giving off carbon dioxide.
   - The PFOB emulsion droplets absorb carbon dioxide generated by the hepatocytes.
   - The hepatocytes perform all the relevant functions on the blood plasma, such as removal of hepatic and neurotoxins, administration of neurotrophic and hepatotrophic factors, and maintenance of coagulability.
5. The treated plasma – PFOB blend exits the reactor and flows through a biomass filter, after which it returns to the PFOB-plasma reservoir. The purpose of the biomass filter is to remove any biological debris such as dislodged hepatocytes.
6. PFOB-plasma blend is continuously withdrawn from the PFOB-plasma reservoir and pumped through a cross-flow membrane separator, where pure blood plasma is separated from the blend. Although there is almost no PFOB left in the blood plasma stream exiting the membrane separator, there is still a significant percentage of blood plasma left in the PFOB stream. This is necessary to maintain the PFOB emulsion integrity and to thus avoid having to re-emulsify the PFOB inline. Thus, the PFOB stream exiting the membrane separator is a concentrated PFOB emulsion. The extent of concentration

is limited by the emulsion viscosity at higher dispersed phase volume fractions and the maximum packing for the specific emulsion.

7. The blood plasma exiting the membrane separator flows into a plasma reservoir. Plasma is continuously withdrawn from the plasma reservoir and returned to the patient at the same rate that plasma enters the system from the plasma separator. The plasma that is returning to the patient is remixed with the separated white blood cells, red blood cells and platelets from the plasma separator, before flowing through a de-aerator back into the patient.

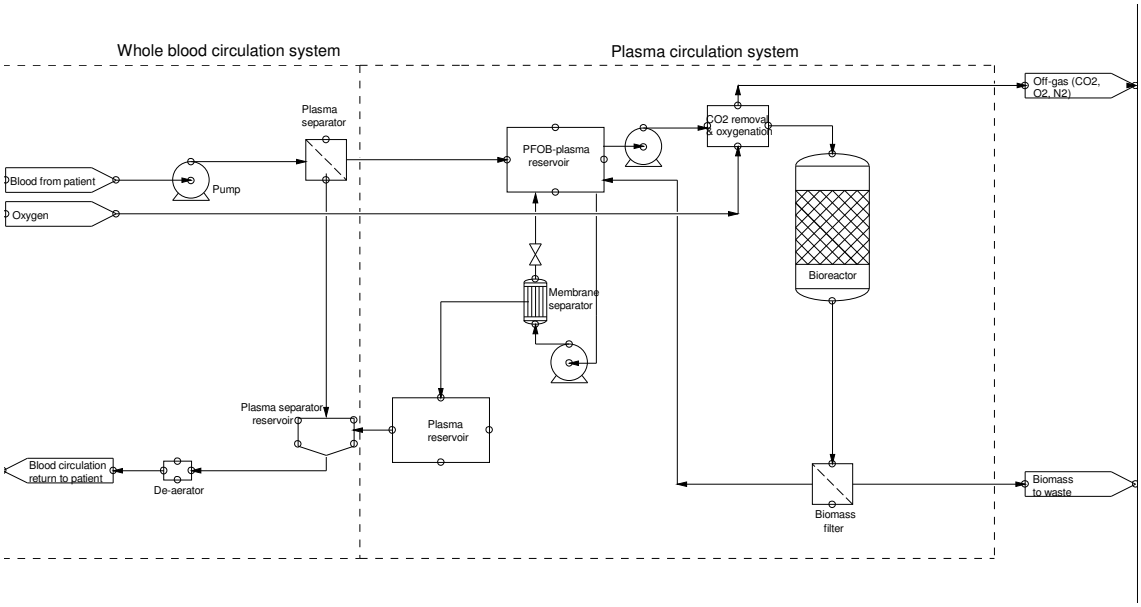

Figure 2-3. Basic flow diagram of the UP-CSIR BALSS

This system complies with the basic requirements for a BALSS as discussed in Section 1.1:

- It provides a suitable environment for hepatocyte adhesion and proliferation through the biocompatible polyurethane foam. The foam density can be manipulated to increase / decrease foam surface area as required for cell adhesion. Internal as well as external experiments (Kurosawa et al., 2000:160; Gion et al., 1999:131; Ijima et al., 1998:213) have shown successful adhesion and proliferation of hepatocytes on polyurethane foams.
- Nutrients for hepatocyte growth and function are supplied by the blood plasma.
- Oxygen is supplied to the cells by the PFOB emulsion, which also regulates carbon dioxide levels.
- Minimization of immune reactions is achieved through the separation of the white blood cells from the blood plasma, and the biomass filter that prevents cell debris from entering the patient's blood stream.
- New bioreactors with improved mass transfer are stressed as a critical area of development for future bio-artificial liver devices (Kamohara, Rozga and Demetriou, 1998:283). In the CSIR-UP BALSS, effective mass transfer between hepatocytes and blood plasma is provided through direct perfusion of the blood plasma through the bioreactor.

A prototype system has been designed, and has been refined based on the first animal (porcine or pig) trial completed in November 2002 (see Figure 2-4 for photograph of prototype I, and Figure 2-5 for photograph of prototype II). A follow-up animal trial for proof of concept purposes is scheduled for January 2004. The intention is to show statistically significant prolonged survival rates for pigs with acute liver failure treated with the UP-CSIR BALSS. Upon successful completion of animal clinical trials, human clinical trials are planned for 2004.

Figure 2-4. Photograph of prototype UP-CSIR BALSS

Before the current UP-CSIR BALSS is connected to a patient, a number of preparatory steps must take place:

1. The whole system must be sterilized. This is done through sterilization of components such as tubes and the bioreactor through gamma irradiation, and subsequent circulation of a Peresal® solution through the connected system. Peresal® is a proprietary formulation for disinfection and decalcification of extracorporeal hemodialysis equipment.
2. Bioreactors must be seeded with freshly harvested hepatocytes. This is done through an automated procedure, where the surgically removed liver is dissolved using an enzymatic collagenase solution and the hepatocytes separated from non-parenchymal cells using a multi-step isolation procedure. The cells are then seeded into the bioreactor in a sterile manner using a sealed transfer apparatus. The seeded bioreactors are placed in a circulation system with oxygenator and culture medium for 24 hours, to

allow the hepatocytes to attach to the bioreactor scaffold surface and overcome the initial shock resulting from the seeding process.

3. All surgical preparations related to the patient must take place.

Figure 2-5. Photograph of prototype II of UP-CSIR BALSS

It is intended that the final UP-CSIR BALSS will take the form of a mobile unit on a bedside trolley, with a number of consumable parts that will be replaced for every patient. These parts will include a number of pre-seeded, cryopreserved bioreactors, tubing, plasma separator, etc. and will be sold pre-packaged and sterilized.

From the above process description and discussion, a number of design aspects relating to the BALSS development emerge that must be carefully considered. These are listed in Table 2-2.

Table 2-2. Aspects relating to BALSS development

Aspect	Impact / considerations
Type of cells	Different types of cells can be used for the bioreactor. These include immortalized human cell lines (e.g. HUH-7 or HEPG2), primary human hepatocytes, and primary animal hepatocytes. Each of these have their own advantages and disadvantages, and the choice will impact on the function and efficacy of the BALSS: ▪ Primary human hepatocytes - although primary human hepatocytes would be preferable, the supply of suitable, viable human livers is very limited, and even when available, such livers should rather be used for transplantation. ▪ Immortalized human cell lines - these are easy to work with in a laboratory setting, but it is difficult to culture sufficient quantities for use in BALSS bioreactors. Also, immortalized cell lines tend to have lost some of the original hepatocyte functionality, and there are concerns about transmission of these cells or tumorigenic products to the patient (Tsiaoussis et al., 2001:3; Allen and Bhatia, 2002:449). ▪ Primary animal hepatocytes (xenogenic) – porcine hepatocytes are preferred due to the very similar physiological characteristics and functionality compared to human hepatocytes (Tsiaoussis et al., 2001:4). These hepatocytes are relatively easily obtainable in large quantities. The biggest concerns are the risk of zoonosis and immune system related problems (Te Velde et al., 1997:229), as well as the inability to divide in culture (Sussman and Kelly, 1997:S67). However, no adverse side effects or immune system reactions have been reported so far (Cao, Esquivel and Keeffe, 1998:89). The UP-CSIR BALSS currently utilizes primary porcine hepatocytes, although other cell types could also be used.
System process volume	The total BALSS process volume must be as small as possible, as only a limited amount of blood plasma can be withdrawn from the patient at any given time. The process volume in the UP-CSIR BALSS is primed using saline. If the process volume is too large, the saline will cause dilution of the patient's blood (i.e. decreased hematocrit) and a decrease in blood pressure. Although the process volume can be primed with donated blood plasma, the requirement for this should be avoided if possible, due to increased procedure complexity and risk.

Aspect	Impact / considerations
Choice of scaffold and cell morphology	The material chosen as scaffold for the bioreactor must be biocompatible, and the hepatocytes must adhere to the surface and proliferate. The material must provide sufficient surface area for cell growth. The morphology of the material will also influence cell growth, association and function. Recent studies (Wu et al., 1996; Ijima et al., 1998; Yamada et al., 1998; Yamada et al., 1999; Yamada et al., 2001) have indicated the importance of spheroid formation in hepatocyte functioning. Spheroids show vastly improved function compared to monolayer-cultured cells. Spheroid volume must be controlled, as hepatocytes in the centre of large (larger than approximately 105 µm – Ijima et al., 1998:224) spheroids are starved of oxygen and thus exhibit reduced function (Flendrig, Te Velde and Chamuleau, 1997:1180). One study has indicated that it might be possible to control spheroid volume through control of the scaffold pore size (Glicklis et al., 2000:344). The scaffold material must be easily sterilizable.
Sterile / aseptic environment	All components of the BALSS must be sterilized where possible, and any exposure of process internals to atmosphere (with the associated risk of contamination) should be avoided if possible. Human intervention in the process must be minimized and all work should be carried out as aseptically as possible.
Instrumentation	Instrumentation is required for real-time monitoring and control of BALSS performance. Basic measurements include flow rates, temperatures (the whole system must be maintained at 37 ºC), pressures, pH and oxygen partial pressures. The instrumentation should require minimal process volume for measurement with maximum accuracy (based on cost and required process volume vs. accuracy considerations).
Hepatocyte (bioreactor) function	The hepatocytes in the bioreactor generally exhibit normal cell culture behaviour – after an initial lag period, cell function and proliferation increases to a maximum level, which is maintained for a number of days. After this maintained functionality period, decreased function and cell death occur. Thus, it is important to determine the bioreactor functionality vs. time under a variety of stress conditions in order to determine the optimal time when a bioreactor should be loaded in the BALSS and when it should be removed.
Reactor design	Apart from the choice of scaffold, the physical design of the bioreactor can also influence the system efficiency. Channel formation or preferential flow through certain parts of the bioreactor and the associated 'dead spaces' (areas with no circulation) should be minimized, as this could lead to reduced function and cell death in the dead spaces.
Cell seeding	The cell seeding procedure must result in as uniform a distribution of cells throughout the bioreactor scaffold as possible. A non-uniform distribution will result in sub-optimal utilization of bioreactor volume. The viability of seeded cells must be maximized through careful design of the cell harvesting and seeding procedure.

Aspect	**Impact / considerations**
Clotting activation	Activation of the plasma clotting cascade must be avoided as far as possible, for example through infusion of heparin into the BALSS.
Co-culturing	Recent studies (Bhatia et al., 1999; Kim et al., 1998; Okamoto et al., 1998) indicate increased hepatocyte functioning when the cells are co-cultured with non-parenchymal cells such as fibroblasts or Kupffer cells.
Scale-up	Some types of bioreactor devices do not lend themselves to easy scale-up due to mass transfer and design limitations. Additionally, some devices have too low cell densities to allow realistic scale-up.

3. OXYGEN CARRIER DEVELOPMENT

"Blut ist ein ganz besonderer Saft." (Translation - blood is a very special fluid) – Von Goethe, 1909.

3.1. Overview of oxygen carriers

The term 'oxygen carrier' is generally used to refer to a molecule that has an unusually high capacity to carry oxygen, either through oxygen bonding to the molecule or through physical absorption of the oxygen. Historically, the chronic shortage of donor blood experienced by blood banks worldwide, as well as the need for large stockpiles of blood during war or civilian disasters provided the main impetus for development of oxygen carriers (Ketcham and Cairns, 1999:326). This application has resulted in the widespread use of the incorrect term 'blood substitute' to describe these oxygen carriers.

There are two main types of oxygen carriers currently under development – hemoglobin-based and perfluorocarbon-based. Hemoglobin-based oxygen carriers consist of hemoglobin molecules stabilized in some way to prevent breakdown of the hemoglobin tetramer into its toxic dimers. Perfluorocarbon-based oxygen carriers consist of an emulsion of one or more perfluorocarbons, which exhibit very high solubility of gases compared to water or plasma. For reviews of the status of oxygen carrier development, see Riess (2001) or Sarteschi et al. (2001).

3.1.1. Hemoglobin-based oxygen carriers

Hemoglobin is a tetrameric protein with two α polypeptide globin subunits and two β polypeptide globin subunits (α1β1α2β2). An iron-containing heme group, which is responsible for oxygen binding, is associated with each of the subunits. The hemoglobin molecule is unstable in the body outside the red blood cell. It is quickly broken down into two dimers (α1β1 and α2β2), which are known to have renal (kidney) toxicity due to build-up in the renal tubules (Chang, 1999:61).

Due to this in vivo instability, the hemoglobin must be stabilized before it can be used in blood substitute applications. There are a number of approaches used for this (Chang, 1998:234; Winslow, 1999:339):

- Cross-linked polyhemoglobin – a number of hemoglobin molecules are cross-linked or polymerized using e.g. glutaraldehyde or *o*-raffinose.
- Cross-linked hemoglobin – the α1 and α2 subunits are cross-linked using e.g. bis(3,5-dibromosalicylic) fumarate.
- Recombinant hemoglobin – the α1 and α2 subunits are fused together to form 'dialpha hemoglobin'. The molecules are produced using genetically engineered E. coli.
- Conjugated or surface-modified hemoglobin – the hemoglobin is conjugated with molecules such as dextran, polyoxyethylene or polyethylene glycol.
- Encapsulated hemoglobin – these include microcapsules, lipid vesicles and nanocapsules.

There are a number of hemoglobin-based oxygen carriers in various stages of clinical development (see Riess, 2001; Ketcham and Cairns, 1999:332; Winslow, 1999:339). Hemopure (a polymerized bovine hemoglobin manufactured by Biopure) was the first hemoglobin-based oxygen carrier approved for human use and received approval in South Africa in 2001.

3.1.2. Perfluorocarbon-based oxygen carriers

Perfluorocarbons (PFC's) are a family of compounds with very high stability and chemical and biological inertness, as well as exceptionally high solubility of gases. They are synthesic compounds, with PTFE (polytetrafluoroethylene) the most well known member of the PFC family. PFC's originally found application in the Manhattan nuclear bomb project in World War II, where they were used as inert solvents in the uranium enrichment process (Faithfull and Weers, 1998:243).

The inertness of PFC's stem from the very high electro-negativity and large size of the fluorine atom compared to hydrogen. These atoms shield the carbon backbone from chemical reactions through steric and electronic protection (Lowe, Davey and Power, 1998:272). The fluorine-carbon bond is very strong (486 kJ/mol – Lowe, 1991:87), which also contributes to the molecules' stability.

Due to the low polarizability electron cloud surrounding the PFC molecules, intermolecular interactions are very weak (only London dispersion forces). This weak interaction leads to high solubility of non-polar gases in PFC's (Riess, 2001:2866). A gas solubility comparison of a number of PFC's and water is given in Table 3-1.

Table 3-1. Gas solubility in a number of PFC's and water

Liquid	**Gas solubility (ml of gas per dl of liquid at 37 ºC and 1 atm)**		**Reference**
	Oxygen	**Carbon dioxide**	
Water	2.5	65	Lowe, 1991:87
Perfluorodecalin ($C_{10}F_{18}$)	42.3	148	King et al., 1989:1037
Perfluorotributylamine ($C_{12}F_{27}N$)	40.3	140	King et al., 1989:1037
Perfluorooctyl bromide ($C_8F_{17}Br$)	50.0	213	Lowe, 1991:87

PFC's are generally both hydrophobic and lipophobic, and require emulsification for use in aqueous environments.

The potential for using PFC's in blood substitute applications was first realized in the 1960s when Clark and Gollan (1966) published their famous paper on the survival of mice breathing oxygenated liquid PFC. For blood substitute applications, there are a number of important considerations regarding the formulation and preparation of PFC emulsions, which are also relevant for cell culture applications. These considerations are discussed below.

Droplet size & size distribution

Droplet size is important in terms of interfacial surface area for mass transfer (the smaller the droplets, the larger the surface area / volume ratio). It is also important in terms of in vivo effects – droplets larger than 0.4 µm can cause embolisms (Shah and Mehra, 1996:181), and even at sizes above 0.2 µm, adverse effects such as fevers have been reported (Krafft, Riess and Weers, 1998:309). Smaller droplets show reduced release of cytokines by macrophages (Chang, 1999:65). Thus, it is generally accepted that the average droplet size must be below 0.2 µm, with a narrow droplet size distribution (Faithfull and Weers, 1998:246; Shah and Mehra, 1996:181). Generally, high-pressure homogenization or microfluidization is used to produce emulsions with these characteristics (see Section 3.2). Droplet size is also important in terms of physical emulsion stability – as the PFC's are generally much denser than water, the droplets need to be very small in order to minimize settling or 'creaming' of the emulsion. Wider droplet size distributions are more prone to Ostwald ripening than narrow size distributions.

Dispersed phase volume fraction

The dispersed phase volume fraction (ϕ_p) determines the oxygen carrying capacity of the PFC emulsion – oxygen carrying capacity increases with increase in ϕ_p. At the same time, there is an upper limit set by the maximum packing density of the emulsion droplets. The emulsion viscosity also increases with increasing ϕ_p (see Section 3.3.2). For monodisperse spheres, the maximum packing density is approximately 0.74 for tetrahedral packing, and ~ 0.64 for random packing (Mandersloot and Scott, 1990:57). For polydisperse emulsions, this value can be somewhat higher. At some ϕ_p close to the maximum packing density, phase inversion will take place, and the emulsion will become a water-in-oil emulsion. The values found by Yamamoto et al. (1994:450) for phase inversion of a perfluorotributylamine-water system were $\phi_p = 0.60 – 0.65$.

Emulsion viscosity

The emulsion viscosity is strongly related to the dispersed phase volume fraction, and is also affected by droplet size (generally, viscosity increases with decrease in droplet size – Pell and Holzmann, 1974:665) and zeta potential. If the zeta potential is close to zero, flocculation of the emulsion can occur, causing a reversible increase in emulsion viscosity. The zeta potential is influenced by the pH, total ionic content, choice of surfactant, and type of ions present.

Choice of surfactant

The choice of surfactant is based on two main considerations: effectiveness of emulsification of the PFC (i.e. stability of the resulting emulsion) and biocompatibility. Earlier PFC emulsions used poloxamers (polyoxyethylene-polyoxypropylene-polyoxyethylene triblock copolymers) such as Pluronic® as surfactant, but

use of poloxamers has decreased due to reported adverse reactions. Clinical studies indicated anaphylactoid-type reactions in a small percentage of patients due to complement activation (Zuck and Riess, 1994:314), although later indications are that the reactions can be substantially reduced by reducing impurities in the surfactant (Riess, 2001:2871).

So-called second-generation PFC emulsions use egg yolk phospholipids as surfactant, which do not cause complement activation. The egg yolk phospholipids typically have a HLB (hydrophilic-lipophilic balance) value of between 18 and 20 (G. Young, 2000).

Stability

The shelf life of the PFC emulsions should be as long as possible. The first generation of PFC emulsions were very unstable, and had to be kept frozen and reconstituted just prior to use. One of these emulsions, Fluosol® DA, was approved by the FDA for use during angioplasty for high-risk patients (Riess, 1992:183). In addition to its instability, the PFC volume fraction was so low (approx. 10 vol.%) that the oxygen carrying capacity of the resulting emulsions was not that much higher than water or plasma alone, especially after dilution in the patient's blood. Second-generation emulsions show much improved stability (shelf lives of longer than a year are reported when refrigerated – Riess et al, 1994:227) as well as increased oxygen-carrying capacity.

Choice of perfluorocarbon

The choice of perfluorocarbon is important for a number of reasons. Perfluorocarbon emulsions are generally eliminated from the body through the reticuloendothelial system (RES). A reasonable residence time in the body is required for therapeutic effect, but elimination time cannot be too long, as this would cause excessive build-up with prolonged use. As molecular weight of perfluorocarbon increases, the rate of excretion decreases exponentially (Zuck and Riess, 1994:307). The rate of excretion is related to the PFC's ability to dissolve in lipids, which decreases with increased molecular weight. The acceptable molecular weight range for PFC's is between 460 and 520 g/mol (Dandliker, Watson and Drees, 1995) – PFC's with lower molecular weights can cause pulmonary complications (Krafft, Riess and Weers, 1998:257). At these molecular weights, organ retention time is too long. By inclusion of a lipophilic moiety, such as the bromine atom, the lipid solubility increases, which causes decreased organ retention time, as well as improved emulsion stability when a phospholipid is used as surfactant (Krafft, Riess and Weers, 1998:258). The presence of a lipophilic bromine atom, together with its high solubility of oxygen, makes perfluorooctyl bromide the PFC of choice for most developers and researchers in the field of injectable oxygen carriers.

3.1.3. Oxygen carrier selection for the UP-CSIR bio-artificial liver support system

The selection of oxygen carrier for use in the UP-CSIR BALSS was based on a number of major selection criteria:

- The oxygen carrier should have sufficient shelf life for ease of use in both laboratory experiment and clinical setting.
- The oxygen carrier should be either commercially available or relatively easy to manufacture.
- Physical separation of the oxygen carrier from plasma should be possible.
- The oxygen carrier should preferably be approved or in development for 'blood substitute' use (if approved, this would remove a complication in obtaining future approval for the UP-CSIR BALSS).

Based on the above criteria and the risk of zoonosis associated with hemoglobin-based oxygen carriers, PFC emulsions were selected as oxygen carriers for the UP-CSIR BALSS. Based on the research data available, perfluorooctyl bromide (PFOB) was selected as PFC of choice.

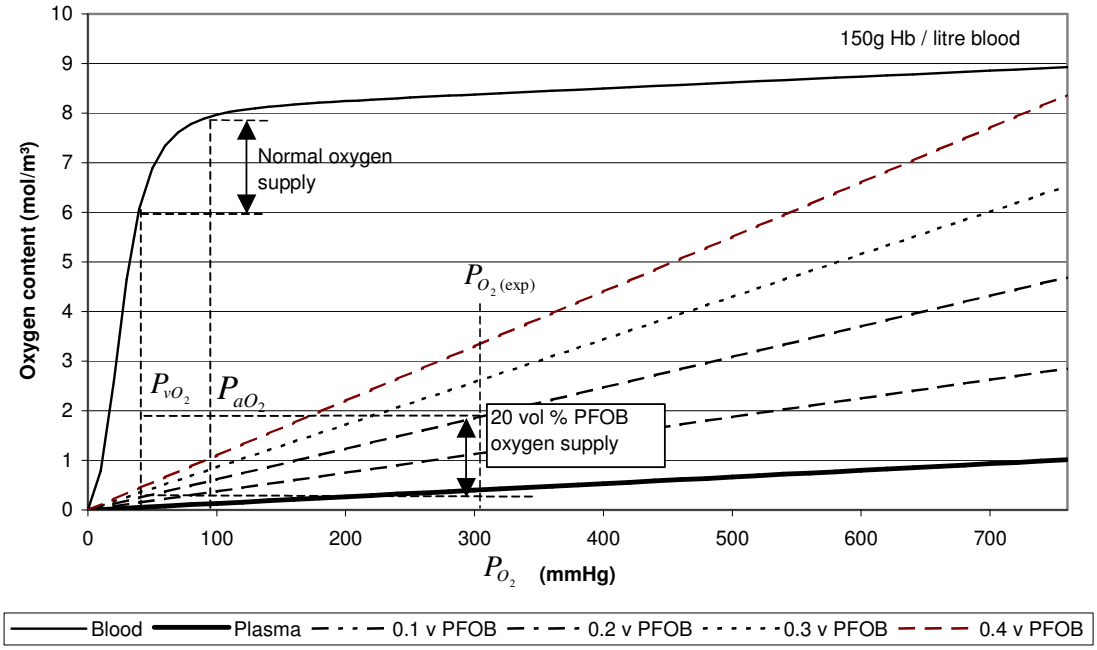

Figure 3-1. Increased PFOB volume fraction increases the oxygen carrying capacity of the emulsions. The oxygen solubility in the emulsions follows a linear relationship with partial oxygen pressure. An experimentally measured partial oxygen pressure in the UP-CSIR BALSS is indicated on the graph, showing similar potential oxygen delivery compared to blood (if exposed to normal venous partial oxygen pressure).

The improvement in oxygen carrying capacity of a PFOB emulsion (dotted lines) compared to water or plasma alone (thick solid line) is clear from Figure 3-1. The oxyhemoglobin dissociation curve (thin solid line) is

included in the figure for comparison purposes. The lines for the PFOB emulsions were calculated using the Henry's constant for oxygen in PFOB (see Section 4.1).

The double-arrowed lines for the 0.2 v/v PFOB emulsion and for hemoglobin on the graph indicate the amount of oxygen delivered by the two fluids for a decrease in partial oxygen pressure typically encountered by the said fluids. For hemoglobin, this typical decrease in partial pressure is the difference between arterial and venous oxygen pressure in the blood. For 0.2 v/v PFOB emulsion, this decrease is the difference in oxygen partial pressure between experimentally measured oxygenated PFOB emulsion (oxygenated with a 60% O_2 gas feed) and venous oxygen pressure in the blood. It can be seen from Figure 3.1 that the oxygen delivery for the two systems are comparable, with hemoglobin oxygen delivery somewhat higher.

When the oxygen partial pressure of the PFOB emulsion is increased (e.g. by increasing the oxygen content of the gas feed to the PFOB emulsion oxygenator), oxygen delivery levels can be achieved that exceed that of hemoglobin under normal arterial and venous oxygen pressure conditions.

The oxyhemoglobin curve was calculated by first calculating the hemoglobin oxygen saturation percentage ($Sat\%$) using the following equation given by Severinghaus (1979:599):

$$Sat\% = \frac{100}{\frac{1}{18033P_{O_2}^3 + 4.8P_{O_2}} + 1} \tag{3-1}$$

The total blood oxygen content (C_{blood}) includes the oxygen carried in the hemoglobin, as well as dissolved oxygen in the blood plasma:

$$C_{blood} = \left(C_{Hb} S_{Hb} \frac{Sat\%}{100} + S_{pl} P_{O_2} \right) \times \frac{P_{atm}}{RT} \tag{3-2}$$

3.2. Emulsion preparation & stability

For reviews of basic emulsion science, see Bibette et al. (2002) or Sherman (1968).

3.2.1. Emulsion formulation

The emulsion formulations and manufacturing procedures used were continuously improved during the project as knowledge and experience increased. Initially, sonication (see Section 3.2.2) was used for emulsification, together with a phosphate buffer solution as continuous phase (Emulsion A). Table 3-2 gives a typical composition for Emulsion A. Emulsion A is prone to flocculation (causing pseudoplastic rheological behaviour), as well as having large droplet sizes (4 µm Sauter mean diameter) and exhibiting severe instability. Later, improved formulations were manufactured by using a buffered saline solution as continuous phase, with high-pressure homogenization (see Section 3.2.2) used for emulsification (Emulsion B). Table 3-3 gives a

typical composition for Emulsion B. These emulsions feature submicron droplet sizes (0.2 µm Sauter mean diameter), exhibit Newtonian rheological behaviour, and are very stable.

Table 3-2. Typical composition of Emulsion A (0.2 PFOB volume fraction)

Component	Composition (weight %)	Supplier / purity	Purpose
PFOB	25.8	Fluorochem / 98%	Oxygen carrier
Egg-yolk lecithin	5.0	Sigma-Aldrich / 60% (PC:PE* ~ 2:1)	Surfactant
Phosphate buffer solution (pH 7.5) – Na_2HPO_4 & KH_2PO_4	68.0	Na_2HPO_4 & KH_2PO_4 from Saarchem	Continuous phase
D-α-tocopherol (Vitamin E)	0.7	BASF	Anti-oxidant to protect egg-yolk lecithin during manufacture, sterilization and storage
Glycerol	0.5	PIC	To increase emulsion viscosity (Lohrmann et al., 1998); as cryoprotector (Garfield, Balaban and Seitz, 1999); as additional surfactant (Clark and Leland, 1996)
Lecithin as % of PFOB	19.4%		
Manufacturing equipment	Sonicator		

*PC:PE is the phosphatidyl choline:phosphatidyl ethanolamine ratio in the specific grade of egg-yolk lecithin

Table 3-3. Typical composition of Emulsion B

Component	Composition (weight %)	Supplier / purity	Purpose
PFOB	30.73	ABCR / 99%	Oxygen carrier
Egg-yolk lecithin	1.91	Lipoid E80S / 80% (PC:PE = 4.7:1)	Surfactant
Sodium chloride	0.5	Merck	Adjust emulsion osmolarity
Sodium bicarbonate	0.15	BDH Chemicals	Buffer
Water	65.67	Demineralized (Millipore – Super-C activated carbon)	Continuous phase
D-α-tocopherol (Vitamin E)	0.99	BASF	Anti-oxidant to protect egg-yolk lecithin during manufacture, sterilization and storage

Component	Composition (weight %)	Supplier / purity	Purpose
EDTA	0.05	Clinical Sciences Diagnostics	Chelating agent for metal cations that could catalyze lecithin degradation or destabilize emulsion (through changing the zeta potential)
Lecithin as percentage of PFOB	6.2%		
Manufacturing equipment	High-pressure homogenizer		

A typical composition of the egg-yolk lecithin used for Emulsion B, Lipoid E80S, is given in Table 3-4. The phosphatidyl choline and phosphatidyl ethanolamine molecules are illustrated in Figure 3-2. The presence of a polar (hydrophilic) phosphate head group and a hydrophobic tail is evident from Figure 3-2. The main components of phosphatidylcholine naturally occurring in egg yolk lecithin are given in Table 3-5 (Wabel, 1998). From this composition, an average molar mass for phosphatidylcholine can be calculated as 753.6 g/mol. If a similar fatty acid side chain distribution is assumed for phosphatidylethanolamine, the corresponding molar mass is 710.6 g/mol. Using these values, an estimate of the molar mass of Lipoid E80S lecithin of 731 g/mol is obtained.

Table 3-4. Typical composition of Lipoid E80S egg yolk lecithin (from certificate of analysis – Lipoid E80S batch no. 120077-7, supplied by Lipoid AG)

Component	Specification, %	Analysis result, %	Molar mass (g/mol)
Phosphatidyl choline	64.0 – 79.0	71.9	753.63
Phosphatidyl ethanolamine	12.0 – 18.0	15.4	710.57
Lysophosphatidylcholine	< 3.0	1.5	355.36
Sphingomyelin	< 3.0	2.0	507.67
Phosphorus	3.5 – 4.1	3.75	
Neutral lipids	< 5.0	2.0	
Triglycerides	< 3.0	1.5	
Cholesterol	< 1.0	< 1.0	386.66
Free fatty acids	< 1.0	< 0.05	
DL-α-tocopherol	0.05 – 0.1	0.07	430.71
Water	< 2.0	0.4	18.01
Ethanol	< 0.2	< 0.2	46.07

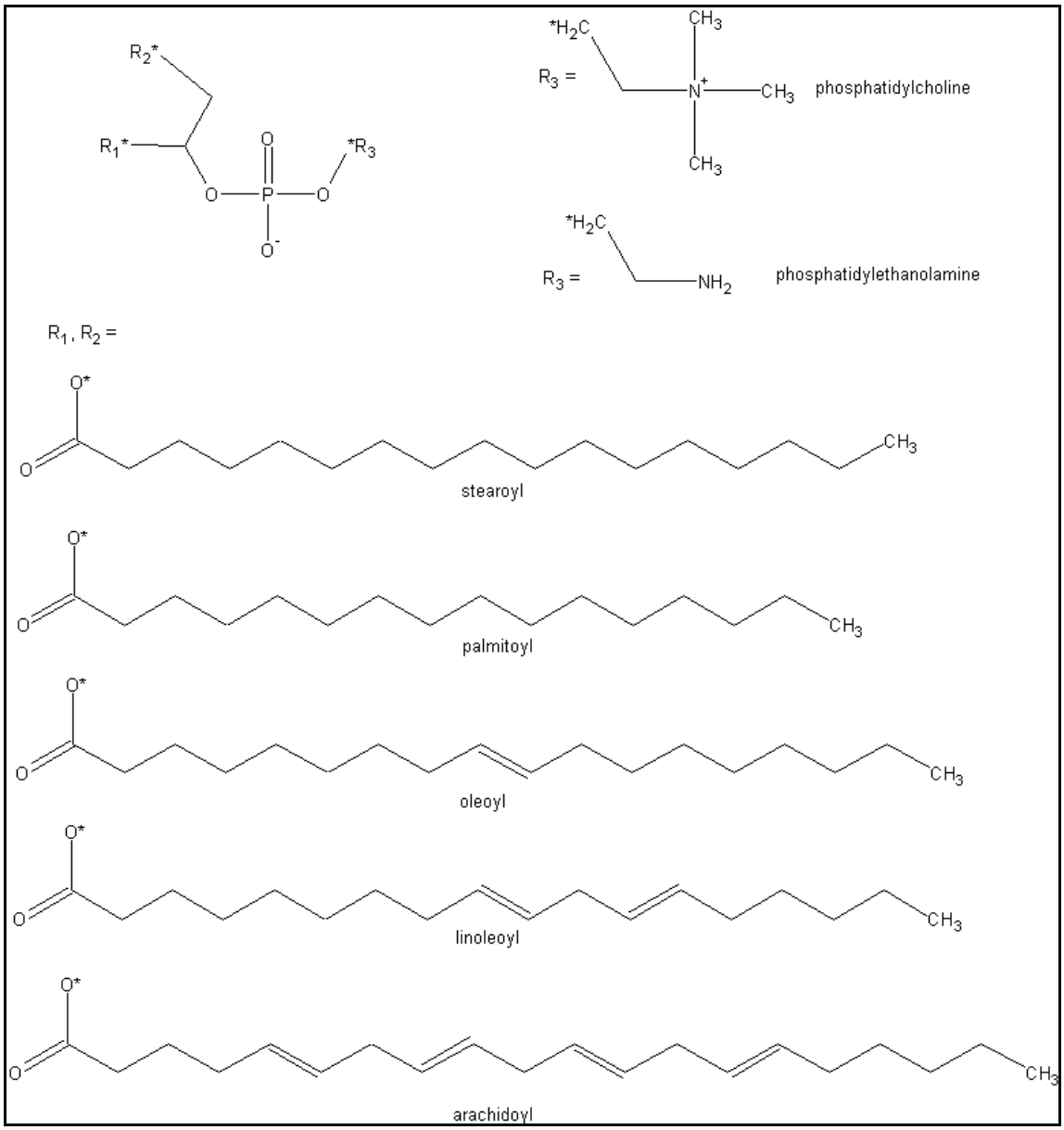

Figure 3-2. Chemical structure of phosphatidyl choline and phosphatidyl ethanolamine (Wabel, 1998)

Table 3-5. Typical components of phosphatidylcholine in egg yolk lecithin

R_1, R_2	**Composition (mol %)**	**Molar mass (g/mol)**
Palmitoyl, oleoyl	38.2	745.56
Palmitoyl, linoleoyl	21.8	743.55
Stearoyl, linoleoyl	11.22	771.58
Stearoyl, oleoyl	9.3	773.60
Stearoyl, arachidoyl	3.36	795.58
Palmitoyl, palmitoyl (dipalmitoyl)	0.72	719.55

The optimal lecithin content as percentage of PFOB for 0.2 µm emulsions is reported as 4 – 6 weight percent (Riess, 1992:187). The choice of lecithin is also important. It has been reported that the ratio of phosphatidyl choline (PC) to phosphatidyl ethanolamine (PE) should be higher than approximately 4:1; otherwise, a drastic reduction in emulsion stability is observed, especially after sterilization (Krafft, Riess and Weers, 1998:289). The PC:PE ratio for Emulsion A was 2:1, while the ratio for Emulsion B was 4.7:1.

For blood substitute and cell culture applications, the continuous phase of the emulsion must preferably be close to physiological conditions - pH = 7.4 (Sherman and Luciano, 1986:34) and osmolarity = 280 - 310 mOsm/ℓ (Sherman and Luciano, 1986:134). The pH should be buffered to prevent large fluctuations in the cell culture environment. The recommended pH is around 8.0 for lecithin-based emulsions that are terminally heat-sterilized (Floyd, 1999:139). Calculated osmolarity for Emulsion A is 1360 mOsm/ℓ and for Emulsion B, it is 350 mOsm/ℓ. Measured pH of Emulsion A was 8.1 and of Emulsion B was 8.4.

For different PFOB volume fractions, the amount of surfactant added was adjusted accordingly, but the salt concentrations in the aqueous phase were kept constant (to maintain pH and osmolarity). At PFOB volume fractions higher than approximately 0.5, the emulsion assumes a creamy solid consistency.

3.2.2. Emulsion manufacturing procedure

The basic mechanism of emulsion manufacture is the creation of interfacial surface area between two immiscible phases, and the stabilization of that interface by using a surfactant that has groups 'soluble' in each of the phases. Enough surfactant must be added to form at least a monolayer on the interfacial surface area created. Thus, at constant dispersed phase volume fraction, more surfactant needs to be added the smaller the droplet size gets.

The amount of energy required for creating the interfacial surface area can be calculated thermodynamically from the following equation (Riess, 2001:2880):

$$\Delta G_{form} = \Delta A \sigma_i - T\Delta S_{config} \tag{3-3}$$

The entropy term is usually negligible compared to the surface tension term for macroemulsions (Riess, 2001:2880). Thus, ΔG_{form} will be positive, and therefore the emulsion is thermodynamically unstable. The actual energy required for emulsification is usually much higher than the value calculated from Equation 3-3, due to the additional energy required as a result of the increase in surface curvature of small droplets, which causes a local increase in the capillary or Laplace pressure. The Laplace pressure can be calculated from the following equation (Krafft, Riess and Weers, 1998:278):

$$\Delta P = \frac{2\sigma_i}{R_d} \tag{3-4}$$

Other factors, such as the presence of a surfactant and the viscosity of the continuous phase, can influence the energy required for emulsification.

As mentioned in Section 3.1.2, droplet size and droplet size distribution is very important for PFOB emulsions in blood substitute and cell culture applications. Narrow droplet size distributions and very small droplets (around 0.2 µm) are preferable for increased stability, improved mass transfer and *in vivo* compatibility.

Generally, two methods have been used for the manufacture of PFC emulsions: sonication and high-pressure homogenization. Literature on PFC emulsions also refers to microfluidization as a separate process, but it is essentially the same process as high-pressure homogenization. Sonication uses ultrasonic waves to cause cavitation within the liquid blend, causing break-up of dispersed phase droplets. High-pressure homogenization forces liquid through a very small orifice ('valve') at very high pressures (in the order of 2000 bar), to cause droplet break-up.

Sonication suffers from some disadvantages: the energy put into the liquid is concentrated around the tip of the ultrasonic probe and is not uniformly distributed throughout the liquid. Thus, emulsification by sonication is not a very repeatable procedure, as position of the probe in the container, probe shape, shape of the container, and even liquid level in the container are all variables influencing the droplet size distribution of the resulting emulsion. Sonication is also not very scalable, and more suited to a laboratory environment. Sonication results in wide droplet size distributions, with average droplet sizes larger than 1 µm.

High-pressure homogenization, on the other hand, is a very repeatable process, as all material in the sample is exposed to approximately the same duration and intensity of energy input. As the number of passes through the homogenizer is increased, the droplet sizes get smaller and the droplet size distribution becomes narrower.

A Cole Parmer Series 4710 Ultrasonic Homogenizer was used in the preparation of Emulsion A (see Table 3-2 for composition), with energy setting at maximum (120 W). The following procedure was used:

1. Mix all ingredients except PFOB – dissolve and stir for 30 min at 40 ºC.
2. Sonicate mixture for 10 minutes.
3. Add PFOB.
4. Homogenize for 1 minute with Ultra Turrax Type TP18/2 rotor-stator type homogenizer @ 20 000 rpm.
5. Sonicate mixture for 7 minutes.
6. Homogenize for 1 minute with Ultra Turrax.
7. Sonicate for 2 minutes.
8. Repeat Steps 6 and 7 another nine times.

For Emulsion B (see Table 3-3 for composition), an APV 2000 Laboratory Homogenizer (high-pressure homogenizer) was used in manufacturing, with homogenizing pressure kept constant at 1800 bar. The number of passes was increased during the course of the project, from an initial four passes, to the current 15 passes.

The following procedure was followed:

1. Dissolve salts, EDTA and Vitamin E in the water.
2. Add lecithin.
3. Agitate for 5 minutes at 5000 rpm with magnetic stirrer.
4. Agitate with Silverson L3R rotor-stator type homogenizer for 1 minute at 8000 rpm.
5. Add PFOB slowly while agitating at 6000 rpm (with magnetic stirrer) for 15 minutes.
6. Homogenize for 15 passes. Catch product in beaker immersed in ice bath and give chance to cool down between passes. Bubble nitrogen through emulsion in feed and product containers to minimize oxidative degradation of lecithin at higher temperatures (Dandliker, Watson and Drees, 1993).
7. Put samples in autoclave bottles and sterilize for 15 minutes at 121 ºC.

The resultant droplet size distributions and stabilities (of Emulsions A and B) are discussed in Sections 3.2.4 and 3.2.5, respectively.

The amount of homogenization performed on the lecithin solution before addition of PFOB also has an impact on the ultimate emulsion stability. If too much homogenization is performed, multilamellar vesicles (MLV's) and eventually single unilamellar vesicles (SUV's) are formed. When these dispersions were used for emulsion manufacture, it was found that their resulting emulsions were less stable than emulsions prepared using lecithin dispersions that were only gently dispersed (Cornélus et al., 1993). This is probably due to the stability of the formed vesicles, making it more difficult to 'rupture' them to make surfactant available for stabilization of the PFOB-water interface.

The longer the phospholipid chain length, the more energy required to rupture or split vesicles – this was seen in interfacial tension experiments, where equilibration for phospholipids with chain lengths > C_{12} could not be reached within 24 hours (Kabalnov et al., 1995:2973). While this creates a problem when the EYP (egg yolk phospholipids) is in the form of vesicles, it probably contributes to the high emulsion stability obtainable using EYP.

When mentioning 'rupturing', the effect is a combination of energetic rupture of the interfacial monolayer and of molecular diffusion of surfactant. The rate of molecular diffusion is also related to the cmc (critical micelle concentration) – the higher this value, the higher the effective concentration of surfactant in the medium, allowing for faster molecular diffusion (Kabalnov et al., 1995:2973).

3.2.3. Emulsion sterilization

The emulsions are autoclaved for terminal sterilization at 121 ºC for 15 minutes. Autoclaving causes a slight increase in droplet size, and the use of a rotating autoclave is recommended (Wabel, 1998). Phosphatidyl choline is hydrolyzed slower than phosphatidyl ethanolamine during autoclaving, and increased pH helps to stabilize the emulsions for autoclaving (Wabel, 1998).

For Emulsion A, severe instability was noted during autoclaving. Figure 3-3 shows a negative staining TEM (transmission electron microscopy) photograph of some large coalesced droplets in Emulsion A, formed during autoclaving. These coalesced droplets did not appear after autoclaving Emulsion B, and Sauter mean droplet diameters of 0.2 to 0.25 µm were achieved after autoclaving.

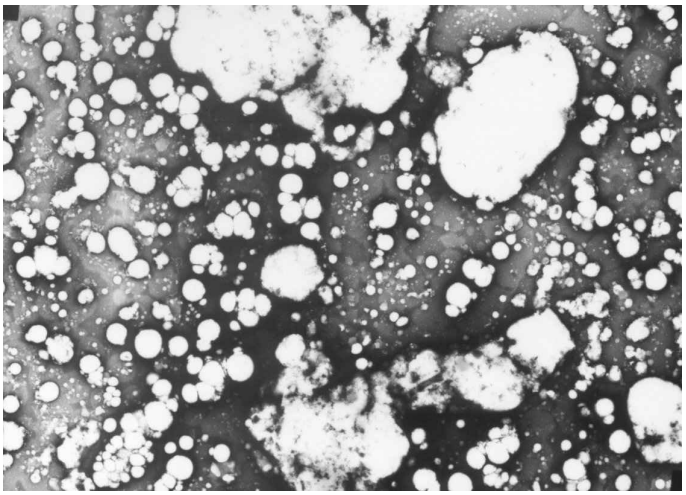

Figure 3-3. Negative staining TEM photograph at 7500x of coalesced droplets in Emulsion A, formed during autoclaving.

3.2.4. Emulsion droplet size distributions

As mentioned earlier, small droplet sizes and narrow droplet size distributions are important parameters of the PFOB emulsions. Thus, it is important to accurately determine droplet size distributions for the emulsions manufactured with the various formulations and processes.

Literature on PFOB emulsions fails, almost without exception, to mention the calculation method for their reported average droplet diameters (e.g. number average, surface average, etc.). This is a critical omission, as it is important for comparison purposes to know how the values were calculated.

In the application of PFOB emulsions as oxygen carriers, the most important criterion is surface area per volume for mass transfer. Thus, the Sauter mean diameter (SMD), which is a surface area per volume average, was used for all emulsions as the yardstick for comparison.

The SMD of droplets or bubbles of phase *a* (d_{sa}) is calculated with the following equation (Allen, 1981:128):

$$d_{sa} = \sum_{i=1}^{N} n_i d_{ai}^3 \Big/ \sum_{i=1}^{N} n_i d_{ai}^2 \qquad (3\text{-}5)$$

The importance of choosing the right criterion for comparison of emulsions is illustrated in Figure 3-4, giving typical cumulative distributions for a high-pressure homogenized sample with four passes.

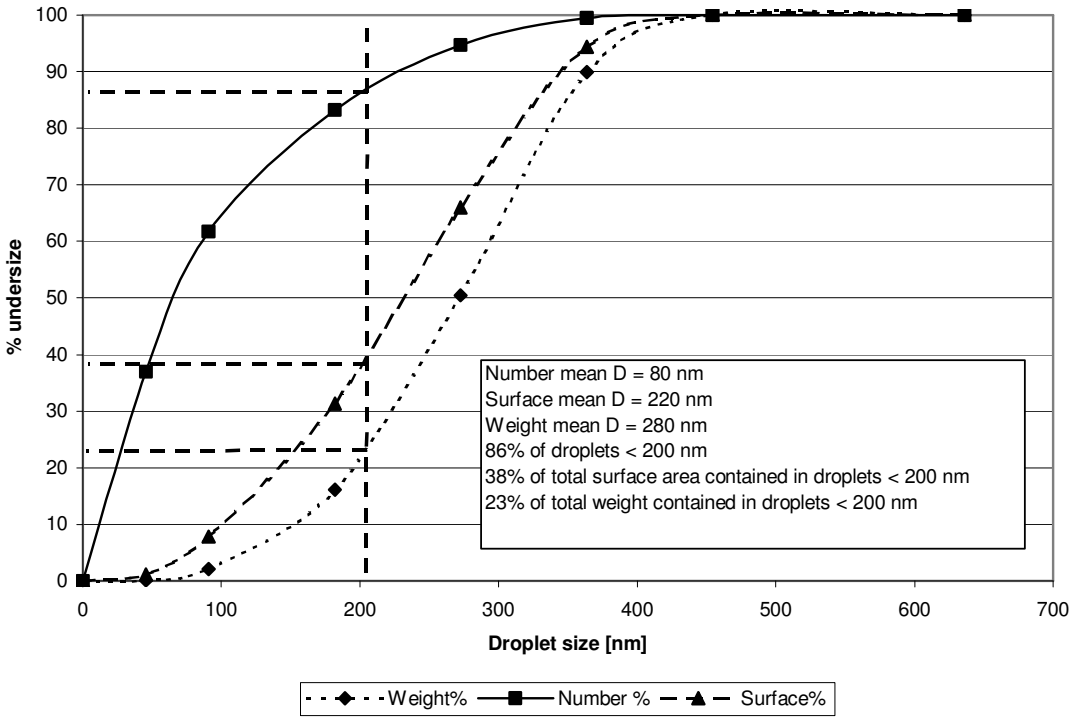

Figure 3-4. Cumulative size distributions for a four-pass high-pressure homogenized PFOB emulsion calculated from different bases – number, surface area and weight (or volume)

The cumulative distribution lines in Figure 3-4 would become steeper with narrower droplet size distributions. The figure illustrates the importance of narrow droplet size distributions for efficient mass transfer of emulsions. Although droplets smaller than 200 nm present 38% of the total surface area, only 23% of the total weight is present in droplets smaller than 200 nm. The oxygen is carried per volume, but the mass transfer takes place per surface area. Thus, a wide distribution would lead to less effective mass transfer, as a lot of the dissolved oxygen is then carried by larger droplets that have smaller surface area to volume ratio's.

Initially, it was intended to get a qualitative picture of the droplet size and size distributions obtained. Cryo-SEM (cryogenic scanning electron microscopy) was attempted, but failed to reveal distinct boundaries between droplets and continuous phase (Figure 3-5).

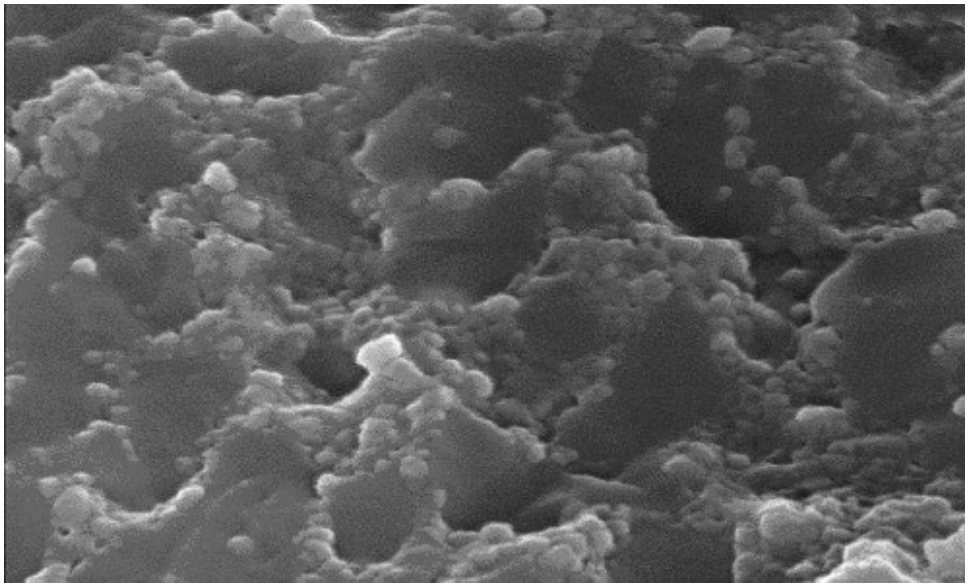

Figure 3-5. Cryo-SEM picture (5000x) of Emulsion A failed to reveal distinct phase boundaries.

Negative staining TEM photographs (stained with uranyl nitrate according to the method given by Hayat, 2000) were taken of the emulsions, and proved to be much more successful than cryo-SEM (Figure 3-6).

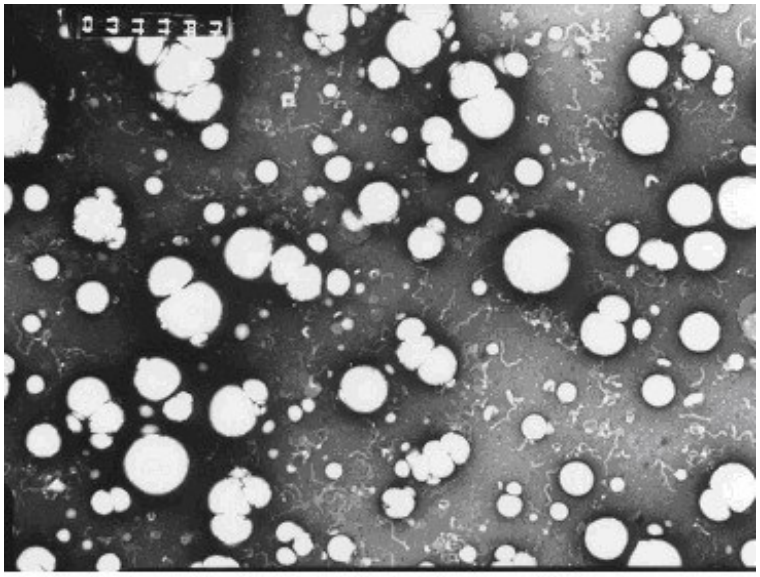

Figure 3-6. Negative-staining TEM photograph (22000x) of Emulsion A clearly showing emulsion droplets. Some flocculated droplets with deformed boundaries are visible in the picture.

The TEM photographs were initially used to generate droplet size distribution data through visual measurement and counting. The project team was aware that this is only a qualitative tool and that it is not very accurate. Another factor compounding the inaccuracy is the fact that one cannot easily distinguish between lecithin vesicles and emulsified droplets. Figure 3-7 is a negative-staining TEM photograph of a background solution containing lecithin but no PFOB. It is clear that the vesicles are in fact very much similar in appearance to the

PFOB emulsion droplets on negative-staining TEM photographs. Typical sizes for lecithin SUV's were reported as 70-80 nm (Wabel, 1998).

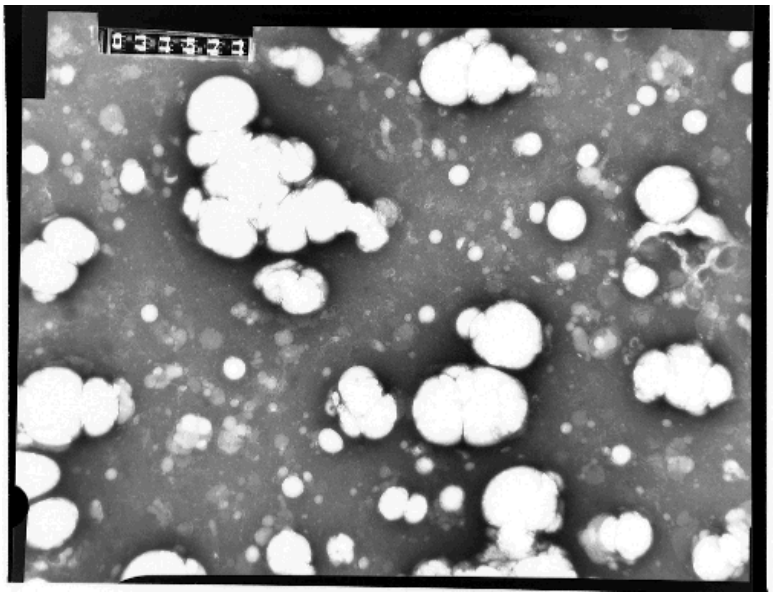

Figure 3-7. This negative-staining TEM photograph (18000x) of a background solution containing lecithin shows that the vesicles formed by the lecithin is similar in appearance to PFOB droplets.

The similar appearance is arguably not such a big problem, as the concentration of micelles and vesicles at higher PFOB volume fractions should be low. Put another way, if stable emulsions at high PFOB volume fractions are obtained, then the droplets must necessarily be coated with surfactant. If the correct amounts of surfactant were added for the droplet size required, then there would not be high levels of free surfactant left in the solution. In fact, high levels of free lecithin can destabilize PFOB emulsions (Krafft, Rolland and Riess, 1991).

Cryo-TEM or freeze-fracture TEM (FF-TEM) can be used to obtain improved discernment between micelles, vesicles and small emulsion droplets (Wabel, 1998). A cryo-TEM picture of Emulsion B is shown in Figure 3-8.

For quantitative droplet size distributions, samples were analyzed with a Malvern Mastersizer 2000 laser light scattering particle size distribution analyzer. Results were converted from number distributions to surface area distributions, as surface area for mass transfer is the most important parameter for these emulsions. Figure 3-9 shows comparative results for Emulsions A and B. It is clear that the high-pressure homogenizer yields smaller droplet sizes and narrower droplet size distributions (polydispersity 0.54 for Emulsion B vs. 1.03 for Emulsion A, where polydispersity $PD = \sigma / d_n$).

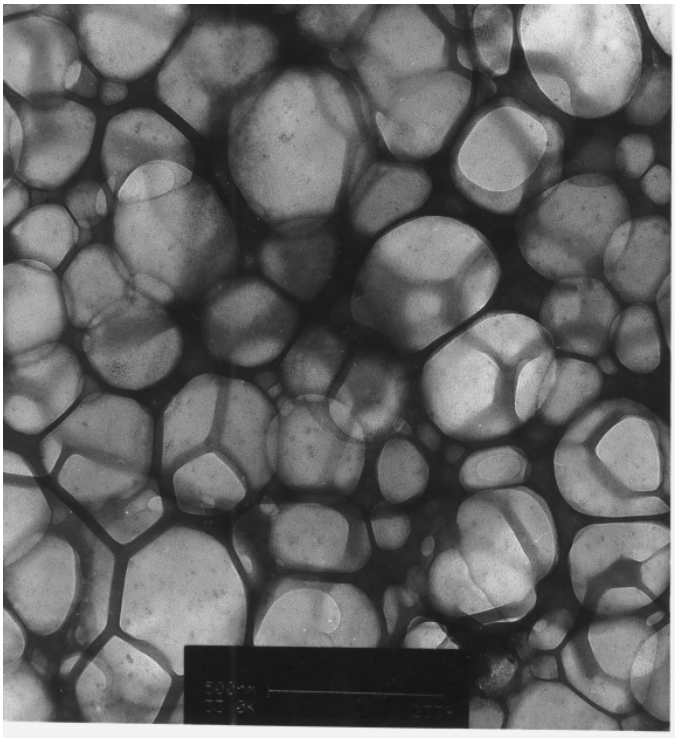

Figure 3-8. Cryo-TEM photo of Emulsion B (33 000x)

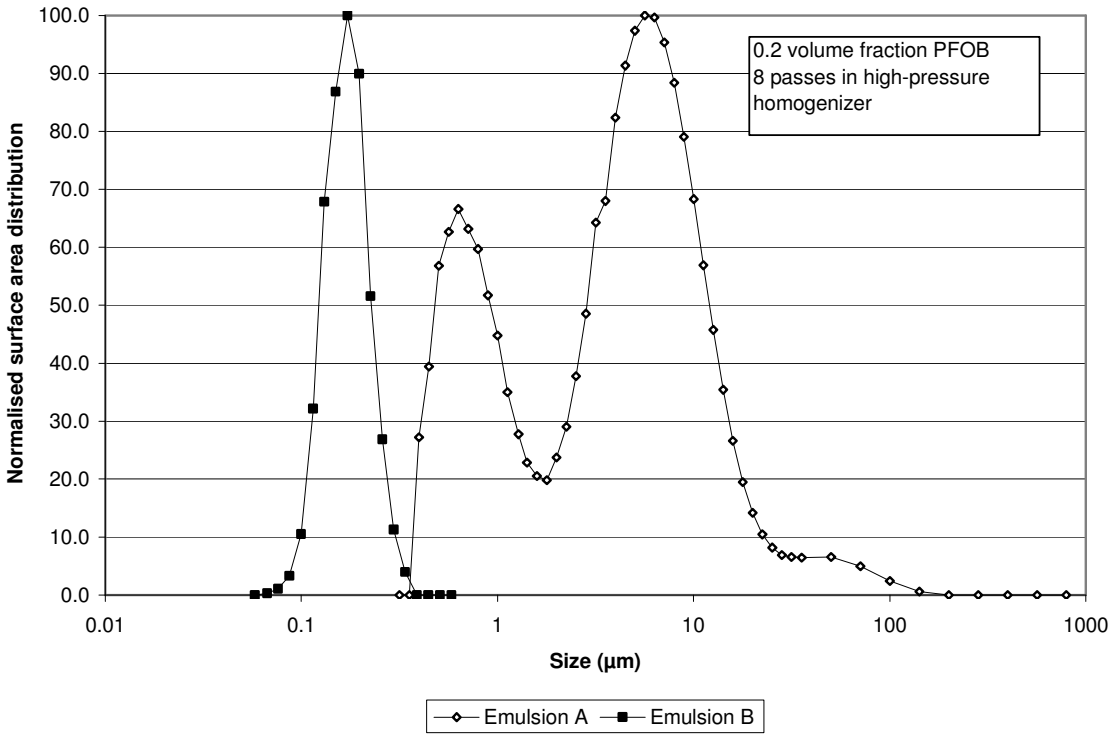

Figure 3-9. Comparative droplet surface area distributions obtained for sonicated (Emulsion A) and high-pressure homogenized (Emulsion B) emulsions.

The bimodal nature of the droplet size distribution obtained for Emulsion A could be due to multilamellar vesicles (the smaller peak), as laser light scattering cannot distinguish between vesicles and emulsion droplets (Wabel, 1998). On the other hand, it could be due to the localized nature of the sonicator's energy input: the larger droplets in the region of 8 – 10 µm could be formed by the homogenization with the rotor-stator type homogenizer, and the smaller droplets could be formed by the sonicator. As not all droplets are sufficiently exposed to the high-energy region surrounding the probe tip, a bimodal distribution is formed.

The influence of number of passes through the high-pressure homogenizer on the droplet size distribution can be seen in Figure 3-10. With increase in number of passes, the average droplet size decreases, and the droplet size distribution becomes narrower (note that the x-axis is on a log scale). As the droplets get smaller, the decrease in droplet size with additional homogenization cycles diminish (Asua, 2002:1283), and a lower practical limit is reached at approximately 100 nm. In addition, further increase in the number of passes through the homogenizer when these droplet sizes have been reached, actually leads to a decrease in emulsion stability. This is postulated to be due to surfactant being removed from the droplet interface through the high energy input and forming free stable vesicles (Krafft, Riess & Weers, 1998:283).

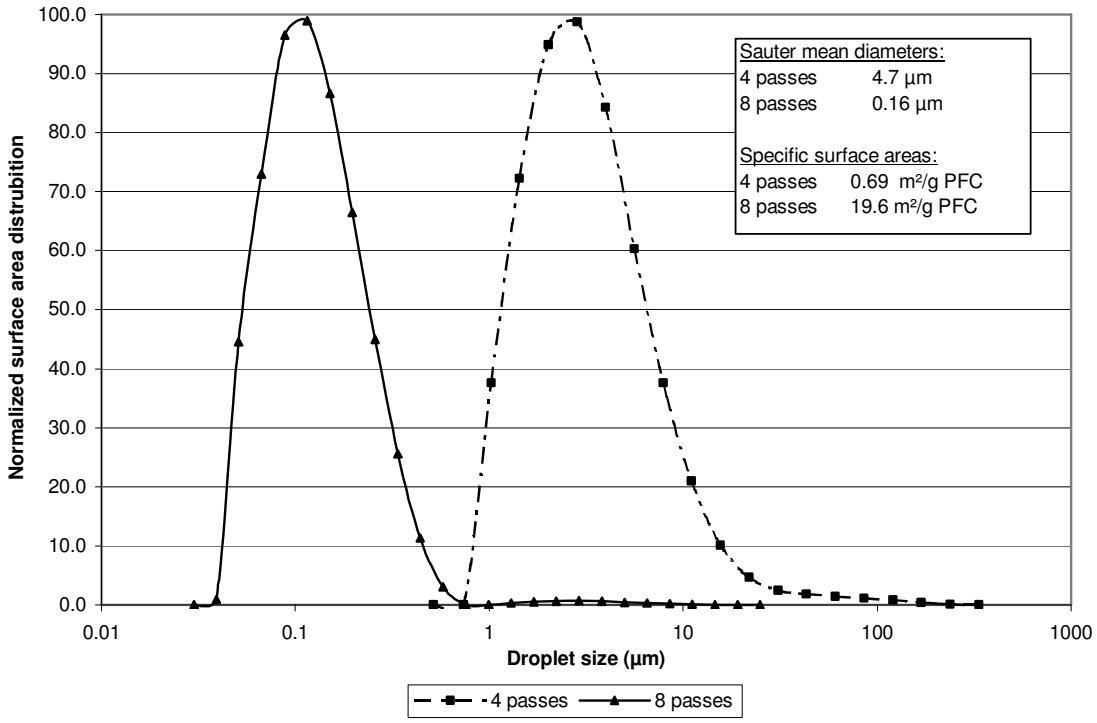

Figure 3-10. Increased number of passes through the high-pressure homogenizer results in smaller droplet sizes and narrower droplet size distributions for a 0.2 volume fraction PFOB emulsion (note that the x-axis is on a log scale).

Other methods that can be used for determination of droplet size distributions of submicron emulsions are field-flow-fractionation (FFF) methods (Janča, 1988:326), and photon correlation spectroscopy (Wabel, 1998).

3.2.5. Emulsion stability

It is important to understand the factors affecting emulsion stability if it is to be used in a clinical setting for mass transfer purposes. The emulsion shelf life is directly affected by its stability.

There are four basic mechanisms by which droplet size can increase or emulsions become unstable over time. These are flocculation, coalescence, sedimentation and molecular diffusion or Ostwald ripening (see Figure 3-11).

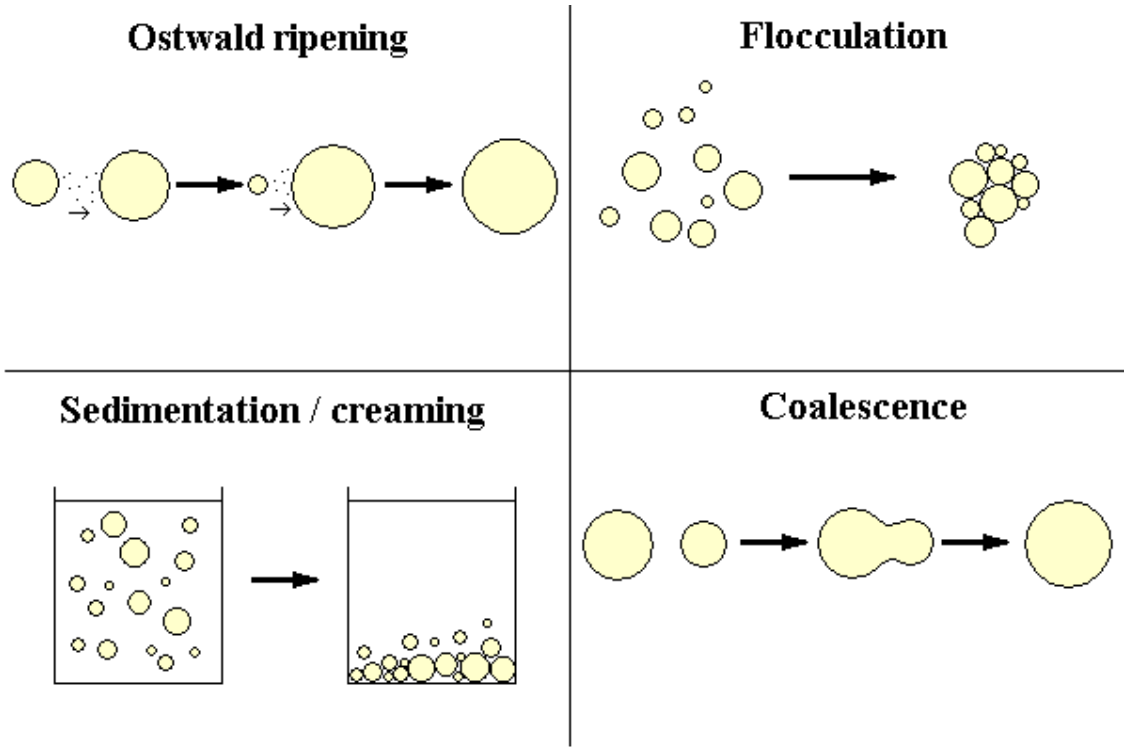

Figure 3-11. Emulsion instability mechanisms

Ostwald ripening (molecular diffusion)

Molecular diffusion occurs when the dispersed phase in an emulsion has a slight solubility in the continuous phase. It is caused by a small difference in dispersed phase chemical potential between droplets with different radii of curvature (this is called the Kelvin effect – Krafft, Riess and Weers, 1998:293). This causes molecules of the dispersed phase to diffuse through the aqueous phase from smaller to larger droplets. Molecular diffusion or Ostwald ripening is only of real impact in submicron emulsions (Riess, 2001:2877).

When diffusion of the oil phase (as opposed to the surfactant) is rate limiting, the Ostwald ripening rate (ω) can be calculated as follows (Kabalnov et al., 1995:2966):

$$\frac{d}{dt}(d_n^3) = \omega = \frac{8\sigma_i D_p c V_{m,p}}{9RT} f(\phi_p) \tag{3-6}$$

where $f(\phi_p)$ is a correction factor for the increase in the ripening rate with increase in dispersed phase volume fraction (ϕ_p), and c is the molecular solubility of PFOB in water, a dimensionless parameter calculated by $c = S_p M_p / \rho_p$. As the dispersed phase volume fraction tends to zero ($\phi_p \to 0$), the correction factor tends to 1 ($f(\phi_p) \to 1$).

An ingenious solution to the problem of Ostwald ripening of submicron emulsions was proposed by Higuchi and Misra (1962). Through the addition of a small amount of a second component to the dispersed phase, molecular diffusion can be dramatically decreased. The second component should be insoluble in the continuous phase. As the first component diffuses from smaller to larger droplets, a small difference in concentration of the first component develops between the smaller and larger droplets (due to the second component not diffusing). This concentration difference changes the chemical potential of the droplets, and molecular diffusion equilibrates (i.e. no net diffusion occurs).

In the case of PFOB emulsions, Ostwald ripening occurs due to the slight solubility of PFOB in water. Through the addition of small amounts (in the region of 0.5 vol %) of a second perfluorocarbon, perfluorodecyl bromide, Ostwald ripening is reduced to an insignificant level (Krafft, Riess and Weers, 1998:310). The addition of perfluorodecyl bromide also enables the production of emulsions with smaller droplet sizes (Riess, 2001:2879).

In addition, it was found that the Ostwald ripening rate is significantly lower for egg yolk phospholipids compared to other hydrocarbon surfactants, which is reportedly due to the much lower interfacial tensions measured for PFOB-water emulsions using egg yolk lecithin as surfactant (Kabalnov et al., 1995:2973). This effect seems plausible when considering Equation (3-6), as the Ostwald ripening rate is directly related to interfacial tension.

Flocculation

Flocculation occurs when the attractive (Van der Waals) forces between droplets exceed the repulsive forces. These repulsive forces can be either steric or electrostatic. Steric (or hydration) repulsion is achieved by providing steric hindrances on the surface (normally through the addition of a polymer which absorbs onto the surface of the droplet). Electrostatic repulsion is related to the zeta potential of the droplets.

Zeta potential is the overall charge a particle or droplet acquires in a particular medium – it is the droplet's potential at the slipping plane (Kaszuba, 2002). If the particles acquire a large enough positive or negative zeta potential (the lower limit for stability is usually taken as 30 mV), they will repulse one another and resist

flocculation. The zeta potential is influenced by a number of factors, such as the characteristics of the particle or droplet itself, the choice of surfactant, the pH of the continuous phase, the total ionic content of the solution, and the specific cations and anions present in solution.

The main component of egg yolk phospholipids, L-α-phosphatidyl choline, has a zwitterionic head group. The combination of phospholipid components in EYP generally leads to the formation of a negative zeta potential around PFOB droplets, which has been measured to be in the region of –24 mV (Riess, 2001:2878). Minor components present in the egg-yolk phospholipid (see Section 3.2.1) may also contribute to stabilization by increasing both electrostatic and steric repulsion (Oleksiak, Habif and Rosano, 1994:71).

Sedimentation or creaming

The basic mechanism for sedimentation is gravity (i.e. separation due to density differences). The terminal settling (or rising) rate (u_t) of a single particle in the Stokes'-law region (Re<0.1) is given by (Perry and Green, 1984:5-63):

$$u_t = \sqrt{\frac{g d_p^2 (\rho_p - \rho_m)}{18 \eta_m}} \tag{3-7}$$

As perfluorocarbon density is generally much higher than water (the density of PFOB at 37 ºC was determined experimentally as 1869 kg/m^3), emulsions of perfluorocarbons are prone to settling. From Equation (3-7), it is clear that, apart from density difference, particle or droplet size also has a major effect on settling rate.

As very small drops behave like rigid spheres (Perry and Green, 1984:5-65), Equation (3-7) can be applied to the PFOB emulsions. At 0.2 µm, the settling rate for a single PFOB drop in water at 25 ºC is calculated from Eq. (3-7) (with d_p = 0.2 µm, ρ_p = 1900 kg/m^3, ρ_m = 999 kg/m^3 and η_m = 8.9×10^{-4} Pa.s) as 1.91 mm/day, with Re = 5×10^{-9}.

From this calculation, it appears that the PFOB emulsions in question would not exhibit excessive sedimentation. In addition, Brownian motion contributes significantly to keeping submicron particles in suspension. In concentrated suspensions or emulsions, settling velocities decrease due to increases in both apparent viscosity and density. The hindered settling velocity (u_{th}) can be calculated from an equation given by Maude and Whitmore (Perry and Green, 1984:5-66):

$$u_{th} = u_t (1 - \phi_p)^n \tag{3-8}$$

For Re < 0.3, the value of the coefficient n is 4.65. Using this equation and the calculated terminal settling velocity from above, hindered settling velocities of 0.68 mm/day and 0.18 mm/day are obtained for 0.2 and 0.4 volume fraction PFOB emulsions, respectively. From this it can be concluded that sedimentation is not a major

problem for PFOB emulsions with droplet sizes of approximately 0.2 µm, especially at higher dispersed phase volume fractions.

Coalescence

Coalescence can occur either due to insufficient addition of surfactant, or through nucleation of a hole in the thin film between two emulsion droplets that are close together. The hole nucleation is generally thermally activated (due to local energy fluctuations), and the hole must reach a critical size above which it becomes unstable and grows further (Bibette et al., 2002:98). As dispersed phase volume fraction increases, hole nucleation frequency increases as well. The critical energy required for creating a hole large enough for coalescence to occur, is known as the *hole nucleation activation energy,* E_a.

Coalescence can also occur after freezing and thawing an emulsion. Rapid freezing (i.e. at very low temperatures) and slow thawing seem to minimize coalescence (Sherman, 1968:133).

Experimental results

Figure 3-12 shows the change in droplet size distribution over 18 days for Emulsion A. The SMD changed from 4 to 34 µm over the same period. While the initial droplet size distribution revealed the same bimodal distribution encountered earlier (see Figure 3-9), the size distribution after 18 days changed considerably. All submicron droplets seem to have disappeared, and a group of very large droplets (between 100 µm and 1 mm) have appeared. This indicates that coalescence of the droplets has taken place. The disappearance of the small droplets would seem to suggest that they are indeed emulsion droplets and not vesicles, as the vesicles would not disappear over time (although there are reports of problems with phospholipid adsorption onto glassware – Kabalnov et al., 1995:2969).

It can be concluded from Figure 3-12 that Emulsion A is not a stable emulsion. This was confirmed by measurement of back scattering of light over the sample height over a period of a month, using a Turbiscan MA 2000 machine. Figure 3-13 gives the change in back scattering over sample height, at different measurement times, for Emulsion A (0.2 volume fraction PFOB). It is clear that sedimentation has occurred even before starting the measurements (indicated by the dramatic change in back scattering levels at a sample height of about 37 mm). This is due to the large droplet sizes obtained in Emulsion A. The settling rate for a 10 µm droplet, calculated with Equation 3-7, is 198 mm/hr, which means that a cream layer would form very quickly in Emulsion A.

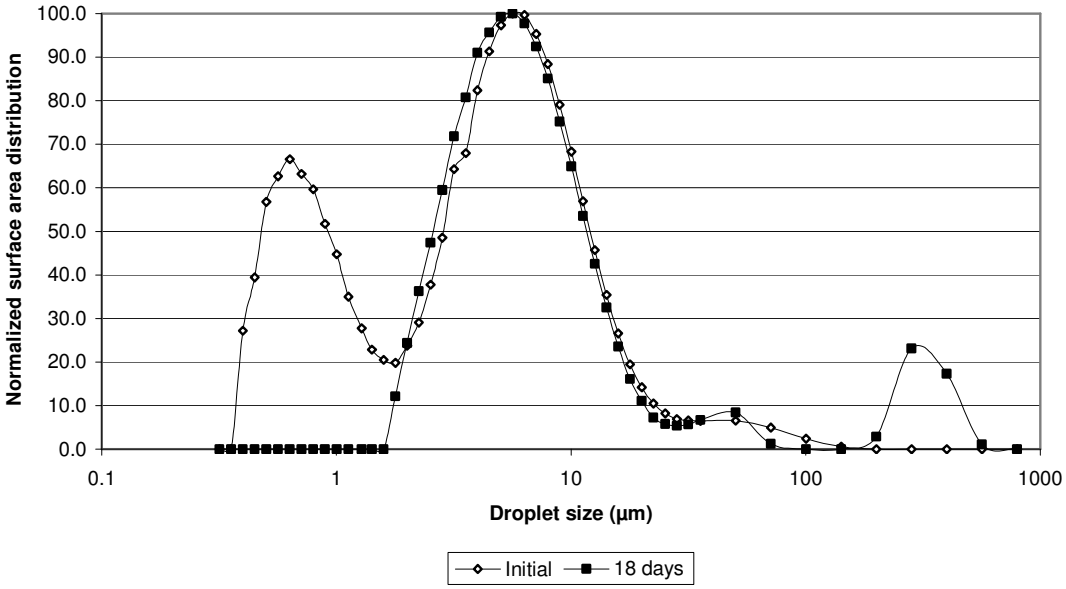

Figure 3-12. A 0.2 volume fraction PFOB preparation of Emulsion A was not very stable over a period of 18 days. Smaller droplets disappeared, while there was significant growth of very large droplets between 100 and 1000 µm.

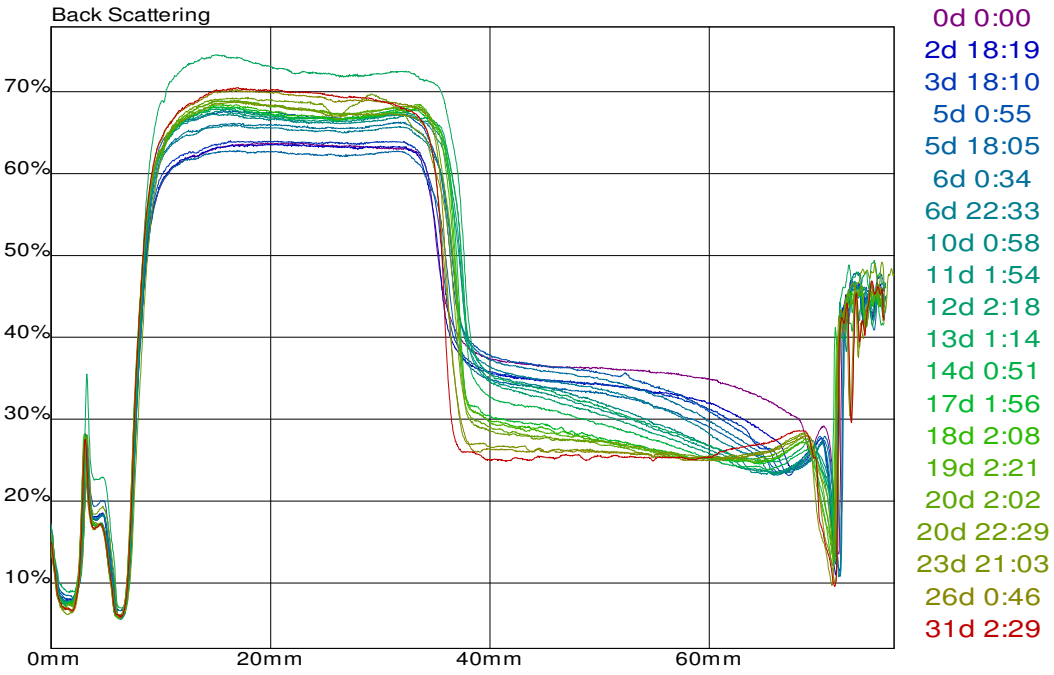

Figure 3-13. Back scattering measurements on Emulsion A (0.2 volume fraction PFOB) show almost immediate formation of a sediment layer, confirming the instability of the emulsion (distance measured from bottom of container).

Apart from sedimentation, coalescence also occurred in Emulsion A, as was evident from the formation of large droplets over time shown in Figure 3-12. This was confirmed by coalescence kinetics data obtained from the Turbiscan MA 2000 measurements. Figure 3-14 shows coalescence kinetics data for two different PFOB

volume fractions of Emulsion A. The 0.4 volume fraction PFOB emulsion was more stable than the 0.2 volume fraction emulsion. This is probably due to decreased settling rates for higher dispersed phase volume fraction emulsions (see Equation 3-8).

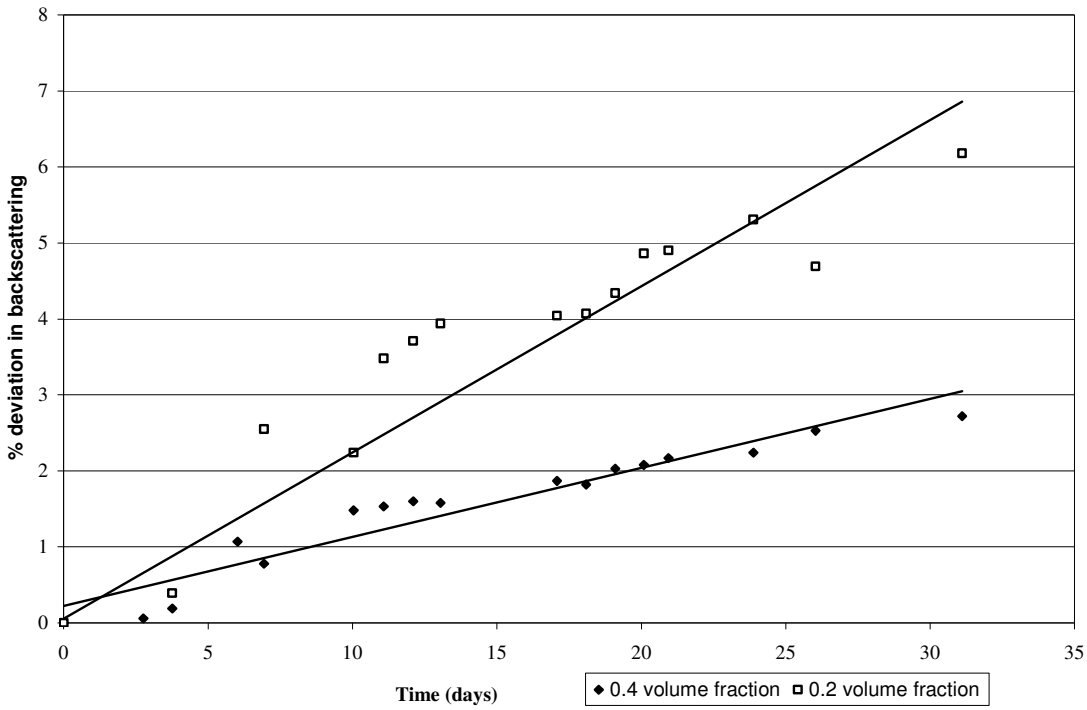

Figure 3-14. Coalescence kinetics data for two different PFOB volume fractions of Emulsion A. The higher PFOB volume fraction emulsion was more stable.

Experimental zeta potential data for Emulsion B with different salt concentrations is given in Table 3-6. One would expect Sample no. 3 to be much more stable than any of the other samples. The value of –25.6 mV compares well with the literature reported value of –24 mV for lecithin-stabilized PFOB emulsions (Riess, 2001:2878). Thus, it would seem that a decrease in salt (NaCl) concentration would improve stability of the UP-CSIR emulsions (previously used salt concentrations were similar to Sample 1). Sample 3's calculated osmolarity is 222 mOsm/ℓ.

Table 3-6. Zeta potential data for Emulsion B

Sample no.	NaCl concentration (g/ℓ)	$NaHCO_3$ concentration (g/ℓ)	Zeta potential (mV)
1	7.6	2.3	-0.8
2	7.6	1.15	-1.6
3	3.8	2.3	-25.6
4	11.4	2.3	-2.9
5	7.6	3.45	-6.6

The instability of Emulsion A can be attributed to a number of factors:

1. The lecithin used in Emulsion A has a PC/PE ratio of 2:1, which is substantially lower than the recommended minimum of four for stable PFOB-lecithin emulsions (Krafft, Riess and Weers, 1998:289).
2. The sonication procedure does not produce small enough droplets or narrow droplet size distributions, causing sedimentation and coalescence of the droplets (as is evident from the above results).
3. The emulsion osmolarity was much too high, leading to a decreased height of the coagulation barrier (Babak, 1994:280) and thus increased rates of coalescence.
4. The zeta potential of Emulsion A was measured as –16 mV, which is too low to prevent flocculation.
5. The absence of a chelating agent means that cations (especially divalent cations such as Ca^{2+}) can collapse the repulsive electrical double layer (zeta potential) between droplets, leading to flocculation. This would be especially important when using an emulsion-plasma mix in the UP-CSIR BALSS, as any dissolved calcium present in the plasma could cause flocculation.

For Emulsion B, much improved stability was observed. Figure 3-15 shows droplet size distributions measured just after preparation of the emulsion and after one month at room temperature. The distributions are almost identical. Emulsion B samples at 0.2 and 0.4 PFOB volume fractions were also kept at 40 ºC for one month. For the 0.2 PFOB emulsion, SMD increased from 0.261 to 0.266 µm. The SMD of the 0.4 PFOB emulsion increased from 0.259 to 0.294 µm during the one-month period at 40 ºC.

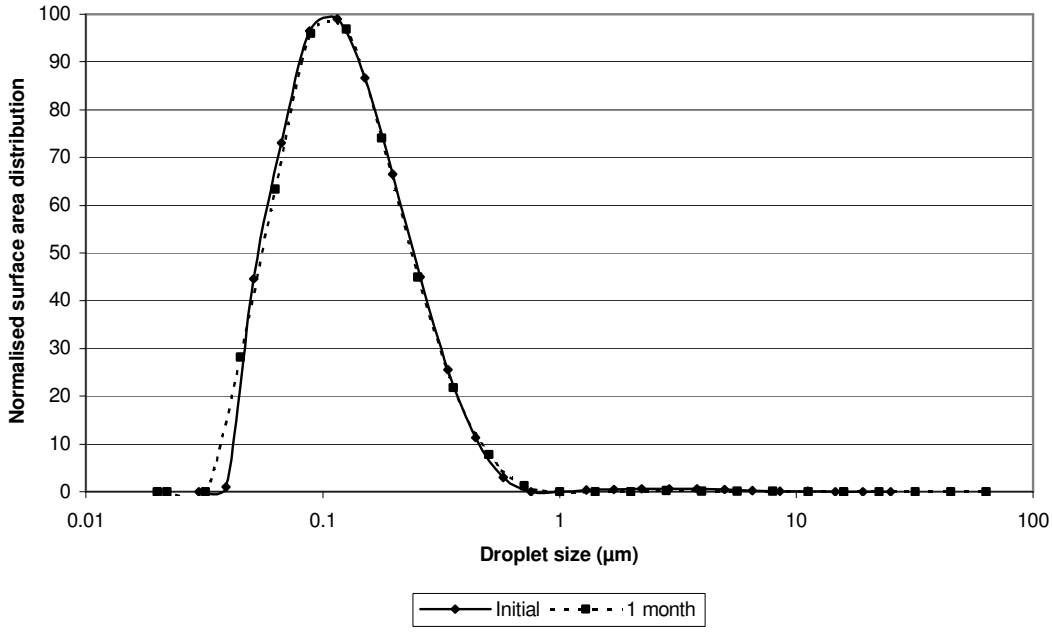

Figure 3-15. The droplet size distribution of Emulsion B (0.4 PFOB volume fraction) remained constant over a period of a month at room temperature.

As PFOB emulsion droplet size growth is very strongly dependent on temperature (a factor of 3 increase in growth rate was observed for a 10 ºC increase in temperature – Kabalnov et al., 1995:2972), this indicates that the stability of Emulsion B would be even better when refrigerated.

Back scattering measurements with the Turbiscan MA 2000 for Emulsion B (0.4 PFOB volume fraction) indicated that no settling occurred for Emulsion B over a period of a month (Figure 3-16). No coalescence could be detected. The negative values at ~ 45 mm indicates some clarification occurring at the top of the emulsion.

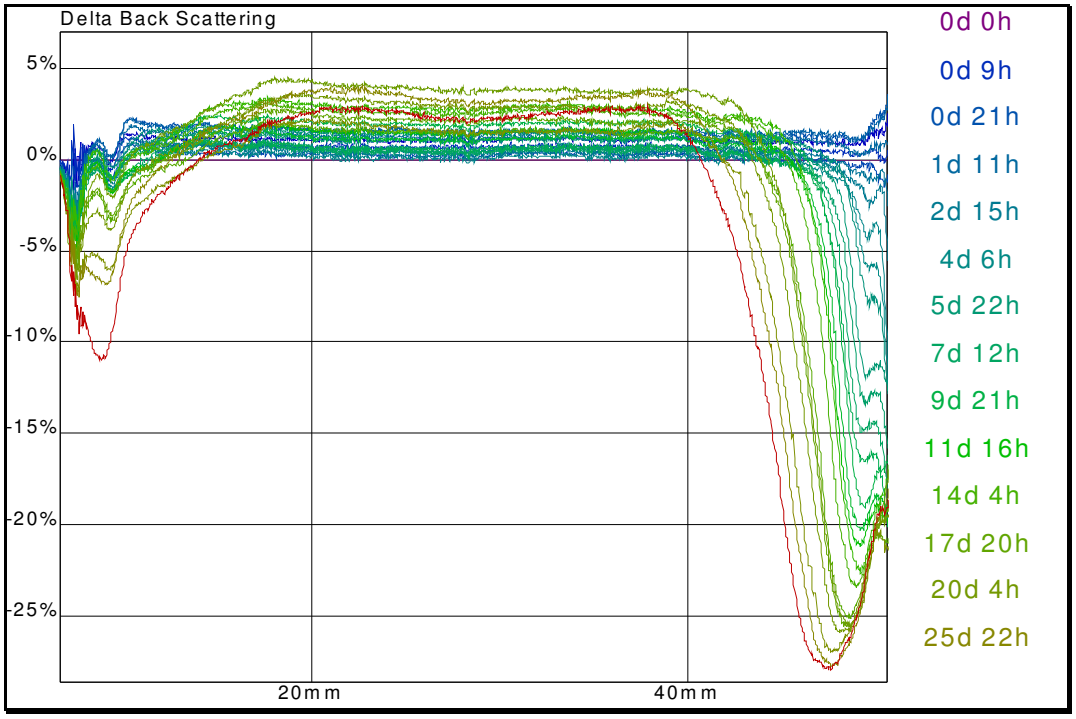

Figure 3-16. Back-scattering data for Emulsion B (0.4 PFOB volume fraction) indicate no settling occurring over a one-month period. Some clarification occurred at the top of the emulsion. Distance was measured from the bottom of the container.

Three different types of lecithin were used in the study: Sigma-Aldrich's 60% PC lecithin, and Lipoid E80 and E80S. Comparative stability data for 0.33 volume fraction PFOB emulsions (Emulsion A) manufactured using these lecithins are given in Table 3-7. The Lipoid lecithins had improved stability compared to the Sigma-Aldrich lecithin, probably due to the higher PC:PE (phosphatidyl choline:phosphatidyl ethanolamine) ratio. Re-emulsification (i.e. a second homogenization treatment) also helped improve stability.

Sediment formed in all the samples, due to the large droplet sizes and low zeta potential of Emulsion A (see discussion earlier in this section).

Table 3-7. Comparative stability data for Emulsion A indicate better emulsion stability for the Lipoid lecithins compared to the Sigma-Aldrich lecithin.

Sample	Sigma-Aldrich	Lipoid E80	Lipoid E80S	Lipoid E80, autoclaved	Lipoid E80S, autoclaved	Lipoid E80S, re-emulsified
Sediment/creaming (vol %)	25	15	25	10	25	5
SMD increase - 2 wks (%)	34.5	5.9	29.3	1.9	6.0	1.3

3.3. Emulsion rheology

An emulsion's macroscopic rheological behaviour depends strongly on (Mason, 1999:231; Pell and Holzmann, 1984:656):

1. Viscosity of the continuous phase
2. Volume fraction of the dispersed phase
3. Droplet size and distribution
4. Interfacial interactions

Experimental rheological data was obtained on a Rheometric Scientific SR5 parallel plate rheometer with plate diameter 25 mm and gap 0.5 mm, with comparative measurements for the Newtonian emulsions made on a Brookfield Digital Viscometer Model DV-I (spindles used were RV1 & RV2). A Brookfield viscometer is not suitable for viscosity measurements of non-Newtonian fluids – end effects cause errors with non-Newtonian fluids in torque viscosity measurement techniques (Whorlow, 1980:139, 158).

When correctly formulated, emulsions with lower dispersed phase concentrations are generally Newtonian. At higher dispersed phase volume fractions, emulsions tend to become pseudoplastic. This was also observed for PFOB emulsions (Krafft, Riess & Weers, 1998:275). The viscoelasticity observed in concentrated emulsions results from the elastic deformation of droplets under shear (Mason, 1999:231), as well as a reduction in the thickness of the associated liquid layer around the emulsion droplets at high shear (Mandersloot and Scott, 1990:63).

The rheological behaviour of Emulsion A was found to be highly non-Newtonian (see Section 3.3.4 for discussion), while that of Emulsion B was Newtonian for the measured dispersed phase volume fractions (up to $\phi_p = 0.5$).

3.3.1. Viscosity of the continuous phase

Viscosity of the continuous phase is one of the main determinants of ultimate emulsion viscosity. The viscosity of the continuous phase is influenced by all components dissolved in it (e.g. surfactants, buffers). The viscosity of the continuous phase of Emulsion A (i.e. the background solution without PFOB) was determined as 10.4 mPa.s, and of Emulsion B was 1 mPa.s (determined with parallel plate rheometer). The high viscosity of

Emulsion A's continuous phase is probably due to the very high concentration of lecithin, as well as the addition of glycerol.

3.3.2. Volume fraction of the dispersed phase

The emulsion viscosity increases with increase in dispersed phase volume fraction (ϕ_p). For emulsions and particle suspensions, there is a maximum limit to ϕ_p, set by the maximum packing attainable for the specific particle or droplet size distribution. For monodisperse spheres, this value is theoretically ϕ_p = 0.74 for tetrahedral packing and ~ 0.64 for random packing, while practical values obtained under shear generally range from 0.60 to 0.66 (Mandersloot and Scott, 1990:57). Polydisperse particle suspensions will have somewhat higher maximum packing, due to smaller particles filling spaces between larger particles. Thus, the narrower the droplet size distribution, the closer the maximum packing value should get to within 0.60 – 0.66.

For emulsions, the maximum packing value can be exceeded, due to the possibility of deformation of emulsion droplets (Mason, 1999:232). As ϕ_p is increased, phase inversion will take place at some critical value. This is of course not allowable for the PFOB emulsions in the UP-CSIR BALSS.

At ϕ_p > ~ 0.55, emulsions prepared by UP-CSIR tended to become viscous cream-like solids. Even before this dispersed phase volume fraction was reached, emulsion viscosity became extremely high, leading to fluid handling problems. Phase inversion for PFOB-in-water was observed to occur at ϕ_p = 0.60 – 0.65 by Yamamoto et al. (1994:450).

As mentioned earlier, various formulations and preparation procedures were used during the course of the project. Rheological measurements were performed on most of these emulsions. Figure 3-17 is a composite graph of all rheological data obtained (including data for sonicated emulsions), as well as two sets of literature data (Ju, Lee and Armiger, 1991a:327; Krafft, Riess and Weers, 1998:275). Although there is appreciable scatter of data, it can be seen that viscosity increases with increased dispersed phase volume fraction.

When literature data and data for Emulsion B is compared, there is a much clearer correlation of viscosity with dispersed phase volume fraction (Figure 3-18). The trend is clearly exponential (r^2 = 0.9825).

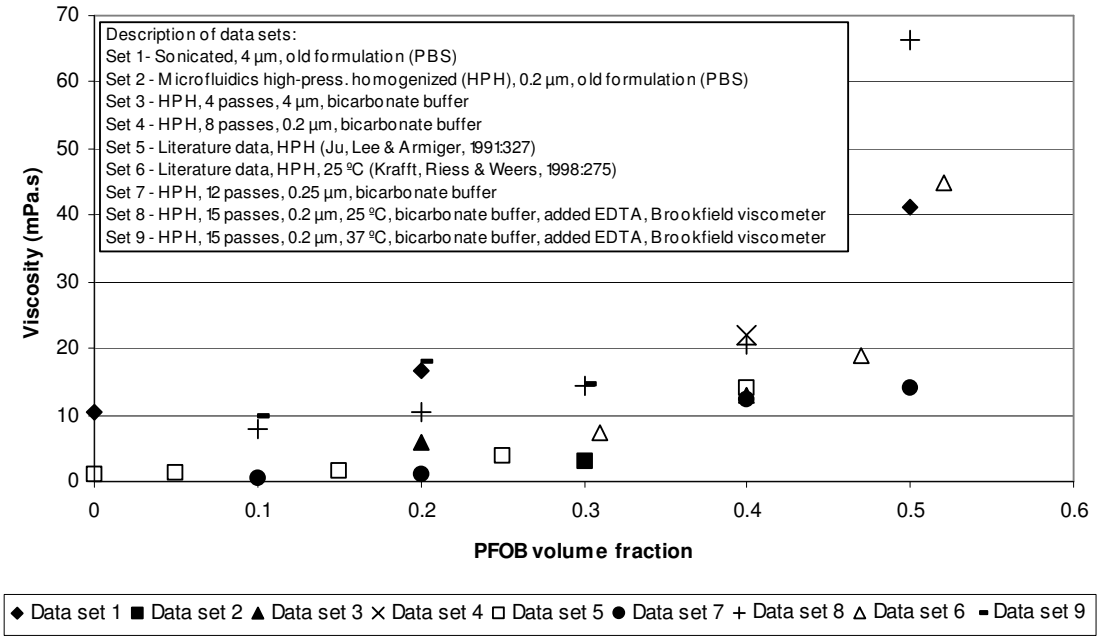

Figure 3-17. This composite graph of experimental rheological data of all emulsions (including sonicated emulsions) as well as two literature data sets shows appreciable scatter, but a general trend of increasing viscosity with increased disperse phase volume fraction can be seen.

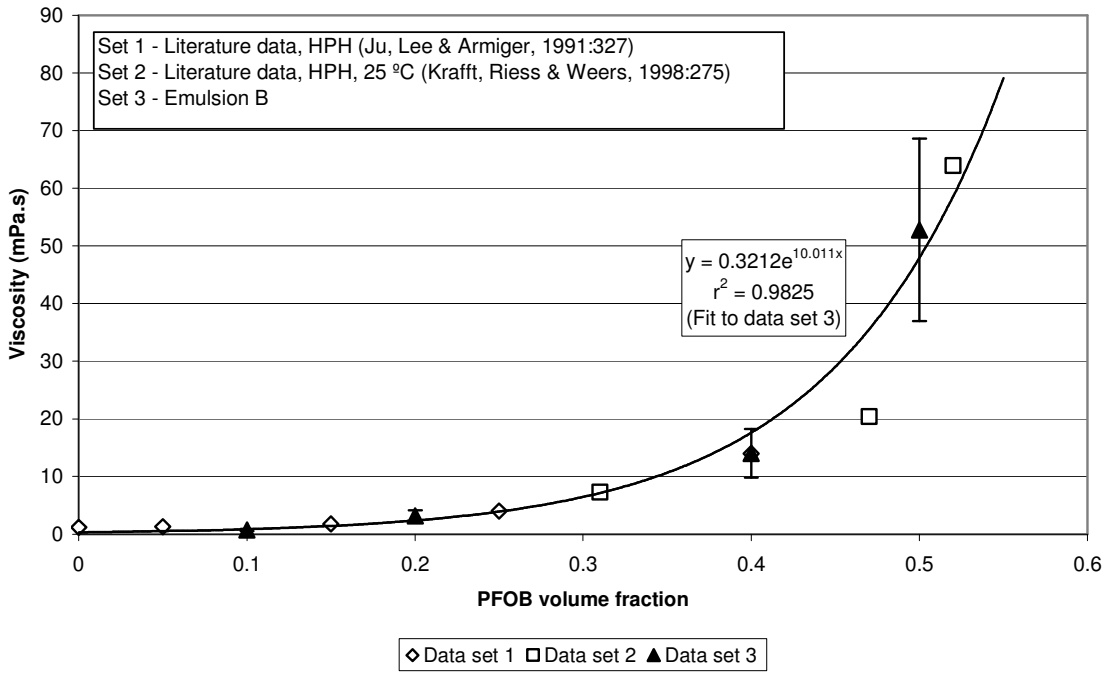

Figure 3-18. Data for Emulsion B and two literature data sets show exponential increase in emulsion viscosity with increase in dispersed phase volume fraction.

For dilute emulsions, the well-known Einstein equation describes the effect of ϕ_p on emulsion viscosity (Mandersloot and Scott, 1990:56):

$$\eta_r = 1 + 2.5\phi_p \tag{3-9}$$

Emulsions may also have an associated liquid surface layer, which increases the effective volume of the dispersed phase (Mandersloot and Scott, 1990:57). At high concentrations and high shear, these associated liquid layers may overlap or become thinner. Equation (3-9) now becomes:

$$\eta_r = 1 + 2.5k_0\phi_p \tag{3-10}$$

where the factor k_0 makes provision for the associated liquid layer. This factor can be determined through fitting of Equation (3-10) to experimental data of dilute emulsions. For the data sets shown in Figure 3-18 (a composite of UP-CSIR data and two literature data sets), the value of k_0 was determined as 1.381.

Mandersloot and Scott (1990) proposed an equation that would be valid for both dilute and concentrated emulsions:

$$\eta_r = \left[1 - \frac{\phi_p}{\phi_{p,\max}}\right]^{-2.5k_0\phi_{p,\max}} \tag{3-11}$$

where $\phi_{p,max}$ is the maximum attainable dispersed phase volume fraction.

Using the determined k_0 value of 1.381, ordinary (non-weighted) non-linear least squares regression was carried out on the 'Mandersloot' equation (Equation 3-11) and the three data sets in Figure 3-18 to obtain $\phi_{p,max}$. The value of $\phi_{p,max}$ was determined as 0.60, with r^2 = 0.977. This value of $\phi_{p,max}$ is in close correspondence with the range of maximum packing values for sheared flow of 0.60 – 0.66 (Mandersloot and Scott, 1990:57).

Figure 3-19 shows a comparison between experimental data and predictions of the Einstein and 'Mandersloot' equations. The Einstein equation correctly predicts emulsion viscosity up to a dispersed phase volume fraction of approximately 0.15, above which it becomes very inaccurate. The Mandersloot correlation predicts viscosity very well over the whole range of experimental data (up to ϕ_p = 0.50).

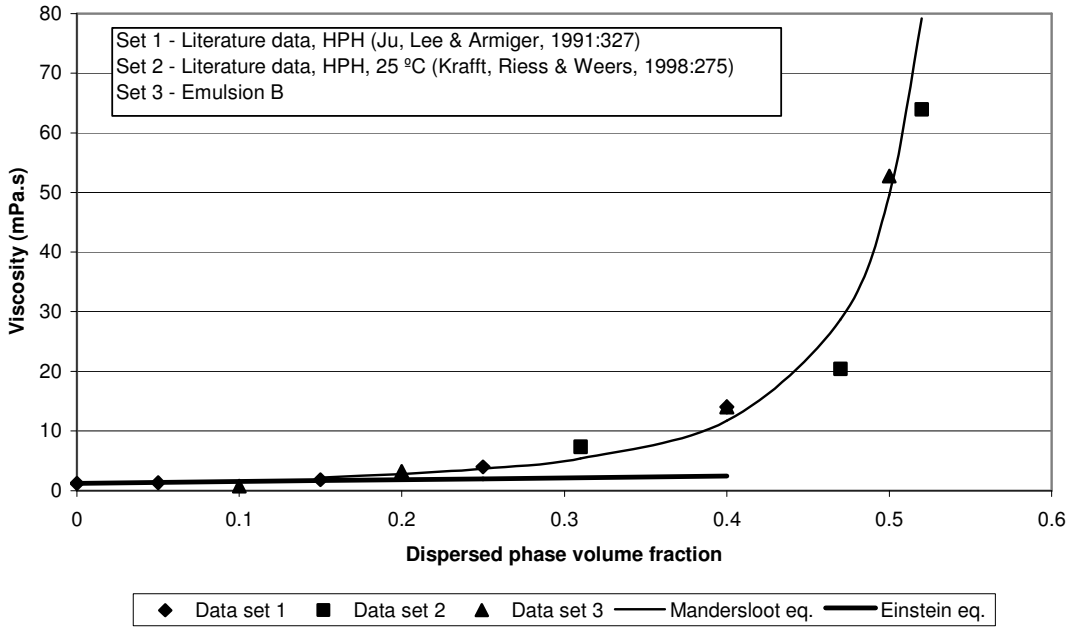

Figure 3-19. Comparison of predictions of Einstein and Mandersloot correlations with experimental data show good correlation for the Einstein equation up to ϕ_p = 0.15 and for the Mandersloot correlation over the whole data range.

3.3.3. Droplet size and distribution

Emulsion viscosity generally increases with decrease in droplet size, due to increased interfacial area and interaction between particles (Pell and Holzmann, 1984:661). Some references report no influence of droplet size and distribution on viscosity, but most report increase in viscosity with decrease in droplet size and decrease in polydispersity (Sherman, 1968:298).

3.3.4. Interfacial interactions

Interfacial interactions between emulsion droplets are determined by the pH, ionic strength, solutes in the continuous phase, and choice of surfactant(s) (see Section 3.2.5). While Emulsion B displayed Newtonian rheological behaviour, Emulsion A displayed non-Newtonian, pseudoplastic behaviour (Figure 3-20), which could be attributed to extensive flocculation occurring in Emulsion A.

Although pseudoplastic behaviour is usually observed only for highly concentrated emulsions, flocculation can cause dilute emulsions to be pseudoplastic, due to the break-up of flocs with shear (Mason, 1999:233; Mandersloot and Scott, 1990:67). The flocculation is thus reversible, and this is illustrated in Figure 3-21, where the viscosity of Emulsion A dropped dramatically with the application of high shear.

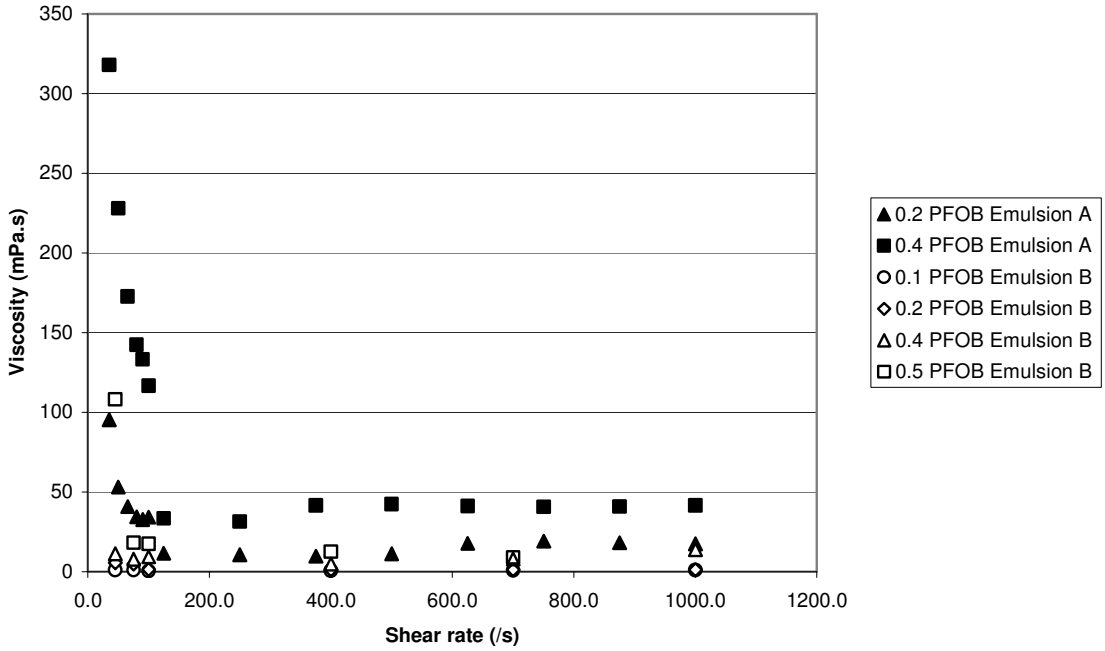

Figure 3-20. Emulsion A (filled data points) displayed non-Newtonian, shear-thinning behaviour. Emulsion B (open data points) displayed Newtonian behaviour, with viscosity remaining constant with change in shear rate. The highest dispersed phase volume fraction, ϕ_p = 0.5, of Emulsion B displayed some pseudoplastic behaviour at low shear, as was also found by Krafft, Riess and Weers (1998:275).

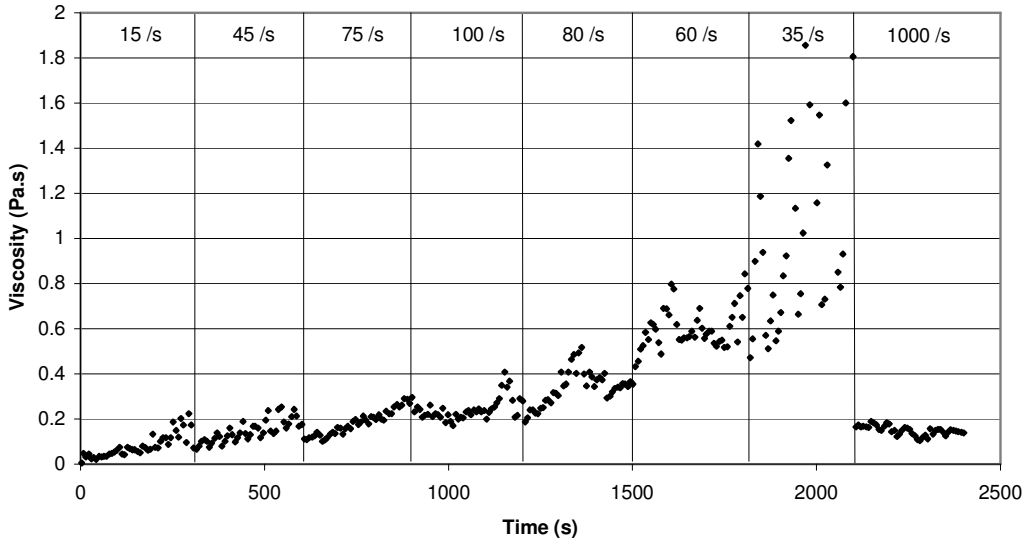

Figure 3-21. At low shear rate, viscosity of Emulsion A increased, even with increase in shear rate, due to flocculation. The flocs can be broken up with high shear, leading to a dramatic drop in viscosity. Rheopectic behaviour of the emulsion was also evident at low shear rate. This was probably due to enhanced flocculation compared to a resting emulsion, caused by the increased droplet contacts per time at low shear.

Figure 3-22 shows a negative-staining TEM photograph of Emulsion A, clearly showing flocculated emulsion droplets. The phase / interfacial boundary between droplets is clearly visible.

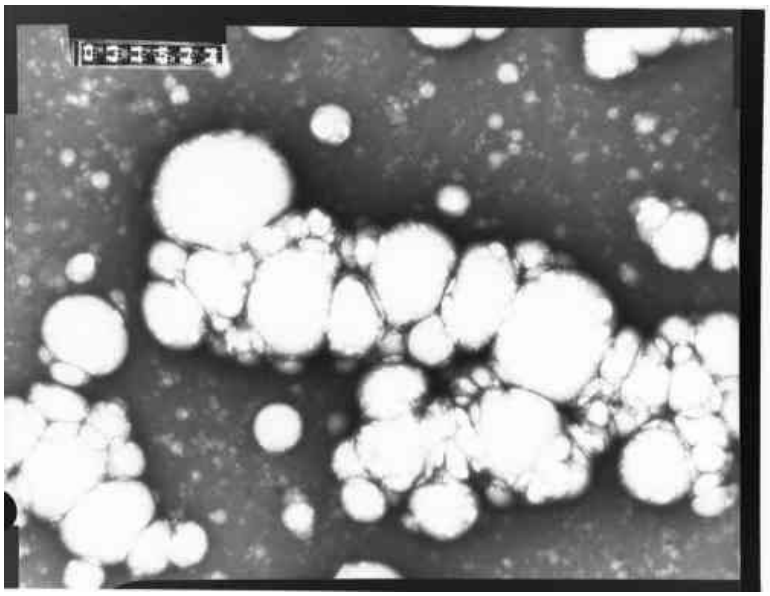

Figure 3-22. Extensive flocculation of Emulsion A occurred with time, as shown in this negative-staining TEM photograph.

Figure 3-23 shows 3D plots of relative viscosity as function of shear rate and dispersed phase volume fraction for two different emulsions. Both emulsions were formulated according to Emulsion A, but were prepared according to two different methods: (a) sonication, and (b) high-pressure homogenization. The emulsion prepared with sonication had a SMD of 4 µm, and the emulsion prepared with high-pressure homogenization had a SMD of 0.2 µm.

The emulsions displayed pseudoplastic behaviour, and viscosity increased exponentially with increase in dispersed phase volume fraction. As the pseudoplastic behaviour was evident for both the 4 µm and 0.2 µm SMD emulsions, it can be concluded that the flocculation (and resultantly pseudoplastic) behaviour was caused mainly by incorrect formulation, as opposed to choice of manufacturing method (sonication vs. high-pressure homogenization).

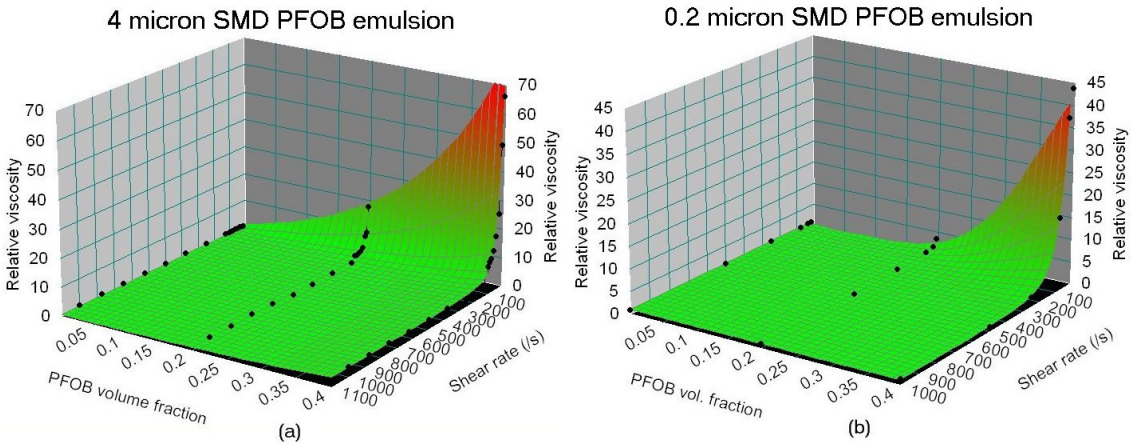

Figure 3-23. Pseudoplastic behaviour is evident for Emulsion A, when prepared with either sonication (a) or high-pressure homogenization (b).

The viscosity of time-independent non-Newtonian fluids can usually be described over a wide range of shear rates with the power law:

$$\eta_e = K_c \dot{\gamma}^{n-1} \tag{3-12}$$

By taking the natural logarithm of both sides of Equation (3-12), the following is obtained:

$$\ln \eta_e = \ln K_c + (n-1) \ln \dot{\gamma} \tag{3-13}$$

Thus, if the power law describes the behaviour adequately over a range of shear rates, a plot of ln η_e vs. ln $\dot{\gamma}$ should give a straight line with intercept $\ln K_c$ and gradient $(n\text{-}1)$. When $n < 1$, the fluid is shear thinning (pseudoplastic), and when $n > 1$, the fluid is shear thickening (dilatant).

The relative / reduced viscosity for a power law fluid is calculated as follows:

$$\eta_r = \frac{\eta_e}{\eta_s} = \frac{K_c}{\eta_s} \dot{\gamma}^{n-1} \tag{3-14}$$

Figure 3-24 shows the determination of coefficients for Equation 3-14 from experimental relative viscosity data on a log-log plot. The intercept gives (K_c/η_s) and the gradient gives $(n\text{-}1)$. The power law equation is only valid for a specific dispersed phase volume fraction and a specific droplet size distribution. The determined values for the power law coefficients are given in Table 3-8.

It can be seen from Figure 3-24 that the lines for the 4 µm SMD emulsions run almost parallel, with a slight decrease in gradient with decrease in PFC volume fraction, which is to be expected (i.e. the dependency of viscosity on shear rate decreases with decrease in dispersed phase volume fraction). The same trend is apparent for the 0.2 µm SMD emulsions, with the 0.2 µm emulsions having lower relative viscosities than the 4 µm emulsions.

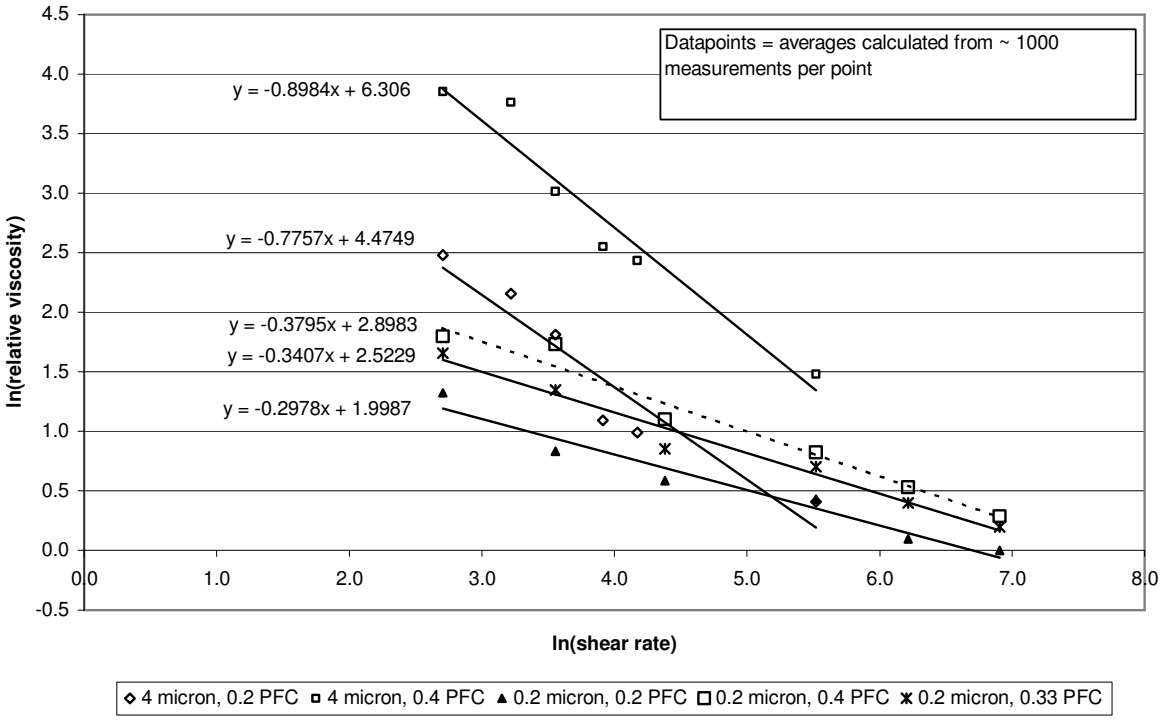

Figure 3-24. Plots of Emulsion A's viscosity-shear relationship on a log-log scale result in straight lines, indicating that the emulsion follows the power law over the given shear range.

Table 3-8. Power law coefficients determined experimentally for Emulsion A (valid for shear rates of 15 – 1000 /s)

Emulsion description	K_c/η_s	**Consistency index** K_c	**Power law exponent** $(n-1)$	**No. of data points**	r^2
Sonicated (d_{sp} = 4 µm) – 0.2 PFC volume fraction	1.05	0.019	-0.78	3169	0.91
Sonicated (d_{sp} = 4 µm) – 0.4 PFC volume fraction	6.57	0.12	-0.90	3186	0.95
High-pressure homogenised (d_{sp} = 0.2 µm) – 0.2 PFC vol. fraction	0.089	$1.6\text{x}10^{-3}$	-0.30	4122	0.96
High-pressure homogenised (d_{sp} = 0.2 µm) – 0.33 PFC vol. fraction	0.15	$2.7\text{x}10^{-3}$	-0.34	4770	0.97

Emulsion description	K_c/η_s	Consistency index K_c	Power law exponent $(n-1)$	No. of data points	r^2
High-pressure homogenised (d_{sp} = 0.2 µm) – 0.4 PFC vol. fraction	0.22	4.0×10^{-3}	-0.38	4122	0.97

3.4. Emulsion concentration

In the UP-CSIR BALSS, it is required that the emulsion is concentrated on-line in the circulation system, without breaking up the emulsion into its constituent components (see Section 2.3). Such a concentration system should preferably be able to operate continuously for seamless integration into the BALSS system. The upper limit for concentration of the dispersed phase is set by the maximum packing density and viscosity considerations. In the UP-CSIR BALSS, this upper limit was arbitrarily set at 0.5 volume fraction PFOB – at higher volume fractions, the emulsions attained a cream-like consistency and viscosities became very high (see Section 3.3), making it impractical from a fluid dynamics perspective.

The requirements for the emulsion concentration system are such that it should:

- Preferably be a physical separation method – it would be preferred not to add any chemicals (e.g. flocculants), as these would either have to be separated out again or would enter the patient's blood stream;
- Not break the emulsion – otherwise in-line re-emulsification would be required;
- Have as small a process volume as possible;
- Be as cost-efficient as possible;
- Be able to separate submicron particles / droplets;
- Be easily sterilizable;
- Let as little PFOB as possible through into the dilute stream – although the PFOB is being used as an oxygen carrier in parenteral applications, all PFOB passing through the separator will be continuously administered to the patient, and large dosages could accumulate over time*.

* PFOB has an organ retention half-time of about 4 days. The PFOB that passes through the separator is not expected to have any harmful effects on the patient - "No toxicity, carcinogenic, mutagenic or teratogenic effects, nor immunological reactions, have ever been reported for fluorocarbons when pure and chosen within the appropriate molecular weight range" (Krafft, Riess and Weers, 1998:258). At an exchange rate of 200 mℓ/min of plasma between BALSS and patient, and a molecular solubility of PFOB in water of 2×10^{-9} mol/ℓ (Riess, 2001:2878), a patient would receive a total dosage of PFOB of 2.9×10^{-4} g per 24-hour treatment period. As a blood substitute, PFOB emulsion is administered to patients at a typical dosage of 1.8 g PFOB/kg body weight (Riess, 2001:2886), and thus the expected PFOB dosages that a patient would receive from connection to the UP-CSIR BALSS should not have any negative effects on the patient.

Based on the above criteria, separation by centrifugation and by ultrafiltration was identified as potential separation methods for separation of particles or droplets in the 0.1 µm size range. Other possible methods for droplets in this size range include solvent extraction, distillation / freeze concentration and gel chromatography (Cheryan, 1986:3), but these do not comply with all of the above criteria.

3.4.1. Centrifugal separation

Centrifugal separation uses centrifugal force to accelerate particles or droplets in the centrifugal field, to amplify a difference in mass in order to cause segregation of the particles or droplets. In a spinning container, the denser material will migrate towards the outer wall of the container.

The centrifugal force (F_c) is given by (Hinton and Dobrota, 1976:48):

$$F_c = m\omega_c^2 r_c \tag{3-15}$$

where m is the mass of the particle or droplet (kg), ω_c is the angular velocity (rad/s) and r_c is the distance of the particle or droplet measured from the axis of rotation of the centrifuge (m). The angular velocity can be calculated from the revolutions per minute (RPM) through $\omega_c = 2\pi \times RPM/60$.

The centrifugal acceleration exerted in a centrifuge is usually described in terms of a multiple of g (the gravitational acceleration) and is then referred to as relative centrifugal force (RCF):

$$RCF = \frac{\omega_c^2 r_c}{g} \tag{3-16}$$

The relative centrifugal force varies according to rotational speed of the centrifuge, as well as position in the centrifuge. A particle or droplet migrating towards the perimeter or outer wall will experience increasing centrifugal force with increasing distance from the axis of rotation.

The settling time for a droplet under a specific centrifugal force can be calculated as follows (Schramm, 1992:41):

$$u_c = \frac{d_p^2(\rho_p - \rho_m)\omega_c^2 r_c}{18\eta_m} \tag{3-17}$$

The location of the inlet and outlets in the centrifuge, as well as the density difference of the materials to be separated, among other factors, determine the purity of the product streams. Usually the outlet of the 'lighter' phase is located near the axis, while the collection point for the denser phase is near the perimeter of the centrifuge. Somewhere in between these radial distances would be the radius of the neutral zone (the interface between the concentrated and dilute phases for the emulsion). Generally, the centrifuge inlet radius is chosen to be close to the neutral zone radius (Young, 2000).

When subjected to high centrifugal forces over a period of time, emulsions tend to quickly form a cream layer, after which centrifugation for a considerable period of time is required for separation (or break-up) of the emulsion into separate phases.

With the UP-CSIR PFOB emulsion, the qualitative separation characteristics determined on a Beckman L7-55 Ultracentrifuge set at 60 000 g's are shown in Figure 3-25. A sediment layer quickly formed at the bottom of the tube, followed by protracted build-up of separated PFOB at the bottom of the tube. A layer of lecithin formed at the water-PFOB interface.

Figure 3-26 shows a photograph of a tube after centrifugation for 96 hours. Four layers are visible (from bottom to top): separated PFOB, remaining sediment (emulsion), concentrated lecithin and aqueous phase. It was possible to separate the PFOB layer from the rest of the material through decanting, but the sediment layer had a solid, cream-like consistency and was difficult to remove from the centrifuge tubes. Even after this centrifugation period of 96 hours, 100% recovery of PFOB was still not achieved - further centrifugation of the other three phases (without the PFOB) yielded still more PFOB.

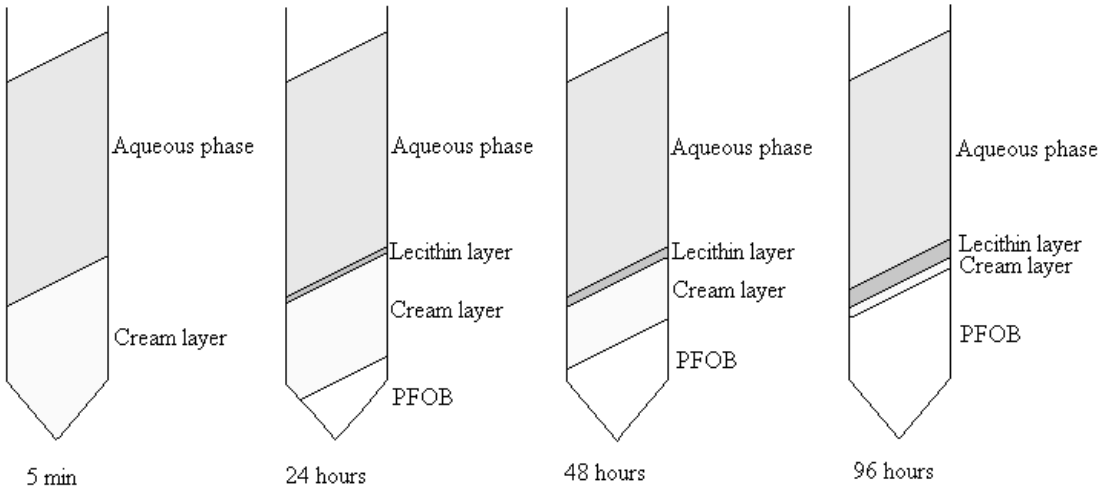

Figure 3-25. A cream layer forms quickly in PFOB emulsions during centrifugation at 60 000 g's. Subsequent phase separation is not complete after 96 hours.

Figure 3-26. Photograph of centrifuge tube containing separated PFOB, after 96 hours of centrifugation at 60 000 g's. A layer of sediment has formed at the water-PFOB interface during centrifugation, consisting of emulsion (bottom) and lecithin (top).

Only a limited number of experimental runs were carried out to determine separation efficiency. Separation efficiency should improve with increased residence time and RCF (or increase in $RCF \times t$). Figure 3-27 shows the results obtained. Although there is considerable scatter in the data, it does appear that improved separation efficiency results from increased $RCF \times t$. Separation efficiencies of between 80 and 100% were achieved (determined by orthophosphoric acid distillation – see Section 3.5), and 100% separation was achieved for $RCF \times t > 2.5 \times 10^6$ s.

As process volume is a critical consideration for the BALSS, the process volume of the centrifuge should be kept to a minimum. By decreasing process volume of the centrifuge, one would simultaneously decrease the radius and thus the centrifugal force at a specific rotational speed. To maintain the same centrifugal force for a smaller process volume, one would have to increase rotational speed.

The required process volume is determined by the circulation flow rate in the BALSS and the residence time required in the centrifuge for droplets to be separated. An estimate of the required residence time can be obtained through using Equation 3-17. The required residence time for a 0.2 µm PFOB droplet to travel 10 mm (at 15 000 rpm and a distance of 50 mm from axis of rotation) can be calculated as 40 s. At a circulation rate of 600 ml/min for the prototype BALSS, the required process volume would be 400 ml, and the required RCF would be 62 500 (calculated from the requirement that $RCF \times t > 2.5 \times 10^6$). A process volume of 400 ml would be too large for the BALSS.

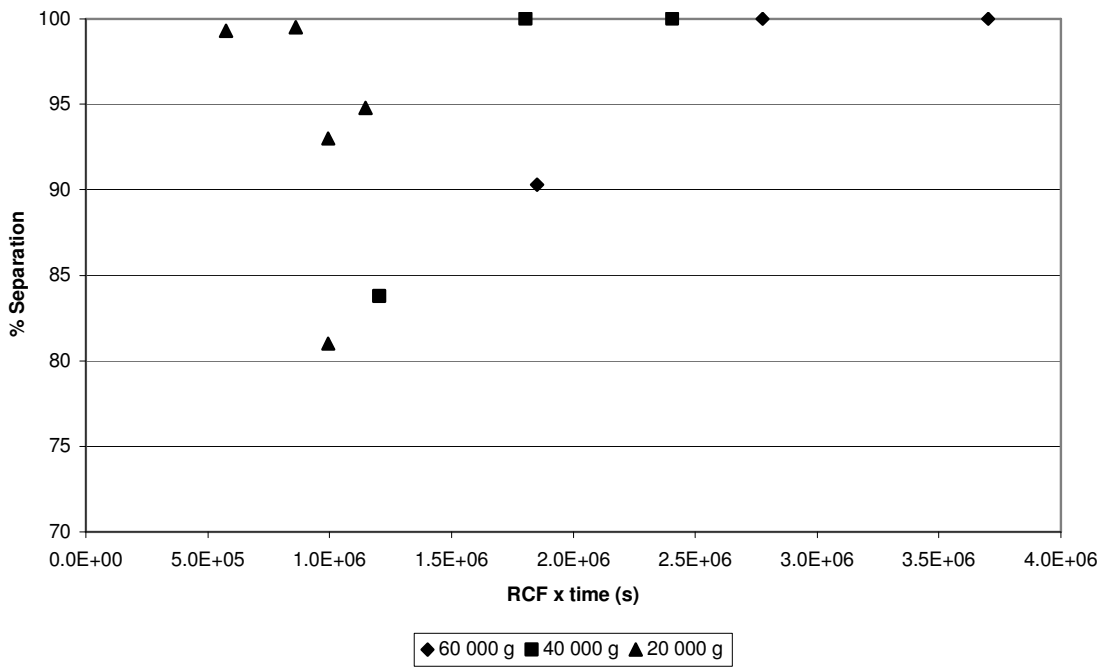

Figure 3-27. Considerable scatter was obtained for centrifugal separation efficiencies for PFOB emulsions. It does appear that improved separation is achieved for higher RCF and longer residence times. With $RCF \times t > 2.5 \times 10^6$ s, quantitative (100%) separation is achieved.

If one assumes a flat disk with height 20 mm for the centrifuge (conservative assumption), the centrifuge radius for the above process volume would be 80 mm. At half this radius (e.g. at the inlet), the required rotational speed for a RCF of 62 500 would be 37 400 rpm (calculated from Equation 3-16). In obtaining this result, a very short settling distance of 10 mm was assumed, as well as a flat disk design (having a large radius / volume ratio).

Centrifugal separation would thus not be suitable for the BALSS, due to the following reasons:

1. The required process volume is too high.
2. Centrifugation of emulsions with phospholipid surfactants can lead to the formation of artifacts (Emulsions with phospholipid surfactants - Wabel, 1998; General discussion - Hinton and Dobrota, 1976:243).
3. Process control would be difficult – stream flow rates must be controlled to maintain the neutral zone radius between the light and dense phase outlet radii.
4. The equipment involves moving mechanical parts and seals, and apart from maintenance and reliability problems, the moving parts could cause contamination of process streams through erosion.
5. The centrifuge cannot be cleaned or sterilized easily between runs and would not be a consumable (i.e. the same machine has to be used for multiple patients).

3.4.2. Ultrafiltration

Background to ultrafiltration

"Membrane filtration is the separation of the components of a pressurized fluid, effected by polymeric or inorganic membranes (generally man-made)." (Paulson, 1995).

There are four different categories of membrane filtration, classified according to the size of the material they filter out (from smallest to largest pore size): reverse osmosis (< 8 Å), nanofiltration (~ 10 Å), ultrafiltration (20 – 500 Å) and microfiltration (0.1 to ~ 10 µm) (Paulson, 1995).

These membranes are all used in cross-flow filtration (as opposed to 'dead-end' filtration), i.e. the feed flow is split into two streams: a concentrate and a permeate stream. Transmembrane pressure is usually controlled with a pressure control valve on the outlet of the concentrate stream.

The use of ultrafiltration (UF) for retention of oil-in-water emulsions has been explored in a number of studies (Faibish and Cohen, 2001a; Koltuniewicz and Field, 1996; Lipp et al., 1988), and retentions of higher than 99% were achieved for droplets as small as 40 nm (Lipp et al., 1998:161).

Classification of ultrafiltration membranes

As membrane pore sizes decrease below 100 nm in the ultrafiltration range, it does not make sense to classify them according to pore diameter anymore. Membrane pore sizes are not uniform – there is a pore size distribution. This means that a specific molecule could be retained by one pore but could pass through another pore. Other factors that complicate the specification of membrane pore sizes, are the orientation of non-spherical particles or molecules, as well as cake build-up. When a solute cake layer builds up on the membrane surface, even molecules much smaller than the pore sizes of the membrane could be retained.

A parameter generally used to classify ultrafiltration membranes is the molecular weight cut-off (MWCO) of the membrane. This value is assigned based on the ability of a membrane to retain more than 90% of a globular solute of defined molecular weight (Pall Gelman Laboratory, 2000:87). The MWCO is not an absolute figure, and the percentage retention for any specific membrane increases from zero to 100% over a range of molecular weights. The narrower this range, the sharper the MWCO of the membrane.

The MWCO of the ultrafiltration membrane for the UP-CSIR BALSS was selected based on the requirement that as little as possible of the plasma constituents should be retained, while as much as possible of the PFOB emulsion is retained. It is recommended that a membrane be chosen with a MWCO three to six times smaller than the molecule that has to be retained. Table 3-9 gives typical solute retentions for ultrafiltration membranes (Pall Gelman Laboratory, 2000:87).

Table 3-9. Typical solute retentions for ultrafiltration membranes (Pall Gelman Laboratory, 2000:87)

MWCO	1K	3K	5K	8K	10K	30K	50K	70K	100K	300K	500K	1000K	0.16 µm	0.3 µm	0.8 µm
Sucrose (0.34K)	a	a	a												
Raffinose (0.5K)	a	a	a												
Vit. B12 (1.3K)	c	b	b	a											
Bacitracin (1.4K)	d	c	c	c	b	b	a								
Insulin (5.72K)	e	e	e	e	e	c									
Cytochrome C (12.5K)	e	e	d	c	c	b									
Ribonuclease A (13.5K)		d	d	c	c	b									
α-Lactalbumin (14.2K)		e	e	c	c	b	a								
Lysozyme (14.4K)		d	d	c	c	c	c								
Myoglobin (17.8K)		e	e	e	e	c	c	b	a						
α-Chymotrypsin-ogen A (24.5K)				e	d	d	b	a	a						
β-Lactoglobulin B (36K)			e	e	e	c	c	b							
Ovalbumin (44K)					e	e	c	c	a						
Albumin (67K)					**e**	**e**	**d**	**c**	**a**						
Alcohol Dehydro-genase (150K)							c	c	b	b					
IgG (160K)							e	e	e	b					
β-Amylase (200K)								e	c	b					
Apoferritin (443K)							e	e	d	c					
Urease (90 – 650 K)							e	d	c	b	b	a			
Thyroglobulin (669K)									e	e	c	a	a	a	
IgM (960K)									e	e	d	c	a	a	
Bovine Serum							e	d	c	c	b	a	a	a	
Latex Beads (0.085 µm)									e	e	c	c	b	a	
Latex Beads (0.137 µm)									e	e	e	e	c	a	
Latex Beads (0.212 µm)											e	e	d	b	
Latex Beads (0.318 µm)													d	c	a
Latex Beads (0.497 µm)													e	e	a
Latex Beads (0.672 µm)															c
Latex Beads (1.08 µm)															e
Yeast															e

a = 1-4% retention b = 5-10% c = 20-80% d = 85-95% e = 96-99%

Hemoglobin has a molecular weight of about 64.5 kDa (Riess, 2001:2808), while the various hemoglobin-based oxygen carriers under development range in size from approximately 7 nm to approximately 225 nm (Riess,

2001:2833). Thus, depending on the size of the specific oxygen carrier, hemoglobin-based oxygen carriers could potentially also be used in the UP-CSIR BALSS in place of the PFOB emulsions.

A MWCO of 300 kDa was selected for the UP-CSIR BALSS. This is large enough to allow albumin (the most plentiful plasma protein and a major transport protein – Lee, 2000) permeation, while small enough to ensure PFOB emulsion retention.

Filtration theory & fouling

It is important for the use of the ultrafiltration membrane in the BALSS that the pressure - flow rate relationship is well understood. All membranes foul over time, causing increased pressure drop and/or decreased permeate flux through the membrane.

Permeate flux (J, m/s) through an ultrafiltration membrane can be described by the following equation (Faibish and Cohen, 2001b:34):

$$J = \frac{\Delta P_b}{\eta_e R_T} = \frac{\Delta P_b}{\eta_e (R_b + R_i + R_c)} \tag{3-18}$$

where R_T is the total membrane resistance, R_b the intrinsic (clean) membrane resistance, R_i the membrane fouling resistance (due to pore plugging and adsorption), and R_c the solute cake layer resistance (m^{-1}).

A useful tool for investigation of membrane fouling is the hydraulic permeability (k_h, m^2), which is calculated by measuring clean water permeate flux as function of transmembrane pressure (Faibish and Cohen, 2001b:32):

$$k_h = \frac{J \eta h_b}{\Delta P_b} \tag{3-19}$$

where h_b is the membrane wall thickness (m).

The hydraulic permeability is measured for a new, clean membrane, and subsequently between runs with experimental fluids, to determine the decline in the membrane hydraulic permeability with use.

Experimental results

The membrane used in the laboratory experiments was a Millipore Pellicon XL Biomax filter with 300-kDa MWCO polyethersulfone membrane (50 cm^2 filtration area). For the animal trials, a PALL Omegasette 0.46 m^2 (open channel) membrane unit was used.

Hydraulic permeability of the clean Pellicon XL Biomax membrane was determined as 5×10^{-17} m^2 (standard deviation 7.9%), compared to values of 3 - 5×10^{-16} m^2 obtained by Faibish and Cohen (2001b:30) for carbon-supported zirconia membranes with 15 kDa MWCO. After completion of all the filtration experiments, the hydraulic permeability of the Pellicon XL Biomax membrane fell to 2×10^{-18} m^2 (standard deviation 3.9%), or 4%

of the original value (this was obtained after aggressive cleaning with caustic soda). This indicated severe fouling of the membrane, but a large number of experiments were performed over several months before this level of fouling was reached.

The efficiency of the membrane in retention of PFOB was determined by distillation of all fractions and measuring recovery (PFOB in the concentrate vs. PFOB in the filtrate). No PFOB was found in the filtrate in any of the experiments.

As most of the experiments were performed at ambient temperature, the effect of temperature on permeate flow rate at constant pressure was investigated (Figure 3-28). It was found that 0.2 PFOB emulsion permeate flow rate increases slightly with increase in temperature (probably due to the associated viscosity decrease).

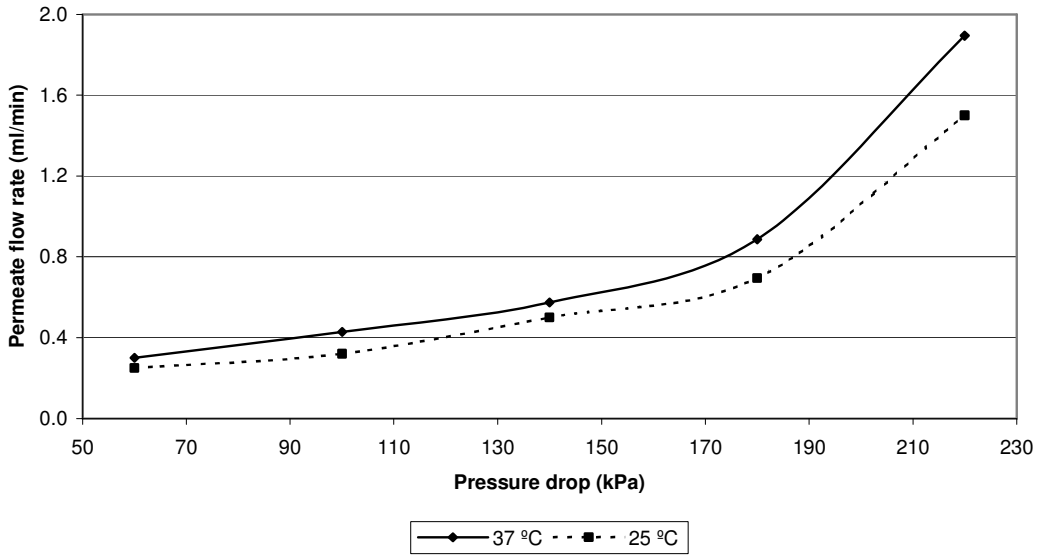

Figure 3-28. Increase in temperature causes a slight increase in 0.2 PFOB emulsion permeate flow rate in the UF membrane.

The percentage of the feed flow going to the permeate is of interest for the UP-CSIR BALSS, as this would contribute to determining the required circulation rate through the UF membrane, in order to separate enough plasma to match the plasma being withdrawn from the patient (other factors, such as membrane filtration area would of course also play a major role). Figure 3-29 shows that, as one would expect, increase in transmembrane pressure leads to an increase in the percentage of the feed flow going to the permeate.

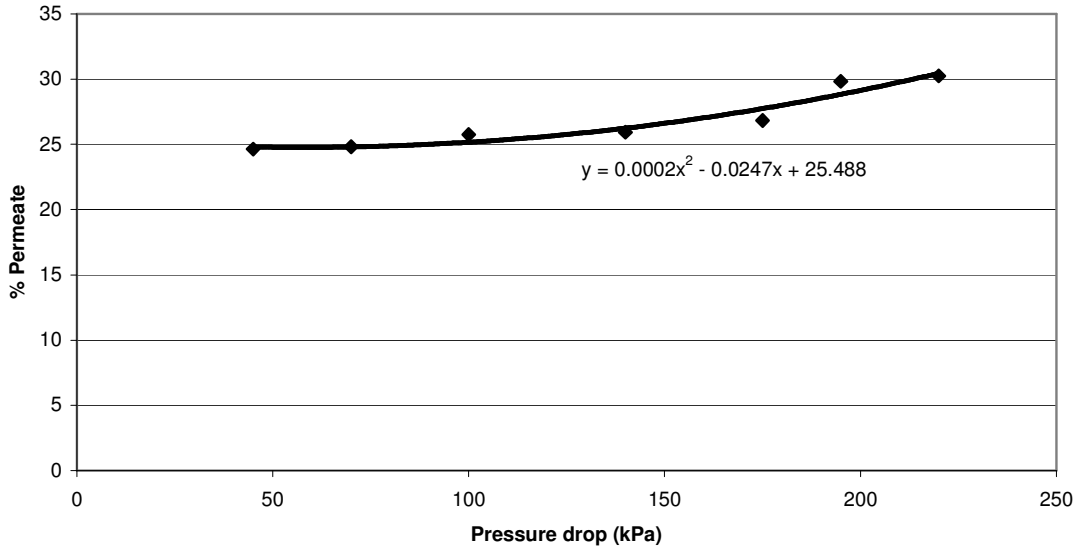

Figure 3-29. Increase in pressure drop leads to a slight increase in the percentage of the feed to the membrane going to the permeate.

Permeate flow rate decreases dramatically with increase in PFOB volume fraction, for both Emulsions A and B (Figures 3-30, 3-31 and 3-32). Increase in pressure drop improves permeate flow rate, as expected.

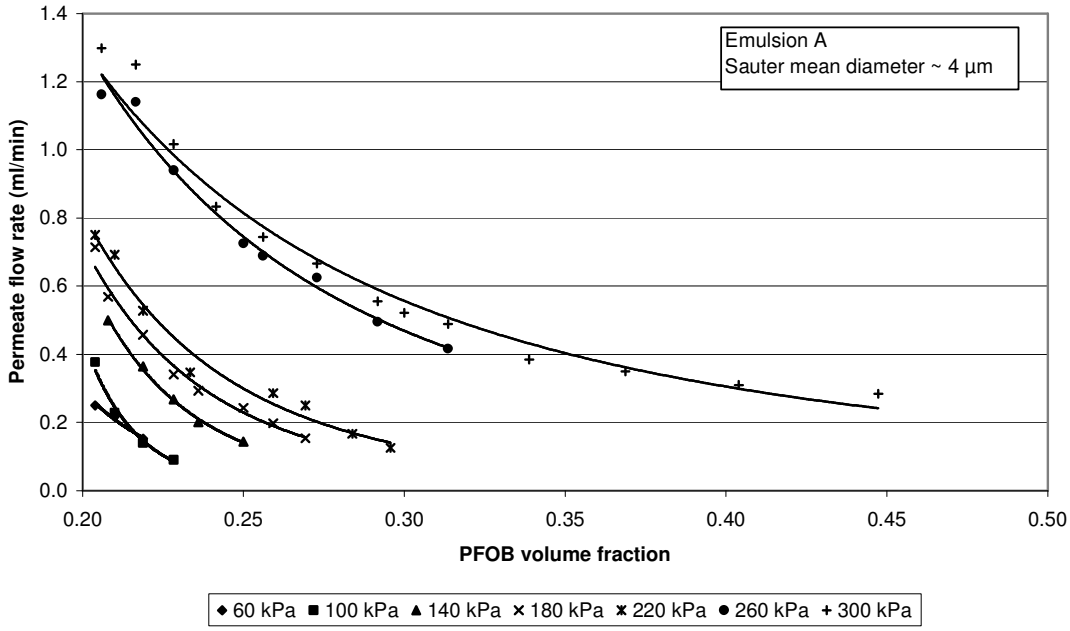

Figure 3-30. Increase in PFOB volume fraction leads to a dramatic decrease in permeate flow rate for Emulsion A. Increase in transmembrane pressure drop leads to improved permeate flow rates.

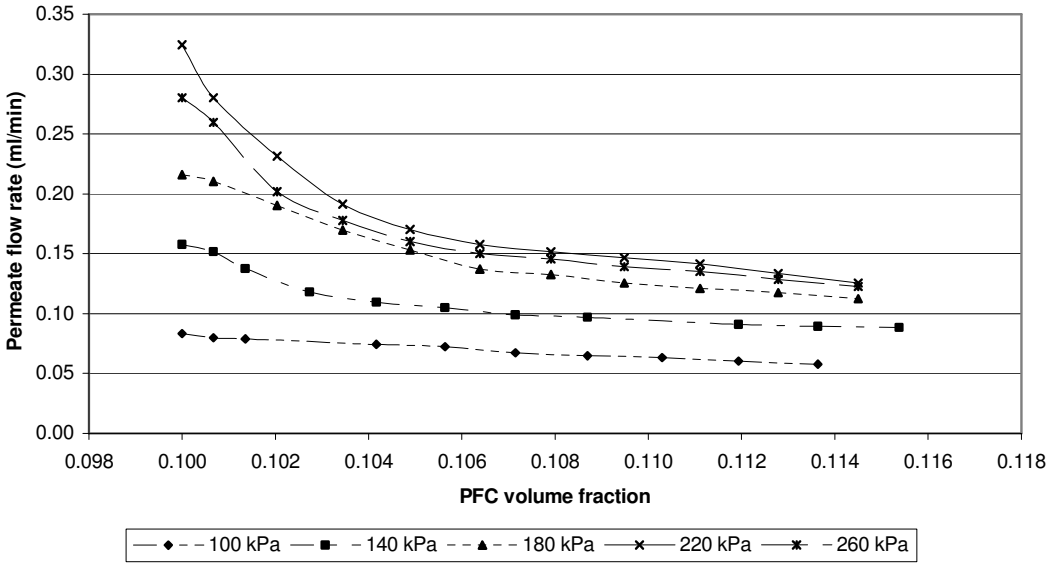

Figure 3-31. Similar trends to Emulsion A are observed for Emulsion B, with permeate flowrate decreasing with decrease in pressure and increase in PFOB volume fraction.

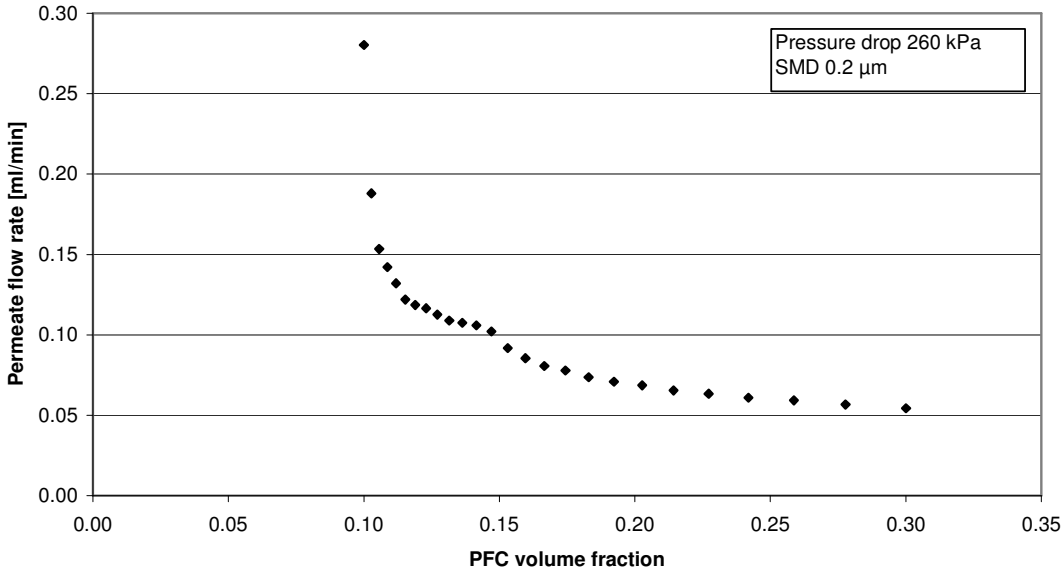

Figure 3-32. Permeate flow rate data for Emulsion B at higher PFOB volume fractions exhibit the same trends as for Emulsion A.

Experimental data for Emulsion B was more erratic than that of Emulsion A, as irreversible fouling of the membrane occurred over the period of use. The fouling could not be completely removed, even with aggressive cleaning for prolonged periods.

The mineral oil-in-water emulsions investigated by Lipp et al. (1988) showed coalescence of emulsion droplets in both the retentate and filtrate. Droplets in the filtrate were much larger than the membrane pore size, indicating coalescence occurring within the membrane. Similar results were obtained in our membrane. No

PFOB could be detected in the filtrate through distillation (indicating close to 100% retention), but some droplets were detected by laser light scattering (Figure 3-33). Although most of the droplets in the filtrate were submicron in size, some very large droplets were evident, which were not present in the feed emulsion. This indicates that coalescence of droplets in the UF membrane also occurs for PFOB emulsions. Fortunately, the fraction of PFOB ending in the filtrate is almost undetectable, as was also found by Lipp et al. (1998:168) for their emulsions.

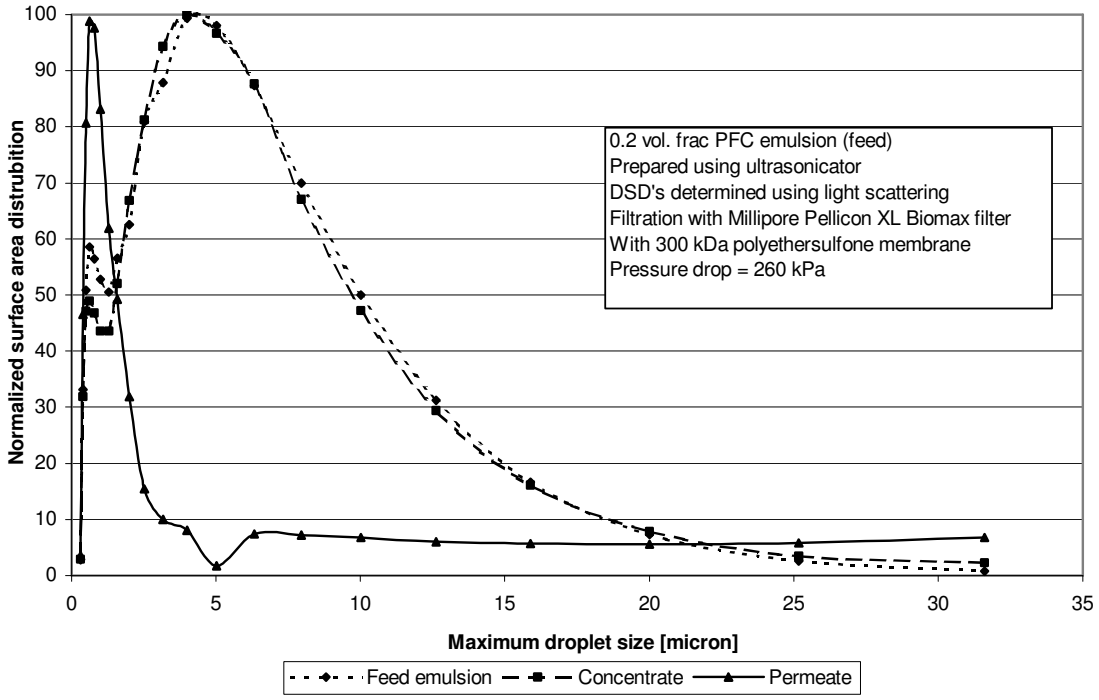

Figure 3-33. Ultrafiltration of Emulsion A resulted in retention of more than 99% of the PFOB, but some of the droplets passing through the membrane coalesced to much larger droplet sizes.

Lipp et al. (1998:175) found that fouling of UF membranes was mostly reversible for their oil-in-water emulsions, but was strongly dependent on choice of membrane. In their case, a regenerated cellulose membrane was most easily cleaned, with a dense polysulfone membrane the most irreversibly fouled. While Faibish and Cohen (2001a:129) concluded that polymeric (PVP) ceramic-supported membranes are fouled less easily than native ceramic (zirconia) membranes, Koltuniewicz and Field (1996:79) concluded that ceramic (zircon; alumina) membranes are fouled less easily than polymeric (PVDF; PS) membranes.

In the case of the UP-CSIR BALSS, there is not much choice with regards to membrane materials. The membrane material is determined by the requirement for minimum protein binding in contact with blood plasma, and is generally manufactured from polyethersulfone (which also has the widest pH compatibility – from 0.5 to 13 – Paulson, 1995).

Fibrinogen build-up

During animal trials of the UP-CSIR BALSS in October 2002, a build-up of fibrous material was noticed in the bioreactor after a number of hours of operation. Experiments are currently being carried out to determine the cause, but it is suspected that this fibrous build-up is due to either fibrin formation or fibrinogen build-up. Fibrin formation is part of the blood-clotting pathway and is formed from fibrinogen, a water-soluble globulin present in the blood plasma and manufactured by hepatocytes (Guillouzo and Guguen-Guillozo, 1986:163).

Even though only blood plasma (and not whole blood) is perfused through the BALSS, all the clotting factors are present in the blood plasma itself, except phospholipids and calcium (Bristoll-Myers Squibb, 2001). It is suspected that the plasma clotting sequence is activated by the glass surfaces in the BALSS, and that the egg yolk lecithin is then the source of phospholipids for the clotting sequence to proceed.

Upon further investigation, it was found that fibrinogen's molar mass is 340 kDa (Haematologic Technologies, 2001). As the ultrafiltration membrane used in the BALSS trials had a MWCO of 300 kDa, this meant that almost all of the fibrinogen in the plasma was being retained by the membrane, causing a continuous build-up of fibrinogen in circulation. This includes fibrinogen entering the BALSS from the patient, as well as fibrinogen synthesised by the hepatocytes within the bioreactor. Even if the fibrous build-up in the bioreactor is not caused by the fibrinogen build-up, this problem should be rectified. The use of UF membranes with higher MWCO's should therefore be investigated, as well as the addition of heparin (an anticoagulant) to the BALSS circuit.

Conclusions

The UF membrane evaluated (300 kDa MWCO) was suitable for quantitative separation of 0.2 µm SMD PFOB emulsions. Membrane fouling should be minimized through maintaining high cross-flow velocities and low transmembrane pressures (Paulson, 1995), which translates into large filtration areas and high circulation rates for the UP-CSIR BALSS. As the PFOB separation in the UP-CSIR BALSS runs on an independent circuit, flow rates can be adjusted as required by the UF membrane.

The issue of fibrinogen retention needs to be investigated further. Membranes with higher MWCO's (500 and 1000 kDa) should be evaluated to determine PFOB emulsion retention and fibrinogen permeation through the membranes.

The ultrafiltration membrane was chosen as method of concentration for the PFOB emulsions in the BALSS for a number of reasons:

1. It has no moving mechanical parts (as opposed to the centrifuge).
2. Process volumes can be kept small.
3. Nearly 100% separation could be achieved for 0.2 µm PFOB emulsions.
4. A tailor-made ultrafiltration unit could be designed for the BALSS that would be a consumable part of the system. It could be pre-packaged sterilely, and one would be used per patient.

3.5. Perfluorooctyl bromide recovery from emulsion

Due to the high cost of the PFOB, it is desirable to recover it from spent emulsions for re-use. Although centrifugation is successful in break-up of the emulsions, it requires over 96 hours of centrifugation in an ultracentrifuge at 60 000 g's (see Section 3.4.1). This is impractical if numerous recoveries have to be performed, and thus an alternative method of demulsification and purification of the PFOB fraction was sought.

There are a variety of possible approaches to demulsification (Sherman, 1968:70):

- Chemical methods – adding e.g. a solvent for the surfactant, a polyvalent salt or acid to destabilize the electrical double layer (i.e. reduce zeta potential), or a different surfactant to try and induce phase inversion;
- Centrifugal separation (as discussed above);
- Electrical methods to induce coalescence;
- Heat treatment – the increase in coalescence rate with heat is probably due to increased frequency of hole nucleation and increased hole size in the thin film.

A number of the above approaches were tested on the PFOB emulsion experimentally:

- Freezing and thawing cycles at –10 ºC and 25 ºC respectively (as mentioned earlier, fast freezing and/or thawing can sometimes induce coalescence);
- Heating at 80 ºC with a 40 % w/v sodium hydroxide solution;
- Heating at 80 ºC with a 50 vol. % hydrochloric acid solution;
- Heating with phenol crystals;
- Incubation with a commercial blend of lipase enzyme mixture – to break down the phospholipid surfactant;
- Refluxing for 30 minutes.

None of these methods achieved significant success, except the last method (refluxing), which resulted in some phase separation occurring. In order to destabilize the emulsion further, it was decided to lower the pH of the emulsion by adding a polyvalent acid, to destabilize the electrical double layer. Orthophosphoric acid was selected, as it has low mammalian toxicity at low concentrations (oral LD_{50} for rats is 1530 mg/kg - Boston University, 1997), and is commonly used in buffer systems for cell culture (Amresco, 2001). Thus, if any small residue remained in the PFOB, it should not have an impact on the BALSS. With the addition of orthophosphoric acid, refluxing resulted in a recovery of 75% of the PFOB.

Distillation (instead of refluxing) with orthophosphoric acid resulted in quantitative (100%) recovery of the PFOB.

The following experimental procedure was used for the distillation:

1. Add 2 g of 85% orthophosphoric acid per 10 g of emulsion in a round-bottom flask.
2. Heat the flask in an oil bath at 125 ºC.
3. Increase temperature to 150 ºC during course of distillation.
4. The distillate will consist of two clear liquid layers (PFOB at the bottom). Add demineralized water to the distillate flask and shake.
5. Measure pH and neutralize with sodium bicarbonate.
6. Separate layers by decanting.
7. Add demineralized water to the PFOB and shake.
8. Repeat steps 6 and 7 another two times to extract any impurities remaining in the PFOB.

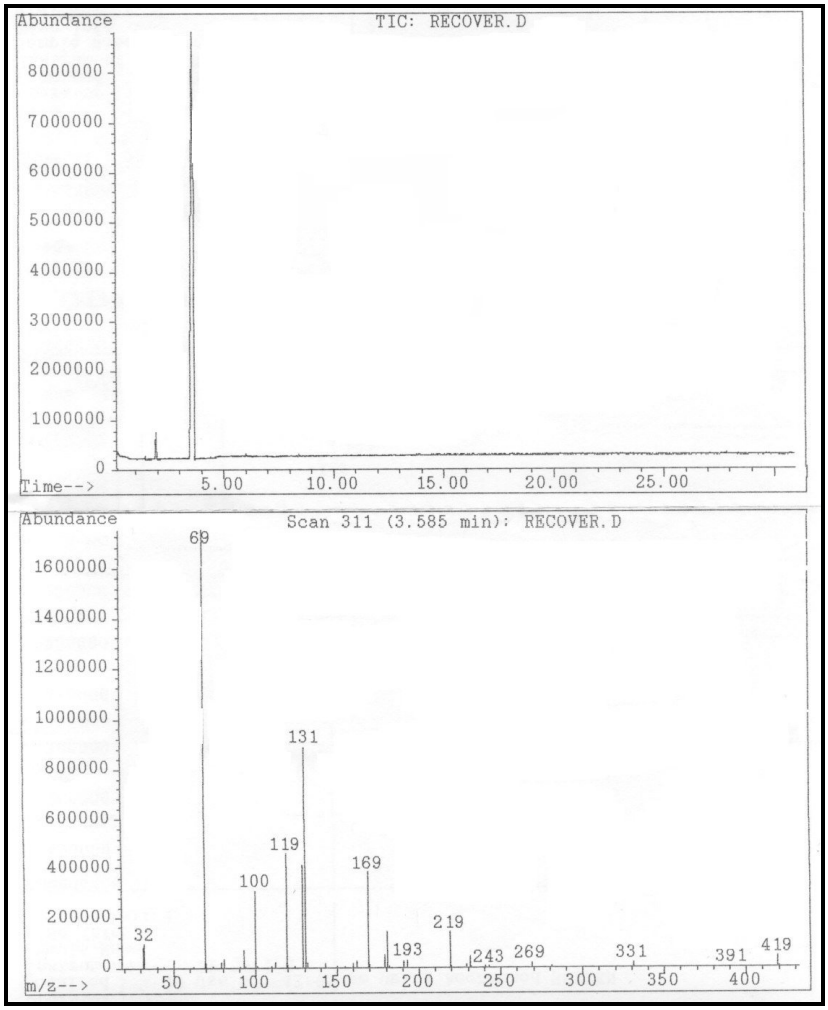

Figure 3-34. GC chromatogram (top) and mass spectrum of PFOB (bottom) recovered from emulsion through distillation with orthophosphoric acid show no other compounds were detected.

GC-MS was used to check the separated phases for impurities. The set-up was a Hewlett Packard 5890 series II capillary gas chromatographer with the following specifications:

- Column: HP-5 capillary column. Length 25 m, diameter 0.20 mm, phase thickness 0.33 µm
- Helium carrier gas at a flow of 1 ml/min
- Oven temperature 30 ºC initially for 3 minutes then ramped at 15 ºC/min to 300 ºC
- Detector: Hewlett Packard 5971 Mass selective Detector (MSD) (small-scale mass spectrometer)
- Total Ion mode m/z 30 to m/z 500, 1.4 scans per second.

Pure PFOB was run as a standard. The chromatogram and mass spectrum for the recovered PFOB (see Figure 3-34) was the same as the standard. No organic material could be detected in the aqueous phase of the distillate.

4. MASS TRANSFER CONSIDERATIONS

"*In theory, there is no difference between theory and practice. But, in practice, there is.*" – Jan L.A. van de Snepscheut.

The main purpose of the PFOB emulsions in the UP-CSIR BALSS is the delivery of oxygen to the hepatocytes in the bioreactor and the removal of carbon dioxide. Thus, it is of vital importance to understand and be able to predict the mass transfer behaviour of these emulsions, both in the bioreactor and in the oxygenator.

In order to measure the oxygen mass transfer rates to PFOB emulsions, and determine experimental mass transfer coefficients, a number of oxygen loading experiments were performed in gas-sparged and membrane oxygenators. Mass transfer models were developed for prediction of mass transfer rates, and the model predictions were verified or tested experimentally.

Although the models were developed for specific components (the gas-sparged and membrane oxygenators), they have application in all parts of the BALSS, including the bioreactor. The basic model will be incorporated in an overarching model for BALSS function, as discussed in Chapter 5.

4.1. Modelling aspects

In this section, concepts and parameters are introduced that are used in the subsequent sections for the model development.

4.1.1. Basic descriptive models for mass transfer

There are two basic approaches that can be used to describe and calculate mass transfer phenomena: the fundamental (diffusion coefficient) approach and the mass transfer coefficient approach. The choice of method will depend on the specific application being analyzed. The diffusion approach has distributed parameters (i.e. concentration varies with both position and time), while the mass transfer coefficient approach has lumped parameters (only gives bulk or average concentration values) (Cussler, 1984:5).

Diffusion approach

The basic equation for one-dimensional unsteady state diffusion was derived by Fick as (Cussler, 1984:19):

$$\frac{\partial C_a}{\partial t} = D\left(\frac{\partial^2 C_a}{\partial z^2} + \frac{1}{A}\frac{\partial A}{\partial z}\frac{\partial C_a}{\partial z}\right) \tag{4-1}$$

where D is the diffusion coefficient (m^2/s) and z is distance measured in the direction of diffusion (m).

When the diffusional area A is constant, Equation 4-1 reduces to the following form:

$$\frac{\partial C_a}{\partial t} = D\frac{\partial^2 C_a}{\partial z^2} \tag{4-2}$$

This equation allows analytical solution only for very simple diffusion problems. For steady-state one-dimensional diffusion through a thin film of thickness l, with the concentration on one side at C_{a1} and the concentration on the other side at C_{a2}, the solution to Equation (4-2) is:

$$C_a(z) = C_{a1} + (C_{a2} - C_{a1})\frac{z}{l} \tag{4-3}$$

A diffusional flux per unit area is defined as follows (generally referred to as Fick's law – Cussler, 1984:19):

$$j = D\frac{\partial C_a}{\partial z} \tag{4-4}$$

When Equation (4-3) is inserted into Equation (4-4) and the differentiation carried out, the following equation results for the diffusional flux:

$$j = \frac{D}{l}(C_{a2} - C_{a1}) \tag{4-5}$$

Mass transfer coefficient approach

The mass transfer coefficient approach is empirical, and is based on the observation that diffusional flux of a material is proportional to the concentration difference of that material by some proportionality constant (Cussler, 1984:3). This proportionality constant is defined as the mass transfer coefficient, k, and the flux equation is then written as follows:

$$j = k(C_{a2} - C_{a1}) \tag{4-6}$$

Note the obvious analogy between Equations (4-5) and (4-6). The diffusion approach is more suited to situations where concentration as a function of distance is important, while the mass transfer coefficient approach is more suited to situations where only bulk concentrations are of interest. When only diffusion is involved, the diffusion approach can be used, especially if the thickness of the diffusional barrier is known. When bulk convection is involved, the mass transfer coefficient approach is more suitable.

Convective mass transfer coefficients are generally calculated from correlations developed for specific geometries and boundary conditions. Through the heat and mass transfer analogy, corresponding equations for heat transfer for a specific geometry can be used by substitution of dimensionless numbers for heat transfer with the appropriate corresponding dimensionless numbers for mass transfer (Incropera and De Witt, 1990:355).

In the development of the mass transfer models described later, a combination of the diffusion and mass transfer coefficient approaches was used.

4.1.2. Emulsion density

The density of PFOB was measured experimentally over a temperature range from 20 to 40 ºC. The results are shown in Figure 4-1. At 37 ºC, the density of the PFOB is 1869 kg/m^3. The experimentally measured density of the background solution (without PFOB) at 37 ºC is 1025 kg/m^3. The emulsion density at 37 ºC depends on the dispersed phase (PFOB) volume fraction as follows:

$$\rho_e = \phi_p \rho_p + (1-\phi_p)\rho_m$$
$$\rho_e = 1025 + 843.7\phi_p \qquad (4\text{-}7)$$

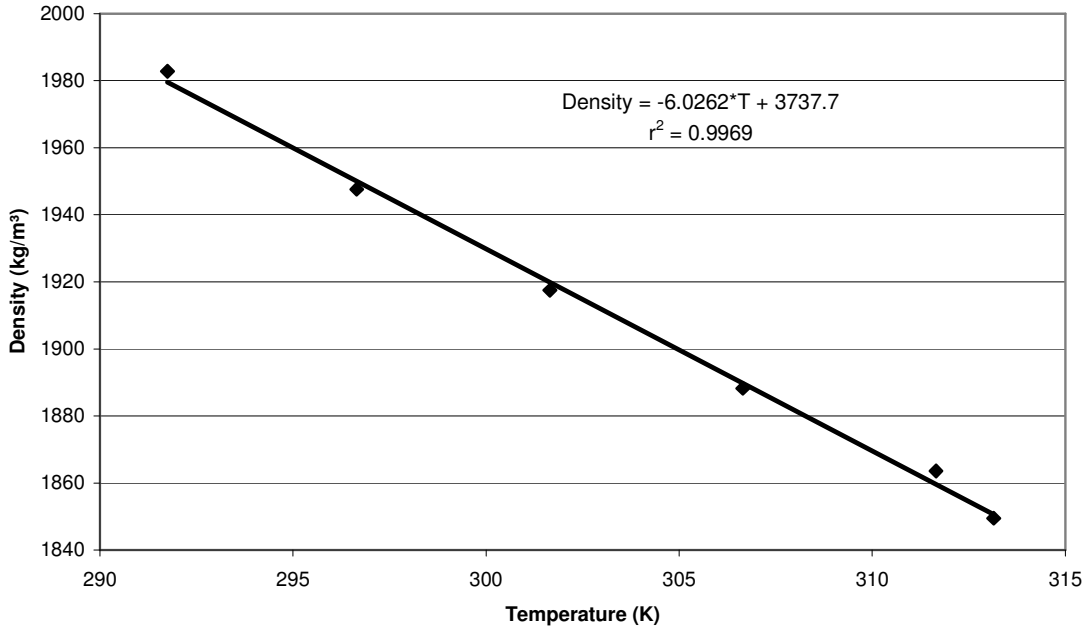

Figure 4-1. Density of PFOB as function of temperature

4.1.3. Emulsion viscosity

Equations and coefficients describing the viscosity of various emulsions were presented in Section 3.3.

4.1.4. Diffusion coefficients

The binary diffusion coefficient of oxygen in water is 2.5×10^{-9} m^2/s at 25 ºC (Perry & Green, 1984:3-259). The diffusivity of oxygen in blood plasma is 2.2×10^{-9} m^2/s at 37 ºC (Patel & Mehra, 1998:145).

The coefficient can be adjusted for other temperatures using the Einstein relation (Perry, Green & Maloney, 1997:5-64):

$$D(T_2,\eta_2) = \frac{\eta_1}{\eta_2}\frac{T_2}{T_1}D(T_1,\eta_1) \tag{4-8}$$

The binary diffusion coefficient of oxygen in PFOB can be approximated with the Wilke-Chang technique for unassociated solvents and low solute concentrations (Perry & Green, 1984:3-286), and the molar volume of liquid oxygen at its boiling point (V_{ob} = 2.8×10^{-5} m^3/mol from Weast, 1985):

$$D_{op} = 1.86\times10^{-18}\frac{M_p^{0.5}T}{\eta_p V_{ob}^{0.6}} \tag{4-9}$$

This equation results in a value for the binary diffusion coefficient of oxygen in PFOB of 3.5×10^{-9} m^2/s, which seems realistic when compared to the values for water and plasma (i.e. similar values, but slightly higher for PFOB). In any event, the accuracy of the coefficient does not have much impact on the results. It is only used in one equation for the calculation of a mass transfer coefficient (Equation 4-52), where it made only a 3% contribution to the value for a typical set of input parameters.

4.1.5. Henry's law

Henry's law states that, for gases that are weakly soluble in liquids, the equilibrium mole fraction of gas in the liquid phase is directly proportional to the partial pressure of that gas, and can be calculated using the following equation:

$$x_g(liq) = \frac{P_g}{H_x} \tag{4-10}$$

where H_x is Henry's constant (bar).

Oxygen dissolution in both PFOB and water obeys Henry's law (Zuck and Riess, 1994). It is appropriate for the model that Henry's law be rewritten in a concentration form. In order to do this, Henry's constant is transformed using the liquid density and molecular weight as follows:

$$H_{g-l} = \frac{M}{\rho}H_x \tag{4-11}$$

Please note that the newly defined Henry's constant, $H_{g\text{-}l}$, has different units than the one in Equation 4-10, namely bar.m^3/mol. With this definition of Henry's constant, Equation 4-10 can be rewritten as follows for the equilibrium concentration of a gas in a liquid at a specified partial pressure:

$$C_g(liq) = \frac{P_g}{H_{g-l}} \tag{4-12}$$

Henry's constant for oxygen in water at 37 ºC is 0.95 bar.m^3/mol (Incropera and De Witt, 1990:A26), and for oxygen in blood plasma (37 ºC) it is 0.988 bar.m^3/mol (Patel & Mehra, 1998:151). Henry's constant for oxygen in PFOB (37 ºC) is 0.0516 bar.m^3/mol and for carbon dioxide in PFOB (37 ºC) it is 0.0121 bar.m^3/mol (calculated using data from Lowe, 1991:87).

4.1.6. Distribution coefficient between PFOB and water

The distribution coefficient of oxygen dissolution in PFOB vs. water is given by the ratio of the equilibrium mass fractions of oxygen in the two phases (Perry and Green, 1984:15-5):

$$K = \frac{(w_{O_2-p})_{equil}}{(w_{O_2-m})_{equil}} \tag{4-13}$$

Define the mass fraction of oxygen in the two phases as follows:

$$\begin{aligned} w_{O_2-p} &= \frac{W_{O_2-p}}{W_{O_2-p} + W_p} \\ w_{O_2-m} &= \frac{W_{O_2-m}}{W_{O_2-m} + W_m} \end{aligned} \tag{4-14}$$

The mass of the various phases is then:

$$\begin{aligned} (W_{O_2-p})_{equil} &= V_p C_{p,equil} M_{O_2} \\ (W_{O_2-m})_{equil} &= V_m C_{m,equil} M_{O_2} \\ W_p &= V_p \rho_p \\ W_m &= V_m \rho_m \end{aligned} \tag{4-15}$$

Inserting Equation 4-15 into Equation 4-14 and then Equation 4-14 into Equation 4-13 yields:

$$K = \frac{C_{p,equil}(C_{m,equil} M_{O_2} + \rho_m)}{C_{m,equil}(C_{p,equil} M_{O_2} + \rho_p)} \tag{4-16}$$

Using Henry's law to calculate equilibrium oxygen concentrations and with $\rho >> C \times M$:

$$K \approx \frac{H_{O_2-m}\rho_m}{H_{O_2-p}\rho_p} \tag{4-17}$$

An example calculation to illustrate that $\rho >> C \times M$ for weakly soluble gases follows:

For oxygen in PFOB, with PFOB density of 1869 kg/m^3, temperature of 37 ºC and oxygen partial pressure of 0.85 bar, the equilibrium solubility of oxygen is 16.5 mol/m^3 or 0.0165 kmol/m^3. Thus:

$C \times M$ = 0.0165×31.9988

= 0.527 kg/m^3 << 1869 kg/m^3

At 37 ºC, the value of *K* from Equation 4-17 is 10.5. Thus, 10.5 times as much oxygen will dissolve in the same mass of PFOB as water. Expressed in volume terms, the ratio is 19.2 (this value is higher due to PFOB's much higher density).

The equilibrium concentration of oxygen in the plasma, at the phase boundary, for a specific concentration of oxygen in the PFOB can be calculated by using the distribution coefficient as defined in Equation 4-17 and rewriting Equation 4-16, with $\rho >> C \times M$:

$$C_{m,equil} = \left(\frac{\rho_m}{\rho_p}\right)\frac{C_p}{K}$$
$$C_{m,equil} = \frac{H_{O_2-p}}{H_{O_2-m}} C_p \qquad (4\text{-}18)$$

4.1.7. Fluid dynamics

The flow properties of the PFOB emulsions are important in terms of determining pressure drops, velocity profiles, and flow regime (laminar, transitional and turbulent). Emulsion A was non-Newtonian and Emulsion B was Newtonian over the range of PFOB volume fractions of interest. Newtonian fluid dynamics is not reviewed here – see Middleman (1998) for a detailed review.

Calculation of basic non-Newtonian parameters

The fluid dynamic behaviour of the non-Newtonian Emulsion A was of interest, especially in the membrane oxygenator, where it has to flow through the extracapillary spaces. Of primary interest were the shear rates at the boundary layer, as one would expect these to have a definite effect on mass transfer rates, as well as shear stress on cells in the BALSS bioreactor.

The velocity profile for laminar flow of a power law fluid in a tube is given by (Skelland, 1967:120):

$$\left(\frac{u}{u_e}\right) = \frac{3n+1}{n+1}\left[1 - \left(\frac{r}{R_f}\right)^{\frac{n+1}{n}}\right] \qquad (4\text{-}19)$$

The shear rate is defined as the rate of velocity change in the radial direction:

$$\dot{\gamma}(r) = \frac{du}{dr} = u_e\left(\frac{3n+1}{n+1}\right)\frac{d}{dr}\left[1-\left(\frac{r}{R_f}\right)^{\frac{n+1}{n}}\right]$$
$$= \frac{u_e}{R_f^{\frac{n+1}{n}}}\left(\frac{3n+1}{n+1}\right)\frac{d}{dr}\left[r^{\frac{n+1}{n}}\right] \qquad (4\text{-}20)$$
$$\dot{\gamma}(r) = \frac{u_e}{R_f^{\frac{n+1}{n}}}\left(\frac{3n+1}{n}\right)r^{\frac{1}{n}}$$

The hydraulic diameter for the extracapillary space in a hollow fibre membrane oxygenator is given by (Lipnizki & Field, 2001:197):

$$d_h = 2R_h = \left(\frac{d_i^2 - N_b V_t (d_f + 2h_b)^2}{d_i + N_b V_t (d_f + 2h_b)}\right) \qquad (4\text{-}21)$$

The Metzner-Reed Reynolds number for a power law fluid can be calculated as follows (Skelland, 1967:110):

$$\mathrm{Re}_{MR} = 8\left(\frac{n}{6n+2}\right)^n \frac{\rho_e u_e^{2-n} d_h^n}{K_c} \qquad (4\text{-}22)$$

where

$$u_e = \frac{Q_e}{A_{flow}} \qquad (4\text{-}23)$$

To calculate the cross-sectional flow area (A_{flow}), the shell-side cross-sectional void fraction (ε_c) of the hollow fibre membrane oxygenator is calculated as follows (Lipnizki and Field, 2001:196):

$$\varepsilon_c = 1 - N_b V_t \left(\frac{d_f + 2h_b}{d_i}\right)^2 \qquad (4\text{-}24)$$

The cross-sectional flow area can then be calculated:

$$A_{flow} = \varepsilon_c A_{cross-section} = \varepsilon_c \frac{\pi}{4} d_i^2 \qquad (4\text{-}25)$$

The viscosity as function of radius for laminar flow of a power law fluid in a tube can be calculated by substituting Equation 4-20 in the power-law equation:

$$\begin{aligned}\eta(r) &= K_c \dot{\gamma}^{n-1} \\ &= K_c \left[\frac{u_e}{R_f^{\frac{n+1}{n}}} \left(\frac{3n+1}{n} \right) r^{\frac{1}{n}} \right]^{n-1} \\ &= K_c \left[\frac{u_e}{R_f^{\frac{n+1}{n}}} \left(\frac{3n+1}{n} \right) \right]^{n-1} r^{\frac{n-1}{n}} \\ \eta(r) &= B\, r^{\frac{n-1}{n}}\end{aligned} \tag{4-26}$$

Average viscosity

In order to evaluate the average viscosity for the non-Newtonian fluid flowing in a tube, an area-average shear rate is calculated:

$$\begin{aligned}\dot{\gamma}_{ave} &= \frac{1}{A} \int_{A=0}^{A=\pi R_b^2} \dot{\gamma} dA \\ A &= \pi r^2 \\ \therefore dA &= 2\pi r dr \\ \therefore \dot{\gamma}_{ave} &= \frac{1}{\pi R_f^2} \int_{r=0}^{r=R_b} 2\pi r \dot{\gamma} dr\end{aligned} \tag{4-27}$$

Inserting Equation 4-20 into Equation 4-27:

$$\begin{aligned}\dot{\gamma}_{ave} &= \frac{2u_e}{R_f^2 R_f^{\frac{n+1}{n}}} \left(\frac{3n+1}{n} \right) \int_{r=0}^{r=R_f} r^{\frac{n+1}{n}} dr \\ \dot{\gamma}_{ave} &= \frac{2u_e}{R_f^2 R_f^{\frac{n+1}{n}}} \left(\frac{3n+1}{n} \right) \left(\frac{n}{2n+1} \right) R_f^{\frac{2n+1}{n}} \\ \dot{\gamma}_{ave} &= \frac{2u_e}{R_f} \left(\frac{3n+1}{2n+1} \right)\end{aligned} \tag{4-28}$$

An average viscosity can be calculated from the average shear rate:

$$\eta_{ave} = K_c \dot{\gamma}_{ave}^{n-1} = K_c \left[\frac{2u_e}{R_f} \left(\frac{3n+1}{2n+1} \right) \right]^{n-1} \tag{4-29}$$

Viscosity at the wall

To evaluate the viscosity at the wall (for shell-side flow of the emulsion in the membrane oxygenator) for power law fluids, the friction factor for laminar flow is given by (Greeff, 1999):

$$f' = 8\left(\frac{6n+2}{n}\right)^{n} \frac{K_c u_e^{n-2} d_h^{-n}}{\rho_e} \tag{4-30}$$

and for turbulent flow (Greeff, 1999):

$$f' = 0.3168 n^{0.675}\, \mathrm{Re}_{MR}^{-0.25} \tag{4-31}$$

The friction factor can now be used in the Darcy-Weisbach equation to calculate pressure drop per unit length:

$$\left(\frac{\Delta P}{L_b}\right) = \frac{f'}{d_h}\frac{\rho_e u_e^2}{2} \tag{4-32}$$

For calculation of the wall stress, a relationship between pressure drop and wall stress is required. Taking a force balance on a fluid element flowing in the extracapillary space of the hollow fibre oxygenator with no acceleration (Figure 4-2):

$$\begin{aligned} &\sum F = 0 \\ &\therefore P_1 A_{flow} - P_2 A_{flow} - \tau_w A_{surface} = 0 \\ &\Delta P A_{flow} = \tau_w N_b V_t \pi (d_b + 2h_b) L_b \\ &\frac{\Delta P}{L_b} = \tau_w \frac{4 N_b V_t (d_b + 2h_b)}{\varepsilon_c d_i^2} \end{aligned} \tag{4-33}$$

Now the viscosity at the wall can be calculated:

$$\begin{aligned} \dot{\gamma}_w &= \left(\frac{\tau_w}{K_c}\right)^{\frac{1}{n}} \\ \eta_w &= K_c \dot{\gamma}_w^{n-1} \\ \eta_w &= K_c \left(\frac{\tau_w}{K_c}\right)^{\frac{n-1}{n}} \end{aligned} \tag{4-34}$$

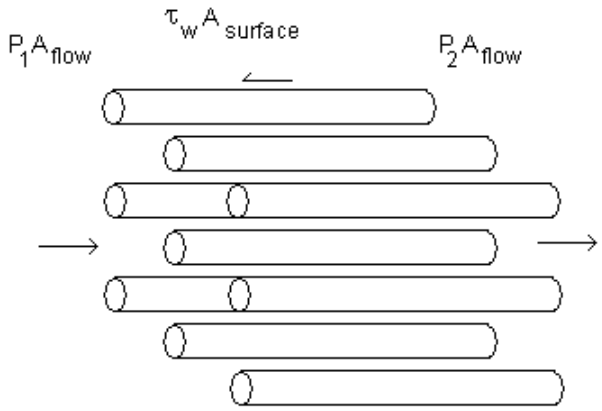

Figure 4-2. Force balance on fluid element for axial extracapillary flow through hollow fibre membrane oxygenator

Length of entrance regions

The length of the hydrodynamic entrance region for axial extracapillary flow in a membrane oxygenator is given by (Lipnizki and Field, 2001:198):

$$L_{HR} = 0.002\,\mathrm{Re}(1-\varepsilon_c)^{0.25} d_h \tag{4-35}$$

The length of the concentration entrance region (Lipnizki and Field, 2001:198):

$$L_{CR} = 0.02\,\mathrm{Re}\,Sc^{0.66}(1-\varepsilon_c)^{0.25} d_h \tag{4-36}$$

Evaluation of flow in membrane oxygenator for non-Newtonian emulsion

Calculated velocity profiles for laminar flow in a tube for the non-Newtonian PFOB emulsions are given in Figure 4-3. These were calculated using the experimentally determined power law coefficients from Section 3.3. The velocity profiles become flatter with increase in droplet size and increase in PFOB volume fraction. Even with the unstable formulation of Emulsion A, the high-pressure homogenized emulsions show flow behaviour closer to Newtonian than the sonicated emulsions.

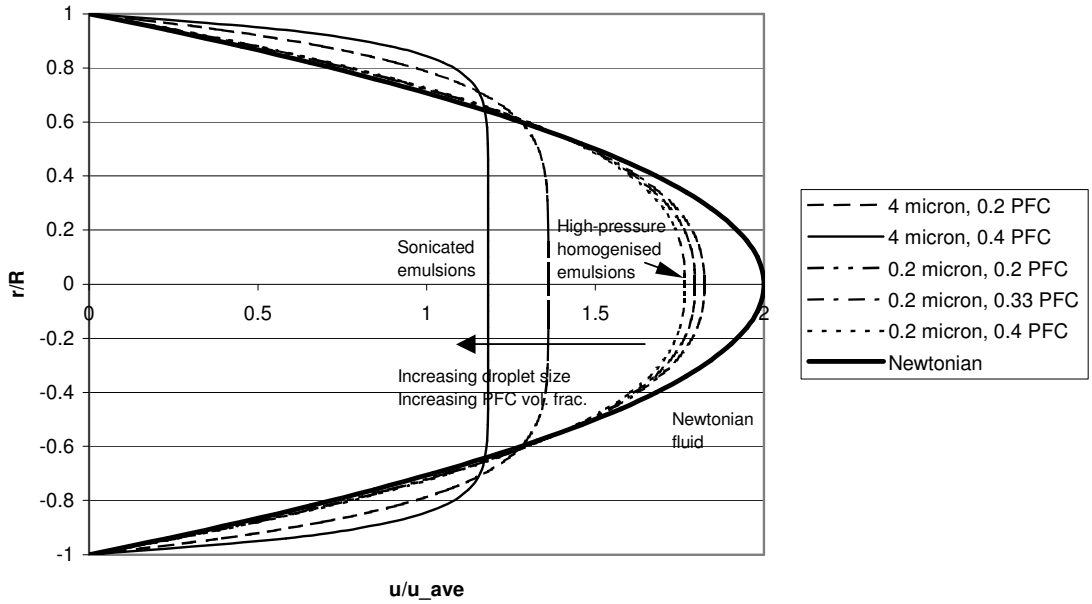

Figure 4-3. Calculated velocity profiles for the non-Newtonian PFOB emulsions with the formulation of Emulsion A. Experimentally determined power law coefficients were used in the calculations. With increase in droplet size and PFOB volume fraction, the velocity profile becomes flatter and approaches that of plug flow.

To determine the flow regime prevalent in the membrane oxygenator, calculations of the Metzner-Reed Reynolds number were done for the allowable range of flow rates through the membrane oxygenator used in the UP-CSIR BALSS (Polystan Safemicro Neonatal Oxygenator – hollow fibre membrane oxygenator with polypropylene hollow fibres). Specifications for this oxygenator are given in Table 4-1. The oxygenator contacts oxygen and fluid in a single-pass, counter-current configuration. These specifications were used in all subsequent calculations involving the membrane oxygenator.

Table 4-1. Specifications for Polystan Safemicro Neonatal Oxygenator

Parameter	Value	Units
Total hollow fibre surface area	0.33	m^2
Fibre inner diameter	280	µm
Fibre wall thickness	50	µm
Fibre length	73	mm
Process volume	26	ml
Maximum process flow rate	800	ml/min

Calculated Reynolds numbers are plotted in Figure 4-4 for Emulsions A and B for the allowable flow range in the Polystan Safemicro Neonatal Oxygenator. The criterion for laminar flow is a Reynolds number below 2300. It is clear from the plot that the flow in the oxygenator will be laminar for all the PFOB emulsions. This was also the conclusion of Shah and Mehra (1998:184).

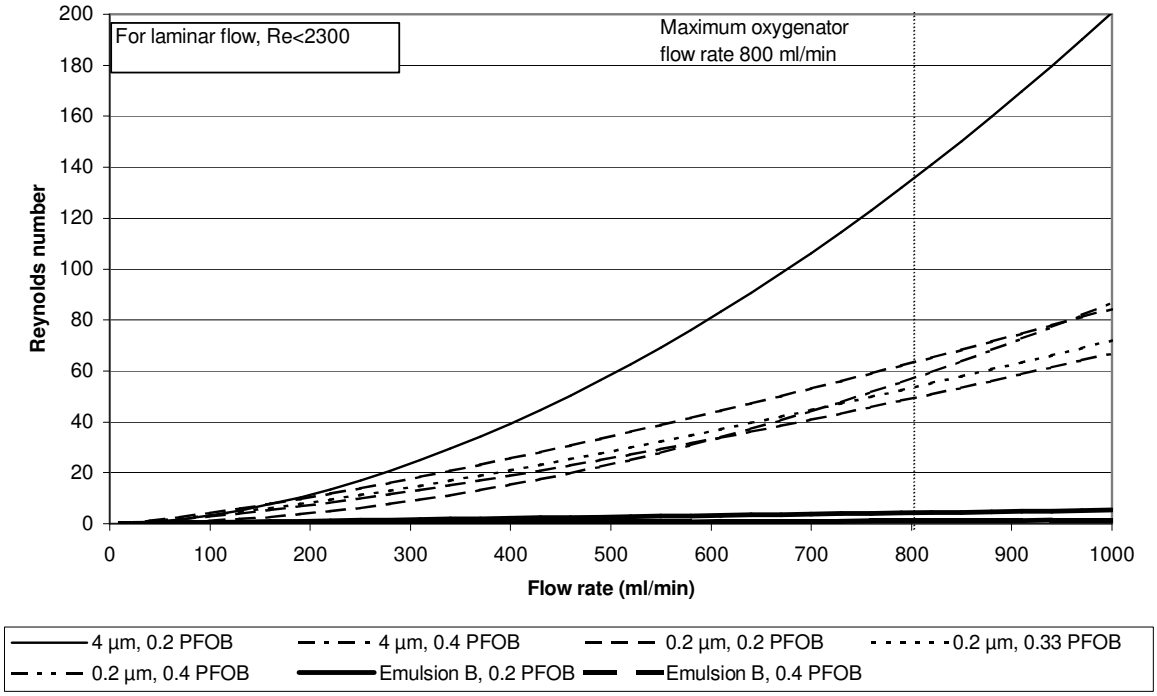

Figure 4-4. Calculated Reynolds numbers for Emulsions A and B in the Polystan Safemicro Neonatal Oxygenator are plotted against flow rate. The flow is laminar for all emulsions at all allowable flow rates through the oxygenator.

4.2. Mass transfer model: gas-sparged oxygenator

4.2.1. Basic approach

In the case of a gas sparger, or an oxygenator where gas bubbles (formed by a sparger) are mixed into the liquid phase using a stirrer, it is assumed that there are two main pathways for oxygen transfer from gas to PFOB droplet in the emulsion – gas to medium to PFOB droplet, and gas to PFOB droplet. In the case of mass transfer from gas to medium to PFOB droplet, the various regions involved in the mass transfer process are illustrated in Figure 4-5. At the top of the figure, a typical one-dimensional concentration profile at a random instant in time before equilibrium is shown. Please note that Figure 4-5 is not drawn to scale.

The mass transfer takes place from the gas bubble, through a boundary layer into the bulk medium, and then from the bulk medium through a boundary layer into the PFOB droplet. The discontinuity in concentration at the phase boundary between the PFOB and the medium is due to the higher solubility of oxygen in PFOB, as calculated from the distribution coefficient (see Section 4.1.6).

Some of the PFOB droplets can, from time to time, find themselves within the boundary layer of a gas bubble (see Figure 4-6). Patel and Mehra (1998:146) reported that uneven droplet distributions occur in capillaries or flow areas of diameter smaller than 300 µm, where there is a tendency for the dispersed phase to migrate towards

the center of the flow area (where there is lower shear). However, this tendency is much lower for small droplets such as PFOB emulsions, and these tend to remain more uniformly distributed over the flow area.

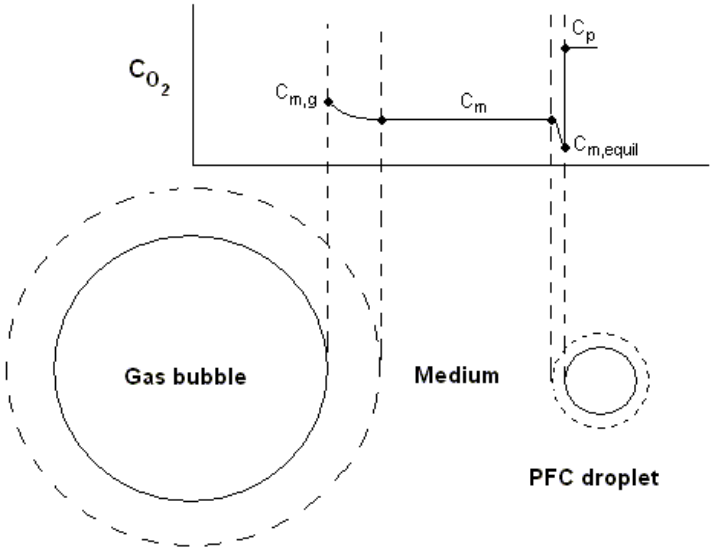

Figure 4-5. Schematic representation of the mass transfer pathway in the gas-sparger. Figure not to scale.

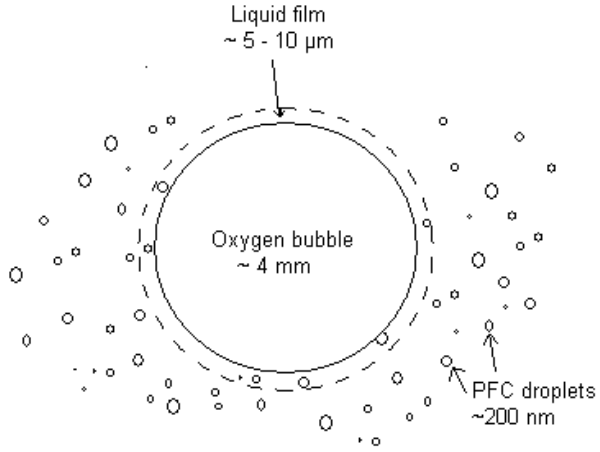

Figure 4-6. PFOB droplets can temporarily enter the boundary layer surrounding the gas bubbles (McMillan and Wang, 1987:574).

The concentration boundary layer typically has a thickness of approx. 5-10 µm (McMillan & Wang, 1987:574). PFOB droplets within the boundary layer are assumed to be separated from the hollow fibre surface by only a thin, stagnant liquid film. Rapid droplet interchange is assumed between droplets within the boundary layer and droplets in the bulk medium (plasma). An alternative approach is to use surface renewal theory to model droplet exchange between the boundary layer and the medium, as was done by McMillan & Wang (1987:581).

A number of assumptions are made for the model:

- The effect of the interfacial surfactant molecules on the PFOB droplet surfaces on oxygen transport through the PFOB-medium phase boundary can be neglected (Ju, Lee and Armiger, 1991b).
- Uniform oxygen concentration is assumed for the bulk medium (due to mixing) and within the PFOB droplets (due to their small size – Shah and Mehra, 1998:183). The mass transfer Biot number ($Bi_m = kd_{sp}/D_{op}$ - Incropera and De Witt, 1990:353) for a 0.2 µm PFOB droplet is calculated as 0.025. This value is much smaller than one, and thus the assumption of uniform oxygen concentration in the PFOB droplets is justified (Incropera and De Witt, 1990:230).
- Due to the low vapour pressure of PFOB (590 Pa at 20 ºC (Vermont Safety Information Resources, 2001) and 1400 Pa at 37 ºC (Lehmler et al., 1999:7)) and the fact that the PFOB is emulsified, it is assumed that the losses of PFOB into the gas phase per pass through the oxygenator are insignificant. Over long periods of use (e.g. in the BALSS), it could become significant, and should be considered in calculations.
- Carbon dioxide removal is not rate limiting (Ju, Lee & Armiger, 1991a:323) and therefore is not considered.
- PFOB droplet density remains constant with varying dissolved O_2 concentration.
- The partial pressure of oxygen in the gas bubbles remains constant. This was checked for the experimental gas sparger by comparing actual oxygen flow rates to actual oxygen consumption. While the oxygen flow rate through the unit was ~ 1.2 mol/hr, the maximum (initial) consumption for a 0.4 volume fraction PFOB emulsion was 0.037 mol/hr (~ 3%). If 100% oxygen is used, partial pressure will remain constant even at high oxygen consumption (gas bubbles will shrink).

4.2.2. Mole balances

Taking an oxygen mole balance over the bulk medium, using the concentrations as defined in Figure 4-5, and with no chemical reaction:

Accumulation of oxygen in medium = flow into medium from gas phase – flow out of medium into PFOB phase

$$V_m \frac{dC_m}{dt} = A_{gm} j_{gm} - A_{mp} j_{mp} \tag{4-37}$$

The surface areas and fluxes in Equation 4-37 can be calculated as follows:

$$\begin{aligned} A_{mp} &= V_{gs} a_{mp} \\ A_{gm} &= V_{gs} a_{gm} \\ j_{mp} &= k_{mp}(C_m - C_{m,equil}) \\ j_{gm} &= k_{gm}(C_{m,g} - C_m) \end{aligned} \tag{4-38}$$

Inserting Equation 4-38 into Equation 4-37, with $V_m = V_{gs}(1-\phi_p(1-\phi_g)-\phi_g)$:

$$V_{gs}(1-\phi_p(1-\phi_g)-\phi_g)\frac{dC_m}{dt} = V_{gs}k_{gm}a_{gm}(C_{m,g}-C_m) - V_{gs}k_{mp}a_{mp}(C_m - C_{m,equil}) \tag{4-39}$$

Dividing by the volume of medium, $V_{gs}(1-\phi_p(1-\phi_g)-\phi_g)$:

$$\frac{dC_m}{dt} = \frac{1}{(1-\phi_p(1-\phi_g)-\phi_g)}\left[k_{gm}a_{gm}(C_{m,g}-C_m) - k_{mp}a_{mp}(C_m - C_{m,equil})\right] \tag{4-40}$$

Taking an oxygen mole balance around a PFOB droplet:

Accumulation of oxygen in PFOB = flow into PFOB from medium + flow into PFOB from gas bubbles

$$V_p\frac{dC_p}{dt} = A_{mp}j_{mp} + A_{gp}j_{gp} \tag{4-41}$$

Defining surface areas and fluxes similarly to Equation 4-38, and inserting them into Equation 4-41, yields:

$$V_{gs}\phi_p(1-\phi_g)\frac{dC_p}{dt} = V_{gs}k_{mp}a_{mp}(C_m - C_{m,equil}) + V_{gs}k_{gp}a_{gp}(C_{p,g}-C_p) \tag{4-42}$$

Dividing by the volume of PFOB, $V_{gs}\phi_p(1-\phi_g)$:

$$\frac{dC_p}{dt} = \frac{1}{\phi_p(1-\phi_g)}\left[k_{mp}a_{mp}(C_m - C_{m,equil}) + k_{gp}a_{gp}(C_{p,g}-C_p)\right] \tag{4-43}$$

The concentration of oxygen in the medium at the phase boundary between medium and PFOB is taken as the equilibrium concentration corresponding to the concentration of oxygen in the PFOB (Hines & Maddox, 1985:153). The equilibrium concentration of oxygen in the medium, at the phase boundary, for a specific concentration of oxygen in the PFOB can be calculated from Equation 4-18.

The concentration of oxygen at the medium and PFOB phase boundaries with the gas phase can be approximated using Henry's law (Hines & Maddox, 1985:152):

$$C_{m,g} = \frac{P_{O_2}}{H_{O_2-m}}$$
$$C_{p,g} = \frac{P_{O_2}}{H_{O_2-p}} \tag{4-44}$$

Equations 4-40 and 4-43 represent a set of simultaneous differential equations. Because the set is generally 'stiff' (due to order of magnitude differences in the various mass transfer rates), numerical solution using general numerical methods such as the 4th order Runge-Kutta method is not possible for larger time intervals. However,

an analytical solution can be obtained for this specific set of differential equations (see Appendix A for derivation of analytical solution).

The analytical solution yields the oxygen concentrations in the medium and PFOB as functions of time. By setting $k_{gp}a_{gp}$ equal to zero, the oxygen mass transfer rates with no direct gas-PFOB transfer can also be determined.

4.2.3. Specific surface areas

The fractional surface area of PFOB droplets in the boundary layer of a gas bubble can be derived in a similar way as was done by McMillan and Wang (1987:580) to yield the following equation (see Appendix B for derivation):

$$\phi_{pg}^{|} = \frac{a_{gp}}{a_g} = \frac{3}{2}\phi_p(1-\phi_g)h\frac{\sum_{i=1}^{N} n_i d_{pi}^2}{\sum_{i=1}^{N} n_i d_{pi}^3} \tag{4-45}$$

This approach works sufficiently well when the dispersed phase droplet sizes are in the same range or larger than the boundary layer thickness. When it is smaller, the approach fails, as it then predicts interfacial surface areas larger than the total gas surface area available, which is of course physically impossible. The reason for this anomalous result is that the model adds up the projected surface areas of all droplets in the boundary layer, and when the droplets are much smaller than the boundary layer thickness, multiple layers of droplets can exist within the boundary layer.

Thus, a different approach is required in the case where the dispersed phase droplets are smaller than the boundary layer thickness (as is the case with the PFOB emulsions). This approach must take into account the effect of both PFOB volume fraction (increase in PFOB volume fraction ≅ increase in viscosity, increase in total oxygen carrying capacity and increase in droplet occurrence in boundary layer) and PFOB droplet size (increase in droplet size ≅ decrease in droplet surface area and increase in diffusion mass transfer distance) on mass transfer rates.

The total volumetric mass transfer coefficient is the product of the mass transfer coefficient (k) and the interfacial specific surface area between phases a and b (a_{ab}) and must make provision for the above effects.

The approach used was as follows:

PFOB droplets finding themselves within the boundary layer of a gas bubble are assumed to be separated from the gas bubble by only a thin, stagnant liquid film separating the gas bubble from the PFOB droplet. Mass transfer of oxygen takes place by diffusion through the liquid film (McMillan and Wang, 1992:287), followed by

diffusion into the PFOB droplet. Thus, the overall mass transfer coefficient is obtained from summation of the resistances to mass transfer in both the liquid film and the PFOB droplet (see next section).

It is assumed that the PFOB droplets in the boundary layer are touching the thin film at a single point. Thus, apart from the thickness of the thin film, there is an additional distance for diffusion through the medium before the PFC droplet surface is reached, due to the curvature of the droplet. This distance is added to the thickness of the thin film for calculation of the diffusion mass transfer coefficient (k_{gp}). It has the effect of making provision in the model for the effect of droplet size on gas-PFOB mass transfer rates, as larger droplets have larger average distances for oxygen diffusion.

Only the droplets closest to the surface of the thin film are included in this mass transfer pathway. The other droplets are assumed to receive oxygen via the other pathway (gas-medium-PFOB).

It is also assumed that the interfacial specific surface area between gas bubbles and PFOB is linearly proportional to the volume fraction of PFOB. At a PFOB volume fraction of 0.64 (maximum random packing density for monodisperse spheres - Jaeger & Nagel, 1992:1524), the total gas bubble surface area is covered with PFOB droplets.

From the last assumption, the interfacial specific surface area between gas and PFOB is given by:

$$a_{gp} = \frac{\phi_p}{0.64} a_g \tag{4-46}$$

The specific surface areas of the gas bubbles and the PFOB droplets can be calculated using the Sauter mean diameter:

$$\begin{aligned} a_g &= \frac{6\phi_g}{d_{sg}} \\ a_p &= \frac{6\phi_p(1-\phi_g)}{d_{sp}} \end{aligned} \tag{4-47}$$

The Sauter mean diameter, d_s, is calculated from Equation 3-5. The interfacial specific surface areas between the gas & medium and medium & PFC can now be calculated as follows:

$$\begin{aligned} a_{gm} &= a_g - a_{gp} \\ a_{mp} &= a_p - a_{gp} \end{aligned} \tag{4-48}$$

4.2.4. Mass transfer coefficients

The overall volumetric mass transfer coefficient for the liquid phase from the gas phase ($k_{gm}a_{gm}$), can be calculated using a correlation developed by Hocker (Perry & Green, 1984:18-70):

$$k_{gm}a_{gm} = 0.105\frac{Q_g}{V_{gs}(1-\phi_g)}\left[\frac{P_{ag}}{Q_g}\rho_e\left(\frac{\eta_e}{\rho_e g}\right)^{2/3}\right]^{0.59} Sc^{0.3} \tag{4-49}$$

where the Schmidt number is given by:

$$Sc = \frac{\eta_e}{\rho_e D_{om}} \tag{4-50}$$

Alternatively, and more accurately (as the adjusted interfacial specific areas can now be used), the mass transfer coefficients for both the gas-liquid and liquid-PFOB interfaces can be calculated by the following correlation for drops or bubbles in stirred solution (Cussler, 1984:230):

$$k_{gm} = k_{mp} = \frac{0.13D_{om}}{d_{imp}}\left(\frac{d_{imp}^4\rho_e^2 P_{ag}}{\eta_e^3 V_{gs}}\right)^{0.25} Sc^{0.33} \tag{4-51}$$

For mass transfer from gas to PFOB through a thin, stagnant liquid film with thickness h_f, the mass transfer coefficient can be approximated by the sum of the diffusional resistances (D/l) (Hines and Maddox, 1987:147; Incropera and De Witt, 1992:81):

$$k_{gp} = \frac{1}{\frac{h_f + d_c}{D_{om}} + \frac{d_{sp}}{2D_{op}}} \tag{4-52}$$

where d_c is the average distance from the surface of a droplet of PFOB to a plane surface tangent to the sphere and just touching the sphere, given by:

$$d_c = \frac{d_{sp}}{6} \tag{4-53}$$

4.2.5. Other gas-sparger parameters

The gas hold-up in the agitated vessel can be approximated using the following correlation from Sensel (Perry, Green and Maloney, 1997:14-79):

$$\phi_g = 0.105\left(\frac{Q_g}{N_{imp}d_{imp}^3}\right)\left(\frac{N_{imp}^2 d_{imp}}{g}\right)^{0.5}\left(\frac{N_{imp}d_{imp}\rho_e}{\eta_e}\right)^{0.1} \tag{4-54}$$

The agitator power input can be calculated using (Perry and Green, 1984:19-8):

$$P_{ag} = N_p \rho_e N_{imp}^3 d_{imp}^5 \tag{4-55}$$

where the impeller power number, N_p, is given by (equations derived by curve-fitting of data from Perry and Green, 1984:19-10 - for 1<Re_{imp}<100 000):

$$N_p(A) = 0.39 + 8.51\frac{\ln \mathrm{Re}_{imp}}{\mathrm{Re}_{imp}} + \frac{55.07}{\mathrm{Re}_{imp}^{0.5}} + 20.65e^{-\mathrm{Re}_{imp}}$$
$$N_p(B,C) = 4.9 - \frac{27.19}{\mathrm{Re}_{imp}^{0.5}} + \frac{121.7}{\mathrm{Re}_{imp}} - 121.8e^{-\mathrm{Re}_{imp}} \tag{4-56}$$

In Equation 4-56, A denotes a top-entering impeller, off-centre, angular, with no baffles. B denotes a top-entering turbine with four or six blades, centred, with four or more baffles. C denotes a side-entering propeller with three or four blades.

The impeller Reynolds number, Re_{imp}, is calculated as follows:

$$\mathrm{Re}_{imp} = \frac{d_{imp}^2 N_{imp} \rho_e}{\eta_e} \tag{4-57}$$

The gas bubble Sauter diameter can be estimated using a gas bubble Reynolds number as defined below, and correlations obtained through curvefitting of data from Perry, Green and Maloney (1997:14-71):

$$\mathrm{Re}_g = \frac{d_{or} u_{or} \rho_g}{\eta_g}$$
$$d_{sg} = \left[\frac{\sigma_s d_{or}^2}{(\rho_e - \rho_g)g}\right]^{0.25} \left(e\,\mathrm{Re}_g + f\right) \tag{4-58}$$

The values of the constants e and f in Equation 4-58 are shown in Table 4-2 for various flow regimes:

Table 4-2: Values of constants for gas bubble diameter correlation

Lower Re_g limit	Upper Re_g limit	Constant e	Constant f
1	100	8.1E-3	1.6
100	2000	4.0E-3	2.0
2000	4000	-3.3E-3	16.5
4000	100 000	-2.6E-5	3.6

4.3. Mass transfer model: membrane oxygenator

Please note: all relevant assumptions made for the development of the mass transfer model in the gas-sparged oxygenator were used for the membrane oxygenator model as well.

4.3.1. Basic approach

The hollow fibre membrane oxygenator consists of a bundle of hollow fibres connected at their ends by manifolds. The extracapillary space (the space outside of the fibres) is perfused with PFOB emulsion, while the intracapillary space (the space inside of the fibres) is filled with pressurised gas. Figure 4-7 shows a schematic representation of the oxygen transfer from gas to PFOB for a single hollow fibre in a hollow fibre membrane oxygenator. A typical one-dimensional concentration profile is also indicated on the figure. Please note that the figure is not drawn to scale.

The two main oxygen transfer pathways from gas to PFOB now look as follows:

1. Gas → membrane → medium → PFOB
2. Gas → membrane → PFOB

The second pathway above refers to PFOB droplets finding themselves in the boundary layer surrounding the hollow fibres.

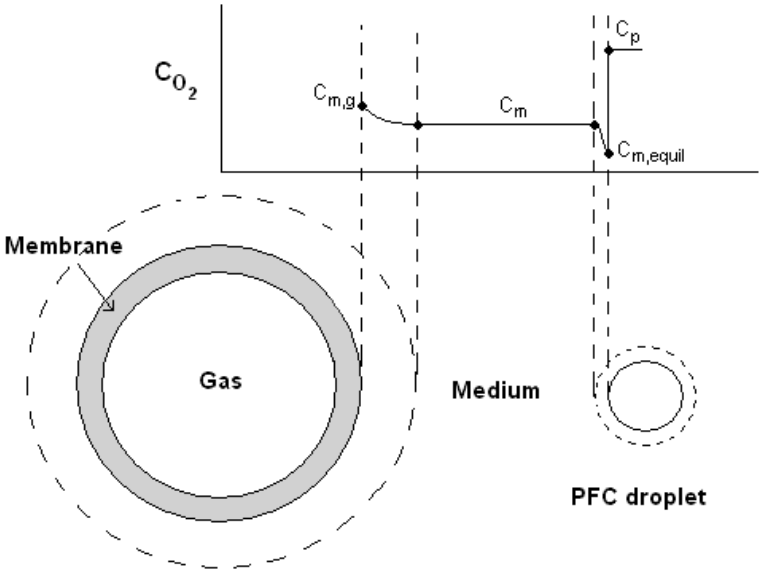

Figure 4-7. Schematic representation of the mass transfer pathway in the membrane oxygenator. Figure not to scale.

There are three resistances to mass transfer involved: the gas-side concentration boundary layer, diffusion through the membrane, and the liquid-side concentration boundary layer. When pure oxygen is used, there is no concentration boundary layer on the gas side. As the membrane is hydrophobic (the Polystan Safemicro

neonatal oxygenator contains polypropylene hollow fibres), it is gas-filled, and thus the membrane resistance to mass transfer is negligible compared to the liquid-side resistance (Goerke, Leung and Wickramasinghe, 2002:2036).

4.3.2. Mole balances

For the membrane oxygenator the assumption of constant dissolved oxygen concentration in the radial direction (except for the boundary layer) in the extracapillary space is made for the generation and solution of the differential equations. In reality there will also be a dissolved oxygen concentration gradient in the radial direction. This model generates average (bulk) results, adequate for the intended purpose.

Taking an oxygen mole balance over a unit cell of medium (flowing through the oxygenator), and rearranging and substituting in the same way as the previous section, leads to the following equation:

$$\frac{dC_m}{dt_m} = \frac{V_t}{V_m}\left[k_{bm}a_{bm}(C_{m,g} - C_m) - k_{mp}a_{mp}(C_m - C_{m,equil})\right] \tag{4-59}$$

Axial diffusion is assumed negligible for the above equation. The average oxygen concentration in the bulk medium for a specific residence time (t_m) in the membrane oxygenator at steady state will be constant.

Taking an oxygen mole balance over a PFOB droplet, and rearranging and substituting in a similar way to the previous section, results in the following equation:

$$\begin{aligned} V_p\frac{dC_p}{dt_m} &= V_t k_{mp}a_{mp}(C_m - C_{m,equil}) + V_t k_{bp}a_{bp}(C_{m,g} - C_{m,equil}) \\ \frac{dC_p}{dt_m} &= \frac{V_t}{V_p}\left[k_{mp}a_{mp}(C_m - C_{m,equil}) + k_{bp}a_{bp}(C_{m,g} - C_{m,equil})\right] \end{aligned} \tag{4-60}$$

Equations 4-59 and 4-60 form a set of two simultaneous linear, first order, ordinary differential equations (Zill and Cullen, 1992:4) describing the mass transfer in a membrane oxygenator. This set of equations can be solved analytically in a similar way as for the gas-sparged oxygenator (see Appendix A) by rearranging to a more convenient form for analytical solution and substituting for $C_{m,equil}$ from Equation 4-18:

$$\begin{aligned} \frac{dC_m}{dt_m} &= \frac{V_t}{V_m}\left(-k_{bm}a_{bm} - k_{mp}a_{mp}\right)C_m + \frac{V_t}{V_m}\frac{\rho_{H_2O}}{\rho_{PFC}K}k_{mp}a_{mp}C_p + \frac{V_t}{V_m}k_{bm}a_{bm}C_{m,g} \\ \frac{dC_p}{dt_m} &= \frac{V_t}{V_p}\frac{\rho_{H_2O}}{\rho_{PFC}K}\left(-k_{mp}a_{mp} - k_{bp}a_{bp}\right)C_p + \frac{V_t}{V_p}k_{mp}a_{mp}C_m + \frac{V_t}{V_p}k_{bp}a_{bp}C_{m,g} \end{aligned} \tag{4-61}$$

4.3.3. Specific surface areas

The interfacial specific surface area between the gas inside the membranes and the membrane itself is equal to the internal membrane surface area divided by the total membrane unit volume:

$$a_{gb} = \frac{N_b V_t \pi d_f L_b}{V_t}$$
$$a_{gb} = \pi N_b L_b d_f \tag{4-62}$$

The external specific surface area of the membrane is equal to the external membrane surface area divided by the total membrane unit volume:

$$a_b = \frac{N_b V_t L_b \pi (d_f + 2h_b)}{V_t}$$
$$a_b = \pi N_b L_b (d_f + 2h_b) \tag{4-63}$$

The interfacial specific surface area between the membrane and the PFOB droplets is calculated in a similar manner as for the gas-sparged oxygenator:

$$a_{bp} = \frac{\phi_p}{0.64} a_b \tag{4-64}$$

The interfacial specific surface area between membrane and medium is equal to the difference between the total membrane external specific surface area and the membrane-PFOB interfacial specific surface area:

$$a_{bm} = a_b - a_{bp} \tag{4-65}$$

The PFOB droplet external specific surface area can be calculated as follows:

$$a_p = \frac{\text{total external droplet area}}{\text{total volume}}$$
$$a_p = \frac{\text{droplet surface area}}{\text{volume PFOB}} \times \frac{\text{volume PFOB}}{\text{total volume}}$$
$$a_p = \frac{6}{d_{sp}} \times \frac{V_p}{V_t}$$
$$a_p = \frac{6\phi_p}{d_{sp}} \left[1 - \frac{\pi}{4} N_b L_b (d_f + 2h_b)^2 \right] \tag{4-66}$$

The interfacial specific surface area between medium and PFOB is equal to the difference between the total PFOB external specific surface area and the membrane-PFOB interfacial specific surface area:

$$a_{mp} = a_p - a_{bp} \tag{4-67}$$

4.3.4. Mass transfer coefficients

Three different calculation methods were used for the membrane oxygenator model to determine the influence of choice of model on the model predictions. Table 4-3 shows the different methods and the alternative calculation approaches used for each. In the first method, Newtonian correlations and average properties are used to evaluate mass transfer coefficients. In the second method, non-Newtonian equations are used. In the third method, Newtonian correlations are used, but properties are evaluated at the high shear conditions at the wall (using the calculated viscosity at the wall) – this was recommended by Cussler (2002).

Table 4-3. Different methods used to evaluate membrane oxygenator mass transfer coefficients

Method	Description of calculation method	Viscosity - curvefitted	Viscosity - power law	Shear rate - power law	Metzner-Reed Re no.	Newtonian Re no.	Lipnizki & Field (2001) correlation	Flat plate correlation	Properties evaluated at wall	Average properties
1	This method calculates viscosity using curve-fitted surfaces and uses Newtonian equations for Sh numbers from Incropera and De Witt (1990) and Cussler (1984).	✓	·	✓	·	✓	·	✓	·	✓
2	This method uses Metzner-Reed Re number for power law fluids, power law for viscosity calculations and the improved mass transfer correlations from Lipnizki & Field (2001).	·	✓	✓	✓	·	✓	·	·	✓
3	This is similar to Method 2 but uses normal Re number and calculates viscosity & other properties at the wall, where most of the resistance to mass transfer is present.	·	✓	✓	·	✓	✓	·	✓	·

The following equation is valid for laminar flow where both the hydrodynamic and concentration profiles are fully developed (Lipnizki & Field, 2001:197):

$$Sh_1 = 3.66 + 1.2\left(\sqrt{1-\varepsilon_c}\right)^{-0.8} \tag{4-68}$$

In the case where the concentration profile is still developing, but with full hydrodynamic development one can calculate the average Sherwood number as follows (Lipnizki & Field, 2001:197):

$$Sh_2 = 1.615\left(1 + 0.14\left(\sqrt{1-\varepsilon_c}\right)^{-0.5}\right)\sqrt[3]{\frac{\mathrm{Re}\,Scd_h}{L_b}} \tag{4-69}$$

For the entrance region of the module, where neither the concentration nor the hydrodynamic profiles are fully developed (Lipnizki & Field, 2001:197):

$$Sh_3 = \left(\frac{2}{1+22Sc}\right)^{\frac{1}{6}}\left(\frac{\mathrm{Re}\,Scd_h}{L_b}\right)^{\frac{1}{2}} \tag{4-70}$$

In practice, using commercially available oxygenators, the concentration profile is generally not fully developed, while the hydrodynamic profile is fully developed (Noda & Gryte, 1979:113). An average Sherwood number for the whole oxygenator for laminar flow can be calculated as follows (Lipnizki & Field, 2001:197):

$$Sh = \left(Sh_1^3 + Sh_2^3 + Sh_3^3\right)^{1/3} \tag{4-71}$$

For turbulent flow, the average Sherwood number can be calculated as follows (Lipnizki & Field, 2001:198):

$$Sh = 0.021\left(\frac{1}{\sqrt{1-\varepsilon_c}}\right)^{0.45} \mathrm{Re}^{0.8}\, Sc^{0.33} \tag{4-72}$$

The mass transfer coefficient from membrane to PFOB (k_{bp}) is calculated in the same way as k_{gp} for the gas-sparged oxygenator:

$$k_{bp} = \frac{1}{\frac{h_f + d_c}{D_{om}} + \frac{d_{sp}}{2D_{op}}} \tag{4-73}$$

The mass transfer coefficients from membrane to medium (k_{bm}) and from medium to PFOB (k_{mp}) are calculated according to Methods 1, 2 and 3 (as described in Table 4-3). The calculation algorithms are given in Appendix C.

4.3.4. Other membrane oxygenator parameters

The total internal volume of the membrane oxygenator, V_t, is calculated as follows:

$$V_t = V_{gb} + V_m + V_p + V_b \tag{4-74}$$

V_{mb} is the volume of gas contained within the membranes in a membrane oxygenator and is given by the following equation:

$$V_{mb} = V_b \varepsilon_b \tag{4-75}$$

The volume of gas in the membrane oxygenator, V_{gb}, is calculated as follows (where N_b is the number of hollow fibres per unit total volume, L_b is the length of a hollow fibre, and d_f is the internal fibre diameter):

$$V_{gb} = \frac{\pi}{4} N_b V_t L_b d_f^2 \tag{4-76}$$

The membrane volume is determined as follows (where h_b is the hollow fibre wall thickness):

$$V_b = \frac{\pi}{4} N_b V_t L_b \left[(d_f + 2h_b)^2 - d_f^2 \right] \tag{4-77}$$

The volume of emulsion ($V_e = V_m + V_p$) in the membrane oxygenator is calculated as follows:

$$V_e = V_t \left[1 - \frac{\pi}{4} N_b L_b (d_f + 2h_b)^2 \right] \tag{4-78}$$

The volume of medium and volume of PFOB can then be calculated as follows:

$$\begin{aligned} V_m &= (1 - \phi_p) V_e \\ V_p &= \phi_p V_e \end{aligned} \tag{4-79}$$

The ratio V_t/V_m in Equation 4-59 can be evaluated using Equations 4-78 and 4-79:

$$\frac{V_t}{V_m} = \frac{V_t}{(1-\phi_p)V_e} = \frac{1}{(1-\phi_p)\left[1 - \frac{\pi}{4} N_b L_b (d_f + 2h_b)^2 \right]} \tag{4-80}$$

The ratio V_t/V_p in Equation 4-60 can also be calculated by using Equations 4-78 and 4-79:

$$\frac{V_t}{V_p} = \frac{V_t}{\phi_p V_e} = \frac{1}{\phi_p \left[1 - \frac{\pi}{4} N_b L_b (d_f + 2h_b)^2 \right]} \tag{4-81}$$

The emulsion velocity through the membrane oxygenator, u_e, is determined by dividing the volumetric emulsion flow rate by the cross-sectional area available for flow:

$$\begin{aligned} u_e &= \frac{Q_e}{A_{flow}} = \frac{Q_e}{\text{Total area - Fibre area}} \\ u_e &= \frac{(V_e / \tau_e)}{\left(\frac{V_t}{L_b} - N_b V_t \frac{\pi}{4} (d_f + 2h_b)^2 \right)} \\ \therefore u_e &= \frac{\left(1 - \frac{\pi}{4} N_b L_b (d_f + 2h_b)^2 \right)}{\tau_e \left(\frac{1}{L_b} - N_b \frac{\pi}{4} (d_f + 2h_b)^2 \right)} \\ u_e &= \frac{L_b}{\tau_e} \end{aligned} \tag{4-82}$$

The concentration of oxygen in the medium at the medium-membrane boundary ($C_{m,g}$) is calculated using Equation 4-44.

For the non-Newtonian fluids, power law coefficients were only available for a finite number of dispersed phase volume fractions (0, 0.2, 0.33 and 0.4 PFOB volume fractions). For prediction of properties at other PFOB volume fractions within this range, values were calculated for the available volume fractions, and the actual values then calculated by linear interpolation.

4.4. Model and experimental results

4.4.1. Experimental setup

Figure 4-8 shows the gas-sparged oxygenator experimental setup. PFOB emulsion is loaded into a 500 mℓ vessel containing a stirrer, sparger, copper heat exchange tubes (for temperature regulation) and oxygen probe (Biological Oxygen Monitor, YSI Model 5300A, YSI Incorporated, USA). The gas sparger is kept at 37 ºC using a water bath, circulation pump and heat exchange tubes. The gas first flows through a gas flow meter before flowing through copper heat exchange tubes in a water bath to regulate the gas temperature. The gas is then bubbled into the emulsion using the sparger, before exiting through a flow meter and oxygen analyzer. Before an experiment, the emulsion in the oxygenator is de-oxygenated by bubbling nitrogen through the emulsion. The oxygen loading profile vs. time is determined by bubbling oxygen through the emulsion at a fixed rate.

Although the choice of 'deoxygenating' gas could have an influence on oxygen load rates, the influence is generally small. In modelling diffusion of two components, there are two extremes: equimolar counterdiffusion, and diffusion of one component through a stagnant second component (Beek, Muttzal and Van Heuven, 1999:240). Generally the difference is small, and in the models developed here, the second extreme was assumed.

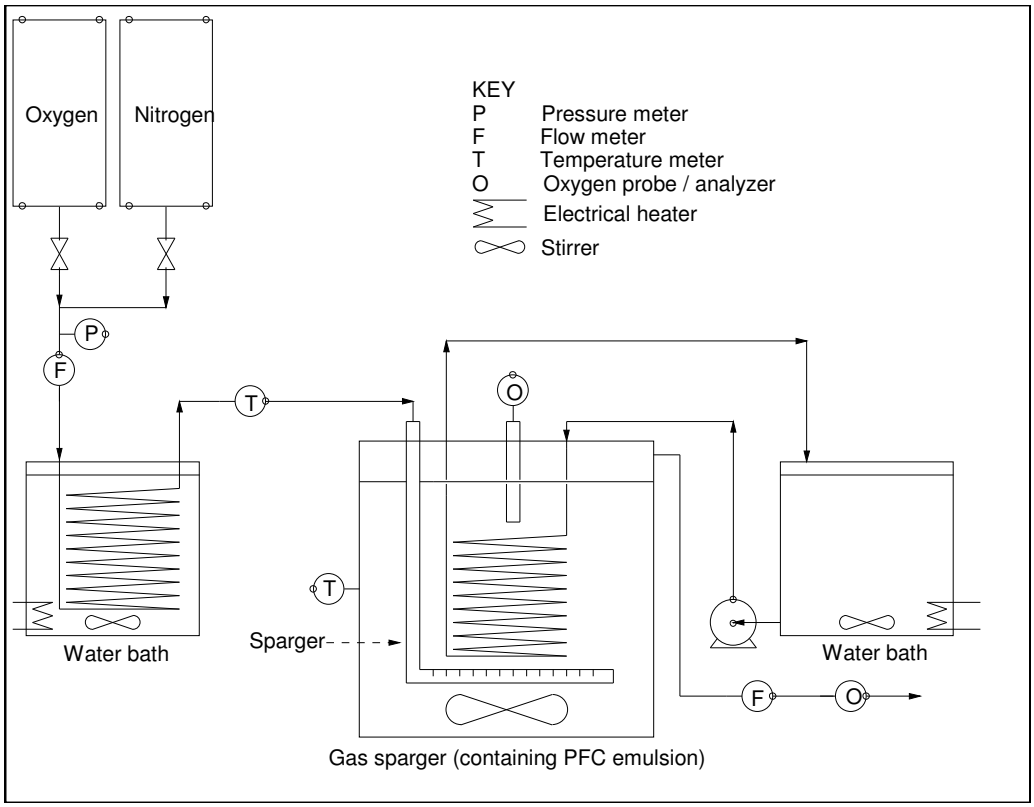

Figure 4-8. Gas-sparged oxygenator experimental setup

Figure 4-9 shows the membrane oxygenator experimental setup. The emulsion is continuously de-oxygenated in the starting container by bubbling nitrogen through it. It is then pumped through a heat exchanger before passing through the membrane oxygenator. The heat exchanger-membrane oxygenator combination used was a Polystan Safemicro Neonatal Oxygenator, with polypropylene hollow fibre membranes. Specifications for this oxygenator are given in Table 4-1. Oxygen-fluid contact takes place in a single-pass, counter-flow configuration.

The oxygen-loaded emulsion is then collected in a container where the oxygen content is measured using an oxygen probe (Biological Oxygen Monitor, YSI Model 5300A, YSI Incorporated, USA). Each experiment yields only one data point for the membrane oxygenator. The emulsion is pumped through the oxygenator at a fixed rate, and the outlet oxygen concentration is measured until it stabilizes. This stabilized reading is the oxygen concentration at steady state in the emulsion for the specific residence time (which is determined by the pumping speed). By varying the pumping speed and taking several stabilized readings, an oxygen loading curve for a specific emulsion is generated.

A review of measurement of oxygen transfer in the absence and presence of microorganisms is given by Sobotka et al. (1982). In this review, the different methods for measurement of oxygen transfer and determination of mass transfer coefficients are discussed, including the methods used in the gas-sparged (“gassing-in liquid”) and membrane oxygenator (“steady state measurement in a continuous-flow system”) experiments.

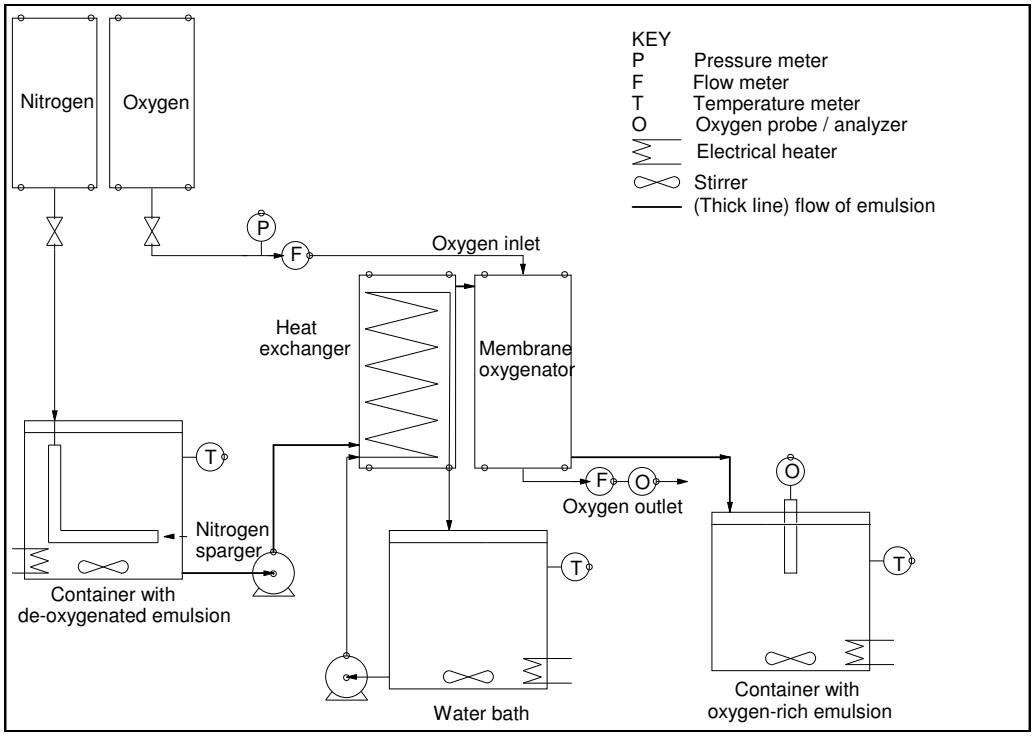

Figure 4-9. Membrane oxygenator experimental setup

In any experiment of this type, lag time of the measurement probe must be considered. The oxygen probes have lag times due to oxygen having to diffuse through the membrane and the probe electrolyte to the electrode surface. This lag time can cause incorrect determination of mass transfer coefficients.

The YSI 5300A Biological Oxygen Monitor used in this study reaches 90% of equilibrium value in 10 s, with a total stabilization time of 60 s (YSI, 2001). For the membrane oxygenator, only steady-state values were measured, and thus probe lag time was not a problem. For the gas-sparged oxygenator, 90% of equilibrium loading was reached after periods of between 400 s (~ 6 min) and 1200 s (20 min). Thus, it was concluded that probe lag time would not seriously affect oxygen loading profile determination.

4.4.2. Determination of experimental mass transfer coefficients

For the gas-sparged oxygenator, the mass transfer coefficient from gas to medium (k_{gm}) could be determined directly by performing oxygen loading experiments on the medium alone. With no PFOB, Equation 4-37 can be rewritten as follows:

$$\frac{dn_m}{dt} = Vk_{gm}a_{gm}\left(C_{m,g} - C_m\right) \tag{4-83}$$

Integrating and rearranging (similar to Sobotka et al., 1982:132):

$$\frac{V_m}{Va_{gm}} \ln\left(\frac{C_{m,g}}{C_{m,g} - C_m}\right) = k_{gm} t \tag{4-84}$$

Thus, a plot of the left-hand side of Equation 4-84 against time should result in a straight line with gradient k_{gm}. Figure 4-10 shows that straight lines were indeed obtained with the experimental data. For 0.5 ℓ/min oxygen flow, k_{gm} = 3.4×10^{-3} m/s (r^2=0.995), and for 1 ℓ/min, k_{gm} = 2.9×10^{-3} m/s (r^2=0.986).

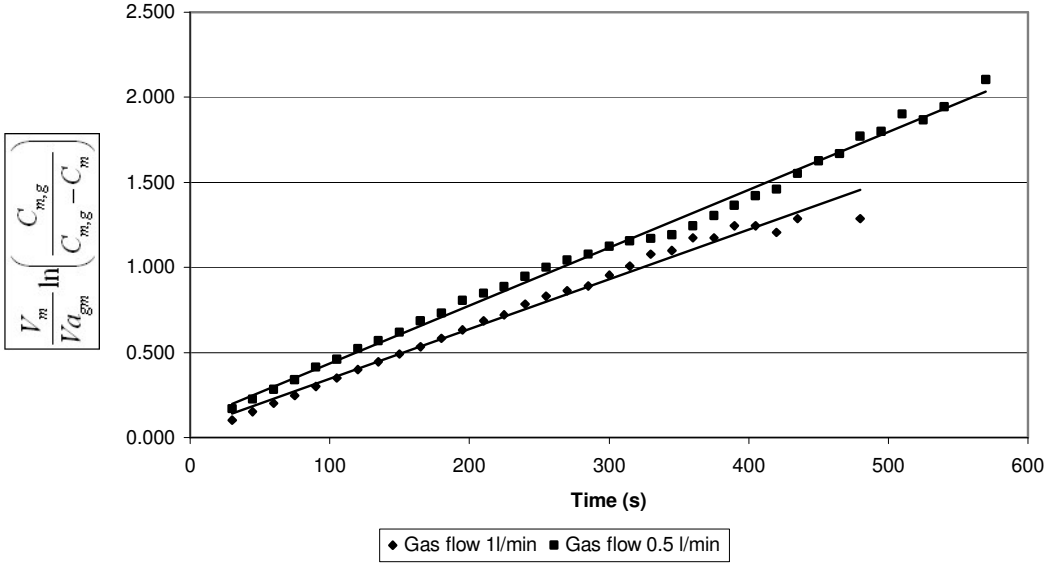

Figure 4-10. A plot of the left-hand side of Equation 4-84 against time (using experimental data for the background solution) for the gas-sparged oxygenator results in a straight line, with gradient k_{gm}.

For the membrane oxygenator, an experiment with background solution also yielded a straight line when plotted against the same function (Figure 4-11). The mass transfer coefficient, k_{bm}, was determined as 3×10^{-5} m/s (the gradient in the plot), with the coefficient of determination r^2=0.952.

Goerke, Leung and Wickramasinghe (2002:2042) determined the following correlation for external flow across fibres in a hollow fibre blood oxygenator:

$$Sh = 0.39\,\mathrm{Re}^{0.59}\, Sc^{0.33} \tag{4-85}$$

When this equation is evaluated at the UP-CSIR experimental conditions, it yields a value of k_{bm} = 2.5×10^{-5} m/s. This value is very close to the experimental value obtained by the UP-CSIR team (3×10^{-5} m/s). Schneider et al. (1995:843) found experimental values ranging form 1.5×10^{-5} to 3×10^{-5} m/s, again in good agreement with the UP-CSIR results.

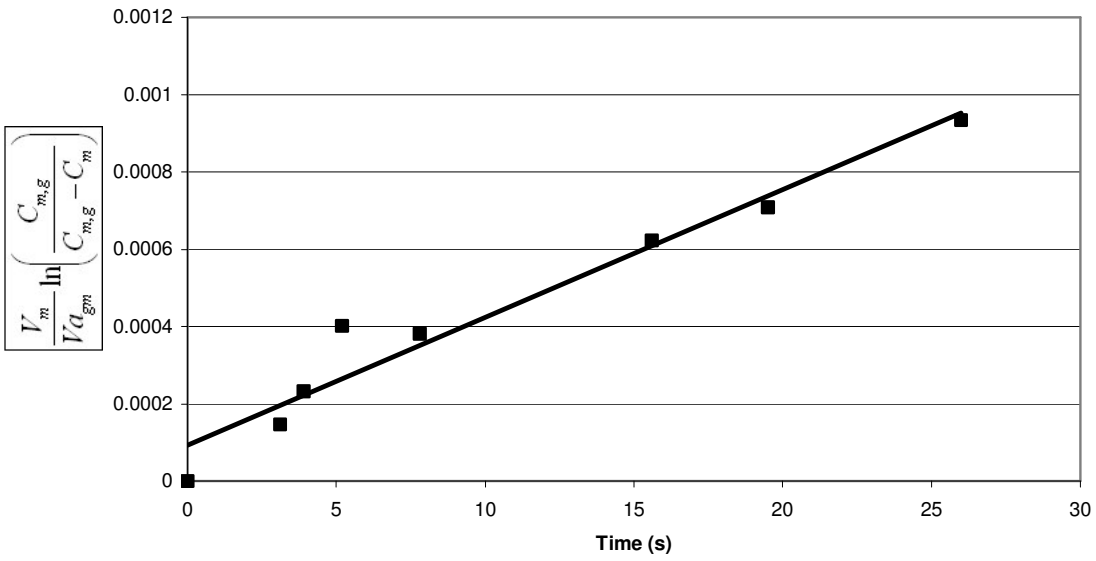

Figure 4-11. A plot of the left-hand side of Equation 4-84 against time (using experimental data for the background solution) for the membrane oxygenator results in a straight line, with gradient k_{bm}.

For the other mass transfer coefficients, rearrangement of the equations to obtain simple plots such as those above was not possible. Experimental values were determined by fitting the model to the experimental data through manipulation of the rate-determining mass transfer coefficient and least squares minimization.

The experimental overall volumetric mass transfer coefficient ($k.a$) for the gas-sparged oxygenator was 8×10^{-4} /s (rate-controlling step - $k_{gp}.a_{gp}$), while the comparable value for the membrane oxygenator was 1 /s (rate-controlling step – $k_{bp}.a_{bp}$), for a 0.2 PFOB volume fraction emulsion. The rate-determining mass transfer coefficients (k) were in the region of 1×10^{-3} m/s for both the gas-sparged and membrane oxygenators, with the big difference in volumetric mass transfer coefficients caused by the much higher specific surface area of the membrane oxygenator compared to the gas-sparged oxygenator.

Yamamoto et al. (1994:454) found volumetric mass transfer coefficients ($k_{mp}.a_{mp}$) of 1.33 /s and 1.65 /s for 0.7 and 0.9 PFOB volume fractions respectively (PFOB as the continuous phase with unemulsified water droplets dispersed in them). Their mass transfer coefficients were in the region of 1×10^{-4} m/s. In the UP-CSIR models, mass transfer from medium to PFOB ($k_{mp}.a_{mp}$) was not the rate-determining step, due to the very large interfacial surface area between medium and PFOB (see next section). Values of $k_{mp}.a_{mp}$ ranged from 200 to 5×10^{5} /s. The much lower values obtained by Yamamoto et al (1994:454) were due to their very large droplet sizes, ranging from 300 to 700 µm. This translates into much lower interfacial surface area for mass transfer.

4.4.3. Model results and discussion

Base parameter sets

In order to investigate the influence of a range of variables on the theoretical oxygen load rates, base sets of parameters were defined for both the gas sparger and membrane oxygenator. When the influence of a specific variable was investigated, all other parameters were kept constant at the base values. The base parameter sets for the gas sparger and the membrane oxygenator are listed in Table 4-4.

Table 4-4. Base parameter sets for gas-sparged and membrane oxygenators

Gas-sparged oxygenator			**Membrane oxygenator**		
Parameter	**Value**	**Units**	**Parameter**	**Value**	**Units**
Thin film thickness	2	µm	Thin film thickness	2	µm
Oxygen pressure	0.85	bar	Oxygen pressure	0.85	bar
Volume of oxygenator	0.48	ℓ	Hollow fibres / volume	4.15×10^{7}	m^{-3}
Oxygenator diameter	0.075	m	Length of fibres	0.073	m
Gas flow rate	0.5	ℓ/min	Fibre internal diameter	280	µm
Orifices	5		Fibre wall thickness	50	µm
Orifice diameter	1	mm	Fibre porosity	0.5	
Impeller diameter	50	mm	Total hollow fibre surface area	0.33	m^2
Impeller rotational speed	2000	rpm	Process volume	26	mℓ
			Process fluid velocity	0.015	$m.s^{-1}$

Oxygen-carrying capacity of PFOB emulsions

One of the fundamental questions asked in this study is: What is the impact of emulsion viscosity on the mass transfer characteristics of the PFOB emulsions? Figure 4-12 illustrates this question. In terms of oxygen carrying capacity, there is an obvious advantage in using higher PFOB volume fraction emulsions, but viscosity increases dramatically at higher PFOB volume fractions. So what would be the optimum PFOB volume fraction for oxygen carrying applications? This question is considered in the next section.

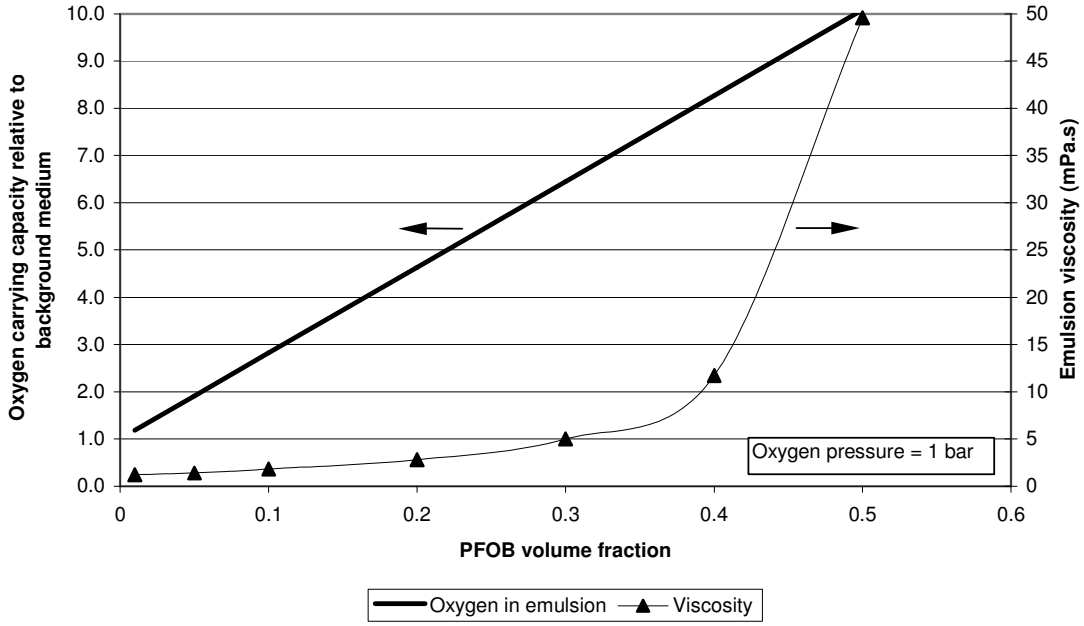

Figure 4-12. Oxygen carrying capacity improves with increasing PFOB volume fraction, but emulsion viscosity increases dramatically at higher PFOB volume fractions.

Rate-determining steps in mass transfer

With mass transfer steps in series, the slowest step is rate determining. With mass transfer steps in parallel, the fastest step is rate determining. Figure 4-13 shows a graphical representation of the mass transfer pathways for the gas-sparged and membrane oxygenators, with theoretical rate determining steps in bold. The volumetric mass transfer coefficient values indicated in the figure were calculated for a 0.2 PFOB volume fraction emulsion, with base parameters as given in Table 4-4.

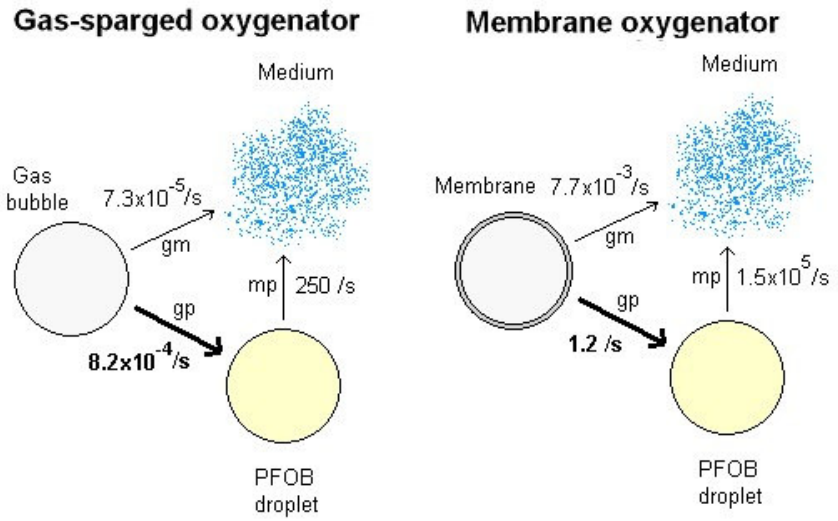

Figure 4-13. Mass transfer rate from gas to PFOB and membrane to PFOB are rate determining according to the theoretical model results. Subscripts indicate: gp = gas-PFOB; gm = gas-medium; mp = medium-PFOB.

A number of observations can be made from Figure 4-13:

- For both oxygenators, mass transfer from the gas surface to the PFOB droplets in the boundary layer is the rate-determining step.
- The mass transfer between PFOB droplets and medium is so fast that equilibrium can be assumed. This is largely due to the very large interfacial surface area between the tiny droplets and the medium. Shah and Mehra (1998:183) came to the same conclusion.
- There is a large difference between the theoretical $k_{mp}a_{mp}$ for the gas-sparged and membrane oxygenators. This is due to the different correlations used to estimate k_{mp}. Inaccuracy in estimation of this value does not have a large influence on the overall mass transfer rates, as it is not the rate-determining step.
- Mass transfer rates from membrane to PFOB and membrane to medium is much higher than the corresponding rates from gas bubble to PFOB and gas bubble to medium. This is due to the much larger interfacial surface areas in the membrane oxygenator ($a_b \approx 3600$ m^2/m^3) compared to the gas-sparged oxygenator ($a_g \approx 2.5$ m^2/m^3). The increased interfacial surface area is the main contributing factor to the improved oxygen mass transfer performance of the membrane oxygenator compared to the gas-sparged oxygenator.

From the data, one can identify potential options for improvement of oxygenator mass transfer performance. For the gas sparger, a decrease in gas bubble size would be a major improvement factor (this is confirmed by the model results in Figure 4-21, as discussed later). This can be done by changing the gas-sparger design to get decreased bubble size and better dispersion of bubbles through the oxygenator. Even with highly optimized gas-sparger configurations, the bubble surface area density cannot approach the surface area density levels obtained with membrane oxygenators.

It would be difficult to improve the mass transfer rates in the membrane oxygenator (as one would expect for a commercially available system). Factors that could improve mass transfer rates are an increase in partial oxygen pressure (with accompanying increase in trans-membrane pressure drop), increase in membrane surface area and possibly a decrease in PFOB droplet size. Increasing the partial oxygen pressure has mechanical/structural integrity implications and is thus limited by the design of the system and material properties.

Increasing membrane surface area is continuously being pursued by membrane oxygenator manufacturers, but is limited by available membrane manufacturing technology and material properties. Decreasing the PFOB droplet size further would not necessarily have a large impact on mass transfer rates, if it is not the rate-limiting factor. Also, limitations in current manufacturing methods preclude much further decrease in droplet size. Another option is to use secondary flow effects to disrupt the concentration boundary layer on the liquid side of the oxygenator (Goerke, Leung and Wickramasinghe, 2002:2035).

Oxygen mass transfer rate comparison: gas-sparged vs. membrane oxygenator

Figure 4-14 shows experimental and theoretical results obtained for oxygen loading of a 0.2 PFOB volume fraction emulsion with SMD 0.2 µm. Very good agreement was obtained between theoretical and experimental results. The superior oxygen mass transfer performance of the membrane oxygenator compared to the gas-sparged oxygenator is evident.

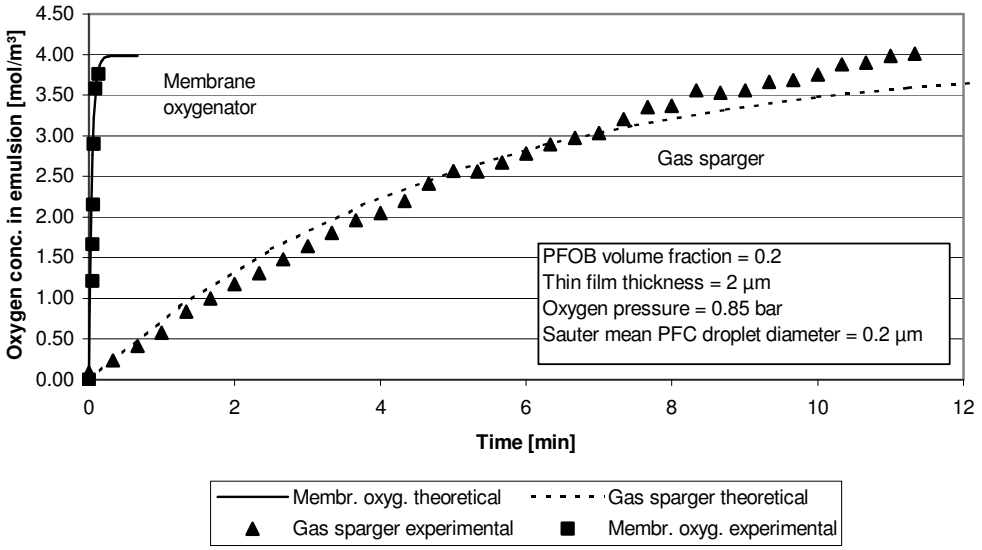

Figure 4-14. Experimental and theoretical oxygen loading profiles obtained in the gas-sparged and membrane oxygenators show good agreement between experimental and theoretical results, as well as much higher mass transfer rates for the membrane oxygenator compared to the gas-sparged oxygenator.

Influence of PFOB volume fraction

Figure 4-15 shows theoretical and experimental oxygen loading curves for different PFOB volume fractions in the gas-sparged oxygenator. There is good agreement between theoretical and experimental trends. With increase in PFOB volume fraction, total emulsion oxygen concentration increases. Mass transfer rates (gradient of the curves) also increase with increase in ϕ_p, but experimental values at higher ϕ_p are lower than theoretical predictions. Similar trends were observed for the membrane oxygenator, as shown in Figure 4-16. Membrane oxygenator experimental data tended to be more erratic than data for the gas-sparged oxygenator.

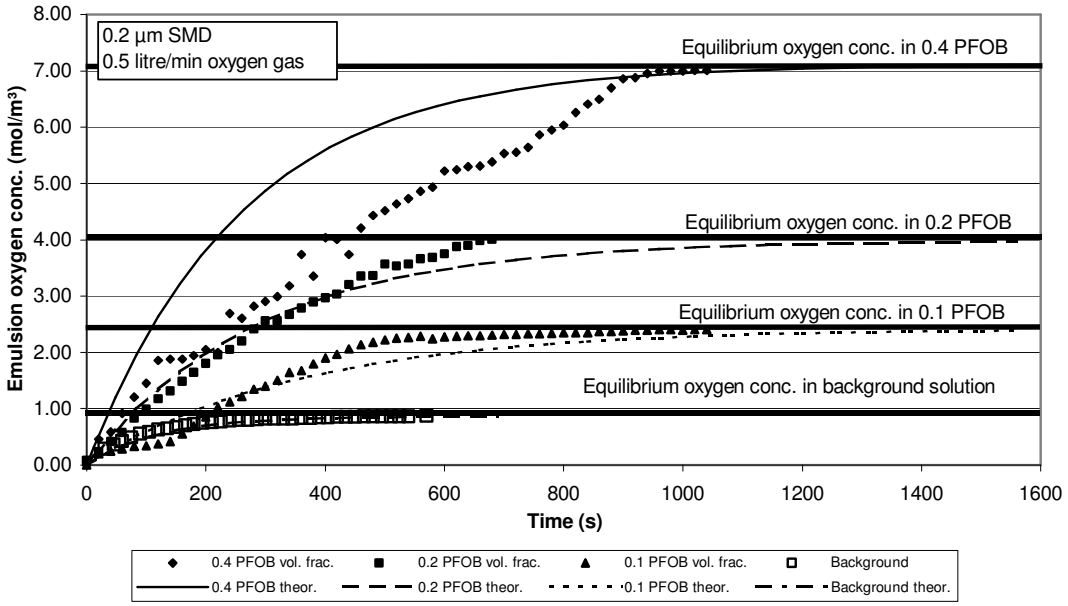

Figure 4-15. Increase in PFOB volume fraction results in increased oxygen content and mass transfer rates for the gas-sparged oxygenator.

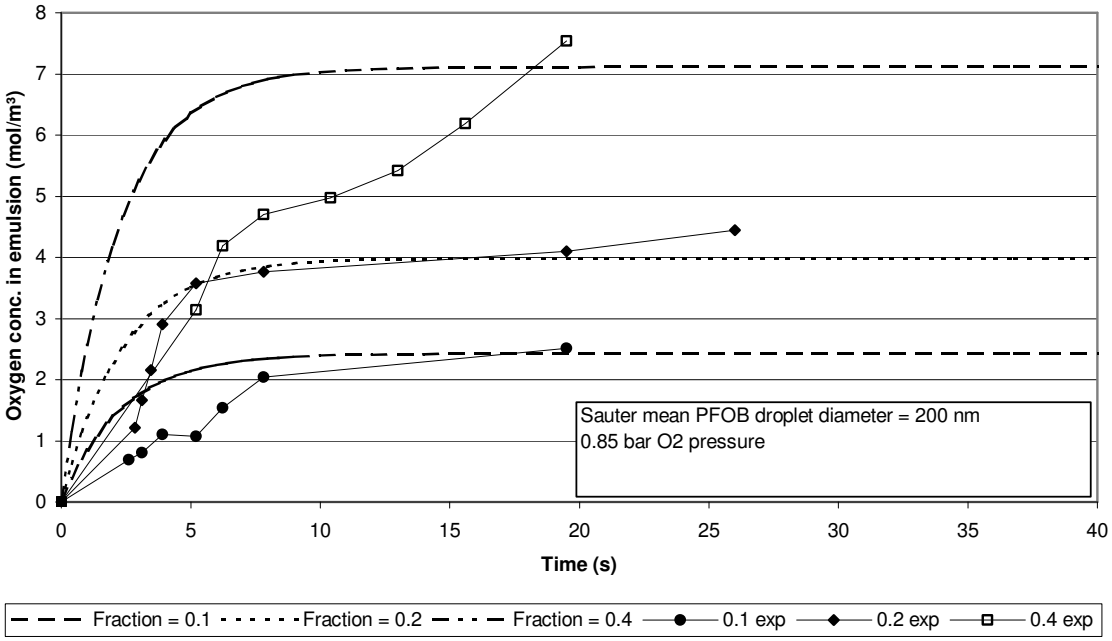

Figure 4-16. Increase in PFOB volume fraction leads to increased oxygen content and mass transfer rates in the membrane oxygenator.

As the oxygen loading rates are liquid-film controlled (Goerke, Leung and Wickramasinghe, 2002:2035; McMillan and Wang, 1992:287; McMillan and Wang, 1987:574), oxygen transfer rates would not be enhanced if PFOB droplets did not penetrate the boundary layer (surrounding e.g. a gas bubble or hollow fibre). Figures 4-

15 and 4-16 clearly show that improved oxygen loading rates were obtained with increased ϕ_p (compared to background medium), which could be plausibly explained by PFOB droplets penetrating the boundary layer.

Possible reasons for the lower than predicted mass transfer rates at higher ϕ_p are discussed in the next paragraphs.

Influence of viscosity

The UP-CSIR model predicts that viscosity does not have a large effect on the mass transfer rates for the membrane oxygenator. Model runs yielded a very small difference in predicted oxygen load rates for a variation in viscosity from 5 mPa.s to 1000 mPa.s (at constant ϕ_p). For the gas-sparged oxygenator, a decrease in mass transfer rates was predicted for large increases in emulsion viscosity at constant ϕ_p (Figure 4-17). This is mainly due to the decreased gas hold-up predicted at higher viscosity (see Equation 4-54) – this leads to decreased gas-liquid interfacial surface area for mass transfer.

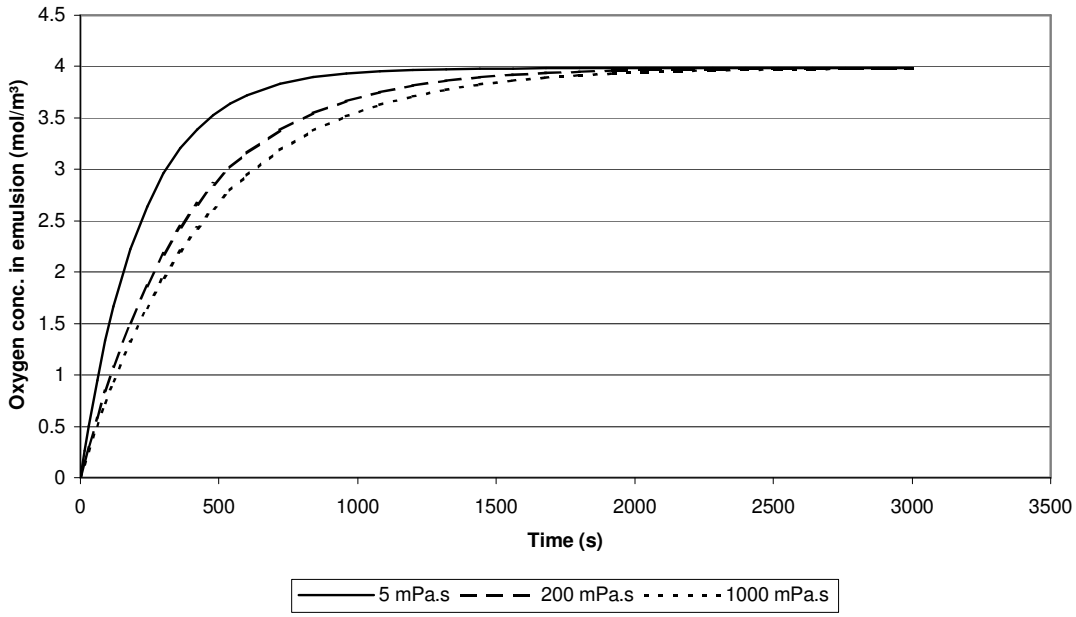

Figure 4-17. The theoretical model for the gas-sparged oxygenator predicts a slight decrease in mass transfer rates with large increases in viscosity.

It would be difficult to verify the effect of viscosity on the mass transfer rates directly with experiments – the viscosity cannot be changed without changing other emulsion properties such as ϕ_p. However, the experimental oxygen loading curves for different ϕ_p (Figures 4-15 and 4-16), indicate that for both the gas-sparged and membrane oxygenators, predicted load rates corresponded well with experimental rates for $\phi_p = 0.1$ and 0.2, but were significantly lower than theoretical values at $\phi_p = 0.4$.

It is interesting to note that for both the gas-sparged and membrane oxygenators, the load rates at ϕ_p = 0.4 are similar to those at ϕ_p = 0.2. This points toward a rate-limiting factor coming into effect at ϕ_p = 0.4.

The rate-limiting effect could be explained by one of three mechanisms:

1. The increased emulsion viscosity causes decreased replacement rates of fluid elements in the boundary layer, counteracting the increased concentration of PFOB droplets in the boundary layer.
2. The concentration of PFOB droplets in the boundary layer reaches a 'saturation' level at ϕ_p around 0.2, and thus further increase in ϕ_p does not increase the mass transfer rate. This could be due to the non-uniform dispersion of dispersed phases in small diameter (< 300 μm) flow paths (Patel and Mehra, 1998:146). Particles tend to migrate to the centre of the flow path, and this tendency increases with increase in particle size. Thus, the volume fraction of dispersed phase is lower near the wall than in the centre of the flow path.
3. No further increase in effective interfacial surface area between PFOB emulsion droplets in the boundary layer and the membrane or gas bubble is achieved above a certain ϕ_p, even though overall PFOB concentration in the boundary layer increases.

The most probable explanation is that the increased emulsion viscosity causes decreased replacement rates of fluid elements in the boundary layer, limiting the rate of mass transfer.

Ju, Lee and Armiger (1991a:327) developed a theory that predicted that oxygen transfer enhancement would increase for increasing ϕ_p. They defined this oxygen transfer enhancement with an 'oxygen transfer enhancement factor', E, as follows:

$$E = \frac{(k.a)_e (H_{g-l})_e}{(k.a)_m (H_{g-l})_m} \tag{4-86}$$

where e denotes the emulsion, and m the medium without emulsion. Thus, in the emulsion, the mass transfer coefficients and Henry's coefficients for the continuous and dispersed phases are lumped into single coefficients.

The lumping of coefficients is dangerous, as it implies that a homogenous fluid m is replaced with a homogenous fluid e, which is not true on the micro scale. It also implies that PFOB droplets are homogenously distributed between the bulk medium and the boundary layer. Doubts regarding this 'lumped coefficient' approach were also expressed by Shah and Mehra (1998:182).

Ju et al.'s model predicted almost a linear increase in E for increase in ϕ_p. What they did find experimentally, however, was an increase in E from 0.1 to 0.15 PFOB volume fraction, and then E did not increase further with further increase in ϕ_p to 0.25.

This finding correlates with the observation made above regarding no further increase in the mass transfer rates above a ϕ_p of 0.2. Ju et al. contributed this stabilization in the value of E to viscosity effects, but as mentioned earlier, it could also be due to some other rate-limiting mechanism related to the boundary layer.

Influence of PFOB droplet size

PFOB droplet size influences the interfacial surface area available for mass transfer. Figures 4-18 and 4-19 show the influence of PFOB SMD on theoretical and experimental oxygen mass transfer rates for the gas-sparged and membrane oxygenators, respectively. With increase in droplet size, mass transfer rates decrease due to the decreased interfacial surface area.

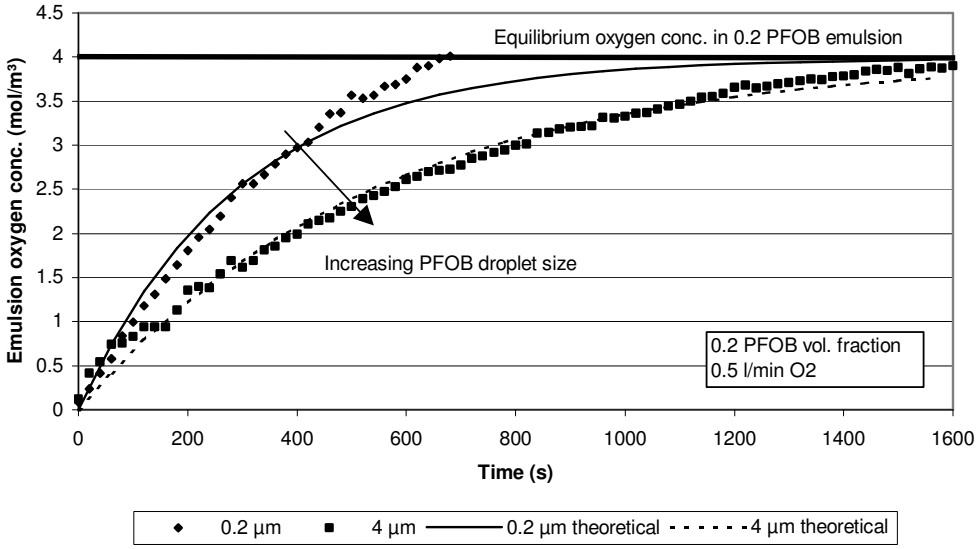

Figure 4-18. Theoretical and experimental oxygen mass transfer rates decrease with increase in PFOB droplet size for the gas-sparged oxygenator.

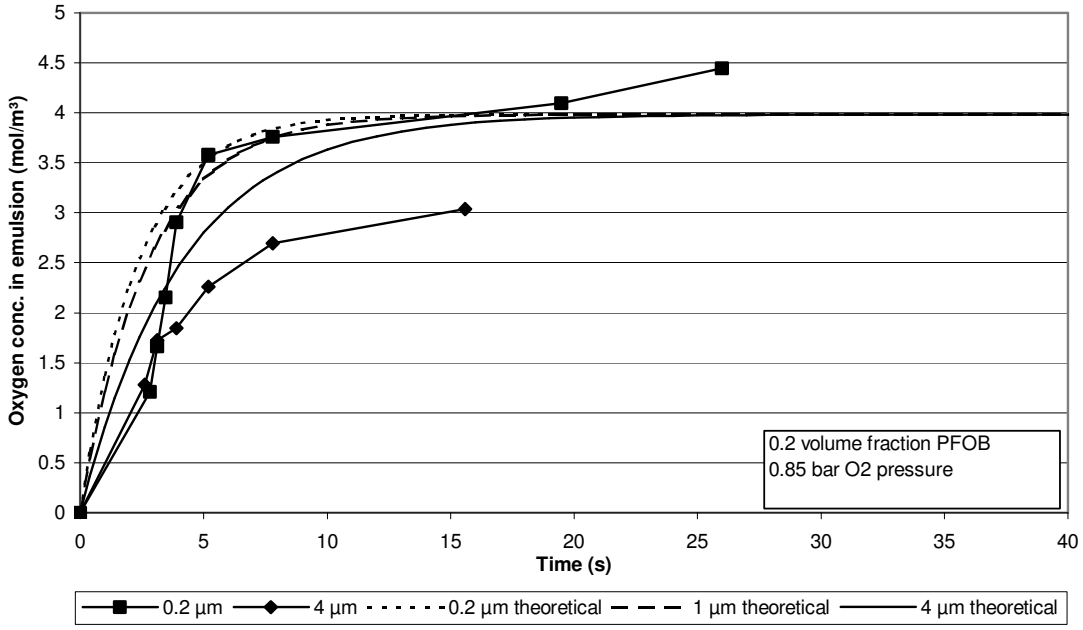

Figure 4-19. Theoretical and experimental oxygen mass transfer rates decrease with increase in PFOB droplet size for the membrane oxygenator.

Gas sparger parameters: gas flow rate and gas bubble size

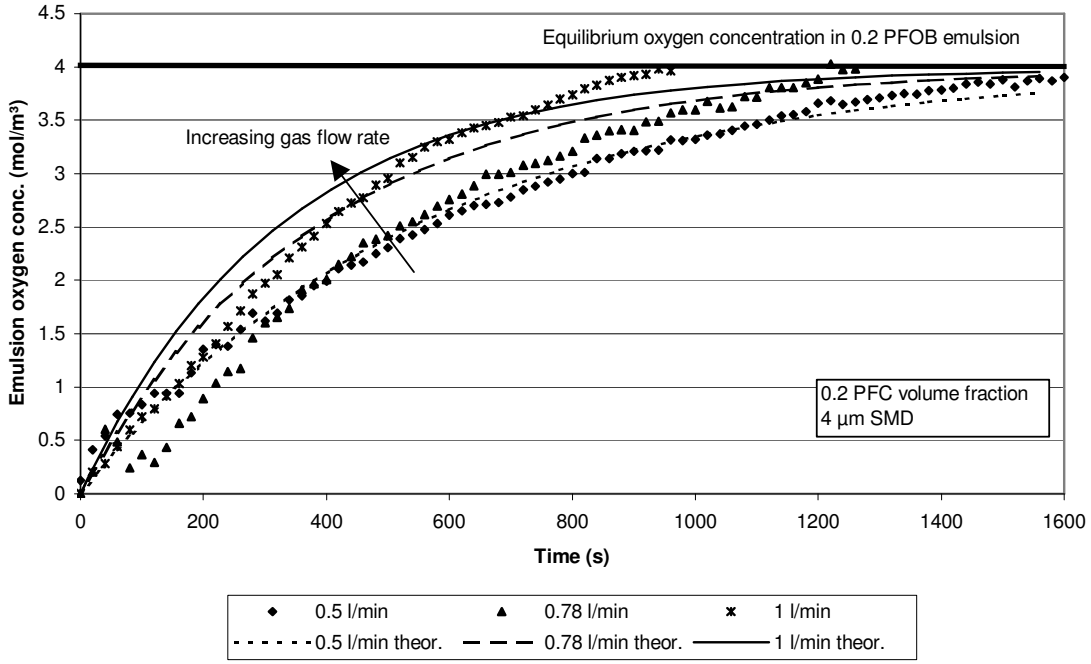

Figure 4-20. Increase in gas flow rate leads to increase in oxygen load rates for the gas-sparged oxygenator.

For the gas sparger, increased gas flow rate and decreased gas bubble size improves oxygen mass transfer rates (Figures 4-20 and 4-21, respectively). Increased gas flow rate leads to an increase in number of bubbles in the sparger at any single time, and thus interfacial surface area for mass transfer is increased (see Equation 4-54 – gas hold-up increases with increased gas flow rate). Decreased gas bubble size has the same effect – an increase in interfacial surface area, leading to an increase in mass transfer rates.

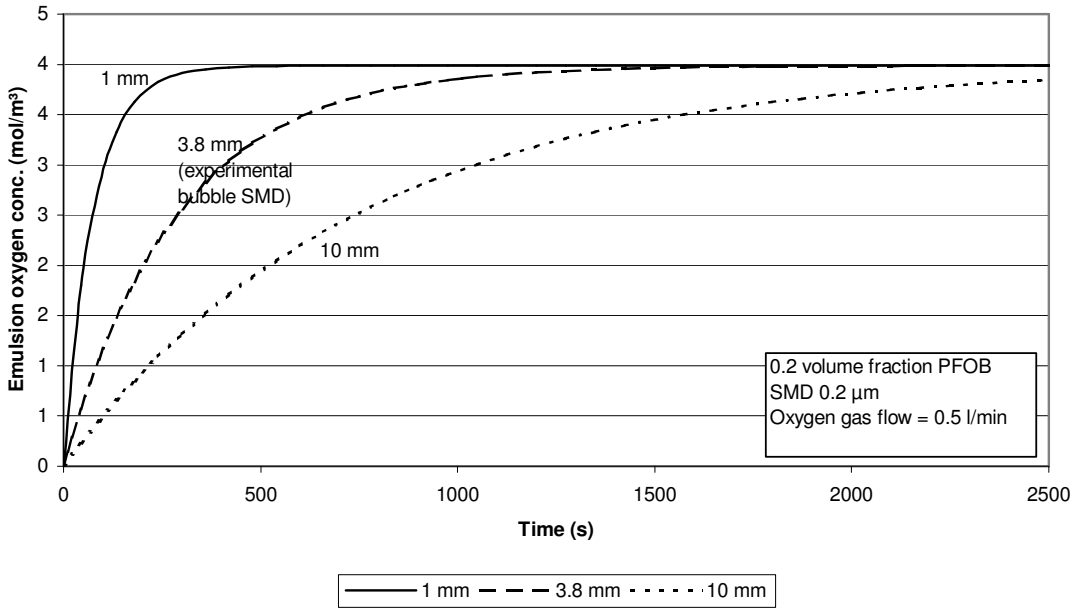

Figure 4-21. Increased gas bubble size theoretically leads to decreased mass transfer rates for the gas-sparged oxygenator.

Membrane oxygenator parameters: emulsion flow rate

In generating the experimental oxygen loading data for the membrane oxygenator, an important assumption is made – that the emulsion flow rate does not have a significant impact on mass transfer rates, as the mass transfer is liquid-film controlled (McMillan and Wang, 1992:287). As oxygen content profile could not be measured along the length of the membrane oxygenator (only exit oxygen concentration is measured), a profile had to be obtained by another approach. With the UP-CSIR experiments, emulsion flow rate was varied to obtain different average emulsion residence times. The steady-state oxygen content was then determined for each different flow rate. From this data, a plot of emulsion oxygen content vs. emulsion average residence time is obtained. This profile is assumed to be similar to the actual oxygen content profile along the length of the oxygenator during steady-state operation.

To verify this theoretically, oxygen loading profiles at different emulsion flow rates were calculated for the membrane oxygenator (Figure 4-22). At least theoretically, emulsion flow rate does not have a significant influence on the oxygen loading profile over the range investigated (1 to 20 s residence times). This is due to the

fact that the model predicts diffusion through the thin liquid film as rate controlling, and the film thickness in the model does not change with change in emulsion flow rate.

One must be careful not to incorrectly interpret this graph. The fact that the loading profiles do not change significantly, does not mean that the oxygen content of the emulsion exiting the oxygenator would be the same, no matter what the flow rate. With increase in emulsion flow rate, average residence time in the oxygenator decreases, and emulsion oxygen content will be correspondingly lower (read off from the graph at a decreased time).

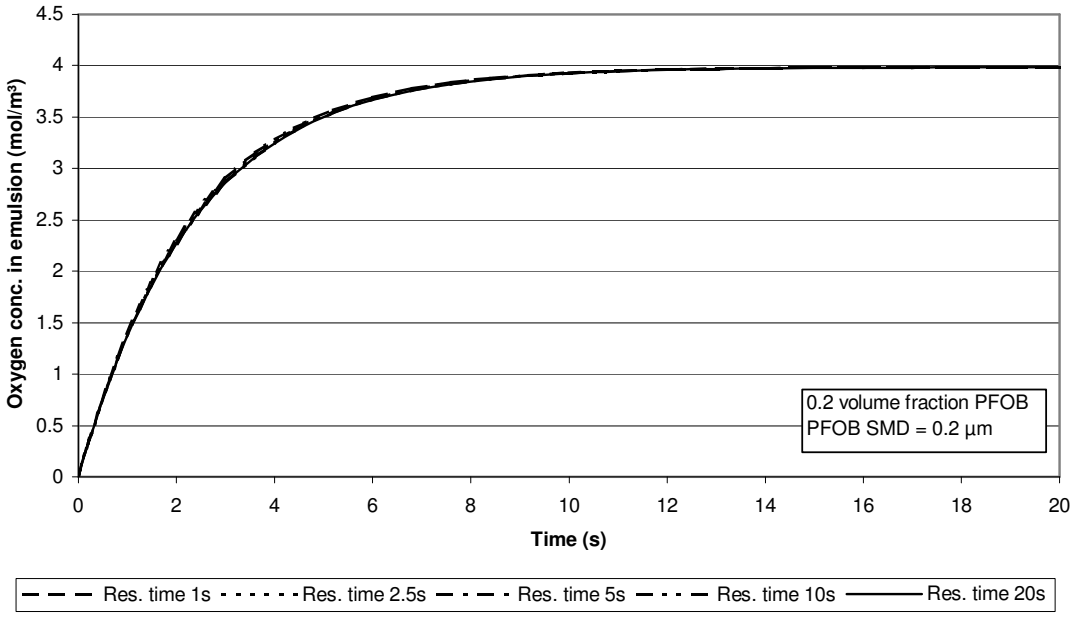

Figure 4-22. Theoretically, emulsion flow rate does not have a significant influence on oxygen loading profiles in the membrane oxygenator.

Experimental verification of this assumption would be difficult. A positive indication is that experimental data does generally follow the same profile as the theoretical data, even though there is considerable scatter.

Influence of calculation method

As discussed in Section 4.3.4, three different calculation methods were used for the membrane oxygenator (these methods were summarized in Table 4-3). The results from the different methods were almost identical (Figure 4-23).

Some of the equations/correlations used in the calculations are of doubtful quality – e.g. while Equation 4.69 is well supported by experiment, Equation 4.71 is not (Cussler, 2003). The effect of this variable quality on the model results is not very high, as the rate-determining step is predicted by the model to be diffusion through a thin film on the liquid side from membrane to PFOB, and this coefficient is not calculated using the said

correlations. This also explains the small variation in predicted mass transfer rates from the three different calculation methods. That said, this very result from the model could be a contributory factor to the difference in predicted mass transfer rates and experimental mass transfer rates at higher PFOB volume fraction.

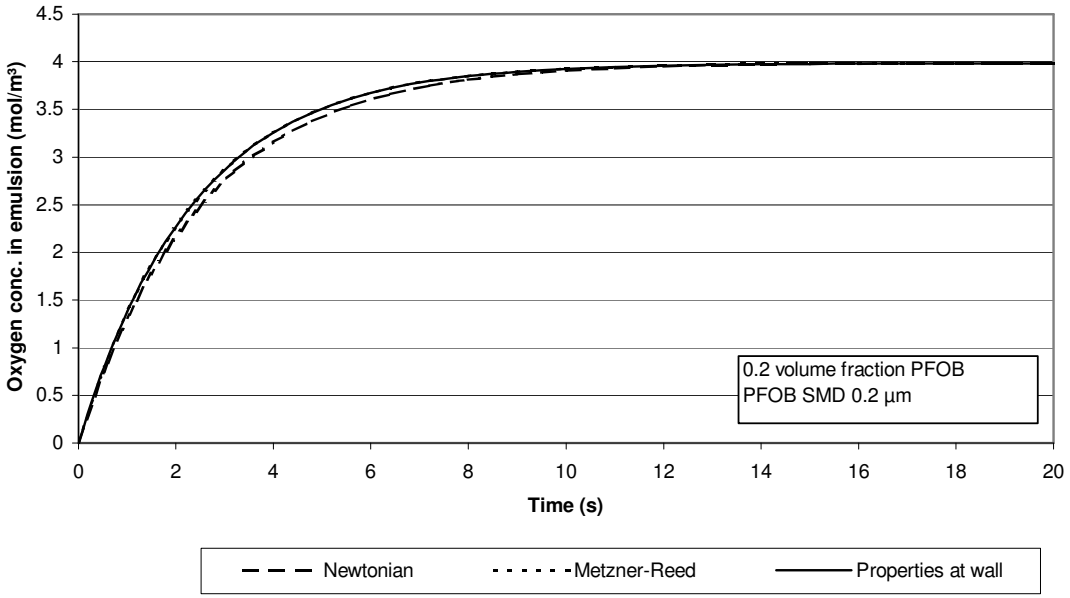

Figure 4-23. The different calculation methods for the membrane oxygenator yielded almost identical results.

Thin film thickness

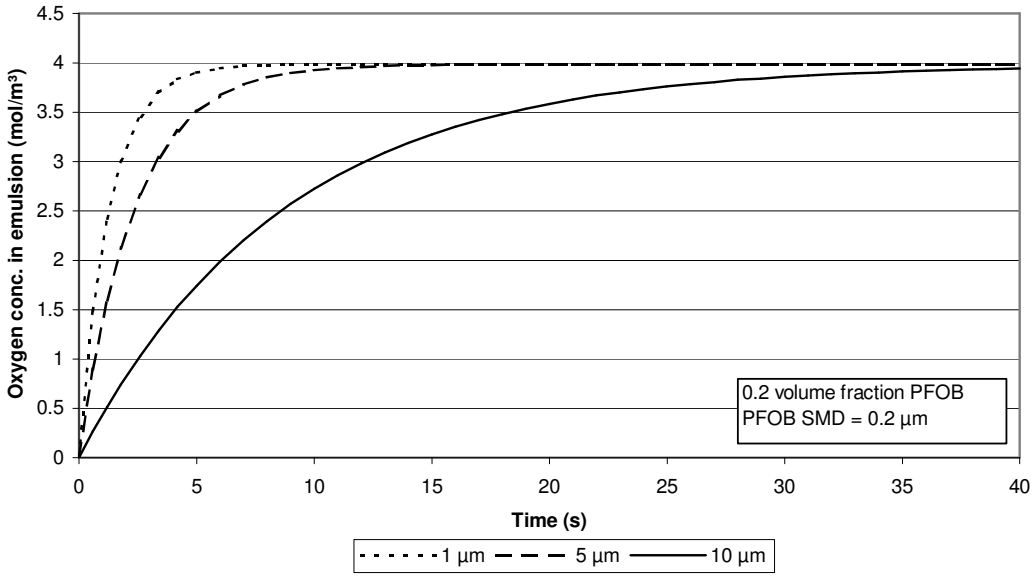

Figure 4-24. Increase in thin film thickness leads to large decreases in mass transfer rates for the membrane oxygenator.

One of the input parameters in the mass transfer models is the thickness of the thin film between the PFOB droplets in the boundary layer and the surface of the gas bubble or membrane. As the theoretical rate-determining step is diffusion through this film, the thickness of the thin film is a critical input parameter. This is illustrated in Figure 4-24, where theoretical mass transfer rates decrease dramatically with increase in thin film thickness for the membrane oxygenator.

The thin film thickness used in all other model calculations was 2 µm. The thickness of the thin film was calculated from penetration theory to be between 5 and 10 µm (McMillan and Wang, 1987:574). However, better correlation between UP-CSIR theoretical and experimental data was obtained for a thin film thickness of 2 µm.

Model predictions made with a thin film thickness of 2 µm resulted in accurate estimates of mass transfer performance for both the gas sparger and membrane oxygenator, including prediction of the influence of varying a number of different parameters. This would seem to indicate that it is a good approximation of the physical reality.

BALSS bioreactor oxygen requirements

Using the determined mass transfer properties of the PFOB emulsions, some basic design calculations can be done for the UP-CSIR BALSS bioreactor. Table 4-5 lists some of the inputs used in the design calculations.

Table 4-5. Input parameters for basic bioreactor design calculations

Parameter	Symbol	Value	Units	Source
Min. number of porcine hepatocytes for adult liver support	N_h	1×10^{10}	cells	Morsiani et al., 2002:985
Maximal oxygen consumption of porcine hepatocytes	$\dot{n}_{h,\max}$	0.9	nmol / s / 10^6 cells	Balis et al., 1999:49
Steady-state oxygen consumption of porcine hepatocytes	$\dot{n}_h$	0.31	nmol / s / 10^6 cells	Balis et al., 1999:49 (Ledezma et al., 1999:59 report a value of 0.25 nmol/s/10^6 cells)
Maximal albumin secretion rate – rat hepatocytes		60	µg / 10^6 cells / day	Glicklis et al., 2000:344
Maximal urea secretion rate – rat hepatocytes		100	µg / 10^6 cells / day	Glicklis et al., 2000:344
Albumin secretion rate - porcine hepatocytes in culture		470	µg / 10^6 cells / day	Unpublished data - cell count through Trypan blue exclusion; average data for 4 pigs

Parameter	Symbol	Value	Units	Source
Maximal albumin secretion rate - porcine hepatocytes		180	µg / 10^6 cells / day	Bader, et al., 2000:103
Maximal urea secretion rate - porcine hepatocytes		2100	µg / 10^6 cells / day	Bader, et al., 2000:102
Typical hepatocyte spheroid diameter	d_{hs}	100	µm	Glicklis et al., 2000:344
Hepatocyte diameter – porcine hepatocytes	d_{hp}	20	µm	Zajicek, 1992:410
Typical oxygen mass transfer coefficient	k_{ph}	1×10^{-3}	m/s	From Section 4.4.2
PFOB volume fraction	ϕ_p	0.2		
PFOB SMD	d_{sp}	0.2	µm	
Oxygen load level of PFOB emulsion exiting oxygenator		70	%	
Equivalent oxygen concentration in plasma at cell surface	C_{cell}	0	mol/m^3	
Polyurethane foam porosity	ε_{PU}	0.967		Supplier (CH Chemicals) data sheet for Polythane EX2048
Polyurethane density	ρ_{PU}	1200	kg/m^3	Supplier (CH Chemicals) data sheet for Polythane EX2048
Polyurethane foam specific surface area	a_{PU}	1.2×10^4	m^2/m^3	Supplier (CH Chemicals) data sheet for Polythane EX2048
Cells currently seeded in UP-CSIR BALSS		2×10^9	cells	

Assumptions made in basic design calculations:

- Available cell surface area for mass transfer is only the projected external spheroid surface area.
- All free volume in the bioreactor is filled with the plasma-PFOB emulsion blend.
- Mass transfer from plasma to cells is insignificant compared to mass transfer from PFOB to cells (based on experimental results reported earlier).
- The maximal oxygen consumption rate is used in the calculations.
- PFOB-hepatocyte interfacial surface area is calculated from (the lesser value of projected surface area of PFOB and projected external spheroid surface area)×(ϕ_p/0.64).

Equations used in these calculations are given in Appendix D.

Results from the calculation for the current 250 mℓ UP-CSIR BALSS bioreactor and current circulation rate of 600 mℓ/min are given in Table 4-6. It seems from the results that the current bioreactor volume is sufficient for

10^{10} hepatocytes, both in terms of volume and surface area requirements. However, the required surface area is strongly dependent on spheroid size.

BALSS bioreactor volumes should be kept as small as possible. Large process volumes for the total BALSS circuit could cause hypotension in the patient being treated – this has been the case in a number of systems, such as those from the Amsterdam Medical School (Flendrig et al., 2002:956) and the Excorp Medical system (Mazariegos et al., 2001:471), but Mazariegos et al. (2001:471) also reported that the hypotension was transient and responded well to an IV fluid bolus at the start of perfusion. Nevertheless, priming of the BALSS circuit with blood plasma before the start of treatment seems a highly probable requirement.

The adult human liver typically secretes 120 mg/kg/day albumin (Bircher et al., 1999:358) or 8.4 g/day for an adult of 70 kg; and 30 g/day urea (Bircher et al., 1999:326). The estimated secretion rates for the bioreactor are 1.8 mg/day albumin and 21 g/day urea for a cell loading of 10^{10} porcine hepatocytes (see Table 4-6), which is 21.4% and 70.0% of normal adult liver albumin and urea secretion levels, respectively. This is within the estimated range of 20 to 40% of normal adult liver function required for liver support in acute liver failure, and confirms estimates by other authors of no. of cells required: $1.5x10^{10}$ (Allen and Bhatia, 2002:451), $2x10^{10}$ (McClelland, MacDonald and Coger, 2003:13) and $1.5–4.5x10^{10}$ (Morsiani et al., 2002:989).

In terms of oxygen supply, it seems that the current circulation rate of 600 ml/min of oxygenated PFOB emulsion-plasma blend is sufficient, both in terms of total oxygen carried and achievable mass transfer rates. Mass transfer rates decrease through the bioreactor as the oxygen gets depleted. The theoretical oxygen transfer rate calculated from the experimental mass transfer coefficient ranges from 1.8 to 2.6 mol/ℓ/hr for a 0.2 PFOB volume fraction emulsion with SMD 0.2 µm. The importance of droplet size is illustrated when comparing this value to the maximum oxygen transfer rate of about 0.25 mol/ℓ/hr found by McMillan and Wang (1992:292) for droplets with SMD between 50 and 250 µm.

Without the addition of PFOB (and assuming a similar mass transfer coefficient from plasma to hepatocytes), a circulation rate of **2.8 ℓ/min** would be required to provide the equivalent mass transfer for 1×10^{10} hepatocytes. This value compares well with the calculated value of 5 ℓ/min for $2.5x10^{10}$ hepatocytes given by Morsiani et al. (2002:990). Thus, required flow rates for oxygen supply can be reduced by a factor 4.7 through the use of a 20 v/v% PFOB emulsion. This factor is slightly higher than the oxygen solubility ratio of 4.5 of a 20 v/v% PFOB emulsion compared to plasma alone. The larger ratio is due to the higher concentration gradient maintained throughout the bioreactor by using a PFOB emulsion.

This illustrates the critical importance of the addition of PFOB and the role it plays in optimizing bioreactor efficiency.

Table 4-6. Results from basic design calculation for UP-CSIR BALSS bioreactor

Result area	Parameter	Value	Units
Reactor size	Percentage of foam substrate surface area covered by spheroids	32.7	%
	Percentage of reactor volume taken up by spheroids / hepatocytes	26.2	%
	Percentage of 'open' volume in bioreactor	70.5	%
Cell function	Estimated maximum albumin secretion rate – rat hepatocytes	0.6	g/day
	Estimated maximum albumin secretion rate – porcine (UP-CSIR)	4.7	g/day
	Estimated maximum albumin secretion rate – porcine (Bader et al., 2000)	1.8	g/day
	Estimated maximum urea secretion rate – rat hepatocytes	1.0	g/day
	Estimated maximum urea secretion rate – porcine (Bader et al., 2000)	21.0	g/day
Oxygen supply	Hepatocyte oxygen requirements	0.032	mol/hr
	Oxygen supply in emulsion entering reactor	0.10	mol/hr
	Oxygen requirements as % of oxygen supply	32.3	%
	Mass transfer rate at entrance to bioreactor	0.928	mol/hr
	Mass transfer rate at exit to bioreactor	0.628	mol/hr
	Req. mass transfer rate as % of actual mass transfer rate: entrance	1.4	%
	exit	2.0	%

Another consideration in bioreactor design is the exposure of hepatocytes to shear stress. High shear stresses could damage cells or even dislodge them from the surface. It is reported that PFC's decrease mechanical damage to cells caused by gas-sparging or stirring and in bioreactors (Lowe et al., 1997:262,264).

In terms of shear stress, Ledezma et al. (1999:60) suggest a conservative maximum shear stress of 1 Pa. In the UP-CSIR BALSS bioreactor, a total pressure drop of approximately 10 kPa was measured over bioreactor, distributors and end connections. If a pressure drop of 5 kPa is assumed over the PU foam itself, a wall shear stress of 6.2 Pa is estimated (using $\tau_w = \Delta P A_{flow} / A_{surf}$). This is somewhat higher than the conservative maximum mentioned above, but more detailed calculation and experimentation is required to verify the results and test cell sensitivity to shear stress in the bioreactor. From a shear stress point of view, addition of PFOB to the system is highly beneficial, as it greatly reduces the required circulation rates to achieve sufficient oxygenation of the hepatocytes.

4.4.4. Conclusions

- The improved oxygen loading efficiency of membrane oxygenators over gas-sparged oxygenators was clearly illustrated, both experimentally and theoretically. Thus, a membrane oxygenator was selected for the UP-CSIR BALSS.

- The mass transfer models developed were sufficiently accurate to predict order-of-magnitude mass transfer rates, as well as the effect of a number of parameters on the mass transfer rate.
- Although the models were developed for specific oxygenator configurations, they can be adapted to other configurations, including modelling of oxygen delivery to cell culture systems, and the experimentally determined coefficients can be used to estimate required flow rates, reactor sizes, etc. (as was illustrated earlier with the calculations for the UP-CSIR BALSS).
- Further refinement of the models could improve accuracy. This could possibly take the form of experimental verification of the theoretical predictions regarding rate-determining step, and closer investigation regarding the exact mass transfer mechanisms involved.
- Definite improvement in both oxygen carrying capacity and oxygen mass transfer rates can be obtained by using PFOB emulsions instead of plasma/medium.
- Even though viscosity increases exponentially with increase in ϕ_p, higher ϕ_p (~ 0.4) still results in better overall mass transfer performance compared to lower volume fractions.
- PFOB droplet size is very important in terms of mass transfer rates – the smaller the droplets, the better the mass transfer performance.
- Oxygenator mass transfer performance can be improved by using higher partial oxygen pressures. This is not a preferred option when applying PFOB emulsions as 'blood substitutes', as it complicates the application due to the need for oxygen cylinders to be available at point of treatment. For the BALSS application, higher than atmospheric partial oxygen pressure availability was included in the design from the start, as it is required in cell culture.
- Basic design calculations for the UP-CSIR BALSS show that the current circulation rate of 600 mℓ/min should be sufficient in terms of oxygen supply to the hepatocytes in the bioreactor, both in terms of total oxygen carried and in terms of achievable oxygen mass transfer rates. They also indicate that the current bioreactor should be large enough for human acute liver failure support and that a cell loading of about 1×10^{10} hepatocytes is probably required. More investigation into the effect of shear stress on cell function is required.

5. INFLUENCE OF EMULSION ON CELL GROWTH KINETICS AND CELL FUNCTION

"*Providing adequate oxygen to the cells without damaging them is perhaps the most important function of an animal cell bioreactor.*" – M.F.A. Goosen, 1999:85.

The main and only purpose and function of the PFOB emulsion in the UP-CSIR BALSS is improved cell function (and thus improved BALSS function). Therefore it is critical to verify that a significant improvement in cell function is indeed obtained in the BALSS with the addition of a PFOB emulsion to the circuit.

5.1. Background

5.1.1. Perfluorocarbons and cell culture

The use of PFC's to improve oxygen supply to cell cultures was patented as early as 1974 (Chibata et al., 1974). Since then, a large number of applications and systems have been investigated (see review by Lowe et al., 1997). Examples of reported experiments and results are given in Table 5-1.

Table 5-1. Examples of experiments on the use of PFC's in cell culture

Cells tested	PFC used	Contact method	Result	Reference
Acetobacter Suboxidans ATCC 621	Perfluorotributyl-amine	Aeration and agitation (gas-sparger)	65% increase in fermentation speed for $\phi_p = 0.4$	Chibata et al., 1974
Escherichia coli K-12	Fluorinert FC-40 (3M) – proprietary composition, but mainly trialkylamines with alkyl chain lengths between 3 and 5	Aeration and agitation (gas-sparger) – 2 ℓ and 14 ℓ reactors – dispersed PFC droplets SMD = 50 – 250 µm	150% increase in total bioreactor productivity for $\phi_p = 0.2$	McMillan and Wang, 1992
Normal rat kidney fibroblasts, transformed with K-NRK and others	Heptacosafluoro-tributylamine (FC43)	Growth on PFC-medium interphase	Anchorage-independent growth assay completed in 3-4 days compared to 10-14 days of control	Sanfilippo et al., 1988
Baculovirus-infected insect cells (*Spodoptera frugiperda* Sf9)	Fluorinert FC-40	PFC-mediated surface aeration (growth in aqueous phase above aerated PFC phase)	Overall mass transfer coefficient 1.6 times higher than normal surface aeration	Gotoh, Mochizuki and Kikuchi, 2001
Escherichia coli K-12	Fluorinert FC-40 and Fluorinert FC-77	PFC emulsion (< 0.2 µm) in culture medium, in gas-sparger	Oxygen transfer enhancement factor of 2 for $\phi_p = 0.1 – 0.25$	Ju, Lee and Armiger, 1991a

Cells tested	PFC used	Contact method	Result	Reference
Protoplasts of albino *Petunia hybrida*	Perfluorodecalin	Growth on PFC-medium interface	52% increase in mean plating efficiency	Anthony et al., 1994
Mouse hybridoma 14-4-4S, ATCC HB32	Fluorinert FC-40	PFC emulsion (< 0.2 µm) in culture medium, in gas-sparger	Oxygen transfer enhancement factor of 1.6 for $\phi_p = 0.1$; cell protection against shear damage	Ju and Armiger, 1992

Yamamoto et al. (1994:452) found no improvement in cell growth rate of *Alcaligenes Eutrophus* for PFC (perfluorotributylamine) volume fractions below 0.7, with dramatic improvement at 0.7 and above. This result warrants further discussion:

- They did not use emulsions, but just stirred water-PFC blends. Consequentially, PFC droplet sizes were in the range of 300 to 700 µm, which constitutes at least a factor 1500 less surface area compared to a 0.2 µm emulsion.
- The reason they found sudden improvement in mass transfer at 0.7 PFC volume fraction and above, was due to the phase inversion at 0.6 – 0.65 PFC volume fraction. With PFC as continuous phase, cell growth was suddenly dramatically improved (as one would expect with the much higher oxygen solubility in the PFC). What the study does tell one is that one can obtain a definite improvement in cell growth and function if oxygen mass transfer to the cells is improved.

High partial oxygen pressures in cell culture medium can lead to oxygen toxicity (hyperoxia) due to the increased generation of free radicals (Balin, Pratt and Allen, 2002:57). The introduction of a PFC dispersed (emulsion) phase to a cell culture medium should not increase the risk of oxygen toxicity as long as the oxygenation partial pressure is not increased. This is because the cells in culture will still see the same partial oxygen pressure in the medium when PFC is present compared to medium alone, when oxygenated to the same level. PFC emulsion droplets act as oxygen reservoirs due to their higher solubility of oxygen at the same partial pressures compared to blood plasma or medium. The main difference between a PFC-medium blend and medium alone is that the oxygen partial pressure will drop more slowly in the PFC-medium blend at the same oxygen consumption rate. As oxygen is depleted from the medium, it is supplemented by oxygen mass transfer from the PFC emulsion droplets.

None of the authors in Table 5-1 have reported the observation of oxygen toxicity. Nevertheless, oxygen toxicity from prolonged exposure to high partial oxygen pressures remains a risk to bio-artificial liver support systems and should be verified.

In summary, it is clear from the literature data that the addition of PFC's to cell culture has a definite enhancement effect on microbial, animal cell and plant cell cultures.

5.1.2. Modelling of UP-CSIR BALSS

Background to BALSS modelling

The goals of trying to mathematically model the UP-CSIR BALSS are two-fold: firstly, to obtain a better understanding of the detailed working of the system, and secondly to enable the automation of as many as possible of the control aspects of the BALSS. Ease-of-use and optimal treatment conditions are prerequisites for a commercially successful BALSS.

This section only briefly discusses the basic model. The final model will include basic liver metabolism reactions.

Modelling of cell growth

Modelling of animal cell growth and function is not simple, especially in a BALSS environment, as it depends on a large number of factors, such as: nutrient supply, oxygen supply, pH, carbon dioxide removal, medium osmolarity, toxins in medium, cell density, removal of cell waste, growth surface characteristics (for anchorage-dependent cells such as hepatocytes), temperature, shear stress, history of cells, etc. Apart from all these factors, hepatocytes have a wide variety of interrelated functions that they perform (as discussed in Chapter 2), which poses particular problems in modelling (Houston and Carlile, 1997:473).

The following references are of particular relevance:

- Houston and Carlile (1997) present a methodology for the determination of *in vitro* drug metabolism using isolated hepatocytes, and how to scale this up for *in vivo* predictions.
- Park, Iwata and Ikada (2001) propose a model for the functional evaluation of a BALSS, in order to try and standardize on quantitative evaluation of liver support systems and enable comparisons to be made.
- Robinson (1991) reviews models of hepatic elimination of drugs and discusses issues surrounding the assumptions made.
- Yuet, Harris and Goosen (1995) and Goosen (1999) modelled the growth of hepatocytes encapsulated in alginate beads.

The rate of cell growth can be expressed as follows (Yuet, Harris and Goosen, 1995:111):

$$\frac{dX}{dt} = u(t - t_{lag})\left[\mu X + \lambda \int_0^t X(v)dv\right] \tag{5-1}$$

where X is cell density, μ is the specific cell growth rate, λ is the cell death constant, the integral function is the cell age distribution, and $u(t\text{-}t_{lag})$ is a step function to make provision for the lag time phase of cell growth and is given by:

$$u(t-t_{lag}) = \begin{cases} 1 & \text{if } t > t_{lag} \\ 0 & \text{if } t < t_{lag} \end{cases} \tag{5-2}$$

The specific cell growth rate is dependent on cell density and the concentration of rate-limiting nutrients (e.g. oxygen and glucose), and can be calculated from (Yuet, Harris and Goosen, 1995:112):

$$\mu = \mu_{\max} \prod_{i=1}^{N} \left(\frac{C_i}{K_{Ci+} C_i} \right) \left[1 - e^{\left(-B \frac{X_{\max} - X}{X} \right)} \right] \tag{5-3}$$

where C_i is the concentration of rate-limiting nutrient i, K_{Ci} is the saturation constant for nutrient i, N is the total number of rate-limiting nutrients, μ_{max} is the maximum specific growth rate, X_{max} is maximum cell density, and B is a parameter to provide for the effect of cell density on growth rate – as cell density approaches X_{max}, growth rate will decrease.

The cell growth model can be related to the rate of consumption of nutrient i by the cells (S_i) as follows (Yuet, Harris and Goosen, 1995:112):

$$S_i = Y_{X/Ci} \mu X u(t-t_{lag}) \tag{5-4}$$

where $Y_{X/Ci}$ is a yield factor, relating the amount of nutrient consumption or metabolite production to the number of cells.

Equation 5-4 is useful, as it relates cell growth rate to nutrient consumption rate and can be used in the UP-CSIR BALSS model's rate equations, of which a basic description is given below.

Basic UP-CSIR BALSS model

While there are various models proposed for individual aspects of a bio-artificial liver, there are no unified models to describe and predict BALSS function. Such a model should include the following aspects:

- Hydrodynamic modelling of flow in the BALSS (pressure drop, flow rates, flow regimes);
- Mass transfer modelling for oxygen (including the effect of PFOB), carbon dioxide, nutrients, toxins, drugs and metabolites;
- Cell growth modelling – cell proliferation during use would influence all other aspects such as oxygen consumption and flow through the bioreactor;
- Cell function modelling – the basic aspects of liver function (not only drug metabolism).

Figure 5-1 shows a simplified process model of the UP-CSIR BALSS.

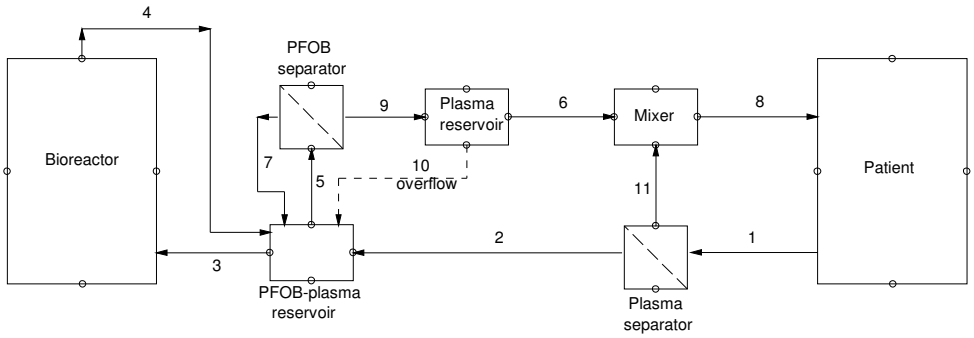

Figure 5-1. Simplified process model for UP-CSIR BALSS

The concentrations of component / chemical i in the bioreactor (C_{BRi}) and the patient's blood (C_{Pi}) can be described by the following set of simultaneous differential equations:

$$V_{BR}\frac{dC_{BRi}}{dt} = r_{BRi} + Q_2 C_{Pi} - Q_6 C_{BRi}$$
$$V_P\frac{dC_{Pi}}{dt} = r_{Pi} - Q_2 C_{Pi} + Q_6 C_{BRi} \quad (5\text{-}5)$$

where r_{BRi} is the clearance / production rate of component i in the bioreactor, and r_{Pi} is the clearance / production rate of component i in the patient.

All other variables are related by algebraic equations. By solving the set of differential equations for a specific set of operating parameters, the influence of a number of variables on the system operation and effectiveness can be investigated. A good example is the effect of circulation rate between the bioreactor and patient on the effectiveness of reduction of a toxin's concentration in the patient. The critical importance of circulation rate for effective treatment of a patient was pointed out by Iwata, Park and Ikada (1998). The model can also be used for optimization of BALSS parameters.

The clearance and production rates of a number of components will be determined experimentally in a closed-circuit BALSS setup (see Section 5.2).

5.2. Experimental setup

Figure 5-2 shows the experimental setup used in the metabolic trials. A medium-PFOB emulsion blend is circulated in a closed circuit. The blend is pumped from a reservoir through an oxygenator before flowing through the bioreactor containing hepatocytes. It then returns to the reservoir. The whole system is contained within a temperature-controlled environment. The temperature is controlled at 37 ºC. The gas blend for the oxygenator is pre-mixed and usually consists of 95% oxygen and 5% carbon dioxide by weight.

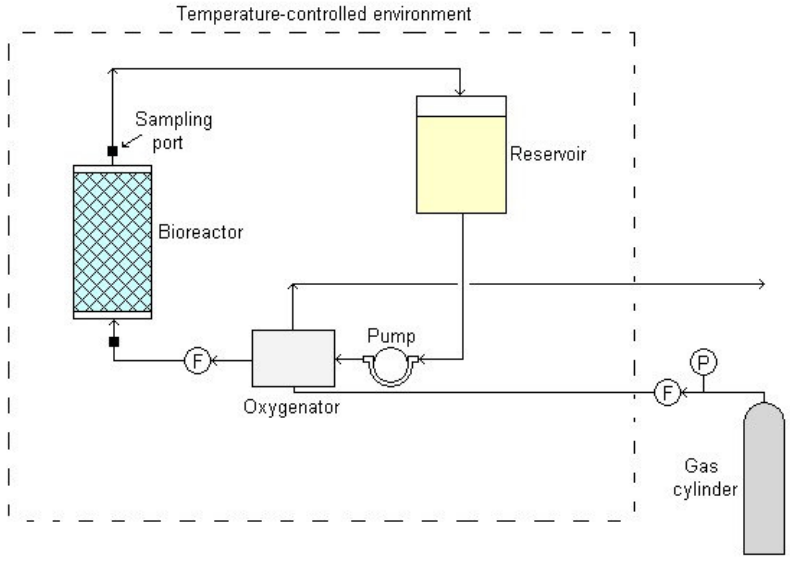

Figure 5-2. Metabolic trial test setup.

Samples are withdrawn from sample ports before and after the bioreactor and analyzed for oxygen content, carbon dioxide content, pH, glucose levels, etc. Toxins can be injected in the same sample ports. The medium-PFOB emulsion blend is replaced every 24 hours during a metabolic trial to replace depleted nutrients in the medium.

5.3. Results & discussion

The first set of metabolic trials showed improved oxygen tension and improved urea production in cultures where PFOB emulsion was included (see Figures 5-3 and 5-4). Details of the experimental setup are provided in Bond et al. (2002). Please note that these are only preliminary results, and that a full set of metabolic trials on primary porcine hepatocytes has commenced in April 2003.

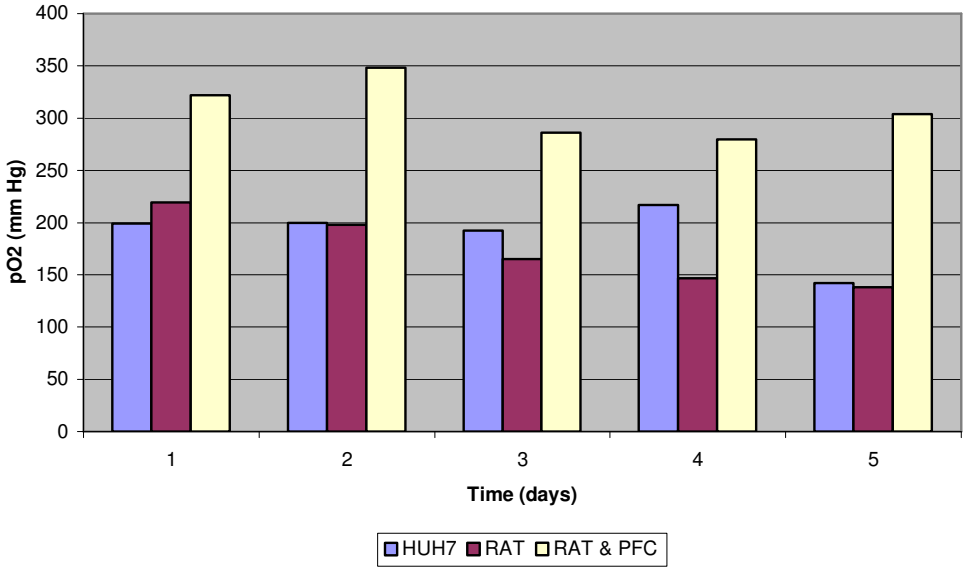

Figure 5-3. The addition of 0.2 volume fraction PFOB emulsion leads to increased partial oxygen pressure in hepatocyte culture (HUH7 - HUH7 cell line; RAT - rat hepatocytes; RAT & PFC – rat hepatocytes cultured with 0.2 volume fraction PFOB emulsion).

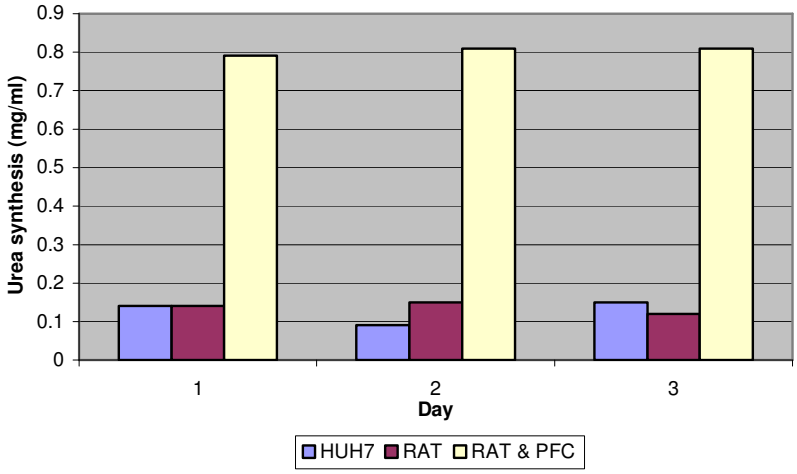

Figure 5-4. Urea synthesis was markedly improved with the addition of 0.2 volume fraction PFOB emulsion in hepatocyte culture (HUH7 - HUH7 cell line; RAT - rat hepatocytes; RAT & PFC – rat hepatocytes cultured with 0.2 volume fraction PFOB emulsion).

6. CONCLUSIONS

"A conclusion is the place where you got tired of thinking." – Martin H. Fischer.

In Chapter 1, important aspects related to the use of perfluorocarbon emulsions in a bio-artificial liver support system were listed:

- How should the emulsion be formulated for maximum stability?
- How can the emulsion be sterilized?
- Which surfactants should be used for emulsification?
- What emulsion manufacturing procedure should be used?
- Does the use of the emulsion result in enhanced oxygen mass transfer compared to plasma only?
- If so, what is the mass transfer enhancement mechanism?
- What are the optimum emulsion droplet sizes and volume fractions that maximize mass transfer and oxygen carrying capacity?
- What separation method can be used to keep the emulsion in circulation in the BALSS without causing it to break?
- How can the PFOB be recovered from spent emulsions?
- Does the emulsion improve BALSS function?

This Chapter will review the answers obtained through this study and summarize the outstanding issues.

6.1. Bio-artificial liver support systems

Although liver support systems have been under development for more than 40 years, no system with proven clinical success is commercially available yet. This is mainly due to the required complexity of the systems (due to the inclusion of live hepatocytes) and the conflicting requirements of efficient mass transfer vs. the provision of a barrier to immune reactions and immunocompetent cells. The UP-CSIR BALSS represents a potential solution to these conflicting requirements, through the use of a direct perfusion system with the addition of an oxygen carrier.

Bio-artificial liver support system design involves many aspects, such as choice of scaffold, choice of cells, process volume of system components, perfusion of plasma vs. perfusion of whole blood, reactor geometry, etc. These were discussed in detail in Chapter 2.

As hepatocytes have very high oxygen demands and a large number of cells are required for human liver support, high cell density in the bioreactor is critical (Hay, Veitch and Gaylor, 2001:119). This can only be achieved through very efficient oxygen supply to all the cells in a bioreactor. The novel UP-CSIR BALSS bioreactor strives towards this goal through the use of the three-dimensional foam matrix and the addition of an oxygen carrier that can deliver oxygen to the cells on a micro scale. Basic bioreactor design calculations for the

UP-CSIR BALSS were performed in Section 4.4.3 and indicated that the current bioreactor volume (250 mℓ) and cell loading (1×10^{10}) should be sufficient to provide approximately 20% of normal liver function for a human patient.

6.2. Perfluorocarbon emulsions

One of the main differentiating aspects of the UP-CSIR BALSS compared to other liver support systems is the use of an oxygen carrier to improve oxygen mass transfer. Oxygen carrier development can be divided in hemoglobin-based and perfluorocarbon-based oxygen carriers. For the UP-CSIR BALSS, a perfluorocarbon-based oxygen carrier was selected as oxygen carrier, due to its relative ease of production, long-term stability, and decreased risk of zoonosis.

Perfluorooctyl bromide was selected as perfluorocarbon, owing to its fast clearance from the reticuloendothelial system, good emulsion stability and its high solubilization of oxygen. As PFC's are hydrophobic, they need to be emulsified for use in aqueous environments, such as cell culture medium or plasma.

In order to use the PFOB emulsions in the UP-CSIR BALSS, it was required to investigate relevant aspects of the emulsions. Two main emulsion systems, A and B, were investigated (see Section 3.2 for details). The main difference between Emulsions A and B was the emulsification procedure. Compared to Emulsion A, Emulsion B was more stable, had a narrower droplet size distribution and smaller droplets.

The conclusions obtained from literature and the current experimental and theoretical study are summarized in Table 6-1.

Table 6-1. Aspects relating to PFOB emulsion properties relevant for its use in the UP-CSIR BALSS

Aspect	Results
Formulation	▪ Egg yolk lecithin as surfactant gives improved stability and fewer adverse effects compared to poloxamers. ▪ Ratio of phosphatidyl choline:phosphatidyl ethanolamine should exceed 4:1. Thus, Lipoid E80 and E80S are more suitable than Sigma-Aldrich egg yolk lecithin for PFOB emulsion preparation. ▪ Sodium chloride is added to the emulsion to adjust osmolarity to approximate physiological values (~ 300 mOsm/ℓ). ▪ Sodium bicarbonate is added to the emulsion to control pH at around 8.0, which is the recommended pH for optimum stability during and after emulsion autoclaving. ▪ EDTA is added as chelating agent for metal cations, in order to avoid emulsion flocculation and catalytic degradation of lecithin. ▪ Vitamin E is added as antioxidant to protect the lecithin surfactant.

Aspect	Results
Preparation	▪ Sonication experiments resulted in unstable emulsions with large droplets (> 1 µm SMD) and high polydispersity. ▪ High-pressure homogenization yields small droplets (~ 200 nm SMD), narrow droplet size distributions, stable emulsions and repeatable results. ▪ 15 passes through the high-pressure homogenizer were sufficient to obtain droplet sizes around 200 nm. ▪ It is necessary to bubble nitrogen through the feed and product containers of the high-pressure homogenizer to minimize oxidative degradation of the lecithin surfactant.
Sterilization	▪ The emulsion can be sterilized by terminal sterilization through autoclaving at 121 ºC for 15 minutes. ▪ A small increase in droplet size occurs with autoclaving, but this can be minimized by using a rotary autoclave.
Droplet size distributions	▪ Laser light scattering was adequate for measuring droplet size distributions. ▪ Emulsions prepared using high-pressure homogenization had smaller droplet sizes and lower polydispersity compared to emulsions prepared using sonication.
Emulsion stability	▪ Ostwald ripening of the emulsion can be limited by the addition of a small percentage (0.5%) of a second perfluorocarbon, namely perfluorodecyl bromide. ▪ Control and measurement of zeta potential is critical in controlling emulsion stability. ▪ Emulsion B's zeta potential was sufficiently high to ensure stability, while Emulsion A was unstable and flocculated.
Emulsion rheology	▪ Emulsion A exhibited non-Newtonian, shear-thinning rheological behaviour, which could be adequately described using the power law. The shear-thinning effect was caused by reversible flocculation of the emulsion. ▪ Emulsion B exhibited Newtonian rheological behaviour. ▪ Emulsion viscosity increases exponentially with increase in dispersed phase volume fraction. ▪ The effect of dispersed phase volume fraction on experimental PFOB emulsion viscosity can be adequately described by the Mandersloot correlation. ▪ The maximum packing density of the PFOB emulsions (Emulsion B) was determined as 0.60 (from the Mandersloot correlation). ▪ Flow in the Polystan Safemicro Neonatal Oxygenator (used in the UP-CSIR BALSS) is laminar for all allowable flow rates of both Emulsions A and B.

Aspect	Results
Emulsion concentration	▪ It is necessary to recirculate the PFOB in the UP-CSIR BALSS. In order to do this, a continuous, on-line concentration unit is required that does not break up the emulsion. ▪ Centrifugal separation of the emulsion, although technically feasible, is not practical for the UP-CSIR BALSS, mainly due to required size, cost and cleaning considerations. ▪ Ultrafiltration was successful and achieved separation efficiencies approaching 100%, with small process volumes. ▪ Membrane fouling occurs with time, and necessitates regular replacement.
PFOB recovery	▪ Distillation with orthophosphoric acid results in quantitative recovery of PFOB from its emulsions with lecithin.

6.3. Mass transfer modelling

Mass transfer models were developed in Chapter 4 for gas-sparged and membrane oxygenators. The model results were verified experimentally, and experimental and theoretical results showed good correlation. Conclusions regarding the mass transfer behaviour of the emulsions are summarized in Table 6-2. Note that the flow was in the laminar regime for all experiments conducted on the membrane oxygenator.

Table 6-2. Summary of mass transfer properties and behaviour of PFOB emulsions

Aspect	Results
Rate-determining step	The theoretical rate-determining step for both the gas-sparged and membrane oxygenators was diffusion through the liquid film.
Experimental mass transfer coefficients	The experimental mass transfer coefficients for the rate-determining step in both the gas-sparged and membrane oxygenators were of the order of 1×10^{-3} m/s.
Oxygen carrying capacity	The emulsion oxygen carrying capacity increases linearly with increase in PFOB volume fraction. At 0.2 PFOB, the emulsion oxygen carrying capacity is approximately 4.5 times that of water alone.
Gas-sparged vs. membrane oxygenator	The membrane oxygenator is superior to the gas-sparged oxygenator in terms of oxygen mass transfer rates. This is due to the much higher interfacial surface area density of the membrane oxygenator.
PFOB volume fraction	Mass transfer rates increase with increase in PFOB volume fraction up to $\phi_p \approx 0.2$. Above this value, the mass transfer rate plateaus but total oxygen carrying capacity increases. Above $\phi_p \approx 0.5$, emulsion viscosity becomes too high and it attains a cream-like consistency. Thus, the optimum PFOB volume fraction is about $\phi_p = 0.4$ - 0.5.

Aspect	Results
Emulsion viscosity	Theoretically, emulsion viscosity should not have a large impact on mass transfer rates to and from emulsions. However, this could not be verified experimentally owing to the direct relation between PFOB volume fraction and emulsion viscosity. Also, the mass transfer rate-limiting effect observed at higher ϕ_p could be due to increased viscosity with increase in ϕ_p.
Droplet size	Smaller droplet sizes lead to improved mass transfer rates.
Gas flow rate and bubble size (gas sparger)	Increase in gas flow rate and decrease in gas bubble size lead to increased mass transfer rates.
Emulsion flow rate (membrane oxygenator)	Theoretically, mass transfer rates in the membrane oxygenator should show only a very weak dependence on flow rate. This should be verified experimentally.
Calculation method (membrane oxygenator)	Calculation method (Newtonian vs. non-Newtonian vs. properties at wall) did not show significant differences in theoretical results for the membrane oxygenator.
Thin film thickness	The thickness of the stagnant film adjacent to the wall is a critical parameter in the model, as the mass transfer is liquid-film controlled. A mean value of 2 µm resulted in a close correlation between theoretical and experimental results for both the gas-sparged and membrane oxygenator.
Bioreactor oxygen supply	The current UP-CSIR bioreactor contains 1×10^{10} hepatocytes in a 250 mℓ reactor. For this design, an emulsion circulation rate of 600 mℓ/min is sufficient to supply oxygen to the current bioreactor loading. When utilizing primary porcine hepatocytes, 1×10^{10} cells should theoretically provide about 20% of adult human liver function, which compares well with other values suggested in the literature. Without PFOB, the required circulation rate for sufficient oxygen supply jumps to 2.8 ℓ/min (a factor 4.7 increase), which would have implications for system design and for shear stress experienced by the cells.

6.4. Perfluorocarbons in cell culture

Several investigators have demonstrated improvements in cell function in cell culture applications, for microbial, animal and plant cells. Preliminary results indicate similar improvements in the UP-CSIR BALSS (e.g. improved urea production and increased partial oxygen pressures), but further verification is required. Improved hepatocyte function is critical to the success of the UP-CSIR BALSS.

A mathematical model of the UP-CSIR BALSS is under development, and will serve as vehicle for improved understanding of the system dynamics, optimization of system parameters, and automation of system control components.

6.5. Recommendations

The following recommendations can be made as a result of this study:

- PFOB emulsions prepared using high-pressure homogenization and the formulation for Emulsion B (as given in Chapter 3) are suitable for use in the UP-CSIR BALSS.
- Ultrafiltration is suitable as an emulsion concentration method for use in the UP-CSIR BALSS.
- Dispersed phase Sauter mean droplet diameters in the range of 0.1 to 0.2 µm are optimal.
- Dispersed phase volume fractions between 0.4 and 0.5 are optimal for enhanced overall oxygen mass transfer.
- The models presented in Chapter 4 can be used for prediction of emulsion mass transfer behaviour.

Further investigation into the following areas is suggested:

- The apparent oxygen mass transfer rate-limiting effect at higher PFOB volume fractions should be investigated in more detail. If this mechanism is better understood, further improvement in oxygen mass transfer with PFOB emulsions could possibly be achieved. This investigation should include viscosity effects.
- Ultrafiltration membranes with larger MWCO's (500 kDa and 1000 kDa) should be evaluated for PFOB emulsion concentration, to avoid the build-up of fibrinogen (MW 340 kDa) in the BALSS circuit. The retention of fibrinogen should be tested for these membranes to ensure minimal retention.
- Experimental verification of the oxygen loading profile assumptions for the membrane oxygenator would be useful. This could possibly be done by modifying such an oxygenator to have oxygen-measuring probes at a number of points along the length of the oxygenator. This could also decrease scatter and experimental error in the data obtained for the membrane oxygenator.
- Detailed shear stress calculations and experimental verification of the effect of shear stress on cell growth and adhesion should be performed to ensure that hepatocyte function in the UP-CSIR BALSS bioreactor is not decreased due to shear stress damage.
- Investigation of the effects of hyperoxia (higher than normal oxygen levels) on the long-term (i.e. days to weeks) function and survival of the porcine hepatocytes would reduce risk in the clinical application of the BALSS.

APPENDIX A: ANALYTICAL SOLUTION OF SIMULTANEOUS DIFFERENTIAL EQUATIONS FOR GAS-SPARGER

From Section 4.2.1, Equation 4-40 can be rewritten as follows:

$$\frac{dC_m}{dt} = \frac{1}{1-\phi_p(1-\phi_g)-\phi_g}\left[k_{gm}a_{gm}(C_{m,g}-C_m) - k_{mp}a_{mp}(C_m - C_{m,equil})\right]$$

$$\frac{dC_m}{dt} = \frac{1}{1-\phi_p(1-\phi_g)-\phi_g}\left[k_{gm}a_{gm}(C_{m,g}-C_m) - k_{mp}a_{mp}(C_m - \frac{\rho_m}{\rho_p K}C_p)\right] \quad \text{(A)}$$

$$\frac{dC_m}{dt} = \frac{(-k_{gm}a_{gm} - k_{mp}a_{mp})}{1-\phi_p(1-\phi_g)-\phi_g}C_m + \frac{k_{mp}a_{mp}\rho_m}{\rho_p K\left[1-\phi_p(1-\phi_g)-\phi_g\right]}C_p + \frac{k_{gm}a_{gm}C_{m,g}}{1-\phi_p(1-\phi_g)-\phi_g}$$

Equation 4-43 can be rewritten as follows:

$$\frac{dC_p}{dt} = \frac{1}{\phi_p(1-\phi_g)}\left[k_{mp}a_{mp}(C_m - C_{m,equil}) + k_{gp}a_{gp}(C_{p,g}-C_p)\right]$$

$$\frac{dC_p}{dt} = \frac{1}{\phi_p(1-\phi_g)}\left[k_{mp}a_{mp}(C_m - \frac{\rho_m}{\rho_p K}C_p) + k_{gp}a_{gp}(C_{p,g}-C_p)\right] \quad \text{(B)}$$

$$\frac{dC_p}{dt} = \frac{-\frac{k_{mp}a_{mp}\rho_m}{\rho_p K} - k_{gp}a_{gp}}{\phi_p(1-\phi_g)}C_p + \frac{k_{mp}a_{mp}}{\phi_p(1-\phi_g)}C_m + \frac{k_{gp}a_{gp}C_{p,g}}{\phi_p(1-\phi_g)}$$

Setting $x=C_p$ and $y=C_m$, and with substitution of single coefficients for the various compound coefficients, Equation A becomes:

$$y' = a_1 y + a_2 x + a_3 \quad \text{(C)}$$

Similarly, Equation B becomes:

$$x' = a_4 x + a_5 y + a_6 \quad \text{(D)}$$

The system of equations shown in Equations C and D can be solved by elimination (Kreyszig, 1983), as follows – first rewrite Equation D to yield y:

$$a_5 y = x' - a_4 x - a_6 \quad \text{(E)}$$

Now differentiate Equation D with respect to time, rearrange and substitute Equation C:

$$\begin{aligned} x'' &= a_4 x' + a_5 y' \\ x'' - a_4 x' &= a_5 y' \\ x'' - a_4 x' &= a_5 (a_1 y + a_2 x + a_3) \end{aligned} \tag{F}$$

Insert Equation E into Equation F:

$$\begin{aligned} x'' - a_4 x' &= a_1 (x' - a_4 x - a_6) + a_2 a_5 x + a_3 a_5 \\ x'' + (-a_1 - a_4) x' + (a_1 a_4 - a_2 a_5) x &= (a_3 a_5 - a_1 a_6) \end{aligned} \tag{G}$$

Equation G is a non-homogeneous second order differential equation with constant coefficients, and can be solved by finding the complementary function x_c and any particular solution x_p of the non-homogeneous equation (Zill and Cullen, 1992:204). Then $x = x_c + x_p$.

The complementary function x_c is solved through solving Equation G's associated homogeneous equation $x'' + (-a_1 - a_4) x' + (a_1 a_4 - a_2 a_5) x = 0$. This is done through the auxiliary equation method (Kreyszig, 1983:131) by using a solution of the form $x = e^{mt}$, so that the associated homogeneous equation becomes:

$$\begin{aligned} m^2 e^{mt} + (-a_1 - a_4) m e^{mt} + (a_1 a_4 - a_2 a_5) e^{mt} &= 0 \\ e^{mt} \left[m^2 + (-a_1 - a_4) m + (a_1 a_4 - a_2 a_5) \right] &= 0 \\ \therefore m^2 + (-a_1 - a_4) m + (a_1 a_4 - a_2 a_5) &= 0 \end{aligned} \tag{H}$$

The equation in m is a normal quadratic equation, with the following general solution:

$$\begin{aligned} m_1 &= \frac{-b + \sqrt{b^2 - 4ac}}{2a} \\ m_2 &= \frac{-b - \sqrt{b^2 - 4ac}}{2a} \\ \therefore m_1 &= \frac{a_1 + a_4 + \sqrt{(a_1 + a_4)^2 + 4(a_2 a_5 - a_1 a_4)}}{2} \\ m_2 &= \frac{a_1 + a_4 - \sqrt{(a_1 + a_4)^2 + 4(a_2 a_5 - a_1 a_4)}}{2} \end{aligned} \tag{I}$$

Now the complementary function x_c is given by:

$$x_c = c_1 e^{m_1 t} + c_2 e^{m_2 t} \tag{J}$$

A particular solution of the non-homogeneous equation is given by (Zill and Cullen, 1992:139):

$$x_p = c_3 \tag{K}$$

Insert Equation K into Equation G:

$$(a_1 a_4 - a_2 a_5)c_3 = (a_3 a_5 - a_1 a_6)$$
$$c_3 = \frac{(a_3 a_5 - a_1 a_6)}{(a_1 a_4 - a_2 a_5)} \tag{L}$$

Now the solution for x is given by:

$$x = x_c + x_p$$
$$x = c_1 e^{m_1 t} + c_2 e^{m_2 t} + c_3 \tag{M}$$

Differentiate Equation M:

$$x' = c_1 m_1 e^{m_1 t} + c_2 m_2 e^{m_2 t} \tag{N}$$

Substitute Equations M and N into Equation E:

$$a_5 y = c_1 m_1 e^{m_1 t} + c_2 m_2 e^{m_2 t} - a_4 (c_1 e^{m_1 t} + c_2 e^{m_2 t} + c_3) - a_6$$
$$y = \frac{(m_1 - a_4)c_1}{a_5} e^{m_1 t} + \frac{(m_2 - a_4)c_2}{a_5} e^{m_2 t} - \frac{a_4 c_3 + a_6}{a_5} \tag{P}$$

Thus, Equations M and P give the solutions for x and y. Now only constants c_1 and c_2 have to be solved. For the set of initial values $y(0)=y_0$ and $x(0)=x_0$, one can solve Equation M at time zero:

$$x_0 = c_1 + c_2 + c_3 \tag{Q}$$

Similarly, solving Equation P at time zero:

$$y_0 = \frac{(m_1 - a_4)}{a_5} c_1 + \frac{(m_2 - a_4)}{a_5} c_2 - \frac{a_4 c_3 + a_6}{a_5} \tag{R}$$

Multiplying Equation Q with $(m_1-a_4)/a_5$:

$$\frac{(m_1 - a_4)x_0}{a_5} = \frac{(m_1 - a_4)}{a_5} c_1 + \frac{(m_1 - a_4)}{a_5} c_2 + \frac{(m_1 - a_4)}{a_5} c_3 \tag{S}$$

Subtracting Equation R from Equation S:

$$\frac{(m_1 - a_4)x_0}{a_5} - y_0 = \frac{(m_1 - m_2)}{a_5}c_2 + \frac{m_1}{a_5}c_3 + \frac{a_6}{a_5}$$

$$\therefore \frac{(m_1 - m_2)}{a_5}c_2 = \frac{(m_1 - a_4)x_0 - m_1 c_3 - a_6 - y_0 a_5}{a_5} \quad \text{(T)}$$

$$c_2 = \frac{(m_1 - a_4)x_0 - m_1 c_3 - a_6 - y_0 a_5}{(m_1 - m_2)}$$

Now c_1 can be calculated from Equation Q:

$$c_1 = x_0 - c_2 - c_3 \quad \text{(U)}$$

The algorithm for solution of the equations for x and y is as follows:

1. Calculate all coefficients $a_{1\ldots n}$ using user inputs.
2. Calculate coefficients m_1 and m_2 using Equation I.
3. Calculate constant c_3 using Equation L.
4. Calculate constant c_2 using the initial values and Equation T.
5. Calculate constant c_1 using Equation U.
6. Now the values for x and y can be calculated at time t using Equations M and P respectively.

APPENDIX B: DERIVATION OF FRACTIONAL GAS-PFOB INTERFACIAL SPECIFIC SURFACE AREA

The interfacial specific surface area between gas and PFOB can be approximated as follows:

a_{gp} = [specific projected area of all PFOB droplets]×[gas boundary layer volume fraction]

$$a_{gp} = \left[\frac{1}{V_{gs}}\sum_{i=1}^{N}\frac{\pi n_i d_i^2}{4}\right]\left[a_g h\right]$$
$$a_{gp} = a_g \frac{\pi h}{4V_{gs}}\sum_{i=1}^{N} n_i d_i^2 \qquad \text{(A)}$$

The total system volume can be calculated as:

$$V_{gs} = \frac{V_p}{\phi_p(1-\phi_g)} \qquad \text{(B)}$$

The volume of PFOB droplets is given by:

$$V_p = \sum_{i=1}^{N}\frac{1}{6}\pi n_i d_i^3 \qquad \text{(C)}$$

Inserting Equation C into Equation B:

$$V_{gs} = \frac{\pi\sum_{i=1}^{N} n_i d_i^3}{6\phi_p(1-\phi_g)} \qquad \text{(D)}$$

By inserting Equation D into Equation A and simplifying, one obtains the fraction of the total gas surface area in direct contact with PFOB droplets:

$$\phi_{pg}^{|} = \frac{a_{gp}}{a_g} = \frac{3}{2}\phi_p(1-\phi_g)h\frac{\sum_{i=1}^{N} n_i d_{pi}^2}{\sum_{i=1}^{N} n_i d_{pi}^3} \qquad \text{(E)}$$

The total PFOB droplet surface area is given as:

$$a_p = \frac{6\phi_p(1-\phi_g)}{d_{sp}} = 6\phi_p(1-\phi_g)\frac{\sum_{i=1}^{N} n_i d_{pi}^2}{\sum_{i=1}^{N} n_i d_{pi}^3} \qquad \text{(F)}$$

By inserting Equation F into Equation E, we obtain:

$$a_{gp} = \frac{h a_g a_p}{4} \qquad \text{(G)}$$

APPENDIX C: CALCULATION PROCEDURES FOR MEMBRANE OXYGENATOR MASS TRANSFER COEFFICIENTS

Please note: calculation methods are given for non-Newtonian fluids. For Newtonian fluids, use Newtonian Re number and Newtonian viscosity in all cases.

Table C-1. Algorithm for calculation of k_{bm} and k_{mp}, Method 1 (using Newtonian correlations, average viscosities calculated from curve-fitted correlations and average shear rate)

Step no.	Description	Equation	Source
1	Calculate hydraulic radius/diameter	$d_h = 2R_h = \left(\frac{d_i^2 - N_b V_t (d_f + 2h_b)^2}{d_i + N_b V_t (d_f + 2h_b)} \right)$	Lipnizki & Field, 2001:197
2	Calculate area-average shear rate	$\dot{\gamma}_{ave} = \frac{2u_e}{R_h}\left(\frac{3n+1}{2n+1}\right)$	Derived (Equation 4-21)
3	Calculate viscosity	d_{sp}= 4 µm: $\eta_e = \eta_m e^{\left[6.6+\frac{16.3}{\dot{\gamma}_{ave}^{0.5}}-2.1\times10^6 e^{-\dot{\gamma}_{ave}}-8.9e^{-\phi_p}\right]}$ d_{sp}= 0.2 µm: $\eta_e = \frac{\eta_m}{6.4 - \frac{34.4}{\ln\dot{\gamma}_{ave}} + \frac{38.3\ln\dot{\gamma}_{ave}}{\dot{\gamma}_{ave}} + \frac{0.57}{\ln\phi_p}}$	Determined experimentally

Step no.	Description	Equation	Source
4	Mass transfer coefficient from membrane to medium	Turbulent flow: $k_{bm} = 0.0164 D_{o,m} \mathrm{Re}_L^{0.8} Sc^{0.33}$ $\mathrm{Re}_L = \frac{\rho_e u_e L_b}{\eta_e}$, $5\times10^5 \le \mathrm{Re}_L \le 10^8$ $Sc = \frac{\eta_e}{\rho_e D_{o,m}}$, $0.6 \le Sc \le 60$ Transitional flow: $k_{bm} = 0.0296 \frac{D_{o,m}}{L_b} \mathrm{Re}_L^{0.8} Sc^{0.33}$ $10000 \le \mathrm{Re}_L \le 5\times10^5$, $0.6 \le Sc \le 60$ Laminar flow: $k_{bm} = 0.664 \frac{D_{o,m}}{L_b} \mathrm{Re}_L^{0.5} Sc^{0.33}$ $\mathrm{Re}_L \le 10000$, $0.6 \le Sc \le 50$	Mass transfer over flat plate (Incropera and De Witt, 1990:439)
5	Mass transfer coefficient from medium to PFC	$Sh = 2 + \left(0.4\,\mathrm{Re}^{0.5} + 0.06\,\mathrm{Re}^{0.67}\right) Sc^{0.4} \left(\frac{\eta_e}{\eta_w}\right)^{0.25}$ where $Sh = \frac{k_{mp} d_{sp}}{D_{o,p}}$ $\mathrm{Re}_D = \frac{\rho_e u_e d_{sp}}{\eta_e}$, $3.5 \le \mathrm{Re}_L \le 76000$ $Sc = \frac{\eta_e}{\rho_e D_{o,p}}$, $0.71 \le Sc \le 380$	Mass transfer to/from spheres (Incropera and De Witt, 1990:439)

Table C-2. Algorithm for calculation of k_{bm} and k_{mp}, Method 2 (using Metzner-Reed Reynolds number and average viscosity)

Step no.	Description	Equation	Source
1	Calculate hydraulic radius/diameter	$d_h = 2R_h = \left(\frac{d_i^2 - N_b V_t (d_f + 2h_b)^2}{d_i + N_b V_t (d_f + 2h_b)} \right)$	Lipnizki & Field, 2001:197
2	Calculate Metzner-Reed Reynolds number	$\mathrm{Re}_{MR} = 8 \left(\frac{n}{6n+2} \right)^n \frac{\rho_e u_e^{2-n} d_h^n}{K_c}$	Skelland, 1967:110

Step no.	Description	Equation	Source
3	Calculate friction factor for **laminar** flow OR **turbulent** flow	$f' = 8\left(\frac{6n+2}{n}\right)^n \frac{K_c u_e^{n-2} d_h^{-n}}{\rho_e}$ OR $f' = 0.3168 n^{0.675} \mathrm{Re}_{MR}^{-0.25}$	Greeff, 1999
4	Calculate pressure drop per unit length	$\left(\frac{\Delta P}{L_b}\right) = \frac{f'}{d_h}\frac{\rho_e u_e^2}{2}$	Greeff, 1999
5	Calculate stress at wall	$\tau_w = \left(\frac{\Delta P}{L_b}\right)\frac{\varepsilon_c d_i^2}{4N_b V_t (d_f + 2h_b)}$	Derived (Eq. 4-33)
6	Calculate viscosity at wall	$\eta_w = K_c\left(\frac{\tau_w}{K_c}\right)^{\frac{n-1}{n}}$	Derived (Eq. 4-34)
7	Calculate area-average shear rate	$\dot{\gamma}_{ave} = \frac{2u_e}{R_h}\left(\frac{3n+1}{2n+1}\right)$	Derived (Eq. 4-28)
8	Calculate average viscosity	$\eta_{ave} = K_c \dot{\gamma}_{ave}^{n-1} = K_c\left[\frac{2u_e}{R_h}\left(\frac{3n+1}{2n+1}\right)\right]^{n-1}$	Derived (Eq. 4-29)
9	Calculate mass transfer coefficient from membrane into medium (k_{bm}) for **laminar** flow	$Sh = \left(Sh_1^3 + Sh_2^3 + Sh_3^3\right)^{1/3}$ where $Sh_1 = 3.66 + 1.2\left(\sqrt{1-\varepsilon_c}\right)^{-0.8}$ $Sh_2 = 1.615\left(1 + 0.14\left(\sqrt{1-\varepsilon_c}\right)^{-0.5}\right)\sqrt[3]{\frac{\mathrm{Re}\,Scd_h}{L_b}}$ $Sh_3 = \left(\frac{2}{1+22Sc}\right)^{\frac{1}{6}}\left(\frac{\mathrm{Re}\,Scd_h}{L_b}\right)^{\frac{1}{2}}$ $Sh = \frac{k_{bm} d_h}{D_{o,m}}$ $\mathrm{Re}_{MR} = 8\left(\frac{n}{6n+2}\right)^n \frac{\rho_e u_e^{2-n} d_h^n}{K_c}$ $Sc = \frac{\eta_{ave}}{\rho_e D_{o,m}}$	Lipnizki & Field, 2001:197

Step no.	Description	Equation	Source
OR 9	Calculate mass transfer coefficient from membrane into medium (k_{bm}) for **turbulent** flow	$Sh = 0.021\left(\frac{1}{\sqrt{1-\varepsilon_c}}\right)^{0.45} \mathrm{Re}^{0.8}\, Sc^{0.33}$	Lipnizki & Field, 2001:197
10	Calculate mass transfer coefficient from medium into PFC (k_{mp})	$Sh = 2 + \left(0.4\,\mathrm{Re}^{0.5} + 0.06\,\mathrm{Re}^{0.67}\right) Sc^{0.4}\left(\frac{\eta_{ave}}{\eta_w}\right)^{0.25}$ where $Sh = \frac{k_{mp} d_{sp}}{D_{o,p}}$ $\mathrm{Re}_{MR} = 8\left(\frac{n}{6n+2}\right)^n \frac{\rho_e u_e^{2-n} d_{sp}^n}{K_c}$ $Sc = \frac{\eta_{ave}}{\rho_e D_{o,p}}$	Incropera and De Witt, 1990:439

Algorithm for calculation of k_{bm} and k_{mp}, Method 3 (using normal Reynolds numbers but evaluating Re and Sc at conditions near wall):

For the third calculation method, values of the viscosity are calculated at the wall (membrane surface), to evaluate mass transfer in the proximity of the wall. To do this, substitute η_w for η_{ave} in Steps 9 and 10 of Method 2, and calculate Reynolds and Schmidt numbers as follows:

- For Step 9, $\mathrm{Re} = \frac{\rho_e u_e d_h}{\eta_w}$, $Sc = \frac{\eta_w}{\rho_e D_{o,m}}$
- For Step 10, $\mathrm{Re} = \frac{\rho_e u_e d_{sp}}{\eta_w}$, $Sc = \frac{\eta_w}{\rho_e D_{o,p}}$

APPENDIX D: BASIC BIOREACTOR DESIGN EQUATIONS

The surface area of a single hepatocyte is given by:

$$A_{hp} = \pi d_{hp}^2 \tag{A}$$

The volume of a single hepatocyte:

$$V_{hp} = \pi \frac{d_{hp}^3}{6} \tag{B}$$

Volume and surface area of a spheroid (assuming that only the external surface of the spheroid is 'available' for mass transfer):

$$\begin{aligned} V_{hs} &= \pi \frac{d_{hs}^3}{6} \\ A_{hs} &= \pi d_{hs}^2 \end{aligned} \tag{C}$$

Number of hepatocytes in a spheroid (where 0.64 is the maximum random packing density for monodisperse spheres):

$$N_{hs} = \frac{0.64 V_{hs}}{V_{hp}} \tag{D}$$

Number of spheroids in bioreactor:

$$N_{sb} = N_h / N_{hs} \tag{E}$$

Surface area and volume of spheroids in bioreactor:

$$\begin{aligned} A_{sb} &= A_{hs} N_{sb} \\ V_{sb} &= V_{hs} N_{sb} \end{aligned} \tag{F}$$

Volume of polyurethane in bioreactor (where V_{bio} is the bioreactor volume):

$$V_{PU} = (1 - \varepsilon_{PU}) V_{BR} \tag{G}$$

'Open' or free volume in bioreactor:

$$V_{open} = V_{BR} - V_{sb} - V_{PU} \tag{H}$$

Projected surface area of spheroids in bioreactor:

$$A_{sb,proj} = A_{sb} / 4 \tag{I}$$

Available surface area on polyurethane foam:

$$A_{PU} = a_{PU} V_{bio} \tag{J}$$

Spheroid surface area as % of available surface area:

$$\%_{sph} = \frac{100 A_{sb,proj}}{A_{PU}} \tag{K}$$

Oxygen requirements of hepatocytes in bioreactor:

$$OR_{h,\max} = \dot{n}_{h,\max} N_h / 10^6 \tag{L}$$

Specific surface area of PFOB in emulsion:

$$a_p = 6/d_{sp} \tag{M}$$

Assume free volume is filled with plasma and PFOB – therefore PFOB volume is given by:

$$V_p = V_{open} \phi_p \tag{N}$$

Projected surface area of PFOB in emulsion:

$$A_{p,proj} = V_p a_p / 4 \tag{O}$$

Interfacial surface area between PFOB and spheroids is chosen as smallest value of $A_{sb,proj}$ and $A_{p,proj}$, and provision is made for the fraction of this area covered by PFOB droplets through the PFOB volume fraction:

$$A_{ps} = \min(A_{sb,proj}, A_{p,proj}) \frac{\phi_p}{0.64} \tag{P}$$

Interfacial surface area between plasma and spheroids is the difference between the total spheroid surface area and the PFOB-spheroid surface area:

$$A_{ms} = A_{sb,proj} - A_{ps} \tag{Q}$$

The rate of oxygen entering the bioreactor is given by:

$$\dot{n}_{O_2,in} = \frac{\%O_2}{100} \left(C_{p,equil} \phi_p + C_{m,equil} (1 - \phi_p) \right) Q_{in} \tag{R}$$

Oxygen requirements as percentage of oxygen supply:

$$\%_{O_2,req} = 100\, OR_{h,\max} / \dot{n}_{O_2,in} \tag{S}$$

The oxygen mass transfer rate from PFOB droplets to hepatocytes is calculated as follows:

$$\frac{dn_p}{dt} = \dot{n}_p = A_{ps} k_{ph} \left(\frac{\rho_m}{\rho_p K} C_p - C_{cell} \right) \quad \text{(T)}$$

where A_{ps} is the interfacial surface area between the PFOB and the hepatocyte spheroids.

The oxygen mass transfer rate from plasma to hepatocytes is given by:

$$\frac{dn_m}{dt} = \dot{n}_m = A_{ms} k_{ph} (C_m - C_{cell}) \quad \text{(U)}$$

Equations (T) and (U) are evaluated at the entrance and exit to the bioreactor, to determine the local mass transfer rates at the entrance and exit. To calculate the exit values, it is assumed that all oxygen requirements of the hepatocytes are met.

REFERENCES

Allen, J.W. and Bhatia, S.N. 2002. Improving the next generation of bioartificial liver devices. *Cell and Developmental Biology*, 13:447-454.

Allen, J.W., Hassanein, T. and Bhatia, S.N. 2001. Advances in Bio-artificial Liver Devices. *Hepatology*, 34(3):447-455.

Allen, T. 1981. *Particle Size Measurement: 3rd Edition.* Great Britain: Chapman and Hall.

Amresco. 2001. The Solution for All of Your Buffer Needs. *Internet:* http://www.amresco-inc.com/catalog/PDF/Buffers.pdf. Accessed: 09/03/2003.

Anthony, P., Davey, M.R., Power, J.B., Washington, C. and Lowe, K.C. 1994. Synergistic enhancement of protoplast growth by oxygenated perfluorocarbon and Pluronic F-68. *Plant Cell Reports*, 13:251-255.

Asua, J.M. 2002. Miniemulsion polymerization. *Progress in Polymer Science*, 27:1283-1346.

Babak, V.G. 1994. Effect of interfacial tension and droplet size on coagulation, adhesion and rheology of concentrated emulsions. *Colloids and Surfaces A: Physicochemical and Engineering Aspects*, 85:279-294.

Bader, A., De Bartolo, L. and Haverich, A. 2000. High level benzodiazepine and ammonia clearance by flat membrane bioreactors with porcine liver cells. Journal of Biotechnology 81:95-105.

Balis, U.J., Behnia, K., Dwarakanath, B., Bhatia, S.N., Sullivan, S.J., Yarmush, M.L. and Toner, M. 1999. Oxygen Consumption Characteristics of Porcine Hepatocytes. *Metabolic Engineering*, 1:49-62.

Beek, W.J., Muttzal, K.M.K. and Van Heuven, J.W. 1999. *Transport Phenomena, 2nd Edition.* USA: John Wiley.

Bhatia, S.N., Balis, U.J., Yarmush, M.L. and Toner, M. 1999. Effect of cell-cell interaction in preservation of cellular phenotype: Cocultivation of hepatocytes and non-parenchymal cells. *FASEB J.*, 13:1883-1900.

Bibette, J., Leal-Calderon, F., Schmitt, V. and Poulin, P. 2002. *Emulsion Science – Basic Principles. An Overview*. Germany: Springer-Verlag.

Bircher, J., Benhamou, J.-P., McIntyre, N., Rizzetto, M. and Rodés, J. 1999. *Oxford Textbook of Clinical Hepatology, 2nd Edition, Volume 1.* Hong Kong: Oxford University Press.

Bond, R., Moolman, F.S., Nieuwoudt, M.J., Van der Merwe, S. and Van Wyk, A.J. 2002. Design, development and experimental verification of a novel bio-artificial liver support system. *10th United European Gastroenterology Week*, 19 – 23 October 2002, Geneva, Switzerland.

Boston University. 1997. Material Safety Data Sheet: Phosphoric Acid. *Internet*: http://www.bu.edu/es/LabSafety/ESMSDSs/MSPhosphoricAcid.html. Accessed: 09/03/2003.

Brems, J.J., Brunson, M. and Salomon, D.R. 2001. Extracorporeal Hepatic Support, in *Liver Transplantation*, edited by G. Klintnalm and H. Sollinger. USA: Centerspan.

Bristol-Myers Squibb. 2001. Blood Clots and Anticoagulants. *Internet*: http://www.cardioliving.com/consumer/Circulatory/Clotting.shtm. Accessed: 07/01/2003.

British Liver Trust. 2001. Guide to your Liver. *Internet*: http://www.british-liver-trust.org.uk. Accessed: 15/09/2001.

Busse, B. and Gerlach, J.C. 1999. Bioreactors for Hybrid Liver Support: Historical Aspects and Novel Designs. *Annals New York Academy of Sciences*, 875:326-339.

Cao, S., Esquivel, C.O. and Keeffe, E.B. 1998. New approaches to supporting the failing liver. *Annu. Rev. Medicine,* 49:85-94.

Chang, T.M.S. 1998. Modified Hemoglobin-based Blood Substitutes: Crosslinked, Recombinant and Encapsulated Hemoglobin. *Vox Sanguinis,* 74(Suppl.2):233-241.

Chang, T.M.S. 1999. Future prospects for artificial blood. *Tibtech*, 17:61-67.

Cheryan, M. 1986. *Ultrafiltration Handbook.* USA: Technomic Publishing Company.

Chibata, I.S., Yamada, S.T., Wada, M.N, Izuo, N.Y. and Yamaguchi, T.Y. 1974. Cultivation of aerobic microorganisms. *US Patent no. 3,850,753*.

Clark, L.C. jr and Gollan, F. 1966. Survival of mammals breathing organic liquids equilibrated with oxygen at atmospheric pressure. *Science*, 152:1755-1756.

Clark, L.C. jr and Leland, C. 1996. Stable perfluorocarbon and oil emulsions. *US Patent no. 5,536,753*.

Cornélus, C., Giulieri, F., Krafft, M.P., Riess, J.G. 1993. Impact of phospholipid dispersions on the stability of fluorocarbon/phospholipid emulsions for biomedical uses. *Colloids Surf.*, 70:233-238.

Cussler, E.L. 1984. *Diffusion: Mass Transfer in Fluid Systems*. USA: Cambridge University Press.

Cussler, E.L. 2002. Personal communication: "Re: Mass transfer in non-Newtonian systems". cussl001@tc.umn.edu (15/03/2002).

Cussler, E.L. 2003. Personal communication: comments on draft thesis (26/06/2003).

Dandliker, W.B., Watson, W.K.R. & Drees, T.C. 1993. Artificial blood containing perfluoro chemicals in presence of emulsifying agents. *US Patent no. 5 434 191*, granted 18/07/1995.

Dixit, V. and Gitnick, G. 1996. Artificial Liver Support: State of the Art. *Scand. J. Gastroenterol.*, 31(Suppl.220):101-14.

Faibish, R.S. and Cohen, Y. 2001a. Fouling-resistant ceramic-supported polymer membranes for ultrafiltration of oil-in-water microemulsions. *Journal of Membrane Science*, 185:129-143.

Faibish, R.S. and Cohen, Y. 2001b. Fouling and rejection behaviour of ceramic and polymer-modified ceramic membranes for ultrafiltration of oil-in-water emulsions and microemulsions. *Colloids and Surfaces A: Physicochemical and Engineering Aspects*, 191:27-40.

Faithfull, N.S. and Weers, J.G. 1998. Perfluorocarbon compounds. *Vox Sanguinis*, 74(Suppl.2):243-248.

Flendrig, L.M., La Soe, J.W., Jörning, G.G.A., Steenbeek, A., Karlsen, O.T., Bovée, W.M.M.J., Ladiges, N.C.J.J., Te Velde, A.A. and Chamuleau, R.A.F.M. 1997. *In vitro* evaluation of a novel bioreactor based on an integral oxygenator and a spirally wound nonwoven polyester matrix for hepatocyte culture as small aggregates. *Journal of Hepatology*, 26:1379-1392.

Flendrig, L.M., Te Velde, A.A. and Chamuleau, R.A.F.M. 1997. Semipermeable Hollow Fibre Membranes in Hepatocyte Bioreactors: A Prerequisite for a Successful Bio-artificial Liver? *Artificial Organs*, 21(11):1177-1181.

Floyd, A.G. 1999. Top ten considerations in the development of parenteral emulsions. *PSTT*, 2(4):134-143.

Fontana, R.J. 1999. Acute liver failure. *Current Opinion Gastroenterology*, 15:270-277.

Garfield, R.E., Balaban, A.T. and Seitz, W.A. 1999. Emulsions of perfluoro compounds as solvents for nitric oxide (NO). *US Patent no. 5,869,539*.

Gerlach, J.C. 1996. Development of a hybrid liver support system: a review. *The International Journal of Artificial Organs*, 19(11):645-654.

Gion, T., Shimada, M., Shirabe, K., Nakazawa, K., Ijima, H., Matsushita, T., Funatsu, K. and Sugimachi, K. 1999. Evaluation of a Hybrid Artificial Liver Using a Polyurethane Foam Packed-Bed Culture System in Dogs. *Journal of Surgical Research*, 82:131-136.

Glicklis, R., Shapiro, L., Agbaria, R., Merchuk, J.C. and Cohen, S. 2000. Hepatocyte Behavior Within Three-Dimensional Porous Alginate Scaffolds. *Biotechnol. Bioeng.*, 67:344-353.

Goerke, A.R., Leung, J. and Wickramasinghe, S.R. 2002. Mass and momentum transfer in blood oxygenators. *Chemical Engineering Science*, 57:2035-2046.

Goosen, M.F.A. 1999. Physico-chemical and Mass Transfer Considerations in Microencapsulation. *Annals New York Academy of Sciences*, 875:84-104.

Gotoh, T., Mochizuki, G. and Kikuchi, K. Perfluorocarbon-mediated aeration applied to recombinant protein production by virus-infected insect cells. *Biochem. Eng.*, 7(1):69-78.

Greeff, I. 1999. *Piping System Design: A Short Course.* Pretoria: Department of Chemical Engineering, University of Pretoria.

Guillouzo, A. 1986. Plasma protein production by cultured adult hepatocytes, in *Isolated and Cultured Hepatocytes.* Guillouzo, A. and Guguen-Guillouzo, C. (Eds.). Great Britain: John Libbey & Company Ltd.

Guyton, A.C. and Hall, J.E. 1996. The liver as an organ, in *Textbook of Medical Physiology*. USA: W.B. Saunders.

Haematologic Technologies Inc. 2001. Catalog: Fibrinogen. *Internet:* http://www.haemtech.com/catalog/Platelet/p1.htm. Accessed: 07/03/2003.

Hay, P.D., Veitch, A.R. and Gaylor, J.D.S. 2001. Oxygen Transfer in a Convection-Enhanced Hollow Fiber Bio-artificial Liver. *Artificial Organs*, 25(2):119-130.

Hayat, M.A. 2000. *Principles and Techniques of Electron Microscopy: Biological Applications, 4th Edition.* Cambridge Press: USA: 367-399.

Higuchi, W.I., Misra, J. 1962. Physical degradation of emulsions via the molecular diffusion route and the possible prevention thereof. *J. Pharm. Sci.* 51:459-466.

Hines, A.L. and Maddox, R.N. 1985. *Mass Transfer: Fundamentals and Applications*. Prentice-Hall, USA.

Hinton, R. and Dobrota, M. 1976. *Density gradient centrifugation.* The Netherlands: Elsevier / North-Holland Biomedical Press.

Houston, J.B. and Carlile, D.J. Incorporation of *in Vitro* Drug Metabolism Data into Physiologically-based Pharmacokinetic Models. 1997. *Toxicology in Vitro*, 11:473-478.

Ijima, H., Matsushita, T., Nakazawa, K., Fujii, Y. and Funatsu, K. 1998 Hepatocyte Spheroids in Polyurethane Foams: Functional Analysis and Application for a Hybrid Artificial Liver. *Tissue Engineering*, 4(2):213-226.

Incropera, F.P. and De Witt, D.P. 1990. *Fundamentals of Heat and Mass Transfer, 3rd Edition.* Singapore: John Wiley & Sons.

Iwata, H., Park, Y.G. and Ikada, Y. 1998. Importance of the extracorporeal circulation rate in a bio-artificial liver. *Mat. Sci. & Eng. C* 6:235-243.

Jaeger, H.M. and Nagel, S.R. 1992. Physics of Granular States. *Science*, 255:1524.

Janča, J. 1988. *Field-Flow Fractionation: Analysis of Macromolecules and Particles*. USA: Marcel Dekker.

Joly, A., Desjardins, J.-F., Fremond, B., Desille, M., Campion, J.-P., Malledant, Y., Lebreton, Y., Semana, G., Edwards-Levy, F., Levy, M.-C. and Clement, B. 1997. Survival, proliferation, and functions of porcine hepatocytes encapsulated in coated alginate beads: a step toward a reliable bio-artificial liver. *Transplantation*, 63(6):795-803.

Ju, L.K., Lee, J.F. and Armiger, W.B. 1991a. Enhancing Oxygen Transfer in Bioreactors by Perfluorocarbon Emulsions. *Biotechn. Prog.* 7:323-329.

Ju, L.K., Lee, J.F. and Armiger, W.B. 1991b. Effect of the Interfacial Surfactant Layer on Oxygen Transfer through the Oil/Water Phase Boundary in Perfluorocarbon Emulsions. *Biotechnol. Bioeng.*, 37:505.

Kabalnov, A., Weers, J., Arlauskas, R. and Tarara, T. 1995. Phospholipids as Emulsion Stabilizers. 1. Interfacial Tensions. *Langmuir* 11:2966-2974.

Kamohara, Y., Rozga, J. and Demetriou, A.A. 1998. Artificial liver: Review and Cedars-Sinai experience. *J. Hepatobiliary Pancreat. Surg.*, 5:273-285.

Kaszuba, M. 2002. What Affects Dispersion Stability and How Can We Predict it? Slide-show presentation downloaded from http://www.malvern.co.uk. Accessed: 12/03/2003.

Ketcham, E.M. and Cairns, C.B. 1999. Hemoglobin-based Oxygen Carriers: Development and Clinical Potential. *Annals of Emergency Medicine,* 33(3):326-337.

Kim, S.S., Utsunomiya, H., Koski, J.A., Wu, B.M., Cima, M.J., Sohn, J. et al. 1998. Survival and function of hepatocytes on a novel three-dimensional synthetic biodegradable polymer scaffold with an intrinsic network of channels. *Ann Surg.*, 228:8-13.

King, A.T., Mulligan, B.J. and Lowe, K.C. 1989. Perfluorochemicals and cell culture. *Biotechnology*, 7:1037-1042.

Koltuniewicz, A.B. and Field, R.W. 1996. Process factors during removal of oil-in-water emulsions with cross-flow microfiltration. *Desalination,* 105:79-89.

Krafft, M.P., Riess, J.G. and Weers, J.G. 1998. The Design and Engineering of Oxygen Delivering Fluorocarbon Emulsions, in *Submicron Emulsions in Drug Targeting and Delivery* edited by S. Benita. Amsterdam: Harwood Academic Publishers:235-333.

Krafft, M.P., Rolland, J.-P. and Riess, J.G. 1991. Detrimental effect of excess lecithin on the stability of fluorocarbon / lecithin emulsions. *Journal of Physical Chemistry*, 95:5673-5676.

Kreyszig, E. 1983. *Advanced Engineering Mathematics, 5th Edition*. USA: John Wiley & Sons, Inc.

Kurosawa, H., Yasumoto, K., Kimura, T. and Amano, Y. 2000. Polyurethane Membrane as an Efficient Immobilization Carrier for High-Density Culture of Rat Hepatocytes in the Fixed-Bed Reactor. *Biotechnol. Bioeng.*, 70:160-166.

Ledezma, G.A., Folch, A., Bhatia, S.N., Balis, U.J., Yarmush, M.L. and Toner, M. 1999. Numerical Model of Fluid Flow and Oxygen Transport in a Radial-Flow Microchannel Containing Hepatocytes. *Journal of Biochemical Engineering*, 121:58-64.

Lee, J. 2000. Metabolic Powerhouse. *New Scientist (11/11/2000)*, 168(2264):135.

Legallais, C., David, B. and Doré, E. 2001. Bio-artificial livers (BAL): current technological aspects and future developments. *Journal of Membrane Science*, 181:81-95.

Lehmler, H.-J., Bummer, P.M. and Jay, M. 1999. Liquid ventilation – A new way to deliver drugs to diseased lungs? *Chemtech*, 29(10):7-12.

Lipnizki, F. & Field, R.W. 2001. Mass transfer performance for hollow fibre modules with shell-side axial feed flow: using an engineering approach to develop a framework. *J. Membr. Sci.* 193, 195-208.

Lipp, P., Lee, C.H., Fane, A.G. and Fell, C.J.D. 1988. A fundamental study of the ultrafiltration of oil-water emulsions. *Journal of Membrane Science*, 36:161-177.

Lohrmann, R., Widder, K.J., Krishnan, A.W., Hong, D.K. and Meng, J. 1998. Emulsions as contrast agents and method of use. *US Patent no. 5,716,597.*

Lowe, K.C. 1991. Perfluorochemicals: Blood Substitutes and Beyond. *Adv. Mater.*, 3(2):87-93.

Lowe, K.C., Anthony, P., Wardrop, J., Davey, M.R. and Power, J.B. 1997. Perfluorochemicals and cell biotechnology. *Art. Cells, Blood Subs. and Immob. Biotech.*, 25(3):261-274.

Lowe, K.C., Davey, M.R. and Power, J.B. 1998. Perfluorochemicals: their applications and benefits to cell culture. *Tibtech*, 16:272-277.

Ludwig, M. 2002. Lecture 13. Oxygen and CO_2 Transport. *Internet:* http://www.mmi.mcgill.ca/Unit2/Ludwig/lect18oxygen&co2transport.htm. Accessed: 06/09/2002.

Mandersloot, W.G.B. and Scott, K. 1990. Rheology of particle suspensions. *South African Journal of Chemical Engineering*, 2(2):53-69.

Mason, T.G. New fundamental concepts in emulsion rheology. *Current Opinion in Colloid and Interface Science*, 4:231-238.

May, M.H. and Sefton, M.V. 1999. Conformal Coating of Small Particles and Cell Aggregates at a Liquid-Liquid Interface. *Annals New York Academy of Sciences*, 875:126-134.

McClelland, R.E., MacDonald, J.M. and Coger, R.N. 2003. Modeling O_2 Transport Within Engineered Hepatic Devices. *Biotechnology and Bioengineering*, 82:12-27.

McMillan, J.D. and Wang, D.I.C. 1987. Enhanced Oxygen Transfer using Oil-in-water Dispersions. *Ann NY Acad Sci* 506, 569-582.

McMillan, J.D. and Wang, D.I.C. 1992. Gas-Liquid Oxygen Transfer in Perfluorochemical-in-Water Dispersions, in *Frontiers in Bioprocessing II.* Todd, P., Sikdar, S.K. and Bier, M. (Eds). USA: American Chemical Society.

Middleman, S. 1998. *An Introduction to Fluid Dynamics: Principles of Analysis and Design.* USA: John Wiley & Sons, Inc.

Morsiani, E., Brogli, M., Galavotti, D., Pazzi, P., Puviani, A.C. and Azzena, G.F. 2002. Biologic liver support: optimal cell source and mass. *Int. J. Artif. Organs*, 25(10):985-93.

Noda, I. & Gryte, C.C. 1979. Mass transfer in regular arrays of hollow fibres in countercurrent dialysis. *AIChE J.*, 25:113.

Okamoto, M., Ishida, Y., Keogh, A., Strain, A. 1998. Evaluation of the function of primary human hepatocytes co-cultured with the human hepatic stellate cell (HSC) Line LI90. *International Journal of Artificial Organs,* 21(6):353-359.

Oleksiak, C.B., Habif, S.S. and Rosano, H.L. 1994. Flocculation of perfluorocarbon emulsions. *Colloids and Surfaces A: Physicochemical and Engineering Aspects*, 84(1):71-79.

Olson, E., Bradley, E. and Mate, K. 1999. Principles of Liver Support Systems. *Internet:* http://biomed.brown.edu/Courses/BI108/BI108_1999_Groups/Liver_Team/Liver.html. Accessed: 05/10/2000.

Pall Gelman Laboratory, 2000. *The Filterbook*. USA: Pall Gelman Laboratory.

Park, Y.-G., Iwata, H. and Ikada, Y. 2001. Derivation of Pharmacokinetics Equations for Quantitative Evaluation of Bio-artificial Liver Functions, in Bio-artificial Organs III, Tissue Sourcing, Immunoisolation and Clinical Trials. Hunkeler, D., Cherrington, A., Prokop, A. and Rajotte, R. (Eds.). *Ann. NY Acad. Sci.*, 944:296-307.

Patel, S. & Mehra, A. 1998. Modelling of Oxygen Transport in Blood-Perfluorocarbon Emulsion Mixtures Part I: Oxygen Uptake in Tubular Vessels. *ASAIO Journal* 44, 144-156.

Paulson, D.J. 1995. Membranes, the finest filtration. *Filtration News*, 1 July 1995.

Pell, E.D. and Holzmann, R.T. 1974. Hydraulic Fluid Emulsions, in *Emulsions and Emulsion Technology Part II* edited by K.J. Lissant. Surfactant Science Series, Vol. 6. USA: Marcel Dekker.

Perry RH, Green D. 1984. *Perry's Chemical Engineers' Handbook, 6th Edition.* USA: McGraw-Hill, Inc.

Perry, R.H., Green, D.W. & Maloney, J.O. 1997. *Perry's Chemical Engineers' Handbook, 7th Edition.* USA: McGraw-Hill Publishing Company.

Raynolds, S. and Dettre, R.H. 1997. Emulsion stability. *US Patent no. 5,595,687.*

Riess, J.G. 1992. Overview of Progress in the Fluorocarbon Approach to *in vivo* Oxygen Delivery. *Biomat., Art. Cells & Immob. Biotech.*, 20(2-4):183-202.

Riess, J.G. 2001. Oxygen carriers ("Blood Substitutes"): Raison d'Etre, Chemistry and some Physiology. *Chem Rev.*, 101:2797-2919.

Riess, J.G., Cornelius, C., Follana, R., Krafft, M.P., Mahe, A.M., Postel, M and Zarif, L. 1994. Novel fluorocarbon-based injectable oxygen-carrying formulations with long-term room-temperature storage stability. *Oxygen Transport to Tissue XV* edited by P. Vaupel et al. New York: Plenum Press:227-234.

Robinson, P.J. 1991. Hepatic modelling and risk assessment: compartmental versus tube models and interspecies scaling. *Drug Metabolism Reviews*, 23(5&6):601-617.

Sanfilippo, B., Ciardiello, F., Salomon, D.S. and Kidwell, W.R. 1988. Growth of cells on a perfluorocarbon-medium interphase: a quantitative assay for anchorage-independent cell growth. *In Vitro Cellular & Developmental Biology*, 24(1):71-77.

Sarteschi, L.M., Sagripanti, A., Carpi, A. and Menchini-Fabris, F. 2001. Rationale for the development of red-cell substitutes and status of the research. *Internal Medicine*, 9:36-44.

Schneider, M., Reymond, F., Marison, I.W. and Von Stockar, U. 1995. Bubble-free oxygenation by means of hydrophobic porous membranes. *Enzyme and Microbial Technology*, 17:839-847.

Schramm, L.L. 1992. *Emulsions: Fundamentals and Application in the Petroleum Industry*. Advances in Chemistry Series 231. American Chemical Society: USA.

Severinghaus, J.W. 1979. Simple, accurate equations for human blood O_2 dissociation computations. *Journal of Applied Physiology*, 46:599-602.

Shah, N. and Mehra, A. 1996. Modelling of Oxygen Uptake in Perfluorocarbon Emulsions: Some Comparisons with Blood. *ASAIO Journal*, 42:181-189.

Sherman, J.H. and Luciano, D.S. 1986. *Human Physiology: The Mechanisms of Body Function, 4th Edition.* USA: McGraw-Hill.

Sherman, P. 1968. *Emulsion Science*. Scotland: Academic Press Inc. (London) Ltd.

Skelland, A.H.P. 1967. *Non-Newtonian Flow and Heat Transfer*. USA: John Wiley and Sons.

Sobotka, M., Prokop, A., Dunn, I.J. and Einsele, A. 1982. Review of methods for the measurement of oxygen transfer in microbial systems. *Annual Reports on Fermentation Processes,* 2:127-210.

Sussman, N.L. and Kelly, J.H. 1997. Extracorporeal Liver Support: Cell-Based Therapy for the Failing Liver. *American Journal of Kidney Diseases,* 30(5) Suppl.4:S66-S71.

Teraklin. 2002. Indications for MARS® liver support therapy. *Internet*: http://www.teraklin.com/eng/indications_liver.html . Accessed: 25/06/2002.

Te Velde, A.A., Flendrig, L.M., Ladiges, N.C.J.J. and Chamuleau, R.A.F.M. 1997. Immunological consequences of the use of xenogeneic hepatocytes in a bio-artificial liver for acute liver failure. *The International Journal of Artificial Organs*, 20(4):229-233.

Trotter, J.F., Wachs, M., Everson, G.T. and Kam, I. 2002. Adult-to-Adult Transplantation of the Right Hepatic Lobe from a Living Donor. *N. Engl. J. Med.*, 346(14):1074-1082.

Tsiaoussis, J., Newsome, P.N., Nelson, L.J., Hayes, P.C. and Plevris, J.N. 2001. Which Hepatocyte Will It Be? Hepatocyte Choice for Bio-artificial Liver Support Systems. *Liver Transplantation*, 7(1):2-10.

University of Newcastle upon Tyne. 2003. On-line Medical Dictionary. *Internet*: http://cancerweb.ncl.ac.uk/omd/. Accessed: 09/03/2003.

Van der Merwe, S.W., Gastroenterologist: Unitas Hospital, Pretoria. 2002. Personal communication. 02/09/2002.

Vermont Safety Information Resources Inc. Material Safety Data Sheet Collection. *Internet*: http://hazard.com/msds2/. Accessed: 06/08/2001.

Von Goethe, J.W. 1909. The Tragedy of Faust, Part I. *The Harvard Classics*, 19(1):1415. New York: P.F. Collier and Son Company. Online access: http://www.bartleby.com/19/1/. Accessed: 05/03/2003.

Wabel, C. 1998. Influence of Lecithin on Structure and Stability of Parenteral Fat Emulsions. Ph.D. dissertation, University of Erlangen. Website: http://www2.ccc.uni-erlangen.de/dissertationen/data/dissertation/Christoph_Wabel/html/Titel.html. Accessed: 25/06/2002.

Weast, R.C. (Ed.). 1985. *CRC Handbook of Chemistry and Physics, 66th Edition.* USA: CRC Press.

Whorlow, R.W. 1980. *Rheological Techniques.* Great Britain: Ellis Horwood.

Winslow, R.M. 1999. New Transfusion Strategies: Red Cell Substitutes. *Annu. Rev. Med.*, 50:337-353.

Wu, F.J., Friend, J.R., Lazar, A., Mann, H.J., Remmel, R.P., Cerra, F.B. and Hu, W.S. 1996. Hollow fibre bio-artificial liver utilizing collagen-entrapped porcine hepatocyte spheroids. *Biotechnol. Bioeng.*, 52:34-44.

Xue, Y.-L., Zhao, S.-F., Luo, Y., Li, X.-J., Duan, Z.-P., Li, W.-G., Huang, X.-Q., Li, Y.-L., Cui, X., Zhong, D.-G., Zhang, Z.-Y. and Huang, Z.-Q. 2001. World Journal of Gastroenterology, 7(6):826-829.

Yamada, K., Kamihira, M., Hamamoto, R. and Iijima, S. 1998. Efficient Induction of Hepatocyte Spheroids in a Suspension Culture Using a Water-Soluble Synthetic Polymer as an Artificial Matrix. *J. Biochem.*, 123:1017-1023.

Yamada, K., Kamihira, M. and Iijima, S. 1999. Enhanced Cell Aggregation and Liver Functions Using Polymers Modified with a Cell-Specific Ligand in Primary Hepatocyte Cultures.

Yamada, K., Kamihira, M. and Iijima, S. 2001. Self-organization of liver constitutive cells mediated by artificial matrix and improvement of liver functions in long-term culture.

Yamamoto, S., Shiragami, N., Unno, H. and Honda, H. 1994. Analysis of Oxygen Transfer Enhancement by Oxygen Carrier in the Autotrophic Cultivation of Alcaligenes Eutrophus under Low Oxygen Partial Pressure. *Journal of Chemical Engineering of Japan,* 27(4):449-454.

Young, G. 2000. Emulsification. *Internet:* http://www.fst.uq.edu.au/staff/gyoung/unitoperations. Accessed: 05/12/2000.

YSI. 2001. Specifications: YSI 5300A Biological Oxygen Monitor. *Internet:* http://www.ysi.com/extranet/BTKL.nsf/447554deba0f52f2852569f500696b21/fb85ef3280e1ecba85256bb100707acc!OpenDocument. Accessed: 09/03/2003.

Yuet, P.K., Harris, T.J. and Goosen, M.F.A. 1995. Mathematical modelling of immobilized animal cell growth. *Art. Cells, Blood Subs., and Immob. Biotech.*, 23(1):109-133.

Zajicek, G. 1992. Time Dimension in Histopathology. *Path. Res. Pract.*, 188:410-412.

Zuck, T.F. and Riess, J.G. 1994. Current Status of Injectable Oxygen Carriers. *Critical Reviews in Clinical Laboratory Sciences*, 31(4):295-324.